Study of refrigerant emissions from mobile air-conditioning compressor shaft seals

David Sousa

ED n° 432 : « Sciences des Métiers de l'Ingénieur »

N° attribué par la bibliothèque

T H E S E

pour obtenir le grade de

DOCTEUR DE L'ECOLE NATIONALE SUPERIEURE DES MINES DE PARIS

Spécialité "Energétique"

présentée et soutenue publiquement par
David SOUSA

le 16 décembre 2008

STUDY OF REFRIGERANT EMISSIONS FROM MOBILE AIR-CONDITIONING COMPRESSOR SHAFT SEALS (ETUDE DES EMISSIONS DE FLUIDES FRIGORIGENES DE JOINTS TOURNANTS DE COMPRESSEURS DE CLIMATISATION AUTOMOBILE)

Directeur de thèse : Denis CLODIC

Jury :

M. Dominique MARCHIO, Mines ParisTech ..... Président
M. René GRAS, LISMMA ..... Rapporteur
M. Eckhart GROLL, Purdue University, USA ..... Rapporteur
M. Denis CLODIC, Mines ParisTech ..... Examinateur
M. Laurent GAGNEPAIN, ADEME ..... Examinateur

Acknowledgements

This research work has been carried out at the Center for Energy and Processes of Ecole des Mines de Paris. This study could not have been completed without the support and help of many people, for which I am very grateful.

Foremost, I would like to thank Denis CLODIC for being a patient supervisor and for supporting this work with ideas, criticism, and for sharing his experience.

Anne-Marie POUGIN, for her administrative support.

Yingzhong YU, for friendship, the support during the experiments and the fruitful advises.

Franck FAYOLLE, for all his help in the preparation of experiments.

I would like to extend my professional acknowledgements to all my colleagues of the Center for Energy and Processes for creating an enjoyable and stimulating environment.

Last but not least, Célia, who gave me the personal support and love, without her none of this would have been possible. To my parents, for their patience and encouragement when it was most required. To my uncles and aunts for their support when I arrived in France. This thesis is dedicated to you all.

Contents

Nomenclature

A	Surface	m^2
C	Concentration	ppm
D	Diameter	m
D_c	Diffusion Coefficient	m^2s^{-1}
E	Young modulus	Pa
E’	Effective elastic modulus	Pa
F	Force	N
h	Thickness	m
H	Hardness	-
J	Gas flux	Mol $s^{-1}m^{-2}$
k	Wear rate	mm^3 N^{-1} m^{-1}
K	Wear coefficient	-
K	Stiffness	N m^{-1}
l	Leakage tube length	m
M	Gas molar mass	g mol^{-1}
$\dot{m}$	Mass flow rate	kgs^{-1}
P	Pressure	Pa
P_e	Permeability coefficient	Mol $mm^{-2}s^{-1}$ MPa^{-1}
Q	Heat transfer	W m^{-2}
G	Gas quantity	mol
r	*R*adius	m
T	Temperature	K
t	Time	s
u	Uncertainty	-
u	Displacement	m
V	Volume	m^3
W	Compressor work	J
w	Strain energy	J
X	Mole fraction	-

Greek letters

λ	Mean free path	m
ρ	Density	kg m^{-3}
ν	Velocity	m s^{-1}
τ	Compression ratio	-
η	Viscosity	Pa.s
ω	Rotational speed	rad s^{-1}
μ	Coefficient of friction	-
σ	Stress	Pa
υ	Poisson ratio	-

γ	Surface tension	mJ m^{-2}
θ	wetting angle	rad
ε	Strain	-

Constants

$M_{HFC-134a}$	Molar mass of HFC-134a (=102.03)	$gmol^{-1}$
R	Universal gas constant (=$8.314x10^{3}$)	kj $kmol^{-1}$ K^{-1}

Non dimensional numbers

Hs	Hersey number
Re	Reynolds number

Subscripts

abs	Absolute
ac	Accumulation Volume
amb	Ambient
av	Net
c	Chamber
ch	Channel
g	Gas
g	Glass Transition
h	Case
HFC	Hydrofluorocarbon
LA	Liquid/Air
max	Maximum
min	Minimum
mix	Mixture
o	Case
oil	Oil
p	Rubber
pr	Peripheral Rides
ref	Refrigerant
SA	Solid/Air
sc	Plastic
sh	Seal Outer Case
SL	Solid/Liquid

Abbreviations

A/C	Air Conditioning
ACEA	European Automobile Manufacturers Association
ACN	Acrylonitrile
ASEAN	Southeast Asian Nations
CCD	Charge Coupled Device
CEP	Center for Energy and Process
CFC	Chlorofluorocarbon
CIPM	Committee for Weights and Measures
CL	Contact Line
CMOS	Metal Oxide Semiconductor
EHL	Elasto-Hydrodynamic Lubrication
EU	European Union
FEM	Finite Element Method
GWP	Global Warming Potential
HFC	Hydrofluorocarbon
HL	Hydrodynamic Lubrication
HNBR	Hydrogenated Nitrile Butadiene Rubber
HVAC	Heating Ventilation and Air Conditioning
ID	Inner Diameter
LCCP	Life Cycle Climate Performance
LED	Light-Emitting Diode
LFR	Leak Flow Rate
MAC	Mobile Air Conditioning
NBR	Nitrile Butadiene Rubber
NDEC	New Europeen Drive Cycle
OCR	Oil Circulation Ratio
OD	Outer Diameter
PAG	Polyalkylene Glycol oil
PID	Proportional–Integral–Derivative
PMMA	Poly-methyl Methacrylate
POE	Polyol-ester oil
PTFE	Polytetrafluoroethylene
PWM	Pulse-width Modulation
R_a	Center Line Average Roughness
R_{max}	Maximum Height Roughness
R_z	Peak-to-valley Height Roughness
TEWI	Total Equivalent Warming Impact
USA	United States of America
UV	Ultra-violet

Introduction

The air-conditioning system is today worldwide standard equipment in the automotive industry improving not only the thermal comfort but also the safety of passengers. This refrigerant system uses HFC-134a, a hydro-fluorocarbon refrigerant, whose emissions contribute to global warming as they accumulate in the atmosphere. The automotive air-conditioning system differs from stationary refrigerant systems, since the components are installed all around the vehicle engine compartment; the compressor is externally driven by the engine and is a so-called open-type compressor. This system configuration results in the use of an important number of seal components, which are the origin of refrigerant gas emissions. Among these components, the compressor has been identified as the most leak prone component representing 50 to 60% of the system emissions. The compressor most emissive component is the shaft seal that represents up to 50% of the compressor emissions, as it will be demonstrated in this dissertation.

The objectives of this thesis are to study the physical principles and to analyze the experimental results of gas emissions in order to contribute to the knowledge on the fundamental mechanisms and the important parameters of the compressor shaft seal gas emissions.

The environmental impacts of the mobile air-conditioning (MAC) system gas emissions are analyzed in Chapter 1. The different types of gas emissions during the system lifetime are described, as well as the leak detection tools used in the field to detect the system leak points. The first chapter ends with the European policies that have been recently approved to control the MAC system emissions.

The physical and experimental study of the compressor gas emissions are presented in Chapter 2. The original experimental setup developed to measure gas emissions when the compressor is at rest as well as when its shaft is rotating are detailed. Unused and aged compressors are tested to demonstrate the major increase in gas emissions with the shaft seal wear process.

The compressor shaft seal emissions are studied in more details in Chapter 3. The evolution of the shaft seal design is presented followed by the description of the original experimental setup developed to study gas emissions in standstill mode. Different shaft seal designs and shaft surface textures have been tested under dry and wet conditions. An experimental setup allows visualizing the shaft seal contact through a transparent shaft and so verifying the seal deformation under different working conditions.

The last chapter presents the beginning of the shaft seal stress analysis study using a finite element method software. The deformation and stress analysis results are presented and compared to gas emissions obtained in Chapter 3.

Chapter 1

MOBILE AIR CONDITIONING (MAC) SYSTEM REFRIGERANT EMISSIONS

Introduction

The first chapter of this study aims at answering the question: Why is it important to study refrigerant emissions from the MAC compressor?

The chapter starts with the description of HFC-134a refrigerant emissions and their contribution to global warming. A description of the MAC system and its leak sources is performed.

Section 3 presents the leak flow rate (LFR) of new MAC systems as well as the contribution of each component to the system emissions. The compressor contribution varies between 50 and 60% of the total system emissions, depending on the system design, making it the most leak prone component.

A description of the different types of gas emissions during the system lifetime is performed and the market growth of air conditioning vehicles is presented. Section 5 introduces the leak detection tools used by professional technicians to search the system leak points and evidences their low sensitivity, as well as the inappropriate use with the shaft seal design.

The chapter ends with the European policies to control MAC system emissions of new vehicles and the most recent designs. The high leak rates due to the aging process, in combination to an increasing impact on the environment, increase the importance of emissions from MAC compressors.

1. Mobile Air Conditioning (MAC) system refrigerant emissions

The Mobile Air Conditioning (MAC) System is an important part of the vehicle Heating Ventilation and Air Conditioning (HVAC) system. The cooling capacity is mainly used to compensate the latent and sensible thermal loads improving comfort of passengers and avoiding the windshield fogging regardless of the external weather conditions.

The air conditioning system is based on a vapor compression cycle that uses a hydrofluorocarbon (HFC) refrigerant, usually HFC-134a, whose emissions contribute to the human induced global warming as they accumulate in the atmosphere. The study of these refrigerant emissions is the main motivation of this work.

As it will be presented, a MAC system emits from leak sources. This chapter examines the MAC system refrigerant emission levels as well as the leak test methods to detect and locate the leaky points. The contributions of each component to the system overall refrigerant emissions are also presented as well as its environmental impact.

1.1. Environmental impact of MAC emissions

The HFC-134a is the most used refrigerant representing 80% of the market [WOR02], and it has been the first HFC introduced in the market, especially in MAC systems, in domestic refrigeration and small commercial systems. Mobile air conditioning has been identified as the most emissive refrigerant domain (see Figure 1-1). The MAC system represents 78% of the worldwide HFC emissions followed by the stationary A/C with 9%. This fact is related to the MAC system design with an open type compressor, and elastomer hoses and fittings to connect the system components, as presented in Section 1.2.

The Global Warming Potential (GWP) of HFC-134a is 1,430 to a time horizon of 100 years [AFE06], which means that one gram of HFC-134a released to the atmosphere is the equivalent of 1.4 kg of carbon dioxide (CO_2). Since HFC-134a does not contain chlorine or bromine, it does not contribute to the ozone depletion. However, HFCs are active gases that contribute to the human induced global warming. HFCs are included in the group of gases listed in the Kyoto Protocol, which has been ratified by the European Union.

The worldwide demand of HFC-134a was about 121,000 tons in 2003 [CLO05] and it is expected to continue to increase mainly due to the rapid growth of the China automobile industry (passenger cars, minibus, other buses and trucks). The passenger cars are highly demanded in China with a growth rate of 24% per year.

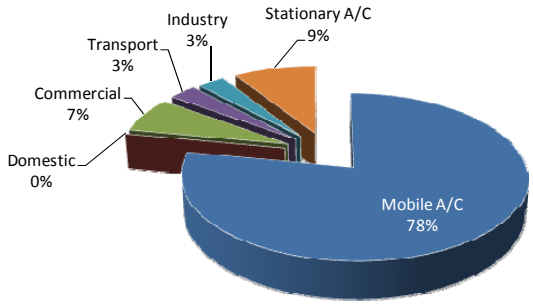

Figure 1-1 Worldwide HFC emissions in 2003 split by domain [CLO05].

HFCs are active gases in the atmosphere. A relatively simple way to verify the global emissions of HFC-134a is to measure its concentration in the atmosphere. Figure 1-2 shows

the evolution of HFC-134a concentration in parts per trillion (ppt) between 1995 and 2007 all around the world: Ireland (Europe), California (West Coast of the United States); Barbados (East of the Caribbean Sea), Samoa (Pacific Ocean) and Tasmania (Australian island).

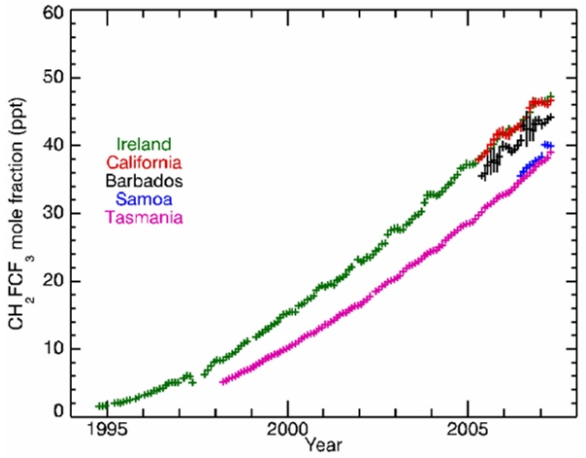

Figure 1-2 Atmospheric concentration of HFC-134a [AGA08].

These measures show that the HFC-134a concentration in the atmosphere has an exponential evolution since 1995 and in 2007 has a value of 38 ppt in Tasmania and 44 ppt in Ireland and California. Therefore, in 12 years, the HFC-134a concentration has been multiplied by a factor of 23 worldwide. The question is: what is inducing such important release of gas to the atmosphere? As mentioned before, the main user of HFC-134a is the refrigeration industry with 80% of the market. Among the different refrigerant applications, the MAC system is clearly the most emissive equipment of the refrigeration industry (see Figure 1-1). Therefore, the air conditioning system used in the automotive industry is the main contributor to HFC-134a emissions.

The next two sections present the MAC system design and its components, as well as the refrigerant emissions at the system and components levels.

1.2. MAC system design

The MAC system is based on the refrigerant vapor compression cycle. Typically, a refrigerant vapor compression cycle is composed of a compressor, two heat exchangers, an expansion device, an accumulator and the working fluid, the refrigerant, that evaporates and condensates during the cycle (see Figure 1-3).

The saturated vapor at low pressure enters the compressor and undergoes an irreversible near adiabatic compression, evolution 1 to 2. Heat is then rejected at constant pressure in evolution 2 to 3 and the working fluid exits the condenser as a slightly sub-cooled liquid. The refrigerant at state 3 enters the expansion valve and expands to the evaporating pressure. The working fluid is then evaporated at constant pressure, evolution 4 to 1, to complete the cycle. Compressor moving parts are oil lubricated to avoid metal-to-metal contact, thus reducing energy losses and wear.

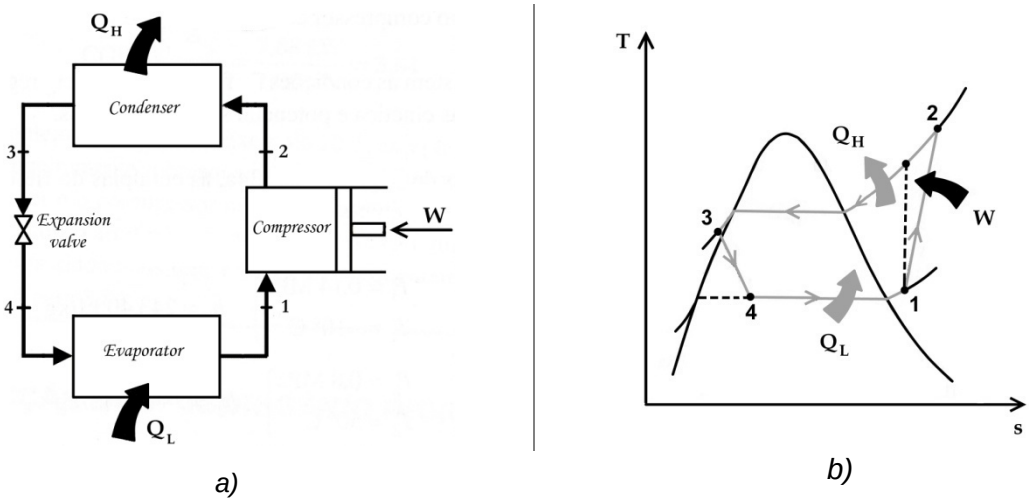

Figure 1-3 a) Refrigerating system lay-out b) T-s diagram for a vapor compression refrigeration cycle.

1.2.1 The system vehicle integration

For a stationary refrigerating vapor compression cycle as used in refrigerators, the compressor work is generated by an electrical motor located inside the hermetical compressor casing. The MAC system differs from these stationary refrigerating systems, since the components are installed all around the vehicle engine compartment and the compressor is driven by the engine through a belt-pulley mechanism (see Figure 1-4). The compressor speed is then proportional to the engine speed. The evaporator is a micro-channel heat exchanger and is normally located inside the dashboard, so that it can absorb heat from the vehicle cabin. The condenser is placed at the vehicle front to ensure a free air flow over it to condensate the refrigerant. Rigid and flexible hoses are used to transport the refrigerant throughout the system. All these components are linked by fittings to allow components replacement during the vehicle life time.

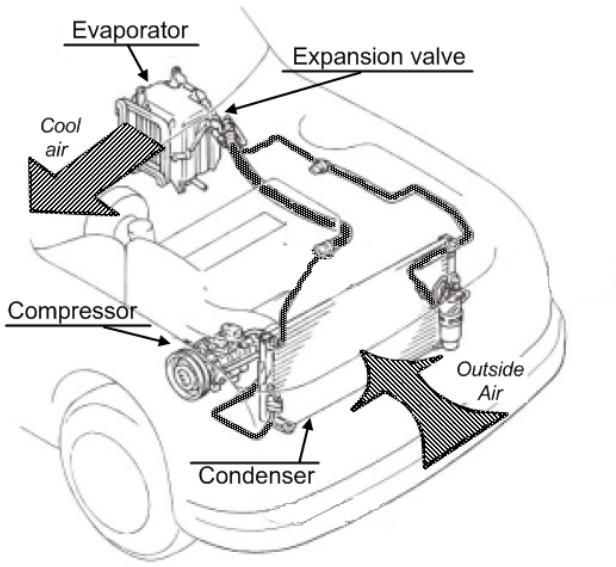

Figure 1-4 Implementation of a car MAC system with a single evaporator.

The compressor is attached to the engine and connected by two flexible hoses to the thermal expansion valve and the condenser (see Figure 1-5). The flexible hoses reduce vibrations coming from the compressor, facilitate assemblage of components and, more importantly, disconnect engine movements from the MAC components fixed on the walls of the engine compartment or inside the dashboard. The liquid refrigerant flows from the condenser to the expansion valve via a rigid aluminum hose. The expansion valve and the evaporator are assembled in the HVAC unit. The pressure sensor and the service valves are brazed on the aluminum hoses, and the receiver is usually coupled with the condenser. If an orifice tube is used as expansion device, the receiver is replaced by an accumulator and placed in the compressor suction line to prevent liquid refrigerant from being drawn into the compressor.

Each component and connections have a sealing system to avoid fluid (refrigerant/oil mixture) to flow out of the circuit. The sealing system is composed by an elastomer seal and its casing. Often the seal is the weakest link in the system and allows losses of fluid that can make the system stop. Any clearance, however small, allows the passage of refrigerant molecules. The fluid flows through micro gaps, the driving forces being the differences of pressures. The seal performance also depends on other variables such as temperature, mating surface topography, seal material properties, seal design, and applied loads.

Some examples of components and fittings sealing technology are presented hereafter.

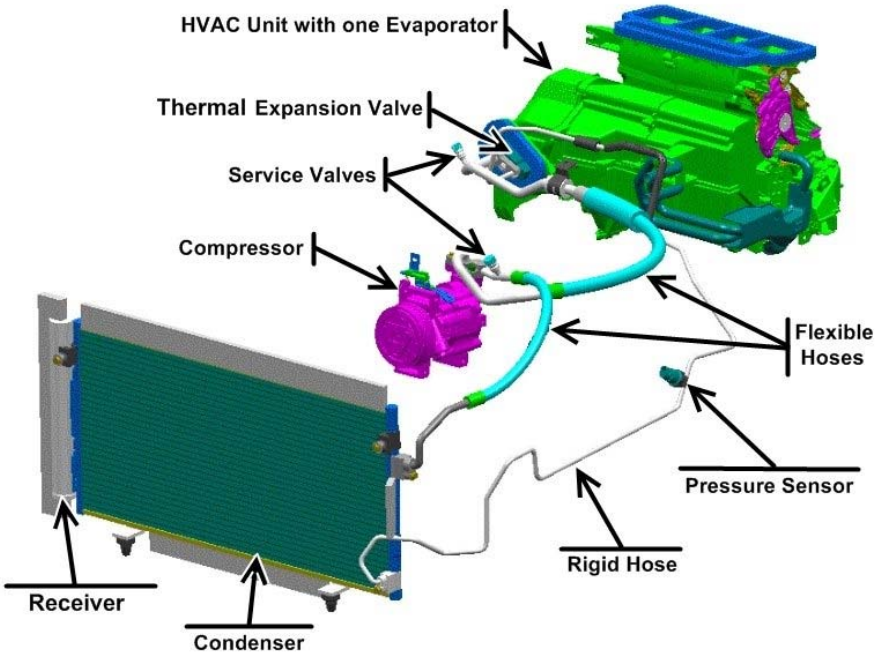

Figure 1-5 Perspective of a single evaporator car refrigerating system.

1.2.2 Heat exchangers and expansion valve

The two compact heat exchangers are located one in the front of the vehicle, the condenser, and the other in the vehicle cabin dashboard, the evaporator. Usually, the thermal expansion valve is fixed to the evaporator and the accumulator to the condenser (see Figure 1-6).

The sealing system is composed of one or several elastomer o-rings that are compressed during assemblage to create a static seal effect. The elastomer o-rings require a low compression force, less stringent machining tolerances and surface finish than metal-gasket seals.

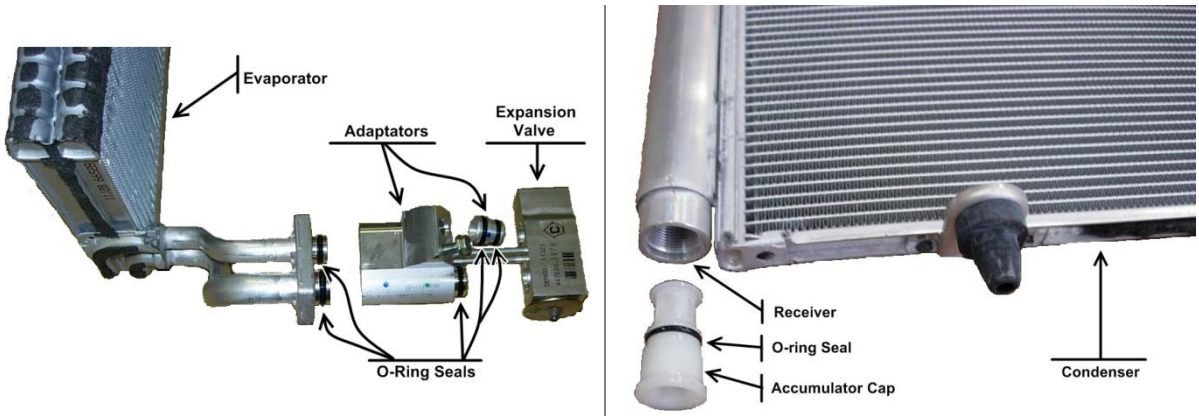

Figure 1-6 Examples of heat exchangers and expansion device sealing system.

1.2.3 Open-type compressor

The compressor is the main component of the MAC system. The compressor body is made of three blocks: rear, cylinder, and front. It encloses the compression mechanism that is belt driven by the vehicle engine. The clutch assembly controls the compressor operation (see Figure 1-7).

Gasket and o-ring static seals are used to seal the compressor body blocks and fittings. As mentioned before, the compressor mechanism is externally driven by the engine (open type), so a particular seal is necessary to seal the space between the shaft and the casing. This particular seal is called the shaft seal. The shaft seal is placed in the compressor front block followed by a felt ring that absorbs the lubricating oil that leaks through the shaft seal.

The complexity of the shaft seal is related to its double working mode: static seal when the shaft is at rest and dynamic seal when the shaft is rotating thus exposed to the wear effect. That is the reason why the shaft seal is the most leak prone component, not only of the compressor, but also of the MAC system, as it will be demonstrated throughout this study.

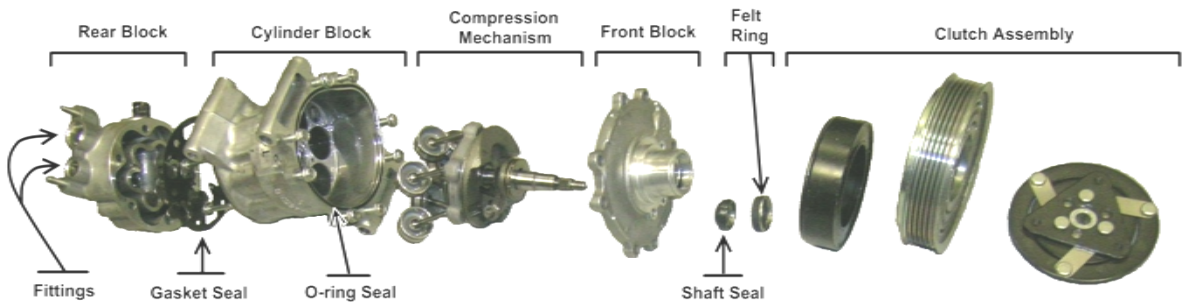

Figure 1-7 MAC compressor exploded view.

1.2.4 Fittings

The component fittings are composed of two aluminum flanges and one or more static seals. Flanges are screwed and seals change of shape in order to contain the refrigerant (see Figure 1-8).

Axial and radial applications are the most common types of o-rings in a MAC system. Figure 1-8a presents a connection with both configurations. The gasket seal can also be found in a connection and it is the combination of two materials: elastomer and metal (see Figure 1-8b).

The number of fittings in a MAC system is variable. A minimum number of 8 to 16 can be found in a single or double evaporator system respectively.

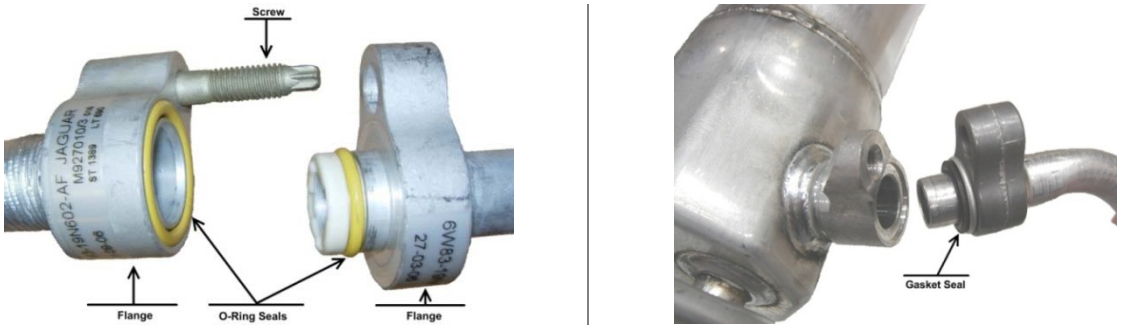

Figure 1-8 Fittings sealing system; a) o-ring type; b) gasket type.

1.2.5 Hoses

The MAC system hoses can be flexible or rigid. The flexible hoses are used to facilitate component assemblage and to avoid compressor and engine vibrations to be transmitted to the refrigerant system.

The size of a typical gas molecule is less than one nanometer. The gas molecules can therefore diffuse through the smallest gap or material pores. The flexible hoses are particularly sensitive to the diffusion phenomenon due to their important elastomer surface in contact with the refrigerant.

The flexible part is linked to the rigid aluminum hose by means of crimps (see Figure 1-9). The flexible hoses are made of one or multiple layers of materials in order to reduce refrigerant permeation and to better absorb vibrations.

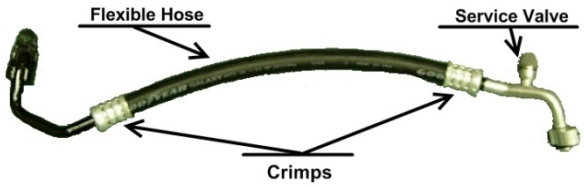

Figure 1-9 MAC system discharge line.

1.2.6 Working fluid and lubricating oil

Before the Montreal Protocol, the MAC systems used CFC-12 as a refrigerant. Since 1990, CFC-12 has been replaced by HFC-134a in developed countries. Today, it is assumed that all vehicles including cars, light commercial vehicles, and truck cabins sold in developed countries have been retrofitted or initially charged with HFC-134a.

HFC-134a is a pure, non flammable refrigerant used primarily as a refrigerant in the refrigeration industry and automobile air conditioners. Another potential use can be the application in plastic foam as a blowing agent, as a solvent for special cleaning applications, and as a propellant in aerosols.

HFC-134a has a strong polarity and is no longer compatible with conventional mineral oils. This fact has led to the introduction of new synthetic lubricants, such as POE (polyol-ester) or polyalkylene glycol (PAG) oil. PAGs are used in the MAC system due to the low water absorption, but they are not used in stationary applications due to their low electric resistivity, which is not compatible with hermetic motor-compressors.

The primary function of the refrigeration lubricant is to provide good compressor lubrication. However, the lubricant oil is miscible with refrigerant and circulates all along the system, so depending on the clearance of the compressor, the oil circulation ratio (average ratio of oil mixed with the refrigerant) varies from 2 to 5%.

1.3. System and components emissions level

An extensive study has been performed by the Center for Energy and Process (CEP) in collaboration with the European Automobile Manufacturers Association (ACEA) in 2006 in order to determine the refrigerant emission levels of new MAC systems [CLO06]. The conclusions point out an annual leak flow rate average value of 10 g/yr for a fleet of 39 vehicles of 10 different types. A comparison study has also been performed to compare the system and the components emission levels. It has been proven that the sum of each component Leak Flow Rate (LFR) is equal to the system LFR and, in all systems, the compressor is the most leak prone component. The compressor contribution varies between 50 to 60%, the lower value corresponding to the use of flexible hoses with high permeation rates.

Figure 1-10 shows the average contribution of components to the system emissions. The compressor represents 57% of refrigerant emissions. It is followed by the suction line and the expansion device with 16% and 10% respectively. The high LFR of the MAC compressor is explained by its complex sealing system, in particular, the shaft seal that performs static and dynamic sealing.

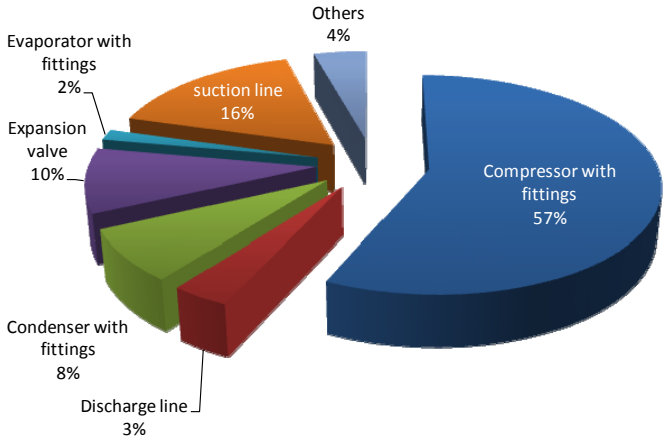

Figure 1-10 Contribution of components to the system emissions at 1020 kPa.

According to the ACEA report [ACE07], the average age of a European car is about 12 years and the average annual distance travelled is about 15,000 km. This means that the vehicle annual operating time is only 300 to 500 hours, which represents only 3 to 6% of the yearly hours. Furthermore, the percentage of the time the air conditioning is switched on never exceeds 70% in the United States and 60% in Europe [JOH04]. Therefore, a MAC system in Europe is 95 to 98% of its lifetime at rest. For that reason, the emission rates at rest define the system leak flow rate as it will be demonstrated further on.

Table 1-1 presents the leak test results in standstill and running modes for three different new MAC systems. The running tests have been done by repeating NDEC cycles.

It is observed that the system refrigerant emissions in running mode are 2 to 3 times higher than those at rest. Nevertheless, as explained before, the running mode represents only 2 to 5% of the vehicle lifetime, so the refrigerant emissions at rest define the system leak flow rate. Notwithstanding, the running mode is extremely important to define the system emissions during the lifetime, since it will change the compressor sealing ability, more particularly, the shaft seal performance (see Chapter 2).

Table 1-1 Annual Leak Flow Rate of new MAC systems.

	At rest			Running mode			Annual LFR [g/yr]
Vehicle	*Duration [hr]*	*Refrigerant loss@20 °C [g]*	*LFR [g/hr]*	*Duration [hr]*	*Refrigerant loss [g]*	*LFR [g/hr]*	**(rest + running mode)**
V1	8529	8.57	1.00E-03	231	0.52	2.25E-03	9.1
V2	8524	7.49	8.79E-04	236	0.54	2.29E-03	8.0
V3	8543	5.07	5.93E-04	217	0.25	1.15E-03	5.3

1.4. Emissions during the MACs lifetime

Emissions are defined as substances emitted to the atmosphere. Those associated to MAC systems are divided in two groups: the refrigerant emissions called direct emissions and the CO_2 emissions called indirect emissions.

The indirect emissions are related to the additional CO_2 emissions due to the vehicle engine fuel consumption while the MAC system operates. They result from two mechanisms: first, by the direct transfer of the mechanical power to the compressor and the increase of vehicle weight and, second, the electrical power used by the fans, blowers, actuators and the control system. The Total Equivalent Warming Impact (TEWI) and the Life Cycle Climate Performance (LCCP) are values used to evaluate these emissions.

1.4.1 Direct emissions

The refrigerant emissions due to MAC systems can occur in three different phases [IPCC06]:

- manufacturing process,
- vehicle lifetime, and
- end-of-life.

At the manufacturing process, refrigerant emissions are usually very low as they result from the charging process. However, at the vehicle end-of-life, emissions depend on the national regulatory policies and on the recovery efficiency. If technicians are not equipped and trained to recover the refrigerant, they will simply vent all the system charge to the atmosphere. The system emissions during the vehicle lifetime are difficult to evaluate as they depend on many issues described hereafter.

The MAC system is permanently pressurized and, in standstill mode, the system emission level is mainly dependent on the refrigerant pressure. The system emissions lead to a progressive reduction of the system refrigerant charge. A computer simulation has been done using REFPROP 7® to calculate the system pressure evolution with the refrigerant charge in standstill mode. Figure 1-11 shows the evolution of pressure and vapor quality with the refrigerant charge for a MAC system with an internal volume of 5.2 liters and an initial charge of 940 g. It can be observed that the system pressure is constant while there is

two-phase equilibrium (vapor quality < 100%). After losing 80% of the charge, there is no more liquid refrigerant in the system and the system pressure drops rapidly.

Unless there is a component failure or an accident, the refrigerant charge will not be lower than 50% since the vehicle owner will recharge it due to the lack of cooled air (see Section 1.4.1.1). Therefore, during the vehicle lifetime, the MAC system refrigerant emissions in standstill mode do not depend on the refrigerant charge. So, as refrigerant is always in the equilibrium phase, the pressure only depends on the temperature of the system coldest point.

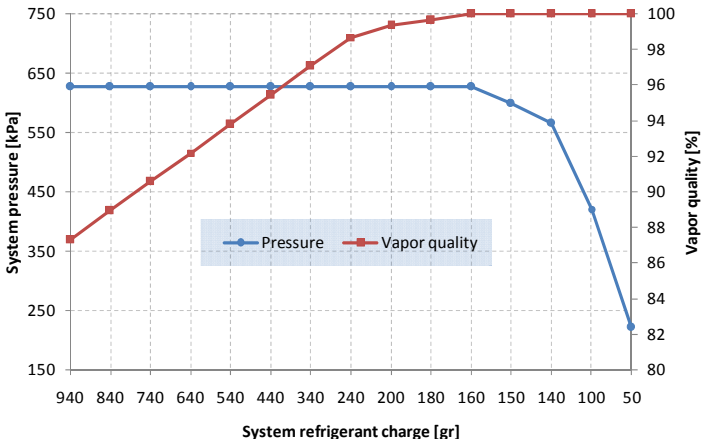

Figure 1-11 System pressure and vapor quality evolution with refrigerant charge at 23°C in standstill mode.

It is more difficult to limit refrigerant emissions during the vehicle lifetime than those emitted during the manufacturing process and at the end-of-life of the refrigerating system. Emissions during the manufacturing process and at end-of-life are only related to the refrigerant charge and recovery process, while those produced during the vehicle lifetime can be divided in:

- regular, and
- irregular.

These different types of MAC refrigerant emissions are discussed hereafter.

1.4.1.1 Regular emissions

Refrigerant leakage is mainly due to a pressure differential between the refrigerant and the atmosphere, separated by a pressure boundary. This pressure boundary can be a seal component or an elastomer hose. The MAC system has an important number of leak sources, see Section 1.2, which are the causes of the refrigerant regular emissions. These emissions depend also on the number of leak points, the leak geometry, the component temperature, and the presence of the compressor lubricating oil in the seal contact.

A leak is defined as a hole or porosity in the wall of an enclosure capable of passing a fluid from one side of the wall to the other. The leakage rate describes the number of molecules leaking per unit of time and is defined both by the leakage rate and the pressure difference across the leak path.

When the refrigeration system is at rest, the refrigerant temperature reaches the equilibrium with the ambient temperature and the system pressure corresponds to the saturating pressure. Figure 1-12a presents the variation of the system pressure with ambient

temperature. Therefore, the system average pressure will be higher in hot climates than in colder ones and, for the same sealing system technology, refrigerant emissions will decrease at lower outdoor temperatures.

When the compressor starts running, a pressure difference is rapidly established: the evaporator pressure (low-pressure side) and the condenser pressure (high-pressure side), see Figure 1-12b. The low-pressure side is relatively stable around 340 kPa and the condenser pressure is strongly dependent on the condenser heat exchange and the outdoor temperature, as well as the air speed. Components bearing the high pressure are parts of the compressor rear block, the discharge hose, the condenser, the receiver, the liquid hose, and partially the expansion valve. The evaporator, the suction hose, and the compressor housing are at the evaporator pressure. Therefore, the compressor housing pressure is generally lower in running mode than at rest.

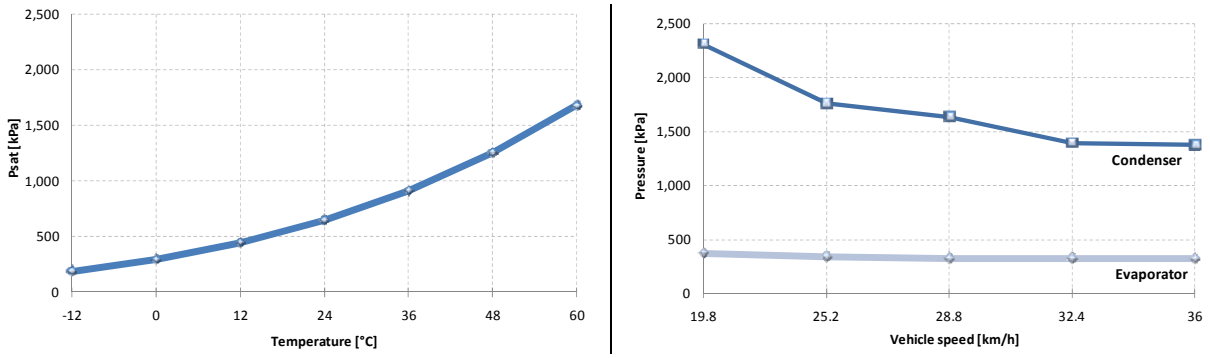

Figure 1-12 MAC system pressure evolution in a) standstill and b) running mode.

Tightness degradation is of major importance to the MAC system regular emissions since it increases refrigerant emissions. Degradation of seals can be caused by their natural ageing or by incorrect servicing procedures.

For static seals, like the o-rings and gaskets, the seal ageing results from the temperature variation in the engine compartment during the year and the switch between running and standstill modes, as well as the pressure cycling and vibrations produced by the compressor and the engine.

For the dynamic seal, the shaft seal, the tightness degradation is related to those factors described for static seals plus the wear of the sealing interface. The shaft seal wear depends on the lubrication during the shaft rotation and, more importantly, when shaft starts running to avoid running under dry conditions, thus increasing the wear rate. This thesis will address this issue in detail in next chapter.

Regular emissions result in a progressive loss of the refrigerant charge. The consequence is the reduction of the system cooling capacity at a given threshold. For a vehicle owner, the single parameter to evaluate the functionality of the refrigerating system is the supply air temperature in the cabin.

A laboratory experiment simulating a slow leak in a steady state regime has been done in order to determine the MAC system performance degradation with the decrease in the system refrigerant charge (see Figure 1-13).

Figure 1-13 shows the evolution of the cabin supplied air temperature with the refrigerant charge variation. When the refrigerant charge is lower than 40 to 50% of the initial charge, the refrigerant mass flow rate delivered by the expansion valve is lower than required and the supply air temperature increases. Therefore, the vehicle owner could not feel significant

changes in the blown air temperature until the system reaches the mid charge and in hot conditions. After that, he will go to a garage to recharge it.

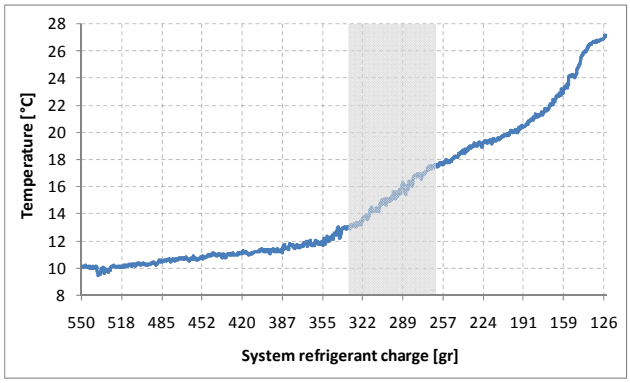

Figure 1-13 Supply air temperature evolution with refrigerant charge in steady state regime.

During the recharge, the potential leak sources occur at the service valves because each time a hose connection is installed or removed, there is a release of refrigerant. This leak is estimated at less than 10 grams. The use of special refrigerant containers, small cans, with emissive valve systems, also contributes to emissions during the system recharge. The refrigerant emissions during service are more pronounced for aged vehicles. As the compressor shaft seal wears out, the refrigerant emissions increase rapidly making the vehicle owner going often to the garage for repair, thus increasing refrigerant emissions during servicing.

1.4.1.2 Irregular emissions

Irregular emissions can take place by seal failures or by accidents. The component failure can generate the complete refrigerant loss of the system. It can be caused by the incorrect design of the sealing system or even by its incorrect installation. The high porosity and cracks of brazed joints, and sealing surfaces with material deposits are characteristic defaults that take place during the manufacturing process of system components, and their levels depend on the quality process. For the compressor shaft seal, an excessive wear of the mating surfaces causes the seal failure. During this study, emissions higher than 1000 g/yr have been measured for aged compressors at rest (see Section 2.8).

Accidents generally affect the integrity of the fittings and components installed in the vehicle front. According to the vehicle impact strength, the MAC system damages can go from the total refrigerant loss in a few seconds to very small perforations in the condenser, which can also be the result of the road or stones impacts. Accidents can lead to a component failure resulting in the release of the total refrigerant charge to the atmosphere.

It is difficult to detect and locate damages caused by the small impacts on the condenser, since the leak points are situated in a vast surface area compared to a component connection. The affordable leak detection tools used by professional technicians are not adapted to detect small leak levels, especially on the shaft seal. The leak detection tools are analyzed in Section 2.6.

The average refrigerant charge of a MAC system depends on the vehicle type. Nowadays, typical values are 500 grams for a single evaporating system and 900 grams for a double evaporating system. If a seal failure of a charged system occurs, the equivalent of 650 kt to 1170 kt of carbon dioxide will be rejected to the atmosphere.

1.4.2 Total direct emissions

In 2003, the total HFC direct emissions have been estimated to 138 kt whereof 85% results from HFC-134a [CLO05]. The two major contributors are the USA with 87 kt and the EU25 with 22 kt, both representing nearly 80% of the total HFC direct emissions.

If only HFCs are considered, the MAC system is the most emissive refrigerating equipment representing 78% of the total emissions followed by stationary refrigerating systems (see Figure 1-1). This fact is related to the rapid switch from CFC-12 to HFC-134a and to the relatively high emission rate of MACs considering all direct emissions.

China has banned the use of CFC-12 in new vehicles as of January 1st, 2002. The same trend has been followed in India where all new MAC systems use HFC-134a.

In order to consider the impact of HFCs in the atmosphere, CO_2 equivalent emissions can be calculated by multiplying HFC emissions by the associated GWP. Values of 115 and 47 million tonnes of CO_2 equivalent emissions are found for USA and EU25 respectively (see Figure 1-14). These high refrigerant emissions and their impact on the environment justify the study of the system sealing mechanism. Next chapter will focus on emissions from the compressor, the most leak prone component, with a specific interest in the shaft seal behavior.

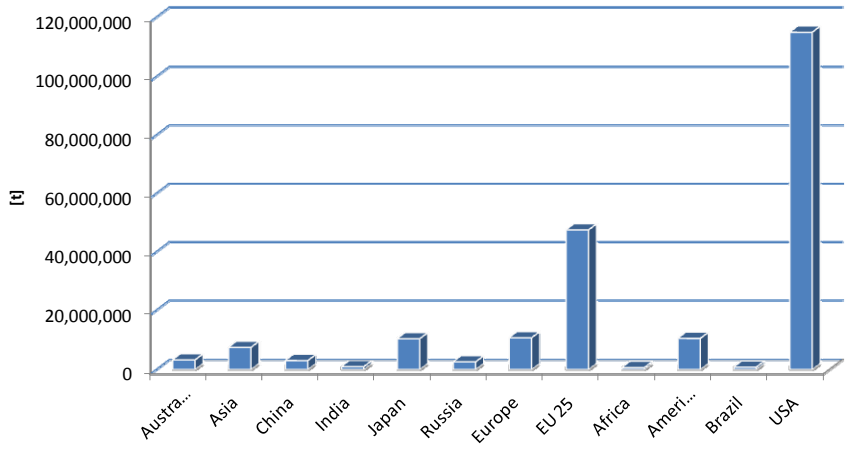

Figure 1-14 Refrigerant CO_2 equivalent emissions in 2003.

1.5. Market evolution

The car industry is the first user of MAC systems. However, the MAC system can also be found in light commercial vehicles, truck cabins, agricultural machines, buses, and coaches.

The worldwide production of motor vehicles in 2006 was 69.2 million units. In 2000, in Europe, 85% of passenger transport was carried by cars, buses and coaches, and 70% of goods were transported by road. The transport activity in EU25 by the horizon of 2000-2020 is expected to growth 55% for road freight transport and 36% for private car transport [ACE07].

Between 2001 and 2006, new car registrations rose 395% in Ukraine and 114% in India. Registration rates higher than 60% can also be found in the Southeast Asian Nations (ASEAN) and in Russia (see Table 1-2). In 2007, 6.2 million passenger vehicles have been

sold in China, around 20% more than in 2006, and only 4% of the population owns a car, compared to 60% in Europe and 80% in America [ECO08].

Safety and thermal comfort of passengers have been considered the most important factors in developing the automobile air conditioning system. The car industry was the first using such a system. In fact, first it has been a large American phenomenon and then in Japan after the '70s. By 1980, more than 80% of American new cars had factory-installed air conditioning system and a large portion of the Asian car industry as well. The number of air-conditioned cars in Europe started to significantly increase in the '90s and it is expected that 9 vehicles in 10 will be air-conditioning equipped by 2010 [BAR03].

The number of automobile air conditioning systems in China has been multiplied by four in seven years (see Figure 1-15) and this market continues to grow. In 2003, the sales of cars in India were 900,000 units and 68% of them were equipped with a MAC system [IPC05].

These facts allow concluding that the automobile air conditioning is a worldwide phenomenon with very high market penetration rates. Therefore, it is essential to study the leak prone component of the MAC system, i.e. the compressor, in order to reduce its emission levels as well as the system direct impact on the environment.

Table 1-2 New car registrations (in thousands) [ACE07].

	2001	2006	Change
South Korea	1468	1218	-17%
ASEAN	1167	1893	62%
India	818	1750	114%
Ukraine	75	371	395%
Russia *(light vehicles)*	1272	2129	67%
MERCOSUR	1778	2389	34%

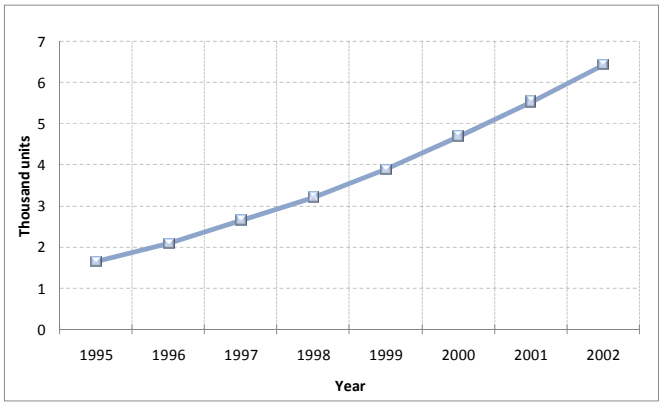

Figure 1-15 Evolution of MACs in buses, trucks, and cars in China (CFC-12 and HFC-134a) [IPC05].

1.6. Leak detection tools

The leak test, usually a non-destructive test, is used for two purposes: the detection and the location of leaks, and the measurement of the fluid flow through a leak, the fluid leakage. The test methods described hereafter are not exhaustive and can only be used to detect and locate component leaks in the field. These test methods have the particularity of using the system operating fluid as the tracer gas: electronic leak detector, soap bubble, and fluorescent leak detector dye.

1.6.1 Electronic leak detectors

The electronic leak detector is a portable equipment used to qualify refrigerant leaks (see Figure 1-16b). There are different leak detector technologies and sensitivities. However, the majority of professional technicians will use inexpensive leak detectors, like the one presented hereafter, which is based on a heated diode technology.

The refrigerant detection is achieved by using a heater and a detector unit (see Figure 1-16a). The detector unit is composed of a cylinder covered externally by a platinum coil and internally by a ceramic layer. The mixture air/refrigerant is sucked from the leak point surroundings, heated, and then reaches the heated detector. If refrigerant concentration is below a certain level, the alkaline atoms from the ceramic layer will naturally travel to the platinum coil. As refrigerant concentration increases, the halogen refrigerant inside the detector ionizes the alkaline atoms and a voltage difference is created between the ceramic layer and the platinum coil. The generated electrical current is proportional to the refrigerant concentration resulting in an audible alarm, which intensifies with refrigerant concentration.

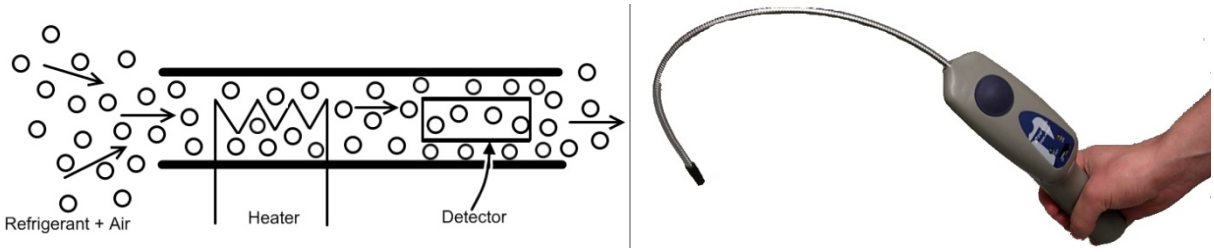

a) *b)*

Figure 1-16 a) Schematic drawing of the heated diode technology; b) electronic leak detector with heated diode technology.

The detector sensitivity is a concentration measure that gives a minimum measurable signal and depends on the minimum gas molecules entering the detector. The operating principle of the heated diode technology implies the degradation of the detector and its consequent replacement.

When the refrigerant passes through a seal, the molecules will diffuse into the atmosphere and, as the distance between the leak point and sniffer increases, the refrigerant concentration decreases rapidly. Therefore, if the sniffer is not close enough to the leak source, the leak will not be detected. Professional technicians must pay attention to the sniffer positioning in order to detect the smallest possible leaks. But, how to detect a compressor shaft seal leak problem? In fact, as the shaft seal is hidden by the clutch assembly, the sniffer will always stay too far away from the leak point, thus making impossible to detect the leak of the shaft seal except large leak (> 50 g/yr). The only way is to disassemble in order to have direct access to the seal, which is never done in the field. Therefore, it can be concluded that the electronic leak detectors are not adapted to leak check the compressor shaft seal.

1.6.2 Soap bubble testing

The soap bubble testing is a wet testing method, which consists in the observation of a pressurized component that has been sprayed or brushed with a soap solution. If the pressure at the end of the leak path is enough to overcome the surface tension forces, then bubbles will be formed and the amount of bubbles per minute can signify the size of the leak.

The bubble size is crucial to the leak detection. Different MAC system component connections can be leak tested using the refrigerant accumulation method. However, this test method is not adapted to the shaft seal because it is hidden by the pulley. Bubbles are visible only for leak rates higher than 120 g/yr. On a connection presenting a leak rate of 120 g/yr, bubble sizes are very small and almost impossible to visualize in the engine compartment environment (see Figure 1-17).

The soap bubble testing is not expensive, but has a very low sensitivity and is not adapted to leak check the shaft seal.

a) *b)*

Figure 1-17 Bubbles formation for an overall leak of; a) 120 g/yr; b) 1,200 g/yr.

1.6.3 Fluorescent leak detector dye

Another leak test method consists in introducing a colored fluid in the MAC system, which is carried by the compressor lubricating oil. When the compressor is running, the lubricating oil travels around the system producing an oil layer around the internal walls. When the oil finds a gap, it will flow through it and reach the exterior. Afterward, an UV blue light is turned to the leaky component and is absorbed by the dye which will emit a visible yellow/green light (see Figure 1-18a).

The dye visualization time mainly depends on the gap dimensions. Table 1-3 summarizes test results for different leak rates using a fluorescent leak detector. The LFR presented in Table 1-3 was calculated with a dry seal contact.

The fluorescent leak detector dye is used by a large number of auto technicians. The dye visualization time increases exponentially with the LFR decrease. It is expected that for low leak rates the oil cannot penetrate the gap and the detection will not be possible.

Table 1-3 Fluorescent leak visualization time.

LFR [g/yr]	662,000	1,490	515	300	7.2	0.28
Visualization time [hr]	0.8	3	11	*	**	**

* No evidence of dye after 14 days of test ** no evidence of dye after 20 days of test

Another drawback of this test method is that if too much dye is added to the circuit, the oil viscosity changes and this can adversely affect the compressor life. Disassembled compressors from used cars have shown a glowed yellow/green color even without a UV light, due to the excess of dye (see Figure 1-18c).

Similarly to the electronic leak detector and the soap bubble, the fluorescent leak detector dye is not adapted to leak check the compressor shaft seal since the dye will be hidden by

the clutch assembly. The dye will be visible only if the oil flow through the shaft is very important to reach the clutch.

a) *b)* *c)*

Figure 1-18 a) Tracer dye visualization; b) New PAG oil; c) Excess of dye in the PAG oil from a used car.

Three different leak test methods used by professional technicians have been presented: electronic leak detector, soap bubble, and fluorescent leak detector dye. It was observed that none of them is adapted to leak check the shaft seal since it is hidden by the clutch assembly. Therefore, leaky compressors are not replaced increasing not only the system emissions but also the number of system recharges with the additional emissions during servicing.

1.7. Policies to control MAC refrigerant emissions

The fluorinated greenhouse gas (F-gas) HFC-134a is included in the basket of gases whose emissions are controlled by the Kyoto Protocol, which was ratified by the European Union (EU) in May 2002. The EU is taking measures to reduce F-gas emissions by 8% from 1990 levels during the period 2008-2012.

The EU has identified the MAC system as one of the major sources of HFC emissions and decided to prohibit the homologation of MAC systems filled with a refrigerant gas with a GWP higher than 150 from January 1st, 2011. From January 1st, 2017, vehicles equipped with a MAC system using an F-gas with a GWP higher than 150 ($GWP_{HFC\text{-}134a}$ = 1300) cannot be sold on the European market. The recharging process of HFC-134a systems will be authorized after that date. Between 2011 and 2017, only MAC systems homologated before 2011 will be filled with HFC-134a [DIR06].

The EU Commission Regulation 706/2007 identifies the components to be leak tested, as well as the leak test method and conditions to determine the system or component leak flow rates. The test method chosen was the refrigerant accumulation method described in Section 1.10.1. The leak test starts with the system pre-conditioning followed by the refrigerant concentration measurement during 24 hours. The calculated leak flow rate is then multiplied by a correlation factor of 0.277. The correlation factor is based on the results of fleet tests of 40 European vehicles [CLO07].

The EU Directive 2006/40/EC also establishes a limit to the leak rate of MAC systems. Nowadays, refrigerating systems filled with a refrigerant whose GWP is higher than 150 are approved if the refrigerant leak flow rate value is smaller than 40 g/yr for systems with a single evaporator or 60 g/yr for double evaporator systems.

The phasing out of HFC-134a from MAC systems is only effective in Europe. Therefore, the use of the HFC-134a as an automotive refrigerant is expected to continue outside Europe.

1.8. Design of new MAC systems

MAC systems have significantly improved since the first comfort cooling system was installed in 1990 [IPC05]. MAC system installations have been progressively improved based on three design criteria: thermal comfort improvements, lower fuel consumption, and refrigerant emissions reduction.

In terms of direct emissions, there are two ways to limit the impact of refrigerant emissions on the atmosphere:

- improve the leak tightness of actual systems and refrigerant recovery at end-of-life or
- replace HFC-134a by a low GWP refrigerant.

The system tightness is directly related to its leak prone component, the compressor. More particularly, the shaft seal, as it will be demonstrated in Chapter 3.

The European HFC-134a phasing-out is accelerating the development of MAC systems with low GWP refrigerants. One of the possible candidates is carbon dioxide (R-744) with a GWP of 1, which is negligible compared to HFC-134a. R-744 is a refrigerant whose properties are very well known and documented, but the system pressure is 10 times higher than that of HFC-134a systems representing a technological challenge to maintain the system leak tightness.

New refrigerant R-1234yf with a GWP of 4 is also under development. It presents a system pressure similar to the HFC-134a, but it is not yet in mass production. Regardless of the refrigerant chosen, the system refrigerant tightness will be fundamental to maintain the initial system performance during the vehicle lifetime.

The development of hybrid vehicles gives the possibility to use hermetic electric compressors and, so, to decouple the MAC system from the engine. The market of electrical vehicles is still irrelevant, but the use of electrical compressors will facilitate considerably the refrigerant containment.

1.9. Conclusions

The MAC system is a permanent pressurized equipment that continuously releases refrigerant to the atmosphere. This release is mainly due to the use of an open-type compressor responsible for 50 to 60% of the system emissions. It has been noticed that HFC-134a atmospheric concentration has been multiplied by 23 in 12 years and these refrigerant emissions are essentially due to MAC systems.

Emission rates at rest define the system leak flow rate because the compressor will run 2 to 5% during the vehicle lifetime in Europe. The refrigerant pressure at rest depends on the ambient temperature, so refrigerant emissions will decrease at lower ambient temperatures and vice-versa. Nevertheless, the component ageing due to the running mode is critical to the compressor dynamic seal degradation.

Several field leak test methods used by car technicians have been compared and it was noticed that they are not adapted to leak check the compressor shaft seal nor sufficiently sensitive to leak test other components. Therefore, leaky compressors are not replaced increasing not only the system emissions, but also the number of system recharges with the additional emissions during servicing. The impossibility to detect relatively small leak rates of the shaft seal gives more importance to the study of the seal degradation due to wear.

In the last decades, there have been significant advances in MAC systems. However, most of the research work has been focused to improve the hose permeation and the fittings. There has been little published work on the compressor refrigerant emissions, particularly, the shaft seal.

The control of MAC system refrigerant emissions is essential to reduce its environmental impact. The EU is phasing-out HFC-134a in the automobile industry. This decision is speeding up the development of new MAC systems with low GWP refrigerants. For R-744 with a GWP of 1 but with a system pressure 10 times higher than that of HFC-134a systems, leak tightness is a challenge and especially for the compressor shaft seal. New blend refrigerants are also under development with saturating pressure in the same range as R-134a.

Regardless of the system refrigerant, the system tightness is fundamental to maintain the initial system performance during the vehicle lifetime and to avoid refrigerant recharging. This work aims at studying the refrigerant emissions of the most leak prone component, the compressor, and more particularly the compressor shaft seal.

Next chapter will detail the compressor emissions in standstill and running modes. The compressor ageing due to the running mode will also be analyzed.

1.10. References

[ACE07] European Automobile Manufacturers Association (ACEA), 2007. European automobile industry report 07/08.

[AFE06] Alternative Fluorocarbons Environmental Acceptability Study (AFEAS), 2006. Contribution of Greenhouse Gases to Climate Forcing Relative to CO_2. www.afeas.org/greenhouse_gases.html.

[AGA08] Advanced Global Atmospheric Gases Experiment (AGAGE). *http://agage.eas.gatech.edu/data.htm*.

[BAR03] Barbusse, S., Gagnepain, L., 2003. La climatisation automobile: impact énergétique et environnemental. ADEME, ref. 4343.

[CLO05] Clodic, D., Palandre, L., Saba, S., 2005. Inventories of the Woldwide Fleets of Refrigerant and Air-Conditioning Equipment in Order to Determine Refrigerant Emissions. ADEME/ARMINES.

[CLO06] Clodic, D, Yu, Y, 2006. Research study on the definition of the implementation of a method of measurement of annual leak rates (LFRs) of MAC systems.

[CLO07] Clodic, D., Yu, Y., 2007. Elaboration of a correlation factor based on the fleet tests and Mobile Air Conditioning (MAC) system laboratory tests. SAE technical paper 2007-01-1187.

[CLO96] Clodic, D., 1996. Zero leaks-Limiting emissions of refrigerants. Ashrae. 189 p.

[DIR06] Directive 2006/40/EC. Emissions from air-conditioning systems in motor vehicles. Official Journal of the European Union, June 14, L161-12.

[ECO08] The Economist, 2008. April 26, pp. 73.

[FRO06] Frost & Sullivan, 2006. U.S. Consumer Buying Behaviors of R-134a Refrigerant for Light Vehicle Applications. Automotive Refrigeration Products Institute (ARPI).

[IPC05] Intergovernmental Panel on Climate Change (IPCC), 2005. Safeguarding the Ozone Layer and the Global Climate System: Issues related to hydrofluorocarbons and perfluorocarbons. pp. 295-314.

[JOH04] John, R., Valerie, H., Stephen, A., 2004. Significant Fuel Savings and Emissions Reductions by Improuving Vehicle Air Conditioning. Proceedings of the 15th Annual Earth Technology Forum and Mobile Air Conditioning Summit, Washington, D.C., April 13-15.

[KHO05] Khoury, G., Clodic, D., 2005. Method of Test and Measurements of Fuel Consumption Due to Air Conditioning Operation on the New Prius II Hybride Vehicle. SAE technical paper 2005-01-2049.

[MOR98] Moran, M. J., Shapiro, H. N., 1998. Fundamentals of Engineering Thermodynamics. John Wiley & Sons.

[PAL03] Palandre, L., Zoughaib, A., Clodic, D., Kuijpers, L., 2003. Estimation of the World-Wide Fleets of Refrigerant and Air-Conditioning Equipment in Order to Determine Forecasts of Refrigerant Emissions. The Earth Technology Forum,

Washington, April.

[WOR02] World Banc, 2002. Production sector presentation. The 19th Ozone Operations Resources Group (OORG), Washington, D.C., March 28.

Chapter 2

COMPRESSOR REFRIGERANT EMISSIONS

Introduction

In this second chapter, gas emissions of new and aged compressors are studied. The chapter begins with the description of the compressor components, its compressor technology and its sealing system.

It goes on with the presentation of an original experimental setup developed to measure gas emissions when the compressor is at rest as well as when its shaft is rotating. Section eight includes the leak test results of new and aged compressors followed by the study of the lubricant oil effect on the shaft seal tightness.

In Section 10, the compressor aging process is investigated by performing endurance tests and analyzing gas emissions changes along the aging process.

A new experimental setup is presented in Section 11 to study the shaft seal emissions directly from the compressor. The shaft seal contribution to the compressor gas emissions is also calculated.

Finally, effects of shaft surface wear in the sealing region as well as of oil leakage resulting from the aging process are pointed out.

2. Compressor refrigerant emissions

The compressor is the most important component of the MAC system because it makes the system running. As shown in the previous chapter, the compressor is the most leak prone component of the refrigerating system, representing in between 50 and 60% of the system refrigerant emissions. Therefore, the understanding of its refrigerant emissions is vital to reduce the system direct impact on global warming.

The literature regarding the MAC compressor is not abundant, even less for its sealing system. This may be due to the fact that this is a technological and production oriented field and very much influenced by the market competition. The compressor market reached about 60 million in 2005; it is shared by several MAC system manufacturers. Sales of the world largest provider of MAC compressors were set to 20.45 million units in 2007, which represented an increase of 6% compared to the previous year [TOY07].

The compressor is an aluminum structure usually composed of three different housings that are assembled and enclose the compression system (see Figure 2-1a). The assembly of the compressor different parts (rear housing, valve plate, oil plug, middle housing, front housing and shaft) introduces seals that are responsible for the compressor gas emissions. The number of parts to be sealed differs depending on the manufacturer and compression mechanism affecting the number of static seals. The dynamic seal, the shaft seal, is always a single one in an open-type compressor.

The compressor is activated by the vehicle engine by means of a belt-pulley driven mechanism. Usually, a clutch is added to the compressor pulley to control the compressor working mode (see Figure 2-1b). When only the pulley/bearing assembly is used, the compressor is designated as clutchless and runs continuously with the vehicle engine.

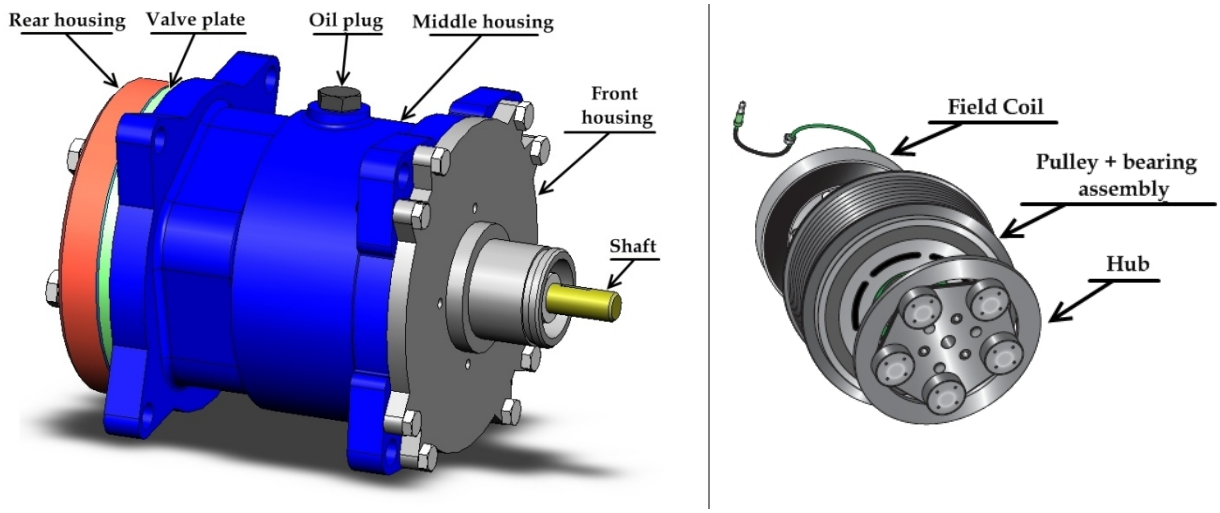

a) Compressor body

b) Clutch assembly

Figure 2-1 The MAC compressor main parts.

2.1. The compression mechanism

MAC compressors are designated according to their compression mechanism. In terms of refrigerant emissions, the compression mechanism is important because it will define the fluid pressure acting on the seals as well as the number of seals used.

In the history of MAC systems, various types of compressors were used. Nowadays, there are three different types of compressors in use: rotary vane, scroll, and reciprocating.

2.1.1 Rotary vane compressor

The rotary vane compressor consists of a rotor with vanes mounted eccentrically in a case placed in the middle housing (see Figure 2-2a). As the compressor is operating, the refrigerant inside the chambers formed in between the vanes is compressed as the chamber volume decreases. This compressor type is used on small vehicles and is characterized by smooth operation.

2.1.2 Scroll compressor

The scroll mechanism, also called spiral or orbital, is composed of a fixed and an orbiting scroll (see Figure 2-2b). The orbiting scroll is attached to the driveshaft in an eccentric position and circles around the fixed scroll with an orbital path. The refrigerant at the scroll enters at the periphery and is compressed as it reaches the scroll center. The displacement volume of a scroll compressor varies from 50 cc to 120 cc according to the spiral dimensions.

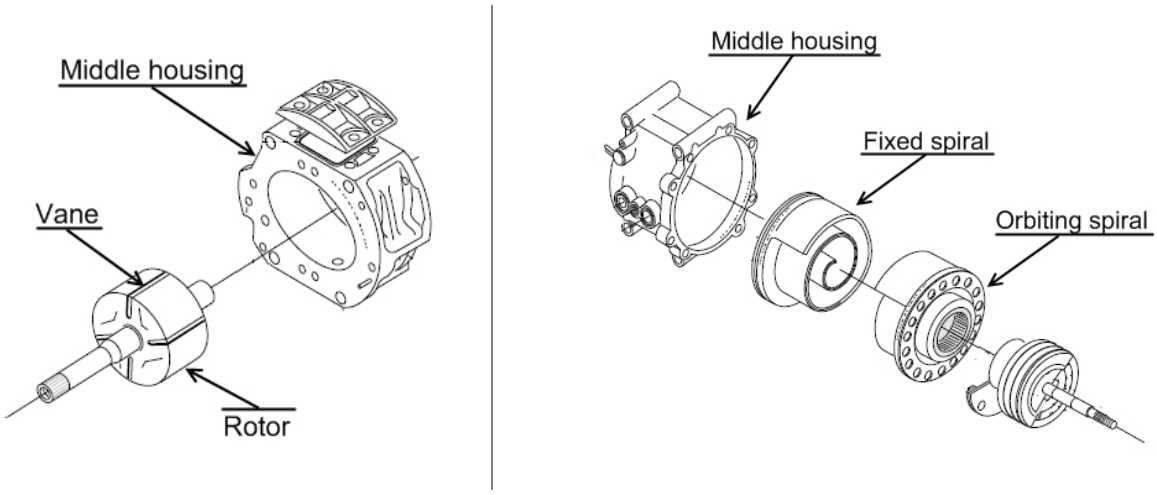

Figure 2-2 a) Rotary vane mechanisms b) Scroll compression mechanisms.

2.1.3 Piston compressor

The reciprocating type is an axial compressor with pistons arranged around a planetary base and parallel to the driveshaft (see Figure 2-3). The displacement volume of a piston compressor is higher than scroll and rotary vane technology and varies from 100 cc to 180 cc.

Depending on the design, the pistons can be driven by a wobble plate or a swash plate. In the wobble plate mechanism (see Figure 2-3a), a wobble plate with a fixed angle is placed on the driveshaft and makes the planetary base wobble, when the shaft rotates, driving the pistons back and forth in their bores. In a swash plate compressor (see Figure 2-3b), the plate rotates itself with the driveshaft. The swash plate is set at an angle to the shaft, so as when it rotates, the pistons are forced back and forth in their bores.

One-way reed valves are placed in a valve plate located between the rear and the middle housings to control refrigerant flow into and out of each cylinder. The discharged refrigerant flow is constant and depends on the number of pistons, its stroke and diameter. The cooling capacity can be adjusted only by on/off cycling of the compressor.

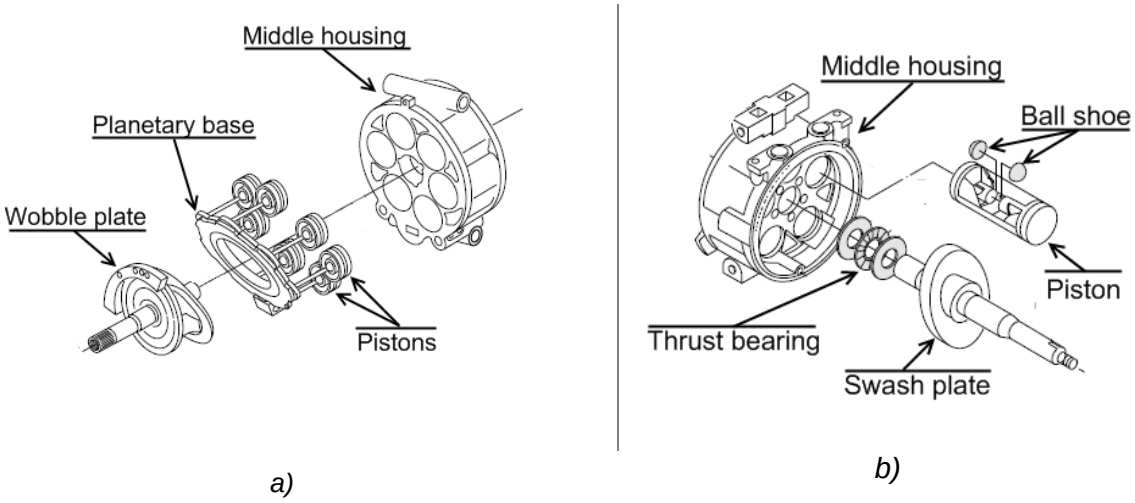

Figure 2-3 Piston type compression mechanism; a) wobble plate; b) swash plate.

In the 80s, a new piston type compressor was introduced, the variable displacement compressor (see Figure 2-4). It is called variable displacement because it has a variable wobble plate angle that changes the piston stroke length and, therefore, the discharge refrigerant flow. This mechanism controls the compressor capacity and is capable to match the cooling demand without compressor cycling.

The wobble plate angle is adjusted by changing the housing pressure. When the housing pressure increases, the pressure exerted on the back side of the pistons keeps them close to the cylinder head, reducing the stroke and the displacement volume. When the housing pressure is reduced, a return spring pushes the wobble plate linkage away increasing the plate angle as well as the piston displacements.

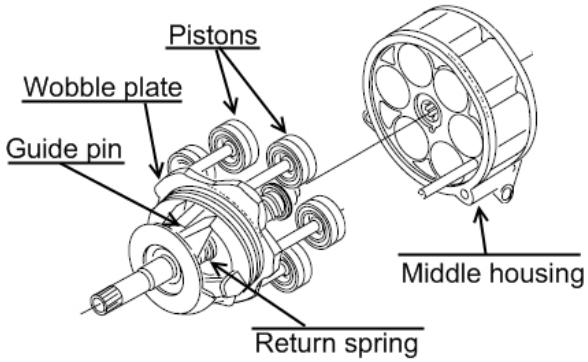

Figure 2-4 Variable displacement compression mechanism.

The housing pressure is adjusted using a control valve with ports and passages that link the suction, discharge, and housing chambers. There are two different types of control valves: mechanical and solenoid (see Figure 2-5).

The mechanical valve (see Figure 2-5a) has a pressure sensitive diaphragm that controls the housing pressure according to the suction pressure level. When evaporator temperature increases (low cooling capacity), the suction pressure increases too. This pushes on the diaphragm, opening a port that vents a small quantity of refrigerant at the housing pressure to

the suction side. As the evaporator temperature decreases, so does the suction pressure. The diaphragm closes the low-side port and, at the same time, opens a port that admits high-side pressure refrigerant into the housing. By increasing the housing pressure, the piston stroke is reduced as well as the refrigerant flow. A compressor equipped with a mechanical valve is considered to have an internal control.

In a solenoid valve (see Figure 2-5b), the diaphragm has been replaced by a coil that produces a controlled magnetic field, which adjusts the opening of venting ports and so the housing pressure. This new configuration allows the MAC system control unit varying the compression volume to match the appropriate evaporator temperature. A pulse width modulated (PWM) signal is given by the control unit to the solenoid valve considering different parameters: passenger selected temperature, cabin temperature and humidity, sun intensity, outdoor temperature, and evaporator and engine coolant temperature. This external control valve represents a great improvement in terms of passenger comfort and fuel savings.

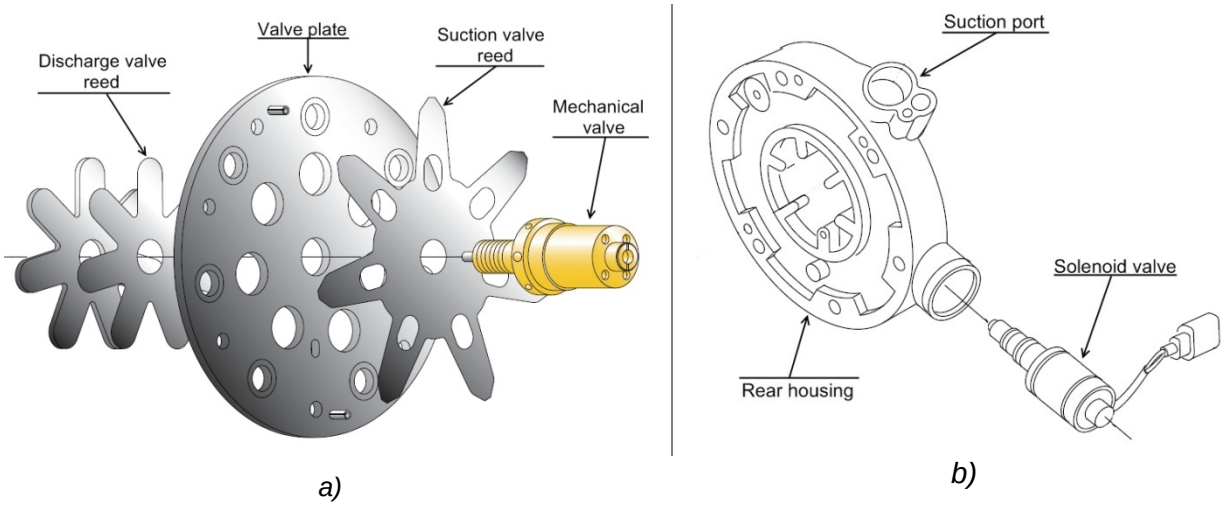

Figure 2-5 Two control valve types for a variable displacement compressor; a) mechanical; b) solenoid.

The variable displacement mechanism changes the compressor displacement volume from 5% to 100%. The variable displacement compressor is the most used technology in new MAC systems; it represented 50% of Denso compressors sales (10 million units) in 2007, an increase of 4-million units from the previous year [TOY07].

In this work, only piston compressors with a variable displacement mechanism are used as it is the most widespread technology.

2.2. Compressor lubrication

The relative motion between the compressor mated parts generates heat and wear from friction. A lubricant is necessary not only to reduce friction, but also to enhance heat dissipation and to allow the compressor working correctly. The lubricant used with HFC-134a in MAC systems is a synthetic lubricant, the Polyalkyl Glycol, generally referred as PAG oil. The lubricant and refrigerant properties are presented in Table 2-1.

The sensitive parts to be lubricated in a piston type compressor are:

- Piston rings (cylinder walls),
- Wobble plate mechanism, and
- Shaft seal

Table 2-1 Properties of 46 ISO VG Polyalkyl Glycol and HFC-134a.

	Lubricant oil	**Refrigerant**
Molar mass (g.mol^{-1})	1550	102.03
Viscosity (µPa.s)	45375.6 (@40°C) 9237 (@100°C)	10.73 (@0°C) 12.37 (@40°C)
Density	975.4 kg.m^{-3} (@15.6°C)	1293.7 **(**kg.m^{-3}) (@0°C) 1146.5 **(**kg.m^{-3}) (@40°C)
Specific gravity	0.978	1.23

The oil film on the cylinder wall is subjected to low temperatures at the suction port and to high temperatures at the discharge port. Both are situated in the cylinder head. Since the oil viscosity decreases with temperature, the oil near the suction port will have a higher viscosity than the oil near the discharge port. Nevertheless, the oil must be rapidly distributed around the pistons as they move back and forth. A high viscosity level will slow the oil distribution inside the housing, thus reducing the lubrication ability.

The PAG oil is highly miscible with HFC-134a to facilitate oil return to the compressor. Due to clearances between the piston and the bore, a small quantity of oil charged is discharged with the refrigerant and circulates throughout the system and returns to the compressor. Some compressor models are equipped with oil separators integrated in the discharge port to separate the oil from the refrigerant, reducing the amount of lubricant that leaves the compressor via the discharge line.

The compressor lubrication system is based on two principles. First, as the oil is miscible with the refrigerant, it circulates inside the housing due to the high gas velocity that provides the force necessary to move the fluid. Secondly, the lubricant collected at the bottom of the housing is drawn up and splashed within the housing by the moving parts, and then circulates to reach the contact between the moving components. This is designated as the splash lubrication method.

For a piston type compressor, the splash effect is achieved by the sliding movement of the swash plate and the pistons (see Figure 2-6). Generally, there is an oil delivery channel to allow the lubricant oil reaching the shaft seal.

However, when the splash lubrication is used, a sufficient amount of lubricant cannot be supplied to some unexposed sliding components within the housing. The lack of lubrication of the shaft seal is more pronounced with the decrease of the wobble plate angle. When the shaft is rotating and the wobble plate angle comes near to 90° relatively to the drive shaft, the pistons and the wobble plate movement decrease. This reduces the oil circulation inside the compressor housing and can increase the wear of those components which are not directly exposed to the oil flow, such as the shaft seal.

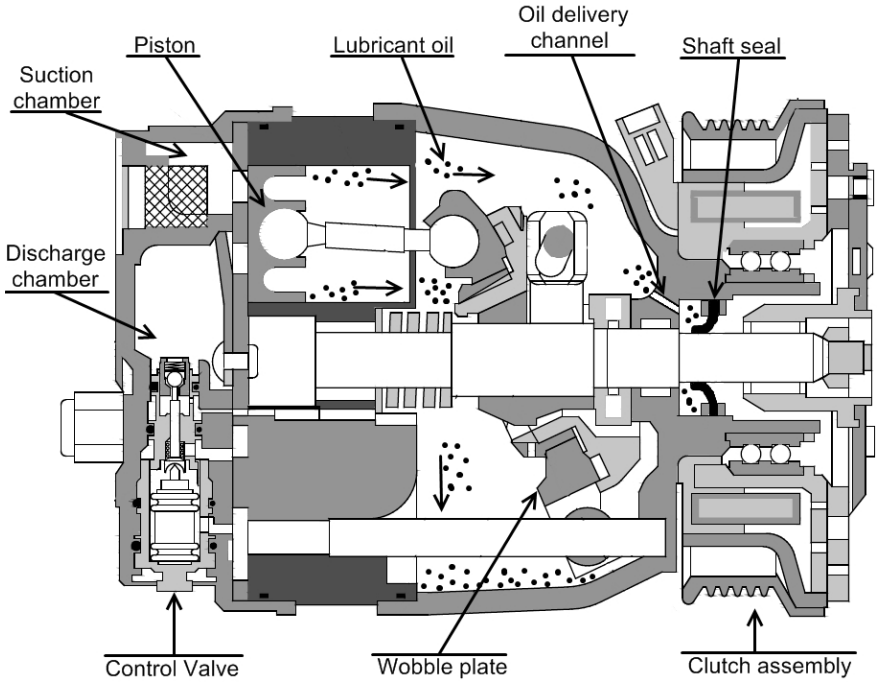

Figure 2-6 Lay-out of the lubrication flow circuit for a variable displacement piston type compressor.

The compressor is charged with oil before being installed in the vehicle. Oil quantity varies according to the compressor displacement range and is indicated by its manufacturer. However, a small portion of oil circulates with the refrigerant flow through the components of the MAC system. The oil return is not always sufficient to maintain a correct lubrication, especially during transient conditions, such as start up and clutch cycling.

The amount of oil carried over with the refrigerant through the vapor compression cycle is referred to as the oil circulation ratio (OCR) and defined in Equation 2.1:

$$OCR\ [wt.\%] = \frac{\dot{m_{oil}}}{\dot{m}_{HFC}+\dot{m}_{oil}} \times 100 \qquad (2.1)$$

Where $\dot{m_{oil}}$ and $\dot{m_{HFC}}$ are the oil and refrigerant mass flow rates respectively.

The OCR is a crucial factor affecting the shaft seal performance. If the OCR of the flowing refrigerant / oil mixture increases, the amount of oil available to lubricate the compressor is reduced, affecting not only the compressor reliability, but also the system performance by reducing the heat transfer in the two heat exchangers. Figure 2-7 shows the OCR variation as a function of time in the system liquid line after the clutch engagement [WAN98]. Oil concentration measurement was carried out using an optical oil concentration sensor based on the oil / refrigerant mixture refraction variation with the oil concentration. These tests have been performed at constant speed, using an electronic expansion valve with different opening values (20, 30, and 35%) and an orifice tube.

An OCR peak value is observed 10 s after the clutch engagement, which corresponds to the oil travelling time between the compressor and the oil concentration sensor placed in the liquid line. After that, the OCR decreases and reaches a steady state-regime with a value of 4%. The same experiment performed under clutch-cycling conditions confirms this behavior. This result indicates that an important oil quantity flows out the compressor during the start-up and this can make the shaft seal lubricating oil film breakdown for a short period of time after a clutch engagement, thus reducing its sealing performance.

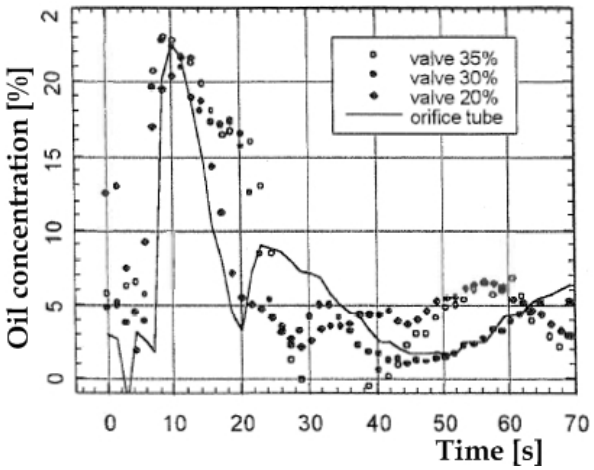

Figure 2-7 Evolution of oil concentration in the liquid line during compressor start-up [WAN98].

The work will be focused on the shaft seal lubrication, since it is a dynamic seal that needs a lubricant oil film between the mating surfaces to work correctly, this means, to contain the refrigerant and the lubricating oil.

2.3. The sealing system

The compressor body is leak tight using different contact seals. These seals are the potential sources of refrigerant leaks. Figure 2-8 shows the exploded view of a piston type compressor with a variable displacement mechanism where we can distinguish different sealing elements used to restrict leakage between the housing and the atmosphere.

In this example, five o-rings are integrated in the control valve, the pressure relief valve and the middle housing. Three fiber gasket seals are installed between the valve plate assembly and the housing, and eight metallic gaskets are used with the oil plug and the housing bolts. The shaft seal is located in the front housing. Accordingly, seventeen sealing elements can be found in this compressor model. This large number of seals explains partially the high compressor gas emission rates. As it will be shown during this work, the issue of compressor emissions is explained by the unsatisfactory performance of the seal placed around the shaft, the shaft seal.

Gasket and o-ring seals are considered as stationary or static seals since there is no relative sliding motion between the mating surfaces. The shaft seal is generally defined as a dynamic seal since there is a relative sliding motion between the shaft surface and the seal. However, the compressor is a permanent pressurized component (Section 1.9) and when the drive shaft is not rotating the shaft seal becomes also a static seal. The shaft seal dual sealing mechanism makes it a very complex and leaky component.

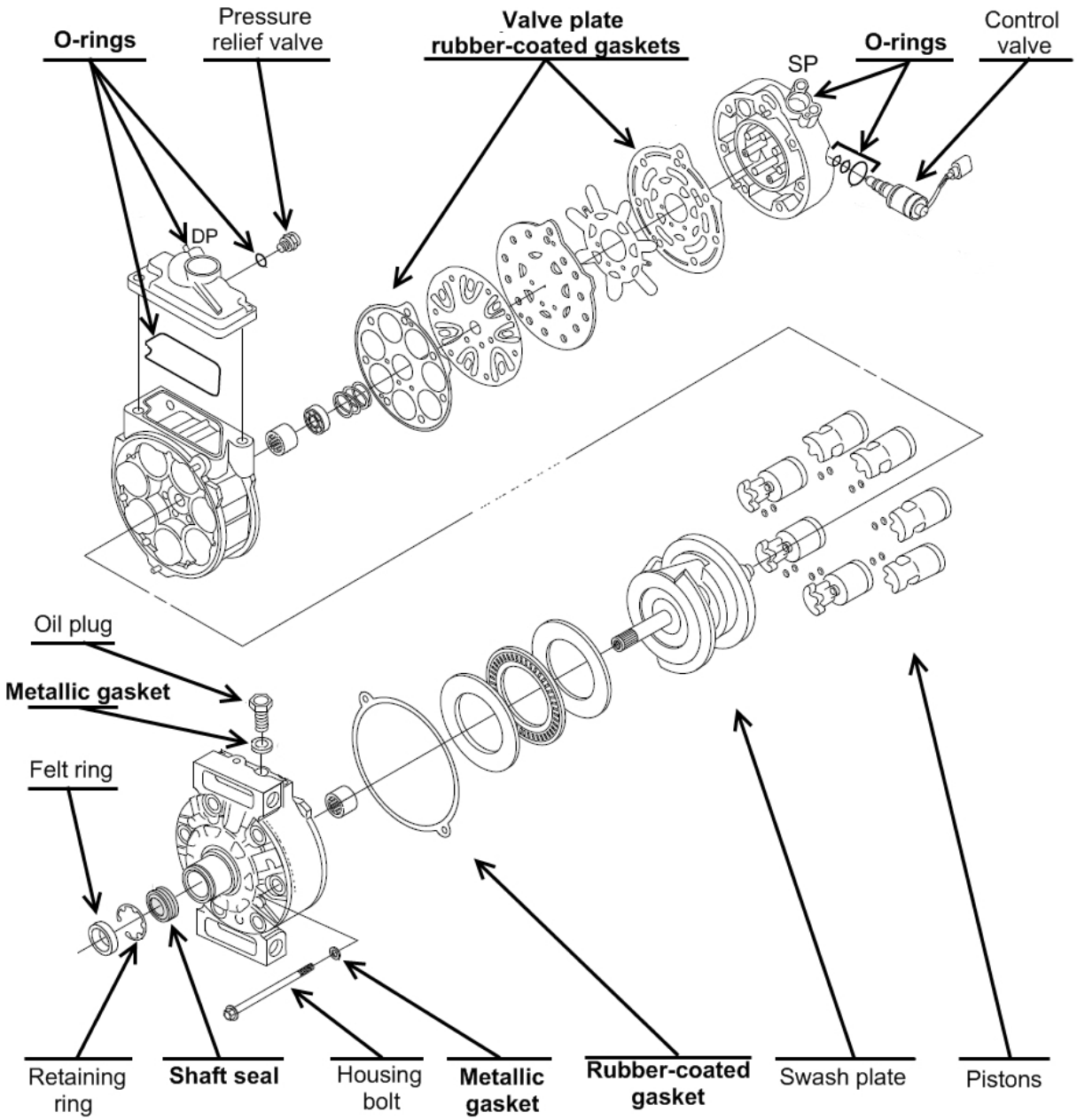

Figure 2-8 Exploded view of a variable displacement compressor with its sealing elements. *DP-discharge port; SP-suction port.*

2.3.1 Static seals

Two metallic parts with good surface finishing joined together will produce a very narrow gap (or channels) in the interface. To close these channels, a third soft material is interposed between the two metallic surfaces that fills up the small surface irregularities, the seal.

An O-ring seal is a rubber circular torus usually used with the control valve and the suction and discharge ports. The inner diameter of an o-ring is smaller than the groove depth. The difference between these two diameters is called interference. After the installation and before pressurization, the contacting surfaces create an interference contact stress. During the compressor pressurization, the fluid pressure will act on the exposed seal surface, so that the contact stress on the three contacting surfaces is increased (see Figure 2-9). Therefore,

the resultant maximum contact stress σ_{max} will be higher than the fluid pressure *p* and will maintain a permanent contact between the mating surfaces. To simplify the illustration, the contact stress is represented only on one contact surface.

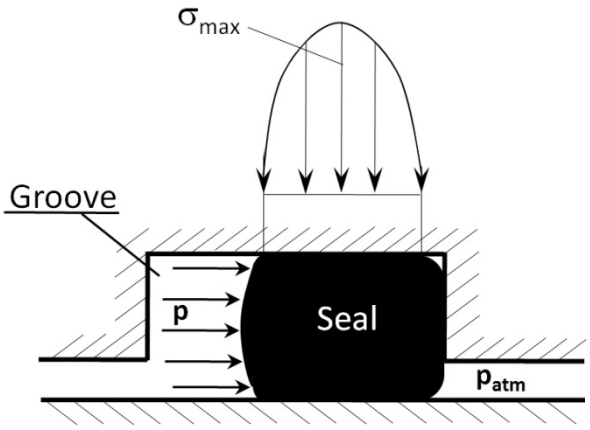

Figure 2-9 Maximum sealing contact stress σ_{max} for an o-ring with fluid pressure *p.*

There are two types of gaskets in the compressor body: metallic and semi-metallic. The metallic gaskets are realized from a single metal sheet and installed with the housing bolts and the oil plug. The semi-metallic gaskets are formed by a thin metal sheet covered with an elastic coating, e.g. nitrile butadiene rubber (NBR). The rubber-coated gaskets are used between the front and the middle housings, and between the valve plate assembly and the rear and middle housings.

During the compressor operation, the valve plate gaskets have a double effect. First, they contain the refrigerant from leaking to the atmosphere and, secondly, they avoid the communication between the suction and discharge refrigerant chambers placed in the rear housing (internal leakage).

Metallic gaskets are used with the housing bolts and require a high contact pressure to be deformed plastically and fill the surfaces irregularities. The metallic seal hardness is lower than the surfaces to be sealed.

2.3.2 Shaft seal

The MAC compressor shaft seal has a unique design. It is a very complex component not only in terms of design, but also by its sealing mechanism, compared to o-rings. The shaft seal has been developed to limit refrigerant and lubricant oil leakages during running and standstill modes. The shaft seal dimensions are typically 14.2 mm for the inner diameter of lips (ID) and 22 mm for the seal outer diameter (OD). This design derives from the oil seals.

A lip type seal is generally composed of four main parts (see Figure 2-10). A rubber lip ring *1* at the high-pressure side, a plastic lip ring *2* at the low-pressure side and peripheral rides *3*, which contact the seal housing surface *8.* They are put all together in a rigid case *6* and *4* to rigidify the assemblage. The rubber lip is bonded to the rigid case and contacts both the shaft and the seal housing surfaces. Both lip rings are in permanent contact with the shaft surface.

The rubber lip *1* has a sharp edge to increase the contact stress on the shaft surface preventing leakage when the shaft is stationary. The rubber ring is made of a synthetic rubber, the hydrogenated nitrile butadiene rubber (HNBR), which is characterized by large strains (typically 90 to 550%) under stress.

The plastic lip ring *2* is made of polytetrafluoroethylene (PTFE). It is typically 1-mm thick and contacts axially the shaft surface over 0.5 to 1 mm when unpressurized. When the shaft rotates, the fluid leaks to the plastic lip ring lubricating the contact and creating a lubricating film in the interface that seals the fluid.

The rubber support ring *5* is used in some seal designs. Its main function is to limit the rubber lip ring deformation with the increase of fluid pressure. Therefore, in stationary mode, the rubber lip will keep a line contact with the shaft surface and, in running mode, the PTFE lip will not be pressed with excessive force against the shaft. This seal design is normally used with variable displacement compressors that generate, for low compression rates, higher fluid pressures than a fixed displacement mechanism.

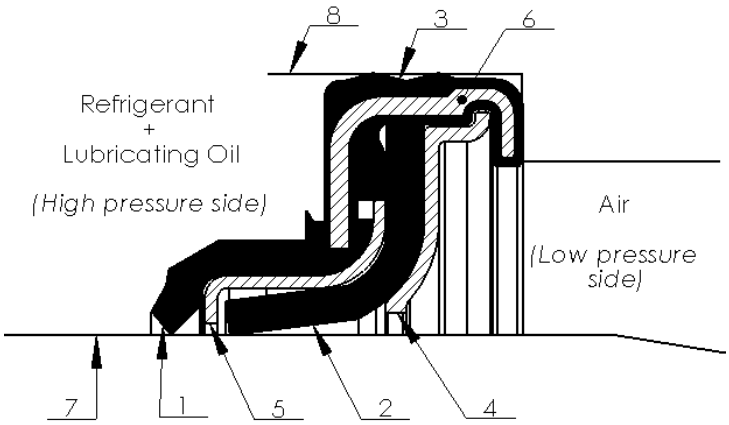

1) Rubber lip ring; 2) PTFE lip ring; 3) Peripheral rides; 4) Backup ring; 5) Rubber support ring; 6) Rigid case; 7) Shaft surface; 8) Seal housing surface

Figure 2-10 Sectional view of a compressor shaft seal.

As for the other compressor seals, the shaft seal leak flow rate (LFR) is due to a permanent pressure gradient between the compressor housing and the atmosphere (see Figure 2-11). As mentioned before, the fluid pressure observed when the compressor is stopped is the saturating pressure of the system coldest point, for example 1020 kPa for 40°C. When the compressor is running, the compression ratio defines the suction and discharge pressures. The shaft seal gas flow can be divided in two groups:

- The fluid flow through the interface with the shaft and the housing, and
- The fluid flow due to the polymeric materials permeation

In the first case, the flow must be classified according to the compressor working mode: stationary or running. This suggests the separated study since the physical mechanisms involved differ from one working mode to the other. In the second case, the gas flow results from the mass transport phenomena. These different sealing mechanisms are presented in more detail hereafter.

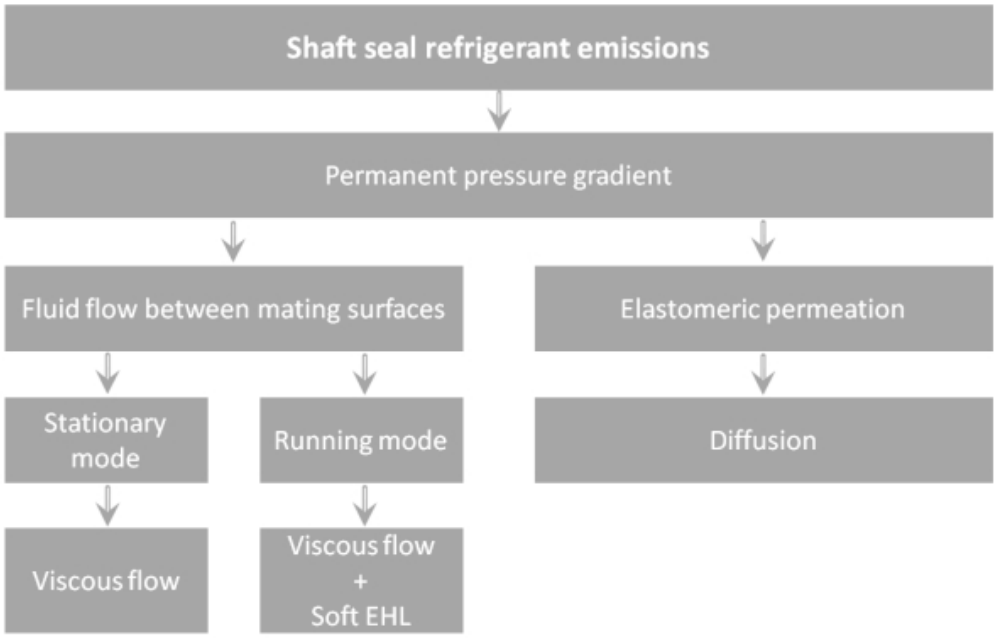

Figure 2-11 Flowchart of shaft seal refrigerant leak paths.

2.3.3 Mechanisms of gas flow through static seals

When the compressor shaft is stationary, the housing pressure is rapidly equal to the saturating pressure, corresponding to the temperature of the refrigerating system coldest point, for example, 1020 kPa at 313 K. Theoretically, a seal presents two different paths where the gas can penetrate to reach a low pressure region (see Figure 2-12). These two possible leak paths are: path *a* micro-flow through the seal interface and path *b* through the seal material itself by permeation.

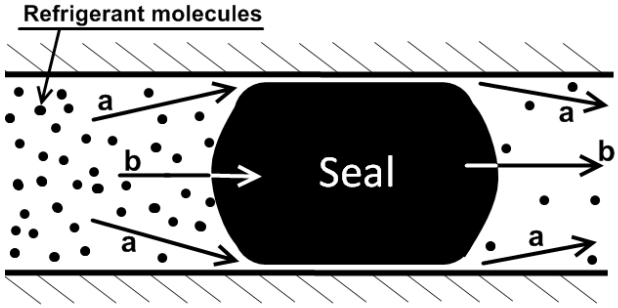

Figure 2-12 The seal possible leak paths.

2.3.3.1 Seal interface mechanism

The profile of metal surfaces, or topography, is partially compensated by the seal elastic/plastic deformation (see Figure 2.13). In order to fill in all the surface irregularities, the seal should have some plasticity and the elasticity is required to keep the contact pressure. Unfortunately, these properties are not always compatible and some free spaces remain among the surface asperities after loading.

The type of flow that occurs through the seal interface depends on different factors, such as: the gas viscosity , the pressure difference causing the flow, and the cross section and length of the leak path. The leak path geometry is very complex, so it will be considered as micro-

channels with constant diameter ranging from 1 to 10 µm in order to simplify the gas flow understanding; those equivalent diameters have been identified by Y. YU [YU08].

The length of the refrigerant gas mean free path can be used to estimate the gas flow mode through the seal interface. The mean free path λ is calculated by Equation 2.2:

$$\lambda = 116.4\left(\eta_g/P\right)(T/M)^{1/2} \tag{2.2}$$

Where η_g is the gas viscosity, *P* is the average pressure, *T* is the absolute gas temperature and *M* is the gas molecular weight. The criterion to determine the gas flow mode is the ratio λ/D_{ch}, where D_{ch} is the diameter of the channel, where:

- Viscous flow for λ/D_{ch} is lower than 0.01,
- Transitional flow for λ/D_{ch} is between 0.01 and 1, and
- Laminar flow for λ/D_{ch} is higher than 1.

Considering the conditions found in the MAC compressor, it is possible to conclude that the flow in the seal interface is viscous. The viscous flow can be divided in laminar flow and turbulent flow. Laminar flow is predominant in leaks and it is distinguished from turbulent flow by the non-dimension Reynolds number, Re:

$$Re = \frac{\rho v D_{ch}}{\mu_g} \tag{2.3}$$

Where ρ is the fluid density, v is the velocity, and D_{ch} is the channel diameter . The turbulent flow is rarely found in leaks.

The viscous flow through a cylindrical tube is defined by the Poiseuille law in Equation 2.4:

$$\dot{m} = \left(\pi r^4/16\mu_g l\right)\Delta P^2 \tag{2.4}$$

Where $\dot{m}$ is the LFR, *r* is the leakage tube radius, *l* is the leakage tube length and ΔP^2 is the pressure difference across the leak.

According to the Poiseuille law, the LFR through a circular channel is directly proportional to the channel diameter and the square of the pressure difference that causes the flow.

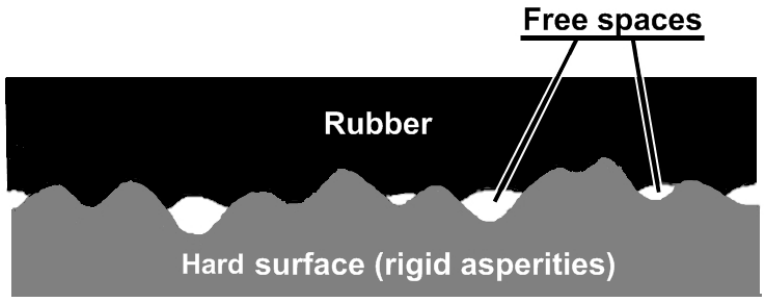

Figure 2-13 Rubber contact with a hard surface.

2.3.3.2 Permeation

The passage of a gas into, through and out of an elastomer barrier is known as permeation, path *b* illustrated in Figure 2-12. The steady state rate of gas flow in these conditions is characterized by the coefficient of permeability. The gas flow through an elastomer is determined using a thin sheet of material, known as a membrane.

The mass transport phenomenon is a process by which a gas moves through an elastomer and can be divided in: absorption, diffusion, and desorption. First, the gas is absorbed into the surface of the membrane at the high-pressure side, and then diffuses through the material at a molecular level to finally emerge on the surface of the material at the low-pressure side.

The gas permeation through polymers is generally described by the Fick's law, Equation 2.5:

$$J = \frac{G}{At} = -D_C \frac{\partial P}{\partial x} \tag{2.5}$$

Where the gas flux *J* is defined as the quantity of gas *G* that goes through a membrane with a surface *A* during time *t*. D_c is the coefficient of diffusion. The gas LFR Q/t can be expressed by:

$$\dot{m} = P_e A \frac{\Delta P}{e} \tag{2.6}$$

The gas leak flow through a membrane is proportional to the permeability coefficient P_e, the membrane with thickness *e* and surface A exposed to the gas pressure and to the pressure difference.

2.3.4 Shaft seal dynamic sealing mechanism

When the compressor starts running, the pistons and the wobble plate bring the viscous lubricant to the shaft seal. Therefore, there is a short delay before the lubricant reaches the shaft seal which depends on the lubricant flow circuit, piston stroke length, oil level, OCR, and fluid temperature. During this period, the lubricant film can be broken making the seal run under dry conditions increasing the wear of lips.

In running mode, the housing pressure is nearly equal to the evaporating pressure (varying from 300 to 400 kPa). For a variable displacement compressor, the housing pressure increases with the decrease of the compression ratio τ and reaches the saturating pressure value of the system coldest point for $\tau = 0$. Thus, the fluid pressure action on the seal is significantly higher in standstill mode than in running mode (except when the outdoor temperature is inferior to 0°C).

The sealing mechanism of lip seals is not well known. There are several complex physical mechanisms that define the seal behavior. Some of these mechanisms are difficult to observe as they are on a microscopic scale. The few publications on the shaft seal performance do not disclose the sealing mechanism in running mode.

The seal life of a shaft seal can be improved through:

- Seal design,
- Materials selection, and
- Lubrication regime

By reducing the rubber lip contact stress when the shaft rotates, it is possible to decrease its temperature, thus reducing the wear rate and material deterioration. The rubber lip temperature of a variable displacement compressor is presented in Figure 2-14. It is observed that a temperature of 200°C can easily be reached for $\tau = 0$. The rubber lip temperature decreases with fluid pressure and speed, which is due to increasing the lubricant film in the contact zone, as explained hereafter.

The rubber lip temperature can also be used as an indication of the lubricant oil viscosity. Let us consider the oil temperature equal to the rubber lip. Taking into account the viscosity values presented in Table 2-1, it is obvious that the oil viscosity at high compressor speeds will be extremely low, making difficult the formation of an oil film sufficiently thick to avoid the asperities contact. At the same time, a thin lubricating film will not fill up the free spaces due to the surfaces imperfections (see Figure 2-13) resulting in an increase of gas emissions.

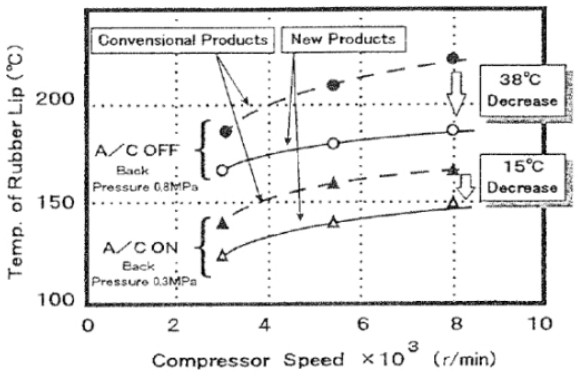

Figure 2-14 Shaft seal rubber lip temperature in running mode for a clutchless type compressor [KIS99]. AC/OFF means $\tau = 0$.

2.3.4.1 Lubrication regime

When the lubricant reaches the rubber lip contact, it is forced by the refrigerant vapor and by capillary effects to penetrate the interface and to reach the PTFE lip. The rubber lip must ensure the oil passage to the plastic lip ring when the shaft is rotating. The principal modes of lubrication are:

- Thick film or hydrodynamic lubrication (HL),
- Mixed lubrication,
- Boundary lubrication, and
- Elasto-hydrodynamic lubrication (EHL)

A helpful concept used to understand the role of these lubrication regimes is the Stribeck curve shown in Figure 2.15. The abscissa of the Stribeck curve is a dimensionless number, usually referred to as the Hersey number (Hs) and defined by:

$$H_s = \frac{\eta_{abs}\omega}{P} \tag{2.6}$$

Where η_{abs} is the oil absolute viscosity, which is the internal friction force that resists to flow, ω is the shaft rotational speed, and *P* the applied pressure. The ordinate is the coefficient of friction μ under steady state conditions, which is the ratio of the frictional force and *p*. In practical situations, it is convenient to use the kinematic viscosity η rather $\eta_{abs.}$

$$\eta = \frac{\eta_{abs}}{\rho_{oil}} \tag{2.7}$$

Where ρ_{oil} is the oil density.

A thick lubricant film corresponds to a high Hersey number, whereas a small number results in a very thin film: the higher the applied pressure, the lower the lubricant film. For an extremely low Hersey number, no real lubricating film is developed in the contact zone and a

significant asperity contact can be observed, resulting in a high friction value and polymer wear rate.

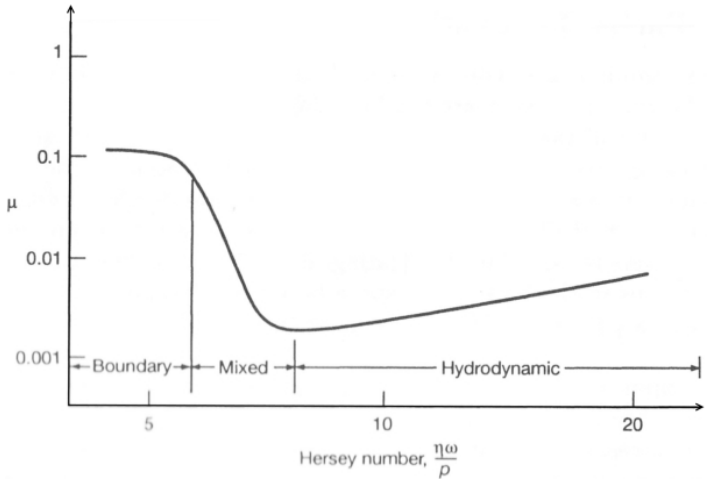

Figure 2-15 Stribeck curve showing the different lubrication regimes.

In a MAC compressor shaft seal, the fluid sealing function in running mode is performed by the PTFE lip ring. At the same time, a lubricant film is also needed in the rubber lip contact to reduce its frictional force that wears the lip edge and affect negatively the seal performances at rest. The PTFE is a thermoplastic polymer with a low coefficient of friction, excellent chemical resistance to many substances, is "non-stick" and has a working temperature range from -260 to 260°C. The PTFE lip is usually filled with glass fibers and carbon graphite, among other additives, to increase strength and rigidity. Generally, the PTFE is not considered as an elastic material, but it possesses sufficient residual elasticity (memory) to maintain the contact with the shaft surface.

The shaft seal lubricant film formation with a rotating shaft can be considered similar to the shaft seals used for oil applications. The rotating shaft together with the rough PTFE surface generates a soft elasto-hydrodynamic oil film that reduces the contact between the shaft surface asperities and the plastic material. The soft EHL regime is normally encountered with materials of low elastic modulus *E*, where the elastic deformation is large, even with light loads, compared to a metal to metal lubricated contact. The soft EHL corresponds to the lower value of μ on the Stribeck curve.

Theoretically, the elastic deformation of the shaft seal lip edges provides a coherent fluid film that avoids the asperities interaction. The refrigerant gas sealing effect results from the formation of a lubricant film that spreads over the surface imperfections, filling up the irregularities and reducing the gas flow. The positive oil effect on leakage is explained by a surface tension that creates a pressure opposite to the gas flow. The minimum lubricant film thickness h_{min} for a sliding motion is:

$$h_{min} = f(p, \omega, \eta_{mix}, E') \tag{2.8}$$

The effective elastic modulus is given as:

$$E' = \frac{2}{\frac{1-\upsilon_1^2}{E_1} + \frac{1-\upsilon_{21}^2}{E_2}} \tag{2.9}$$

In Equation (2.9), subscripts 1 and 2 refer to the two contact bodies. In soft EHL, the low contact pressure has a negligible effect on the viscosity throughout the contact.

2.3.4.2 Fluid viscosity

The fluid in the seal contact is a mixture of refrigerant gas and lubricant oil. Consequently, the viscosity depends on the fluid properties, such as temperature *T* and the mole fraction of refrigerant in the lubricating film X_{refr}. Therefore, the mixture viscosity η_{mix} is:

$$\eta_{mix} = f\left(T, \eta_{refr}, \eta_{oil}, X_{refr}\right) \tag{2.10}$$

The viscosity of mineral oil decreases with increasing temperature. As shown in Table 2-1, from 40 to 100°C the PAG-46 viscosity varies of five orders of magnitude. The refrigerant viscosity also decreases with temperature but of a lower order. The lubricant regime is considered as a soft EHL where the contact pressure has a negligible effect on the oil viscosity variation throughout the contact. Consequently, the fluid viscosity decreases with increasing temperature.

The combination of the fluid mixture viscosity with the lubricant film thickness in the interface will define the gas flow through the seal in running mode.

2.4. Experimental setup

A new experimental setup has been developed at the Center for Energy and Studies to measure the compressor refrigerant emissions in standstill and running modes (see Figure 2-16). The measurement principle is based on the gas rising concentration inside an accumulation volume.

The compressor to be tested, as well as the drive motor, is installed inside a hermetical volume or chamber with rigid walls, the accumulation volume. The compressor is connected by rigid tubes to an external refrigerant circuit that includes:

- a condenser,
- a receiver,
- a filter,
- an electro-valve,
- a sight glass,
- an electronic expansion valve and
- an evaporator.

The accumulation volume temperature is controlled by heating and cooling units. Heat exchange at the evaporator and the condenser is controlled by a water circuit. A picture of the experimental setup is presented in Figure 2-17.

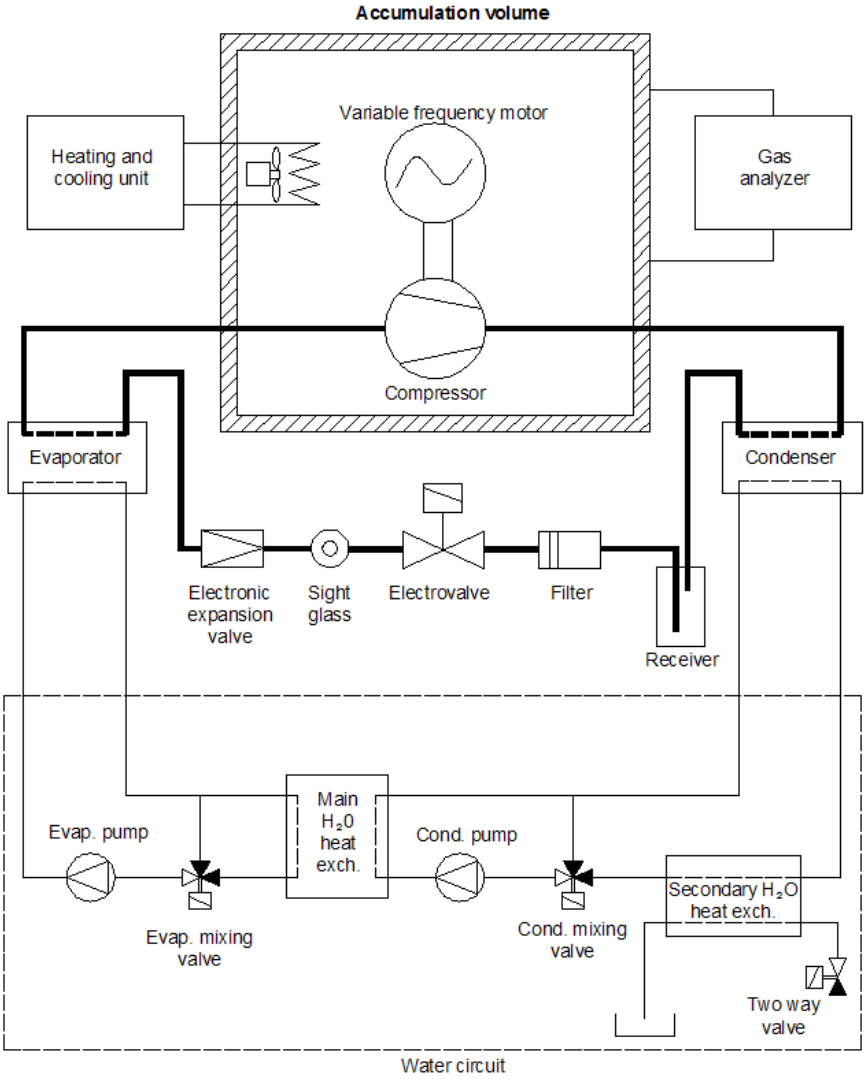

Figure 2-16 Lay-out of the experimental setup.

This experimental setup allows simulating different driving conditions since heat exchangers load and compressor speed can be independently controlled. The electronic expansion valve provides independent control of the refrigerant mass flow rate and allows the control of different operating regimes. The valve position of the electronic expansion valve is controlled by an electric stepper motor that covers the full travel of the stem.

Therefore, all the refrigerant leaking out the compressor through the body seals in standstill or running mode will accumulate in the tight volume and its concentration will be measured by a gas analyzer.

In this experiment, an infrared spectrophotometer is used to measure continuously the gas concentration inside the accumulation volume. The gas absorbs a specific infrared wavelength when the infrared light is radiated to the sample gas. A monitor measures the concentration by the analysis of the absorbed wavelengths, also known as a non-dispersive method. The measurement principle of the ABB Uras-14® infrared gas analyzer is shown in Figure 2-18.

The measurement device is composed of an infrared source whose emissions reach the sample cell via a chopper wheel. The sample cell is divided in two parts: the air sample volume and the reference air volume. The sample coming from the accumulation volume

enters the sample volume and is restituted to the accumulation volume in a continuous process.

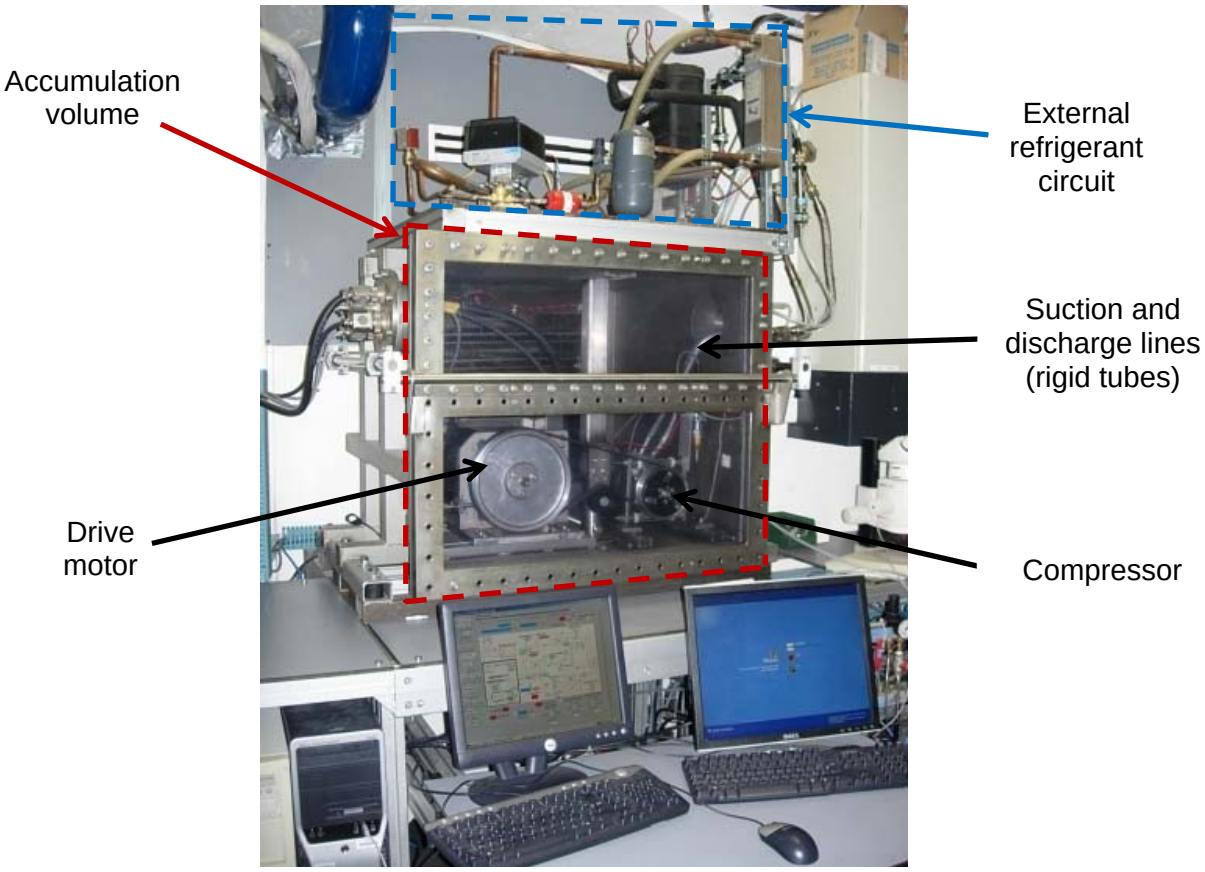

Figure 2-17 Picture of the experimental setup.

As the chopper rotates, two equal-energy infrared beams are directed through these two volumes. The effect produced in the receiver is a pressure raise resulting from the chopper frequency. The pressure effect is received by a diaphragm capacitor and converted into an electrical signal by an attached pre-amplifier. The quantity of absorbed infrared radiation is proportional to the concentration. The receiver is a two-layer device. The back of the receiver has an optically transparent window, so that any residual radiation can reach a second receiver, sensitive to a second sample component.

By adding a second beam path with an emitter, a sample cell and receivers, the photometer can measure up to 4 sample components at the same time. The apparatus used in the test bench can measure HFC-134a as well as CO_2 components with two measurement ranges: 0-50 ppm and 0-500 ppm. The sensitivity is lower than 1% of the measured value.

All the experimental setup inputs and outputs are connected to a compact FieldPoint programmable automation controller from National Instruments®. A LabWindows/CVI® interface is used to visualize and record the data.

Once the gas concentration evolution reaches a steady state, the compressor leak flow rate $\dot{m}_{HFC-134a}$ is calculated by multiplying the gas molar mass $M_{HFC-134a}$ by the number of moles increase along the time $\frac{\partial n_{HFC-134a}}{\partial t}$, (see Equation 2.11).

$$\dot{m}_{HFC-134a} = M_{HFC-134a} \frac{\partial n_{HFC-134a}}{\partial t} \tag{2.11}$$

Where the number of moles of HFC-134a is:

$$n_{HFC-134a} = \frac{C \cdot V_{ac} \cdot P_{amb}}{R \cdot T_{amb}} \tag{2.12}$$

C is the refrigerant concentration inside the accumulation volume, V_{ac} is the chamber net volume, R is the gas constant ($= 8.314\ kJ(kmol \cdot K)^{-1}$), P_{amb} and T_{amb} are respectively the pressure and the temperature inside the accumulation volume.

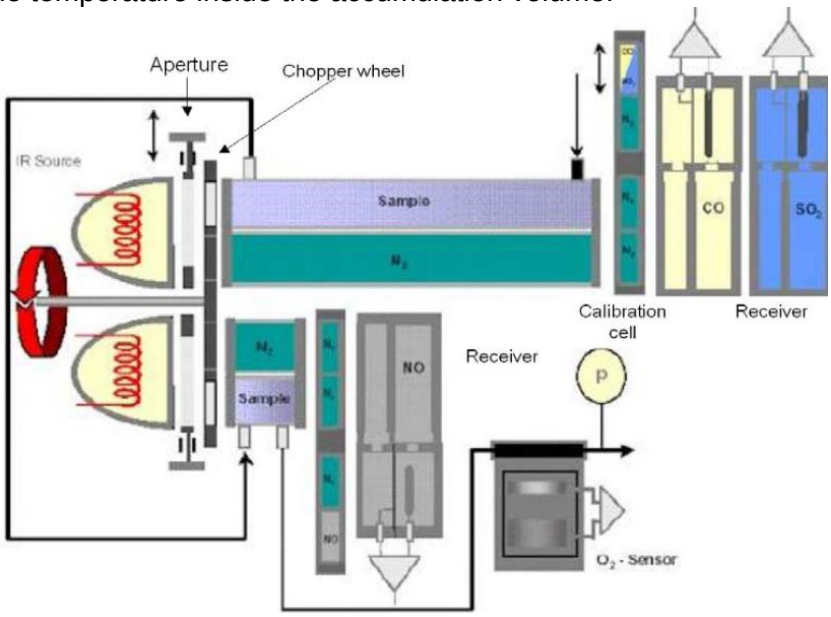

Figure 2-18 Measurement principle of the Uras-14 infrared spectrophotometer (by courtesy of ABB).

2.5. Uncertainty analysis

The measurand is the result of an experimental measurement that is an approximation of the value of the measured quantity. Thus, an experimental result is complete only when accompanied by its uncertainty. The evaluation of uncertainty requires the analysis of all possible sources of uncertainty, such as pressure, temperature, etc.

According to the International Committee for Weights and Measures (CIPM), uncertainties may be grouped in two categories:

A- Those evaluated by statistical methods,
B- Those evaluated by other means.

The compressor leak flow rate is calculated according to Equations 2.11 and 2.12. In this case, the combined standard uncertainty $u_c(y)$ is given by:

$$u_c(y) = y\sqrt{\left(\frac{u(a)}{a}\right)^2 + \left(\frac{u(b)}{b}\right)^2 + \cdots} \tag{2.13}$$

The uncertainty sources to determine the leak flow rate are: T_{amb}, P_{amb}, V_{av} and $^{\partial C}/_{\partial t}$. Then the leak flow rate combined standard uncertainty is:

$$u_{\dot{m}} = \dot{m}_{HFC-134a}\sqrt{\left(\frac{u(T_{amb})}{T_{amb}}\right)^2 + \left(\frac{u(P_{amb})}{P_{amb}}\right)^2 + \left(\frac{u(V_{av})}{V_{av}}\right)^2 + \left(\frac{u(^{\partial C}/_{\partial t})}{^{\partial C}/_{\partial t}}\right)^2} \tag{2.14}$$

The uncertainty sources are analyzed based on the experimental data shown in Figure 2-19.

2.5.1 Temperature

The standard uncertainty for the accumulation volume is calculated by combining types A and B uncertainties (see Equation 2.15).

$$u(T) = \sqrt{u^2_{T(type\ A)} + u^2_{T(type\ B)}}$$
$$= \sqrt{\frac{\sum_{i=1}^{n}(T_i - \bar{T})^2}{n-1} + \left(\frac{\Delta T}{\sqrt{3}}\right)^2} = \sqrt{7.4 \cdot 10^{-3} + 1.8 \cdot 10^{-2}} = 0.16\ K \quad (2.15)$$

Type A uncertainty is estimated from experimental results. Type B uncertainty is standard deviation calculated using a rectangular distribution.

The temperature sensor tolerance (PT100 class A) is given by:

$$\Delta T = 0.15 + 0.002|T| \quad (2.16)$$

Where *T* is the measured temperature expressed in degree Celsius.

2.5.2 Pressure

The pressure sensor used in the accumulation volume ranges from 0 to 200 kPa with a full scale accuracy of 0.2%. As for the temperature, the pressure accuracy is given by:

$$u(P) = \sqrt{\frac{\sum_{i=1}^{n}(P_i - \bar{P})^2}{n-1} + \left(\frac{\Delta P}{\sqrt{3}}\right)^2} = \sqrt{3.5 \cdot 10^{-5} + \left(\frac{400}{\sqrt{3}}\right)^2} = 230.9\ Pa \quad (2.17)$$

2.5.3 Volume

The internal volume of the accumulation chamber is calculated by subtracting the compressor volume from the accumulation chamber net volume (considering all volume internal components, such as the drive motor, the fan, the heat exchanger, etc.) (see Equation 2.18).

$$V_{av} = V_c - V_{compressor} \quad (2.18)$$

V_c is determined using a calibrated leak, see Section 2.6.

$$\frac{u(V_{ac})}{V_{ac}} = \frac{\sqrt{u(V_c)^2 + u(V_{compressor})^2}}{V_{ac}} = \frac{\sqrt{(0.06 \cdot 0.298)^2 + (0.1 \cdot 0.002)^2}}{0.3} = 6\% \quad (2.19)$$

2.5.4 Concentration variation with time

The concentration evolution along the time, for a given compressor, is plotted in Figure 2-19. The data is fitted by the method of the least squares. The best fit curve is that of the model for which the sum of squared residuals has its least value. The residual is the difference between the measured value and the value given by the model.

The standard deviation for $\partial C/\partial t$ is:

$$u\left(\partial C/\partial t\right) = \sqrt{\frac{\sum(C_i - \hat{C}_i)^2/n-2}{\sum(t_i - \bar{t}_i)^2}} = 1.43 \cdot 10^{-3}\ ppm \tag{2.20}$$

Where n is the number of samples, t_i is the measurement time, $\bar{t}_i$ is the mean value of t_i and $\sum(C_i - \hat{C}_i)^2$ is the sum of residuals.

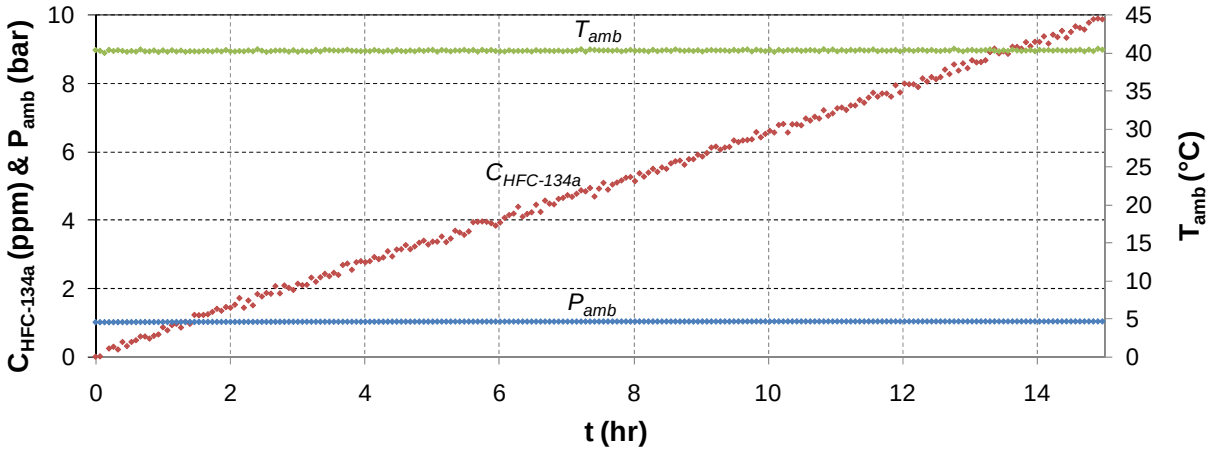

Figure 2-19 Experimental data to determine the compressor leak flow rate.

By replacing the uncertainty sources in Equation 2.14, it comes:

$$\frac{u_{\dot{m}}}{\dot{m}_{HFC-134a}} = \sqrt{(5.1 \cdot 10^{-4})^2 + (2.3 \cdot 10^{-3})^2 + (6 \cdot 10^{-2})^2 + (2.2 \cdot 10^{-3})^2} = 6\% \tag{2.21}$$

The most significant source of uncertainty is the accumulation chamber volume V_{av}, more specifically, the net volume V_c. The other uncertainty sources contribute to less than 1%, so they can be neglected. As the net volume V_c is the same for all experiments to be made, the estimated value for all leak flow rates is set to 6%.

2.6. Test procedure

2.6.1 Volume calibration

The accumulation chamber net volume is determined using a calibrated leak (see Figure 2-20b). The known leak is installed in the accumulation chamber and the gas concentration evolution is recorded (see Figure 2-20a).

Using Equation 2.11 and knowing the ambient pressure and temperature, the leak flow rate and the gas concentration, the net volume V_c can be calculated. The accumulation volume is calculated using Equation 2.18.

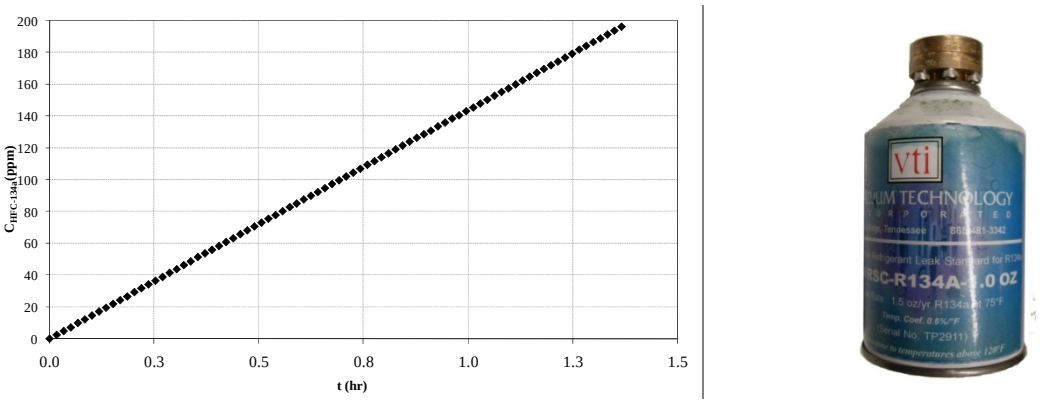

a) *b)*

Figure 2-20 Evolution of the gas concentration in the accumulation volume *a)* using a calibrated leak b*).*

2.6.2 Gas analyzer calibration

The gas analyzer (see Figure 2-21a) is calibrated with three points. The zero point calibration is made with an inert gas, N_2. The two other points are made using two standardized concentrations with a concentration value of 50±1 ppm and 450±9 ppm (see Figure 2-21b).

As for N_2, the standardized concentration is connected to the analyzer inlet port. Once the measured concentration value is constant, the user verifies the error and, if necessary, the analyzer will compensate the electrical signal to match the gas sample concentration. This process is repeated each two months.

a) *b)*

Figure 2-21 *a)* Infrared gas analyzer and *b)* standardized concentration.

2.6.3 Accumulation volume tightness

The measurement system can be divided in three different parts, and leak tightness of each of them has to be controlled:

- accumulation volume,
- gas analyzer, and
- air circuit between the two last ones

The system tightness is always verified at two levels:

- before the leak test, and
- during the leak test

Before leak tests, a small quantity of HFC-134a, about 0.012 g, is introduced inside the volume and the refrigerant gas concentration evolution is recorded for four hours. The accumulation volume is considered tight if the final concentration reading does not differ more than 5% from the initial reading.

During the compressor leak test, the system tightness is continuously monitored by the measurement of the CO_2 concentration. The CO_2 readings will point out any circuit leak trouble that will allow rejecting the measurements.

2.6.4 Compressor lines preparation

The compressor is connected to the external refrigerant circuit by rigid aluminum tubes. These tubes are brazed in the original compressor fittings. To verify the tightness of brazed joints, the compressor with the suction and discharge lines is charged with refrigerant, and then N_2 is used to raise the pressure level to a value of 1500 kPa (see Figure 2-22).

Each brazed joint is wrapped up with a vinyl sheet, as shown in Figure 2-22. The envelopment is tight enough to prevent any air leakage into the enclosure and to create an accumulation volume. At the end of the accumulation time, the envelopment is broken and the sniffer of an electronic leak detector, see Section 1.10, is rapidly inserted in the envelopment to measure the concentration value.

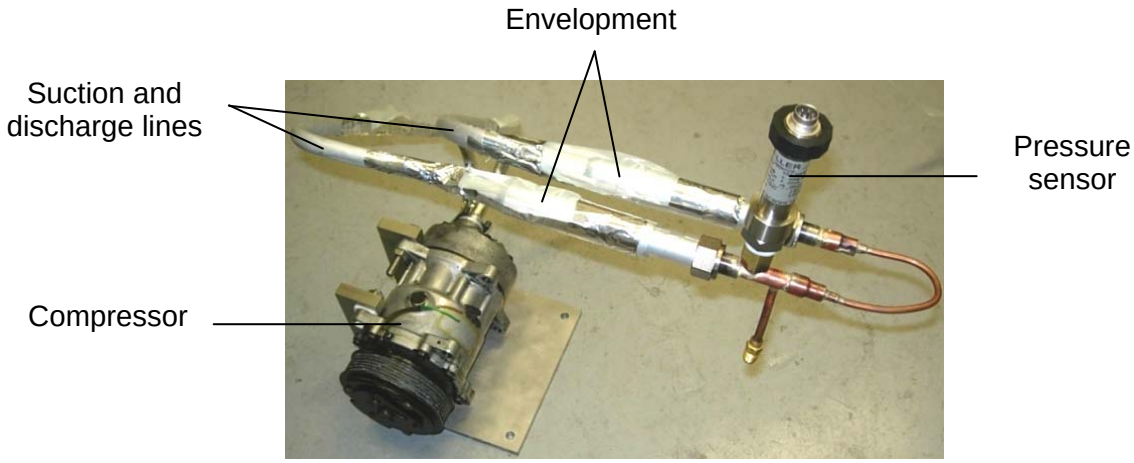

Figure 2-22 Envelopment of the compressor lines brazed joints.

To estimate the minimum detected LFR, it will be considered an envelopment of 0.25 liter at a pressure of 100 kPa and a temperature of 20°C. The accumulation time is 12 hours and the electronic leak detector sensitivity is 20 ppm. Using Equations 2.11 and 2.12, the calculated

leak flow rate value is 0.02 g/yr. Therefore, by using this test method, it is possible to reject any brazed joint with a leak rate higher than 0.02 g/yr.

The minimum compressor LFR value measured during this work is 3.2 g/yr at 1320 kPa. Therefore, the contribution of any brazed joint will never be higher than 0.9%. By considering this worst case, the contribution of line brazed joints to the compressor emissions is considered negligible.

2.6.5 Compressor installation

The compressor is charged with PAG oil according to the manufacturer instructions. Then, it is installed in the accumulation volume and connected to the external refrigerant circuit. A belt tension mechanism having an adjustable pulley is used to put the drive belt under tension.

The accumulation volume and the refrigerant circuit are evacuated to 10 Pa abs. The accumulation volume is filled up with N_2 / O_2 (80 / 20%) and the refrigerant circuit is charged with HFC-134a.

The accumulation volume temperature is regulated to overheat the compressor and to avoid inside refrigerant condensation. When the temperature and pressure inside the accumulation volume are stable, the gas concentration measurement begins.

2.7. Housing fluid pressure and temperature

The fluid in the compressor housing is a mixture of gas and lubricant. When the shaft is not rotating, the fluid pressure varies only with the ambient temperature. When the shaft rotates, the fluid pressure depends on the compressor operating conditions.

In a fixed displacement compressor, the housing pressure is the same as the suction line pressure and depends mainly on the compressor speed and the evaporator load. It has an average value of 300 kPa. In a variable displacement compressor, the housing pressure differs from the suction pressure, which allows the change of the piston stroke length, see Section 2.1.3.

The housing temperature and pressure variation of a variable displacement mechanism have been experimentally determined and are presented hereafter.

2.7.1 Variable displacement mechanism

In a variable displacement compressor, the housing pressure is regulated by a control valve that changes the compressor capacity, see Section 2.1.3. The housing fluid (lubricant + refrigerant gas) temperature and pressure are of particular interest as they act directly on the compressor seals defining the compressor leak flow rate.

A variable displacement compressor has been instrumented to measure its housing fluid temperature and pressure with different control valve signals (see Figure 2-23). The compressor is installed in the accumulation chamber; the chamber temperature is set to 303 K and the suction superheat to 5 K. The refrigerant concentration is not recorded.

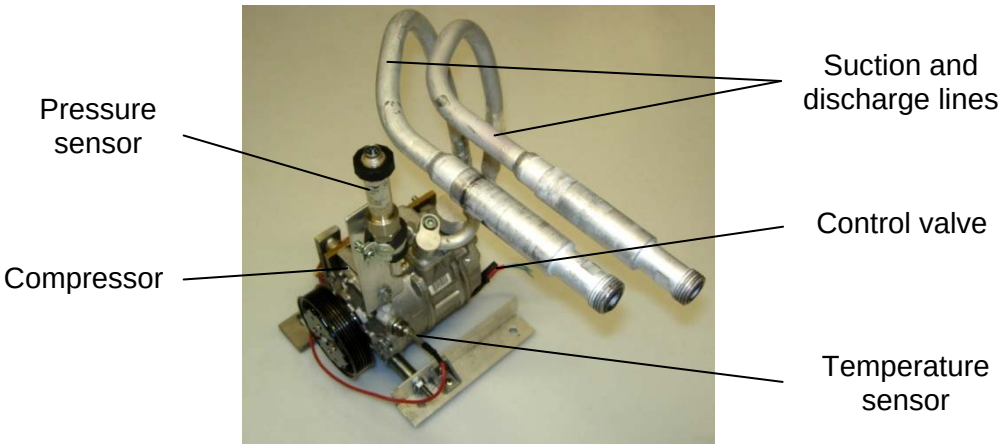

Figure 2-23 Variable displacement compressor equipped with pressure and temperature sensors.

The variable displacement compressor is connected to the refrigerant circuit that has been first evacuated and then charged with refrigerant. The compressor valve is controlled by a PWM signal that defines the duty cycle. The duty cycle represents the PWM signal in percentage to match the cooling demand. The evolution of the housing fluid pressure and temperature at two different speeds is recorded and presented hereafter (Figures 2-24 to 2-26).

Figure 2-24 shows the compression ratio evolution with the control valve signal for two different speeds. For duty cycle values lower than 25% and 35% for 1000 rev^{-1} and 3000 rev^{-1}, there is no refrigerant compression. For higher values, the compression ratio increases to reach a maximum value for a duty cycle signal of 100%.

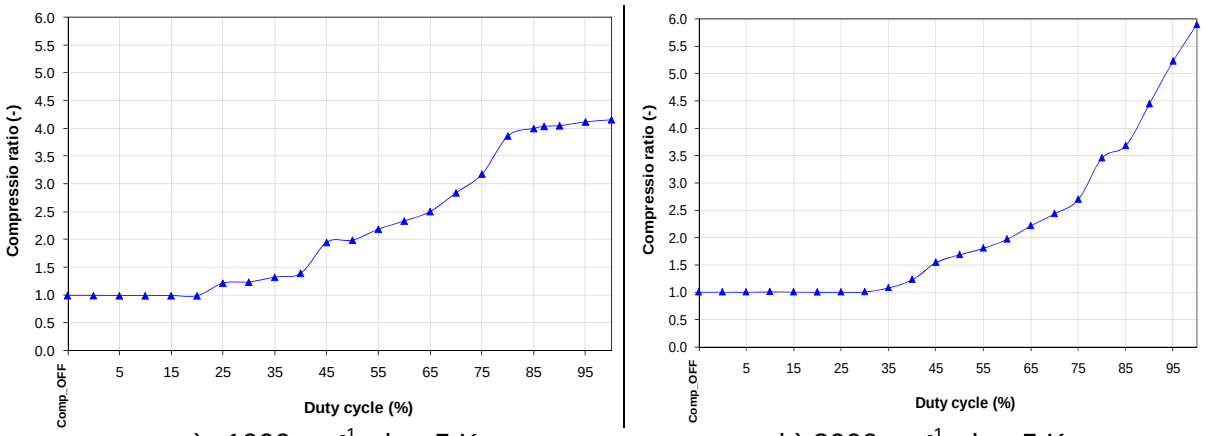

a) 1000 rev^{-1}, sh = 5 K

b) 3000 rev^{-1}, sh = 5 K

Figure 2-24 Compression ratio of a variable displacement compressor.

The evolution of the housing fluid pressure and temperature for the compressor rate evolution presented in Figure 2-24 is plotted in Figure 2-25. While the compressor is off, the fluid pressure corresponds to the saturated value of the system coldest point and remains stable until the compression ratio starts to increase, about a duty cycle of 25%. The fluid temperature evolution is related to the compressor internal friction losses. The increase in the pistons stroke length associated to the rising wobble plate loading generates heat that is transferred to the fluid, thus increasing its temperature and so the higher the shaft speed and compressor ratio, the higher the fluid temperature. A value of 365 K has been found for 3000 rev^{-1} at maximum duty cycle.

The housing pressure decreases with the duty cycle to reach the lowest value at the maximum compression rate. The compression ratio starts to increase when the housing pressure becomes higher than the suction pressure. The raising of this pressure difference increases the piston stroke length and, consequently, the compression ratio. The housing pressure follows the evolution of the suction pressure with a variation that is never higher than 60 kPa. Therefore, by measuring the suction pressure, which is a compressor non-intrusive method, it is possible to know the fluid pressure acting on the compressor seals.

In terms of refrigerant emissions, the coexistence of two different phenomena with the increase in the compression displacement volume is observed:

- First, the housing pressure reduction that lowers the pressure difference acting on the seals. In that case, LFR reduction is expected, as demonstrated by Equations 2.4 and 2.5.
- Second, the significant rising of the fluid temperature that will inevitably affect the shaft seal lubricant film has to be considered. According to the Hersey number, see Equation 2.7, the lower the fluid viscosity, the lower the lubricant film thickness. And, as already explained, a thin fluid film generates high gas emissions through the shaft seal contact.

The next section analyses the compressor emissions to find which one of these two phenomena is more relevant to the compressor emissions.

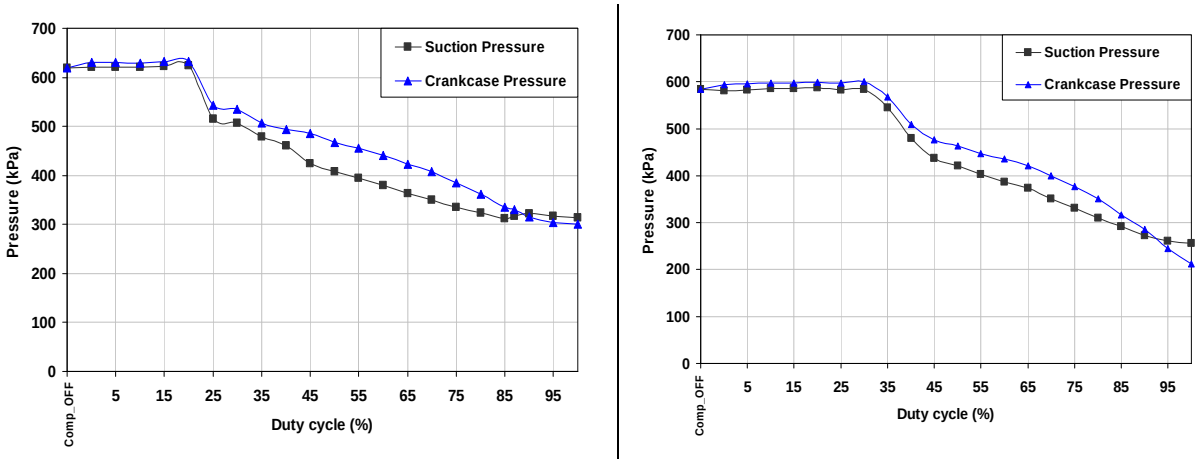

b) 1000 rev^{-1}, sh=5 K b) 3000 rev^{-1}, sh=5 K

Figure 2-25 Housing and suction pressure of a variable displacement compressor.

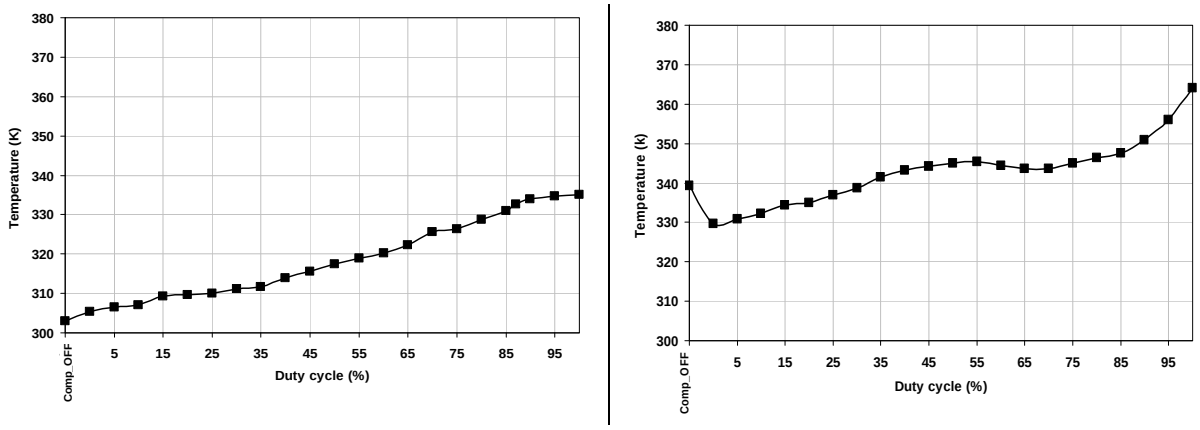

a) 1000 rev^{-1}, sh = 5 K b) 3000 rev^{-1}, sh = 5 K

Figure 2-26 Housing fluid temperature of a variable displacement compressor.

2.8. Compressor emissions

This section analyzes the effect of the operating parameters on compressor emissions. Unused and aged compressors will be leak tested both in standstill and in running modes.

2.8.1 Standstill mode

As mentioned in Chapter 1, in Europe, a MAC system is 97% to 98% of its lifetime at rest. This fact shows the importance of studying unused and aged compressor emissions in standstill mode since it defines the compressor gas emissions.

2.8.1.1 Unused compressors

Eight unused compressors taken from new MAC systems have been leak tested in standstill mode to measure their contribution to the system emissions. They have been pre-conditioned during three days at 323 K and then leak tested at three pressure levels. The compressor temperatures during the leak tests are presented in Table 2-2. The test results are presented in Figure 2-27.

Table 2-2 Compressor temperatures during the leak tests in standstill mode.

Pressure (kPa)	Temperature (°C)
770	35
1020	45
1320	55

At rest, the compressor emissions are strongly related to the fluid pressure, not only in terms of material permeation, but also the gas flow through the seal interface. The gas emissions of compressors A to H are in accordance with these principles. It is obvious from Figure 2.27 that the higher the fluid pressure, the higher the LFR. The relation between these two parameters is quadratic, as described by the Poiseuille law, see Equation 2.4.

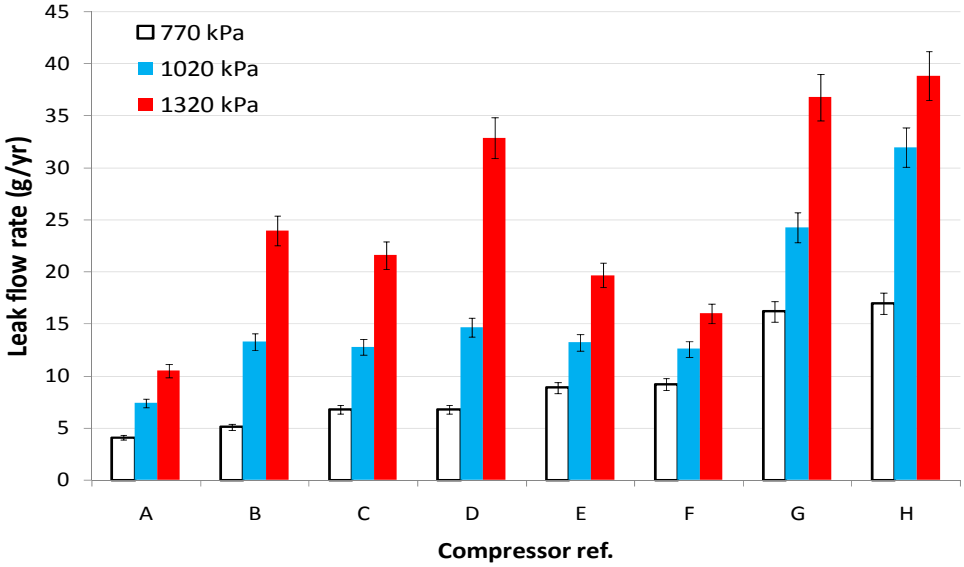

Figure 2-27 Refrigerant emissions of new MAC compressors.

These test results also show the high dispersion among the compressor emissions. Compressor A, the tightest one, presents a LFR of 4 g/yr at 770 kPa compared to 17 g/yr for compressor H under the same test conditions. The highest LFR value has been found for compressor H at 1320 kPa with a value of 38 g/yr.

The dispersion of gas emissions is not related to the number of seals, since all tested compressors have approximately the same number of seals. The reason to the compressor high emissive rates and dispersion values is due to the used sealing technology and, more particularly, to the shaft seal, as it will be demonstrated throughout this work.

The eight compressors tested in standstill mode have also been leak tested with the corresponding MAC system. The LFR comparison allows quantifying the compressor contribution to the system emissions. Accordingly, the compressor represents 50 to 60% of the system gas emissions.

2.8.1.2 Aged compressors

Two aged compressors have been recovered from MAC systems in a scrap yard. They have been charged with PAG-46 oil. Table 2-3 presents the main characteristics of the two compressors.

Table 2-3 Characteristics of used compressors.

Brand name	Vehicle		Compressor			Number of seals		
	km	Year	Control type	Displacement volume (cm^3)	Cylinder number	O-ring	Gasket	Washer
C1	300 000	1997	IC	160	7	4	2	0
C2	85 000	2003	IC	120	6	4	2	0

EC: External control, IC: Internal control

Compressor C1 is a piston type and was installed in a 1997 passenger car with 300 000 km. It is a ten-year old model. Compressor C2 is also a piston-type compressor installed in a small car. It is a four-year old compressor with 85 000 km.

Compressor C1 and C2 have been leak tested in standstill mode at 1030 kPa before and just after the running mode tests presented in next section. Leak flow rate values are presented in Table 2-4.

Table 2-4 LFR of aged compressors at 1030 kPa before and after running mode tests (g/yr).

Compressor ID	Before	After
C1	181	96.6
C2	1411	1779

The interesting point of these test results is to show the significantly high emissive rates of aged compressors. The MAC system of compressor C2 needs to be recharged every two months if the compressor is not replaced. Compressor C1 has also a very high leak rate and presents a significant reduction of emissions after the running tests. On the contrary, compressor C2 gas emissions have increased with the running tests. It is clear that, for both compressors, there is a problem with the sealing system. Further leak test results, which will be presented later, prove that the “problem” is the shaft seal.

The shaft seal is the only wearing seal part of the compressor. So, these leak test results evidence the catastrophic effect of the shaft seal wear on gas emissions. The shaft seal wear will be analyzed in more details in Section 2.12.

2.8.2 Running mode

The running mode represents a small part of the compressor life. However, it cannot be neglected since it will wear the shaft seal, thus increasing the compressor emissions along the time. This section presents unused and aged compressor emissions in steady state.

The gas emissions in steady state regime are related to the compressor oil return. For a constant speed, a stable oil return will enhance the compressor lubrication and stabilize the housing fluid temperature. Accordingly, before measurements, the compressor runs about three hours at constant high speed and compression rate.

2.8.2.1 Unused compressors

Two new and unused variable displacement compressors have been leak tested in running mode, compressors A1 and A2. The difference between them relies on the control valve system, which is either an external or an internal control.

The external control compressor A1 has been tested at different speeds and duty cycle, see Section 2.7. The compressor gas emissions are presented in Figure 2-28 and should be compared to the housing fluid temperature and pressure plotted in Figures 2-24 to 2-26. For 1000 rev^{-1} and 3000 rev^{-1}, emissions are stable for a duty cycle lower than 40%, which corresponds to a very low compression ratio, low fluid temperature, and high fluid pressure. Gas emissions start to increase for higher duty cycle values to reach 45 g/yr at high compression ratio, high compressor speed, high housing fluid temperature, and low housing pressure.

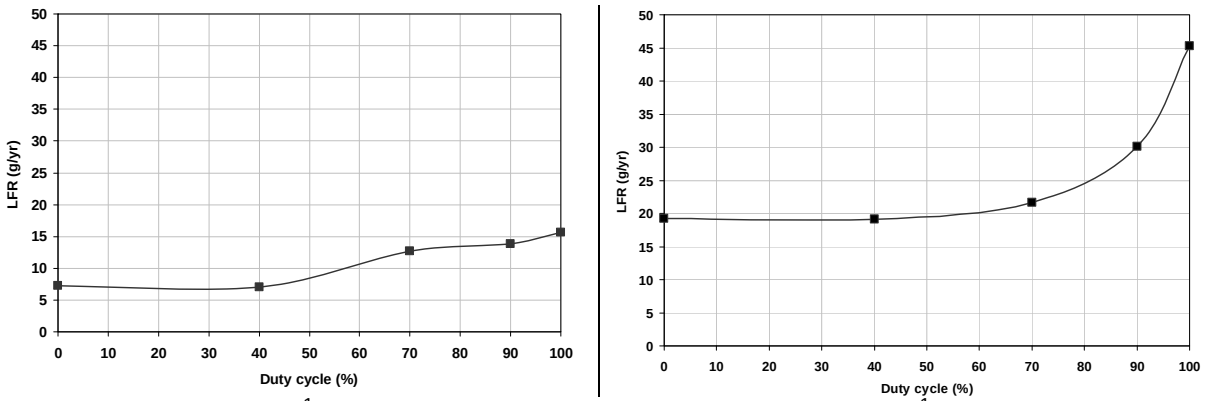

a) 1000 rev^{-1}, sh = 5 K b) 3000 rev^{-1}, sh = 5 K

Figure 2-28 Variable displacement compressor A1 gas emissions.

The relevance of the fluid temperature to the gas emissions is related to the lubricant film formation in the seal interface. As explained before, the oil film thickness defines the distance between the shaft surface and the PTFE seal ring. A thicker oil film will easily fill up the surfaces irregularities reducing the number and dimension of the leak paths. According to the Stribeck curve, the lubricant film thickness will be improved by increasing the fluid viscosity and reducing the lip load.

The increase in the compressor ration reduces the fluid pressure causing:

1. Reduction of the pressure difference that originates the leak
2. Reduction of the load of shaft seal lips

These two factors increase the lubricant film thickness, which should result in reducing gas emissions. On the other hand, the rising of the fluid temperature, up to 365 K at 3000 rev^{-1} reduces the fluid viscosity and, so, the h_{min}, which is the opposite effect of the fluid pressure decrease.

These test results show that the housing fluid temperature explains the evolution of gas emissions, rather than the housing pressure. Accordingly, compressor A1 emissions in running mode are mainly dependent on the housing fluid temperature.

With an external control valve, it is possible to study separately the effect of the housing temperature and speed on the compressor gas emissions. By adjusting the accumulation volume temperature, the compressor housing fluid temperature is controlled. The fluid temperature is measured in the outer housing wall since they have the same value. By acting on the other system controls, it is possible to vary only the compressor speed. Test results for different fluid temperatures and shaft speeds are presented in Figure 2-29. Test results show the increase of gas emissions with the fluid temperature and with decreasing speed. The LFR is divided by two when the shaft speed goes from 1000 rev^{-1} to 4000 rev^{-1}. The combination of the results presented in Figures 2-29 clearly show the significant contribution of the fluid temperature and shaft speed to the compressor emissions. In practice, the increase in the compressor speed is always followed by a fluid temperature rising due to internal friction losses. Therefore, the fluid temperature determines the compressor gas emissions in running mode.

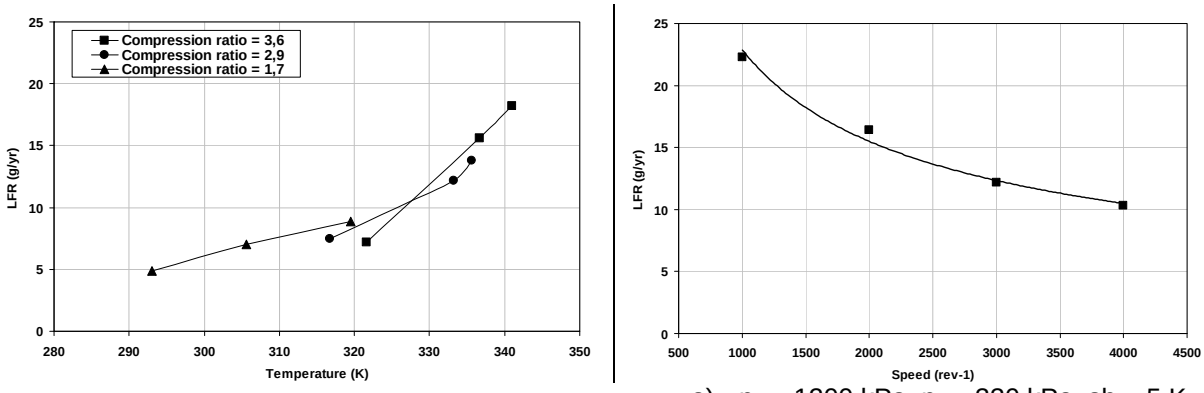

a) sh = 5K, Speed = 1000 rev^{-1}

a) p_d = 1200 kPa, p_s = 330 kPa, sh = 5 K, T_c = 343,2 K

Figure 2-29 Temperature and speed contribution to the compressor gas emissions of compressor A1.

Compressor A2 gas emissions are plotted in Figure 2-30. In this experiment, the accumulation temperature is set to 303 K and the housing fluid temperature is free to change according to the working conditions. The results corroborate the previous statement: the gas emissions increase with the compressor speed due to the rising of the fluid temperature.

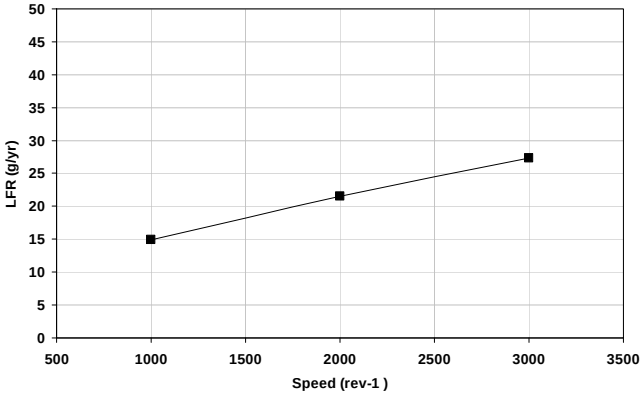

Figure 2-30 Gas emissions for an internal control compressor A2, sh = 5 K.

Both compressors, A1 and A2, have high LFR values even at low speed. As speed increases, the compressor becomes leakier. Values of 45 g/yr and 27 g/yr have been found at 3000 rev^{-1} for compressor A1 and A2 respectively.

2.8.2.2 Aged compressors

Aged compressors C1 and C2 have been leak tested at different compressor speeds and at a constant accumulation volume temperature, 303 K. Test results are presented in Figure 2-33. These two compressors, which presented extremely high emission rates at rest, (see Table 2-4), are tighter than A1 and A2 compressors (see Figures 2-31).

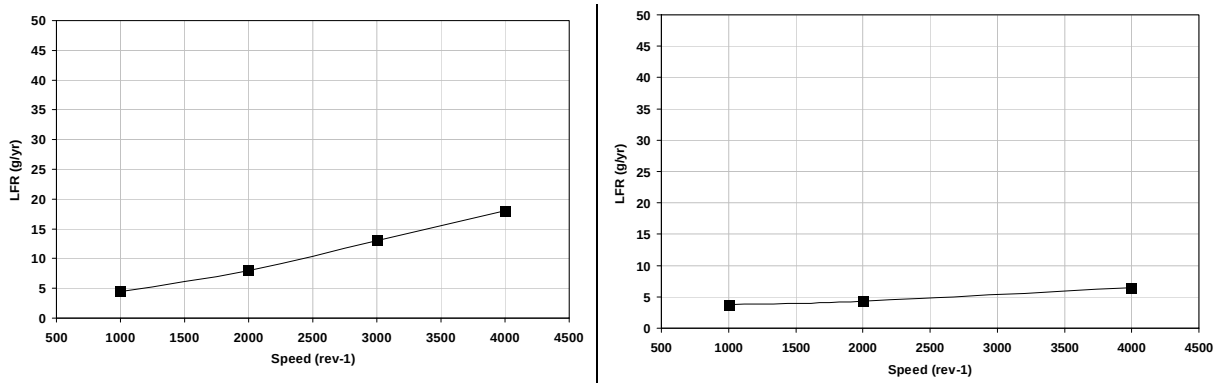

a) Compressor C1, sh = 5 K b) Compressor C2, sh = 5 K

Figure 2-31 Gas emissions in running mode for the aged compressors.

This low LFR was not expected. The increase in gas emissions with speed is in accordance with the reduction of the shaft seal lubrication ability, but higher leak rate values were expected due to seal wear evidenced by the leak test results in standstill mode, (see Table 2-4). Compressor C2, with a LFR value of 1411 g/yr at 1030 kPa at rest, presents emissions lower than 6 g/yr in running mode.

We have to be cautious when comparing the results obtained for different test conditions. The fluid pressure is 3.5 times higher in standstill mode than in running mode. However, such high emission rates indicate the shaft seal failure. For both aged compressors, it is clear that the shaft seal wear deteriorates leak tightness in running mode. Accordingly, an aged MAC compressor presents improved sealing performance when running, and poorer

when at rest. A MAC compressor is 97 to 98% of the time at rest; consequently, the shaft seal emissions at rest are predominant.

2.9. Shaft seal oil effect

This section shows the shaft seal oil effect on the compressor emissions in standstill mode. The following experiment has been done. Two unused compressors, I and J, have been charged with oil and refrigerant. Afterward, they have been hand rotated during 10 minutes and leak tested just after in the horizontal position. The chosen positions were 0°, 45°, and 90° (see Figure 2-32). The two inclined positions, 45° and 90°, will normally bring some lubricant to the shaft seal, depending on the shaft seal oil delivering system. The resultant gas concentration evolution is presented in Figure 2-33.

Figure 2-32 Different compressor positions during the shaft rotation.

The gas concentration evolution shows two different slops, initial and final, for each rotating position. Each angle of inclination, represented in broken lines, corresponds to a leak flow rate. For the same accumulation volume, the lower the inclination angle, the higher the leak flow rate. The LFR for each slope is presented in Table 2-5. The LFR for both compressors before these hand rotating tests is 15.28 g/yr and 13.3 g/yr for compressors I and J respectively.

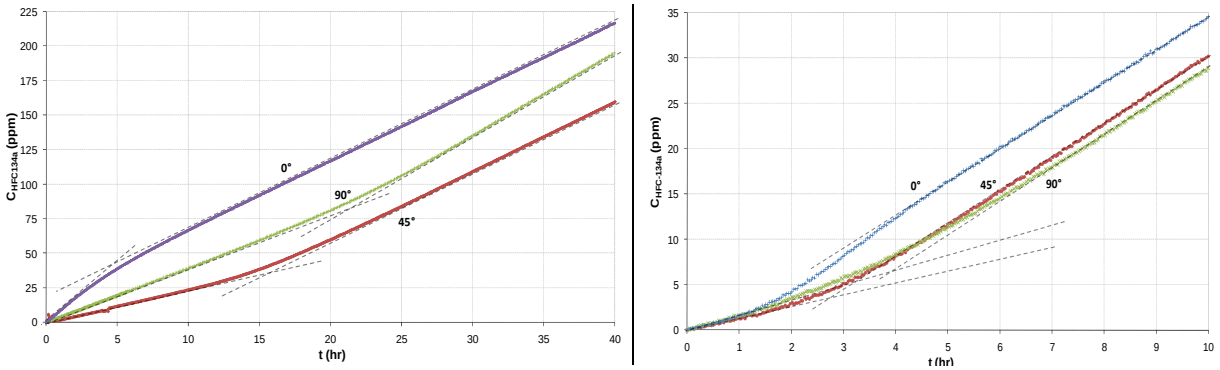

a) Compressor I b) Compressor J

Figure 2-33 Gas concentration evolution after the compressor shaft rotation at different positions.

Table 2-5 Leak flow rate after the compressor shaft rotation at 1030 kPa and 40°C (g/yr).

	0°			45°			90°		
Compressor ID	*Initial*	*Final*	*Variation*	*Initial*	*Final*	*Variation*	*Initial*	*Final*	*Variation*
I	33.81	20.1	**68%**	9.4	20.1	**114%**	15.86	23.87	**51%**
J	5.49	14.22	**159%**	5.05	14.78	**193%**	6.33	14.83	**134%**

The existence of the initial slope reveals a transitory phenomenon that results from the presence of oil in the shaft seal. This temporary process works as a gas barrier since it

allows gas emission reductions up to 190%. For compressor I at 0°, it increases emissions about 68%. The fluid reaches the shaft seal contact during the shaft rotation. At the beginning of the leak test, the fluid in the contact reduces the leak path dimension, thus reducing the gas leak rate. This first step is effective between one and fifteen hours. As time goes on, the gas forces the lubricant to go through the contact and reaches the atmosphere side. When the contact starts to dry, gas emissions raise and reach a steady regime when there is no more fluid in the contact, which corresponds to the final step.

From these static test results, it can be concluded that the shaft seal lubrication reduces substantially the compressor gas emissions in standstill mode but only for a limited period of time. The lubricating oil gas barrier effect on the shaft seal will be studied in more detail in next chapter.

2.10. Endurance tests

The study of the aged compressors C1 and C2 shows significant changes on the compressor gas emissions in standstill and running modes. These two aged compressors had improved performances in running mode. However, they generate extremely high gas leak rates in standstill mode, up to 1411 g/yr.

Two new compressors B1 and B2 have been aged using the experimental setup described in this chapter (see Section 2.4). Compressor B1 has a variable displacement mechanism with internal controls and B2 is a clutchless variable displacement compressor with external control. The aging process consists of running the compressor under the New European Driving Cycle (NEDC) and constant speeds by modifying the suction and discharge pressures, ambient temperature, evaporator load, and the duty cycle. However, this laboratory test is only an approximation of the compressor real working conditions throughout its life.

As mentioned previously, the compressor is 97% to 98% of its lifetime at rest. However, it is switched on and off an undefined number of times. Figure 2-33 shows that the shaft seal contact dries in the first hours following the compressor stop, thus making the shaft seal running temporarily under dry conditions after each compressor engagement, which increases the shaft seal wear. So, the shaft seal wear rate will be lower in this endurance test than during the compressor life. Another important factor affecting the shaft seal emissions is the seal material aging phenomena, specially the PTFE. These plastic material properties are time dependent and exposed to creep due to the permanent load and high temperature cycles. For a matter of endurance test duration, the compressor cycling and aging of polymeric materials will not be considered.

The test procedure consists to leak test each compressor in standstill mode and then start the running mode by repeating NEDC cycles or running under constant speeds. The compressors will be stopped a few times during the test to study the oil effect on gas emissions. The endurance test conditions and the leak test results are presented in Figures 2-35 to 2-44. Before, a brief description of the NEDC cycle is given.

2.10.1 The NEDC cycle

The NEDC cycle is used in the European automotive industry to measure the vehicle energy consumption and exhaust gas emissions. This cycle is divided in urban and extra-urban cycles. This driving cycle takes about 20 minutes (1180 s) with an average speed of

33.8 km/h. Figure 2-34 shows the compressor speed evolution during the cycle considering a drive pulley ratio of 1.

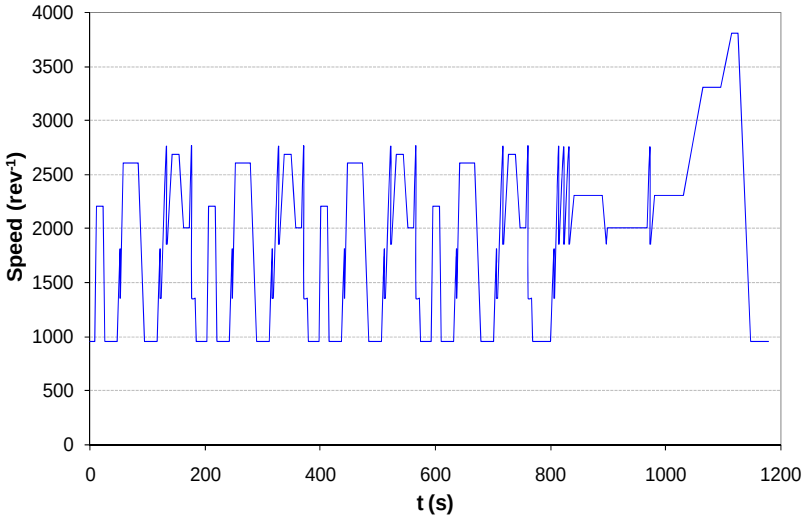

Figure 2-34 Compressor speed rotation during a NEDC cycle.

The suction and discharge pressures, as well as the evolution of housing and suction temperatures during a NEDC cycle, are presented in Figure 2-35. The compressor parameters are controlled using different Proportional–Integral–Derivative (PID) controls that continuously define the valve opening positions to match the input value. The suction temperature is constant during the cycle. However, the housing temperature increases with time and speed during the first cycle. The continuous repetition of cycles will stabilize the housing temperature to a value that depends mainly on the rotational speed, compression ratio, suction superheat and ambient temperature.

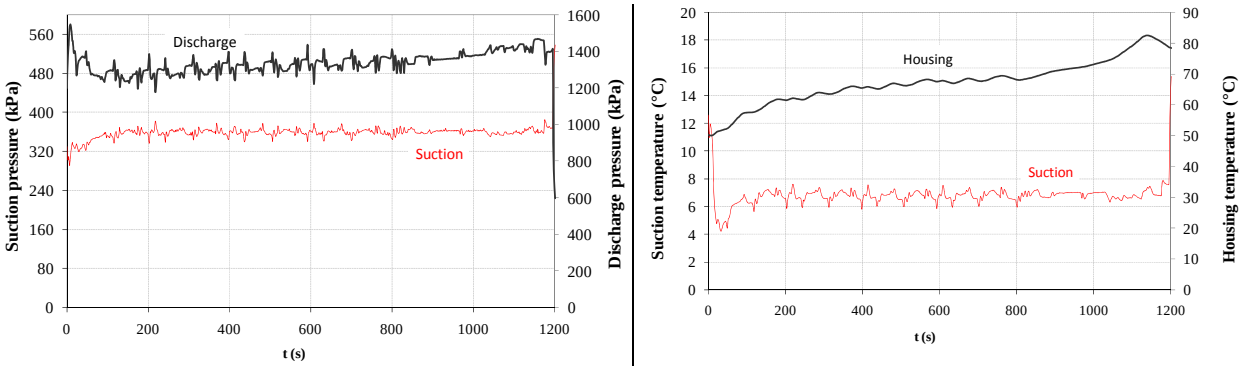

Figure 2-35 Compressor working conditions during a NEDC cycle.

2.10.2 Compressor B1 test results

Compressor B1 has been pre-conditioned during three days at 1320 kPa and 55°C followed by a leak test at rest before the endurance tests. A value of 6.2 g/yr has been obtained at 1020 kPa. This unused compressor has been aged according to the test conditions presented in Table 2-6. The endurance test takes about 872 hours with 584 hours running and 288 hours at rest.

Table 2-6 Endurance test conditions for compressor B1.

Step	Duration (h)	Compressor speed (rev^{-1})	Suction/discharge pressure (kPa)	Evap Load (kW)	Accum. Volume temperature (°C)
1	40	NEDC	350/1200	4.7	30
2	1	0	750/750	0	40
3	200	NEDC	350/1400	4.7	40
4	75	0	870/870	0	44
5	8	0	1100/1100	0	48
6	40	NEDC	350/1500	4.7	50
7	50	NEDC	350/1500	4.5	60
8	70	0	800/800	0	45
9	10	0	1020/1020	0	45
10	40	3000	330/1400	4.5	50
11	140	NEDC	330/1300	2	40
12	24	0	1200/1200	0	50
13	24	5000	360/1300	2	50
14	25	5000	340/1300	1.3	50
15	10	0	1020/1020	0	45
16	25	5000	340/1100	3,8	45
17	90	0	1020/1020	0	45
Running	*584*				
At rest	*288*				
Total	**872**	**hours**			

Step 1 represents the first compressor running hours and the corresponding refrigerant concentration evolution is plotted in Figure 2-36a. It can be noticed that the steady state regime is achieved after 25-hour running. The first 25 hours correspond to the necessary time to establish a constant oil circulation ratio (OCR) inside the compressor and to lubricate the shaft seal. The first hours of running release an important gas quantity to the atmosphere since the shaft seal contact is dry. The steady state LFR is about 6.7 g/yr.

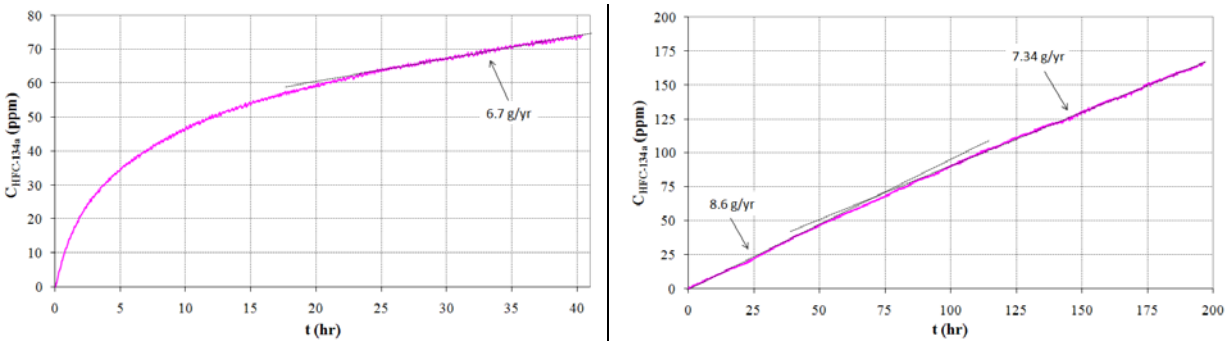

a) Step 1 *b) Step 3*

Figure 2-36 Refrigerant concentration evolution in a NEDC cycle.

Step 2 corresponds to a compressor stop of one hour. It is followed by Step 3 with 200 hours repeating NEDC cycles. In that case, the dry running observed in Step 1 does not take place, since the refrigerant concentration during the first hours is linear (see Figure 2-36b). Therefore, the one-hour stop does not break the shaft seal lubricant film. The LFR obtained for the first 50-hour test is slightly higher than in Step 1. After that point, the compressor emissions decrease to Step 1 level. The linear refrigerant concentration evolution in a NEDC cycle proves that fluid temperature equilibrium is reached by repeating the cycles. To note that the ambient temperature, suction and discharge pressures, evaporator load as well as the suction superheat are maintained constant during the drive cycles.

The compressor was stopped for a long period in Step 4 and maintained at constant temperature and pressure, 44°C and 870 kPa, respectively. The refrigerant concentration evolution during these 74 hours is plotted in Figure 2-37a. This result points out two steady state regimes. The first one corresponds to 3.2 g/yr and the second one to 8.4 g/yr. LFR increase of 160% caused by the shaft seal interface drying effect has already been explained in Section 2.9.

The shaft seal contact is now dry. Let us run the compressor again to see what happens to the refrigerant emissions. The refrigerant concentration evolution for Step 6 under NEDC cycles is presented in Figure 2-37b. If we compare Step 6 and Step 1 refrigerant curves, it will be noticed that they have basically the same progress. At the initial time, about 25 hours are needed to reach a stable shaft seal lubrication regime followed by a steady state regime corresponding to a steady shaft seal lubrication regime. At Step 6, a LFR of 67.2 g/yr was found for the first hours of test, which clearly indicates the shaft seal high emission rate under dry conditions. The LFR value under steady oil lubrication regime reached in Step 6 is slightly higher than the one obtained in Steps 1 and 3. This is due to higher temperature in the accumulation volume, which reduces the fluid viscosity.

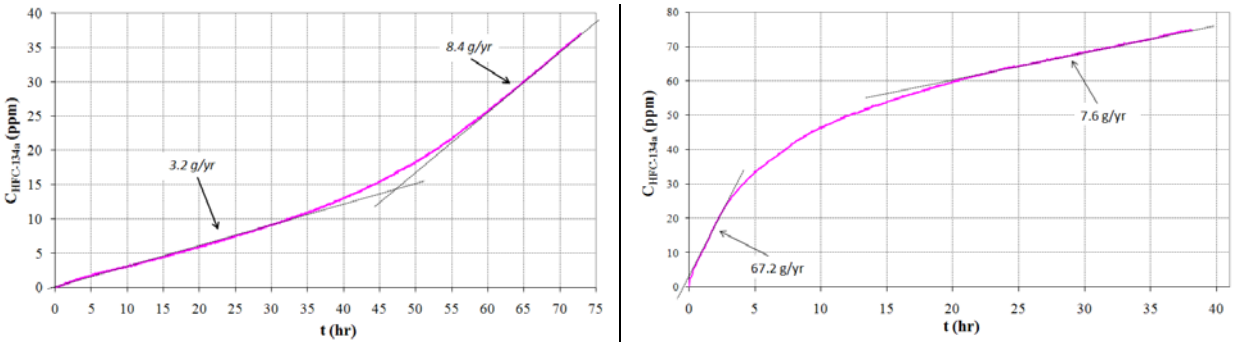

a) Step 4 *b) Step 6*

Figure 2-37 Refrigerant concentration evolution in standstill mode, Step 4, and the NEDC cycle, Step 6.

Step 8 shows again the oil effect on gas emissions in standstill mode, see Figure 2-38. The test was carried out at 800 kPa, which corresponds to an ambient temperature of 32°C, and demonstrates that the steady state regime is obtained only after 55 hours at rest. The sealing system degradations have already started since the LFR of Step 8 is almost the double of the Step 4 one: 8.4 g/yr for Step 4 and 15.1 g/yr for Step 8.

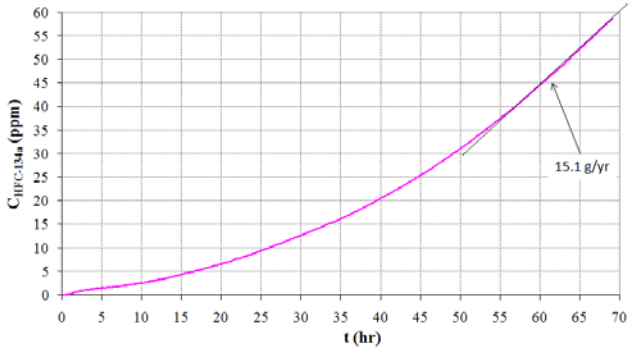

Figure 2-38 Refrigerant concentration evolution at rest for Step 8.

Step 10 takes place just after a stop period of 80 hours. This time, the compressor runs at a constant speed, 3000 rev^{-1}, for 40 hours. The refrigerant concentration evolution as well as the suction and discharge pressures, and the housing temperature are plotted in Figure 2-39. The gas concentration evolution evidences three steady state regimes with increasing LFR

values. This behavior shows that the shaft seal lubricant film properties can rapidly change under steady state conditions producing different gas emission levels.

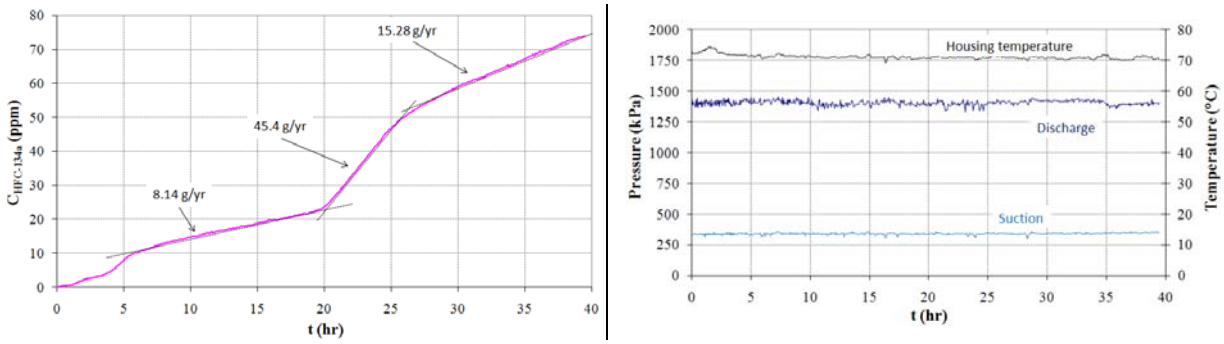

a) *b)*

Figure 2-39 a) Refrigerant concentration and b) Pressure and temperature evolution at constant speed, Step 10.

Figure 2-40a presents the evolution of the refrigerant gas concentration as well as the compressor housing temperature at constant speed of 5000 rev^{-1}. The first seven hours correspond to the standstill mode test of Step 15. The calculated LFR value for Step 15 is 20.91 g/yr, which should be compared to the initial compressor LFR that has a value of 6.2 g/yr representing an increase of 240% due to the aging process. The compressor starts to run at $t = 7\ hours$. The refrigerant concentration and the fluid temperature increase rapidly for 3 hours corresponding to the dry running. The combination of the lubricant film formation and the fluid temperature equilibrium results in gas emission steady state with a value of 17.2 g/yr. The increase in the compressor temperature of 2°C reduces the fluid viscosity and results in a rapid increase in gas emissions (14.8 g/yr).

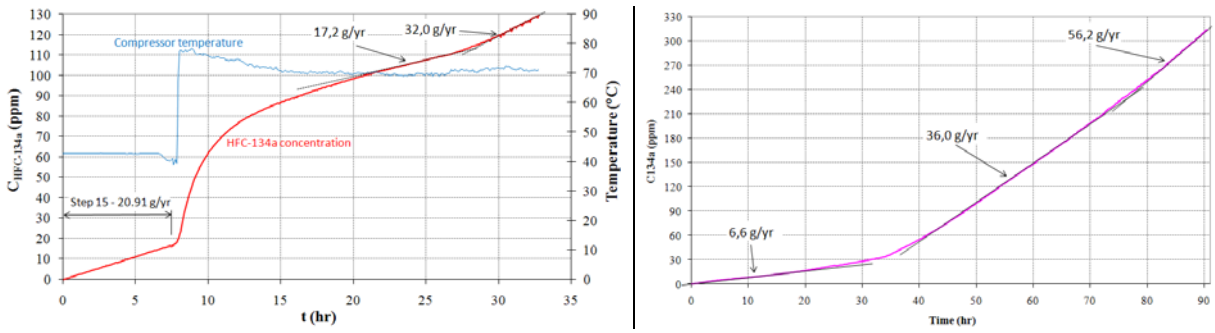

a) Step 16 *b) Step 17*

Figure 2-40 Refrigerant concentration evolution a) at 5000 rev^{-1} and b) at rest.

The last step quantifies the increase in the compressor gas emissions during 872-hour testing: 584-hour running and 288-hour at rest. Test results are presented in Figure 2-40b. The gas barrier effect of the shaft seal lubricating film is observed during the first 30 hours, followed by the increase in gas emissions as the shaft seal interface dries out. The last steady state regime found after 90-hour test corresponds to a LFR of 56.2 g/yr. The oil effect period has been reduced by about 5 hours compared to the one obtained in Steps 4 and 8, suggesting that the higher the fluid pressure, the faster the oil will leave the shaft seal contact.

Summary of this first endurance test

1. This aging process rises compressor emissions from 6.2 g/yr to 56.2 g/yr at 1020kPa, representing an increase of 800%,

2. After a stop period, the seal contact dries and when the compressor starts working again, the shaft seal will run under dry conditions for a period of 5 hours,
3. After a running period longer than 5 hours, the compressor emissions at rest can be divided by a factor 8 due to the lubricant oil in the shaft seal contact. The drawback of this barrier effect is that it is time dependent since the oil is washed out of the contact driven by the gas pressure,
4. A dry contact always results in higher emission rates compared to a lubricated one.

2.10.3 Compressor B2 test results

Compressor B2 has a variable displacement mechanism that can be externally controlled by a PWM signal. Another difference from compressor B1 is the suppression of the clutch eliminating the possibility of disconnecting the compressor from the vehicle engine. This feature constrains the compressor manufacturer to use a shaft seal system that resist to long periods with very low oil circulation, corresponding to $\tau = 0$ (A/C off).

The compressor has been preconditioned during three days at 1320 kPa and 55°C followed by a leak test at rest before the endurance tests. A value of 14.0 g/yr has been obtained at 1020 kPa. This unused compressor has been aged according to the test conditions presented in Table 2-7. The endurance test takes about 587 hours with 385 hours running and 202 hours at rest.

Table 2-7 Endurance test conditions for compressor B2.

Step	Duration (h)	Compressor speed (rev^{-1})	Suction/discharge pressure (kPa)	Duty cycle (%)	Evap Load (kW)	Accu. Vol. temp. (°C)
1	40	0	1020/1020	0	0	50
2	50	5000	300/1400	90	5.0	50
3	25	5000	300/1400	90	5.0	60
4	65	0	1020/1020	0	0	50
5	14	NEDC	260/1400	90	5.0	40
6	70	NEDC	260/1400	90	5.0	50
7	50	0	1020/1020	0	0	50
8	60	NEDC	310/1200	70	2.5	50
9	47	0	1020/1020	0	0	50
10	50	NEDC	610/610	0	0	50
11	7	5000	610/610	0	0	50
12	10	800	610/610	0	0	50
13	22	3000	610/610	0	0	50
14	7	3000	830/830	0	0	50
15	70	3000	610/610	0	0	60
16	70	0	1020/1020	0	0	50
Running	*385*					
At rest	*272*					
Total	**657**	**hours**				

Step 2 represents the first compressor running hours and the corresponding refrigerant concentration evolution is plotted in Figure 2-41. The dry running effect evidenced by the compressor B1 is not observed with this compressor. The first two-hour test results in a LFR value of 43.11 g/yr, which is an extremely high emission rate (see Figure 2-41a). The transition to a lubricated steady state regime is observed after 6 hours with a reduction of gas emissions of 12 g/yr (see Figure 2-41b).

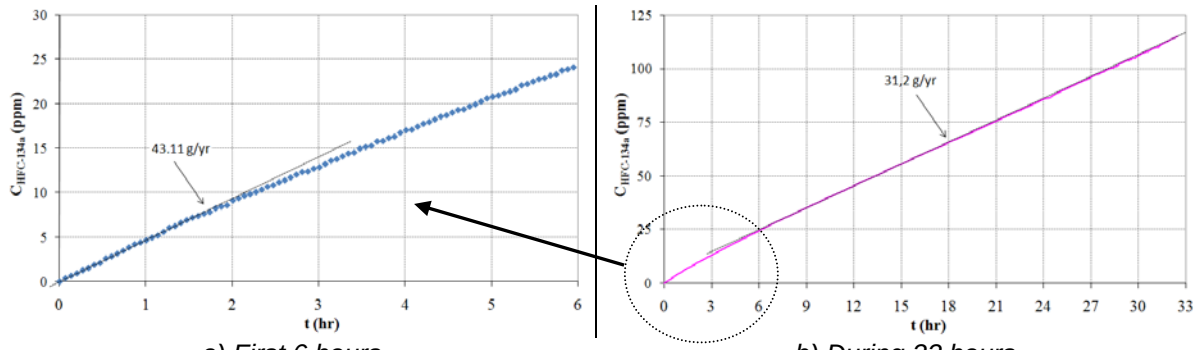

a) First 6 hours *b) During 33 hours*

Figure 2-41 Refrigerant concentration evolution at 5000 rev^{-1}, Step 2.

When the compressor is stopped for a long period, Step 4, the shaft seal oil effect is observed for the first 15 hours (see Figure 2-42a). After 10-hour transitory period, the LFR is established at 12.1 g/yr, which is slightly lower than initial compressor LFR. However, the LFR difference during the oil effect and after is lower than the one observed for compressor B1.

Step 9 corresponds to a running time of 219 hours and an increase in emissions is observed (see Figure 2-42b). The oil effect is observed but still with a smaller impact on emissions, compared to B1 compressor.

The combination of the absence of a dry running and a small oil effect in standstill mode suggests that the shaft seal contact never dries completely for the considered time. This assumption is supported by next test results and by oil leakage observations presented in Section 2.13.

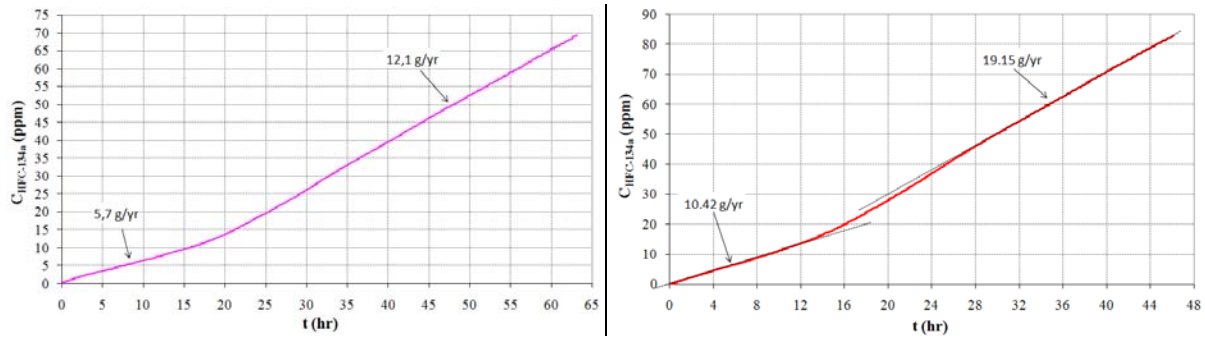

a) Step 4 *b) Step 9*

Figure 2-42 Refrigerant concentration evolution at rest.

As already mentioned, the specificity of a clutchless compressor is to run continuously with the vehicle engine, even when the air conditioning is off. Figure 2-43 shows the refrigerant concentration and compressor temperature evolution when $\tau = 0$. It is observed that the compressor housing temperature is constant during the 50-hour test and the steady state regime is reached after 20 hours with a LFR value of 26.7 g/yr. The LFR obtained for the same shaft speed but with a duty cycle of 90%, in Step 6, was 30.11 g/yr. Therefore, it can be concluded that the shaft seal runs continuously under a lubricated film even when the oil circulation inside the compressor is reduced.

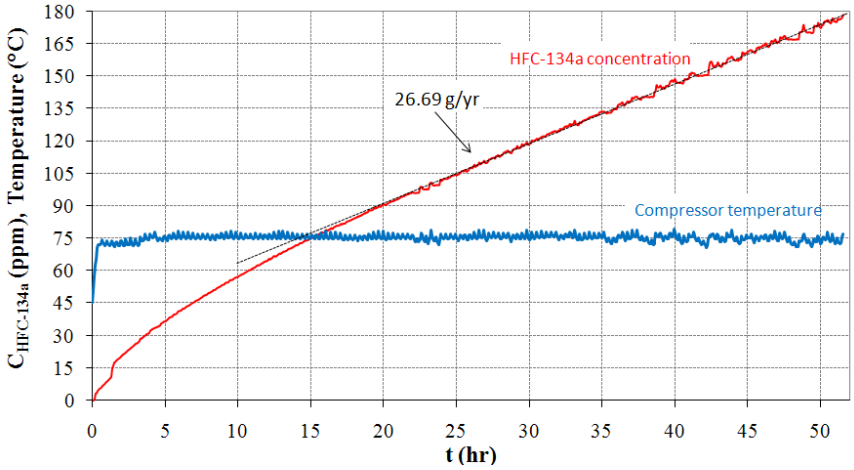

Figure 2-43 Refrigerant concentration evolution for a NEDC cycle and $\tau = 0$, Step 10.

Steps 10 to 13 correspond to the study of the shaft seal on gas emissions when $\tau = 0$, see Figure 2-44a. It can be observed that emissions increase with speed from 8.6 g/yr at 800 rev^{-1} to 39.6 g/yr at 5000 rev^{-1}. The NEDC cycle presents lower emission values due to the lower mean speed. The increase in the compressor speed rises the heat generation in the shaft seal contact, reduces the lubricant viscosity and the film thickness, and thus increases the gas flow through the seal interface.

The evolution of compressor emissions at rest during the endurance test are presented in Figure 2-44b for 1020 kPa. As for compressor B1, the aging process results in a significant increase in compressor emissions.

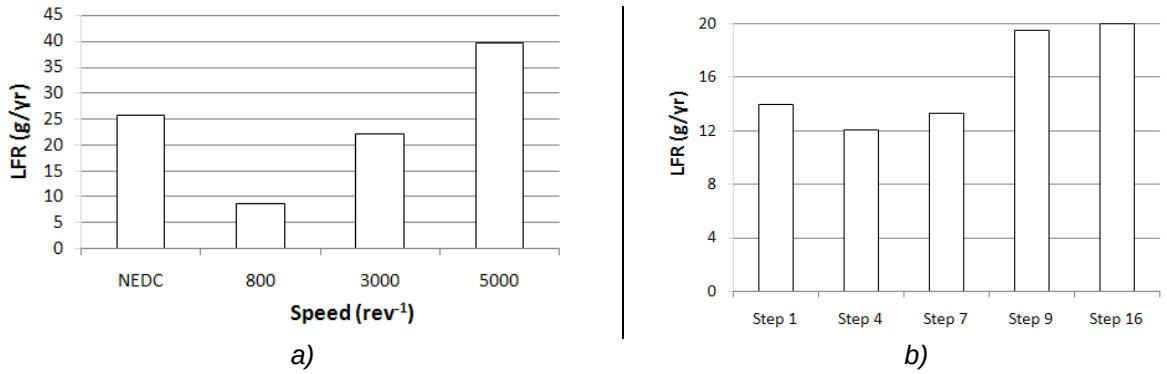

a) *b)*

Figure 2-44 Compressor refrigerant emissions: a) with shaft speed when $\tau = 0$, b) in standstill mode at 1020kPa.

Compressor B2 has gas emission levels higher than compressor B1 for standstill mode and running mode. On the other hand, it preserves the shaft seal lubricant film in both working modes, which eliminates the dry running effect. Even though, the increase in gas emissions due to the shaft wear is not avoided.

The endurance test of compressors B1 and B2 shows that the steady state regime of gas emissions is strictly related to the shaft seal lubrication. However, the lubricant steady state regime is hardly achieved since the compressor never runs constantly for 10 hours. Therefore, the shaft seal always runs under poor lubrication conditions increasing wear and gas emissions throughout the compressor life, where the wear effect is more pronounced

than during these endurance tests. The leak tests of compressors C1 and C2 show such behavior (see Section 2.8).

2.11. Shaft seal refrigerant emissions of aged compressors

Two aged compressors, C1 and B1, have been chosen to study the shaft seal gas emission contribution at rest. Consequently, a new experimental setup has been developed to measure the shaft seal gas emissions in standstill mode directly from the compressor.

2.11.1 Measurement principle

A new hermetical volume has been developed to match the compressor dimensions, see Figure 2-45. The accumulation volume used to recover the gas leaking from the shaft seal is installed in the compressor front housing and recorded with the infrared gas analyzer presented in Section 2.4.

The accumulation volume tightness is achieved by using two o-rings: one between the accumulation volume and the aluminum housing, the other in the accumulation volume middle plane to allow disassembling. The accumulation chamber volume is calculated using a calibrated leak as presented in Section 2.6. The volume tightness is verified by injecting a small quantity of HFC-134a and monitoring its concentration evolution during five hours, as explained in Section 2.6. The leak flow rate uncertainty is 5.6%.

This configuration ensures that all the gas leaking from the shaft seal, and only that one, will be recovered in the accumulation volume at atmospheric pressure. During the experiment, the compressor and the accumulation volume (see Figure 2-46) are installed in a closed chamber to be temperature controlled.

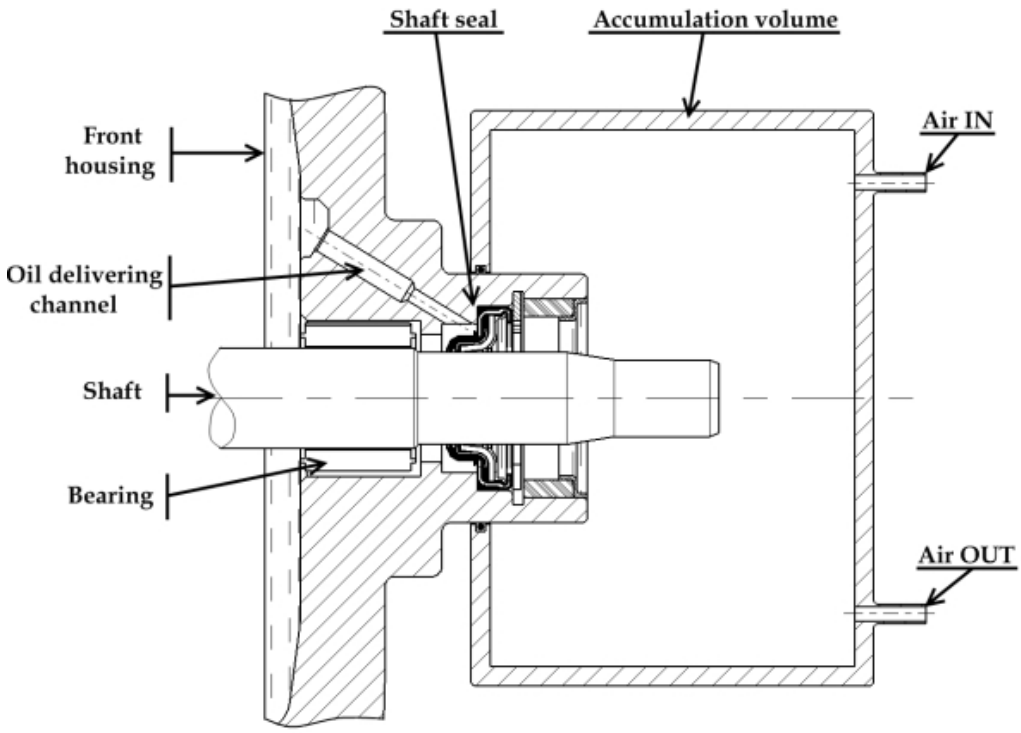

Figure 2-45 Experimental setup to leak test the shaft seal in standstill mode.

Figure 2-46 Photo of the accumulation volume to leak test the shaft seal in standstill mode.

2.11.2 Test results

Compressors C1 and B1 have been tested at three different pressures: 770, 1020, and 1320 kPa. Compressor C1 has been recovered from a MAC system in a scrap yard and has been leak tested previously. Compressor B1 has been submitted to an endurance test in the laboratory, as presented in Section 2.10. Test results for the pressure and temperature conditions presented in Table 2-8 are shown in Figure 2-47.

At rest, the shaft seal emissions are strongly related to the fluid pressure; the higher the fluid pressure, the higher the LFR. The relation between these two parameters is quadratic as described by the Poiseuille law, see Equation 2.4. Compressor C1 shaft seal is an extremely high emissive component with LFR values up to 140 g/yr. Compressor B1 shaft seal high LFR value is 37 g/yr at 1320 kPa. These test results confirm the high emission rate of the shaft seal, especially with aged compressors.

Table 2-8 Compressor temperatures during the leak tests in standstill mode.

Fluid pressure (kPa)	Compressor Temperature (°C)
770	35
1020	45
1320	55

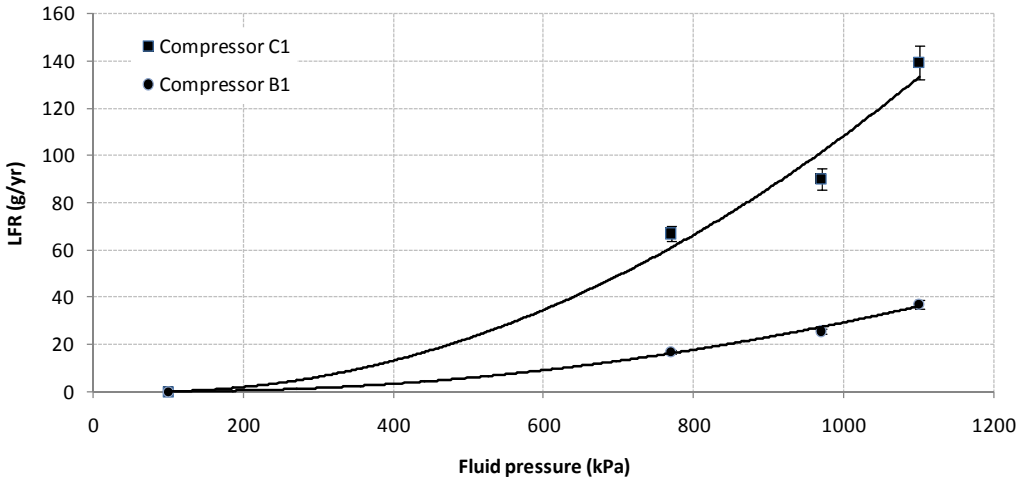

Figure 2-47 Shaft seal gas emissions for aged compressors C1 and B1.

Shaft seal emissions have been compared to the corresponding compressor LFR in order to quantify the shaft seal contribution. Table-2-9 presents the shaft seal emission contributions at 1020 kPa. The result confirms the interest of studying the shaft seal emissions since they represent 93% of compressor C1 gas emissions. This contribution is even greater as the shaft seal wear goes on.

Table 2-9 Shaft seal LFR contribution to the compressor gas emissions for two aged compressors at 1020 kPa.

Compressor I.D.	Compressor LFR (g/yr)	Shaft Seal LFR (g/yr)	Shaft seal contribution
C1	96.60	90.30	**93%**
B1	36.0	25.72	**71%**

Next chapter deals with the shaft seal wear and is based on observations and measures on compressors C1 and B1.

2.12. Wear

The degradation process, known as wear, occurs at the interfaces between the interacting bodies and leads to the progressive loss of material resulting from their relative motion. There are different wearing components in a MAC compressor such as pistons, shoes, drive-shaft, and the shaft seal, among others. In this work, the focus will be given to the shaft seal wearing components, especially the shaft surface.

The shaft seal tribological system is composed of two sliding contacts (see Figure 2-48):

- HNBR/shaft surface, and
- PTFE/shaft surface

The shaft seal lip rings are pressed against the shaft surface by the addition of two forces: the preload and the fluid load. The first one is obtained during the shaft installation due the diameter difference between the shaft and the lip rings, and the second is obtained when the compressor is charged with refrigerant and varies with the working conditions. When the shaft starts to rotate, a lubricant oil film is necessary between surfaces to increase the gap avoiding the contact of asperities.

The shaft seal friction and wear is a very complex phenomenon, controlled by the thin films of material present between the interacting surfaces. The wear of the shaft seal sliding surfaces is important since the sealing performances in standstill and running modes are directly related to the surfaces texture. The shaft parameter hardness and diameter tolerance will also contribute to the wear rate.

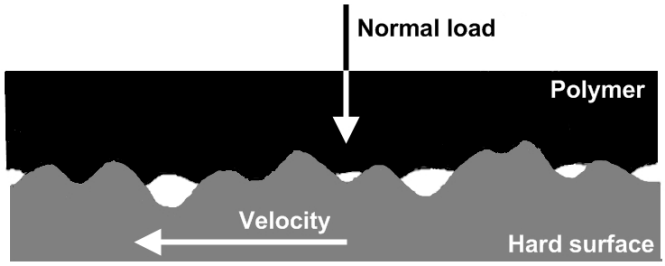

Figure 2-48 Contact of asperities between soft and hard materials.

The shaft surface texture is of primary importance since it defines the mating surface contact conditions that affect the sealing performance by defining the gas leak path dimensions in standstill mode and the lubrication regime in running mode. The surface profile, or texture, of the machine surface represents the deviation from the nominal surface, the perfect flat surface, and includes roughness (nano and micro-roughness) and waviness (macro-roughness). Roughness is formed by fluctuations of the surface and is characterized by hills or bumps, and valleys of short wavelengths. Waviness is the surface irregularity of longer wavelengths and may result from different production factors such as heat treatment, machine or work piece vibrations, as well as wear.

2.12.1 Shaft parameters

The roughness values of three unused compressor shafts are presented in Table 2-10. Measurements have been performed by a stylus tracer instrument that amplifies and records the vertical motions of a stylus displaced at a constant velocity by the surface to be measured. The calculated values to characterize the surface are as follows: the center line average (R_a), the average peak-to-valley height (R_z), and the maximum height (R_{max}).

The shaft hardness is also a relevant factor to the seal performance since it will affect the shaft surface wear rate. For the same sealing system, a high hardness value prevents excessive wear. The hardness value of a compressor shaft is typically of 584HV.

Table 2-10 Surface roughness of unused compressor shafts measured in the seal area.

Shaft I.D.	Diameter (μm)	Ra (μm)	Rz (μm)	R_{max} (μm)
No.1	14.264	0.09	0.76	1.0
No.4	14.268	0.18	1.56	2.12
No.6	13.489	0.12	0.99	1.27

The shaft diameter will determine the contact stress in the sealing interface. A high contact stress value is favorable to the static sealing effect but will reduce the seal contact lubrication during the shaft rotating, thus increasing wear. A lower contact stress value is achieved with a small diameter shaft and improves the seal lubrication. However, a high gas leak rate value can be observed in standstill mode, especially if the contact pressure value is lower than the fluid pressure. A typical value of the shaft diameter tolerance is of ±0.08 mm. The shaft eccentricity relatively to the seal case affects the seal performance only in running mode. The eccentricity can be partially compensated by the PTFE lip deformation that follows the shaft movements. A high eccentricity value makes the lip contact pressure drop locally, producing high gas and oil leakage levels.

2.12.2 Wear rate

Theoretically, the shaft seal runs under a soft EHL film that avoids the contact between the mating surfaces. As shown in previous experiments, in Section 2.10, the contact between the sealing surfaces cannot be avoided during the shaft rotation, therefore, it is expected to observe wear on both surfaces.

The wear rate for rubbers can be defined by:

$$k = \frac{K}{H} \tag{2.22}$$

k is the specific wear rate ($mm^3\ N^{-1}\ m^{-1}$) for a material with an indentation hardness *H* and a wear coefficient *K*. Therefore, the wear rate can be reduced by increasing the wearing surface hardness and lowered by improving the contact lubrication.

The PTFE has been chosen to leak tight the compressor shaft in running mode since it exhibits a very low coefficient of friction and retains useful mechanical properties at temperatures from -260 to 260°C. There are many kinds of PTFE-based composites for sliding applications since various fillers are incorporated in the matrix polymer to improve the mechanical properties and match the application requirements.

The size and shape of plastic debris generated during the shaft rotation may change during sliding under a dry or lubricated contact. Metallic wear debris with a particle size of 0.01-1 µm can also come from the compressor housing, and more particularly, from the front housing bearing adjacent to the shaft seal, to reach the seal contact by the action of the fluid flow.

In this work, the focus is given to the shaft surface texture variation as the measurement techniques are available.

2.12.3 Shaft surface texture

Shaft surfaces from aged compressors show wear tracks in the sealing zone, see Figure 2-49. These tracks correspond to the contact between shaft seal lip rings and the metallic surface.

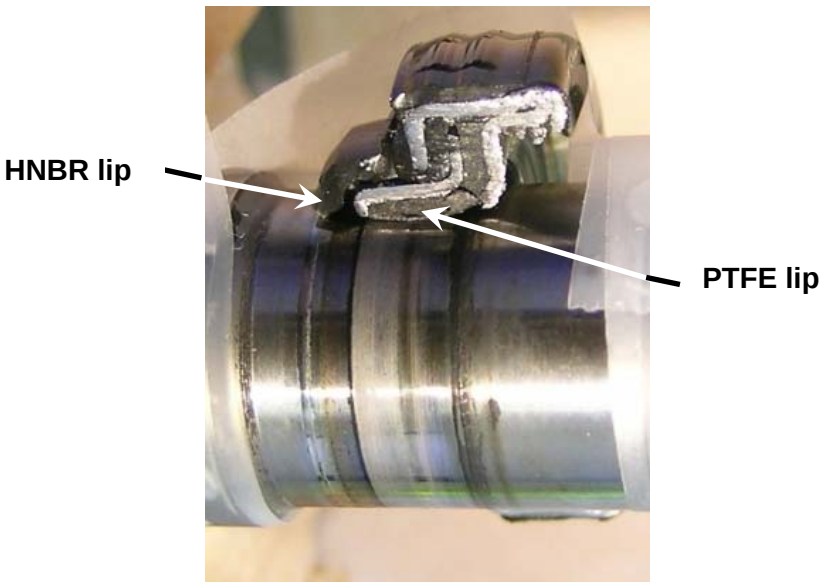

Figure 2-49 Shaft surface wear tracks of an aged compressor.

During compressor operation, wear particles from metallic surfaces can be transported by the lubricant and reach the shaft seal contact. Debris with dimensions under the micrometer penetrate the HNBR contact and abrasion can take place. Some of the debris leave the HNBR contact to reach the PTFE contact.

The profile of a used compressor shows the existence of two grooves resulting from the wear process, as shown on Figure 2-50. The groove corresponding to the rubber contact is deeper than the PTFE contact. The roughness profile of a new and an aged shaft surface is shown in Figure 2-51. The wearing process is different from the rubber lip to the PTFE lip and the

shaft surface roughness in the rubber contact zone increases with the shaft rotation time. This can be explained by the metallic wear debris that gets trapped in the rubber sealing zone accelerating the shaft wear.

The increase in the surface roughness due to wear impacts the shaft seal emissions at two levels:

- at rest, and
- in running mode

When the compressor shaft is stopped and the contact is dry, the gas leak rate rises with the square of the pressure difference and the increase in the dimensions of gas channels. By increasing the shaft surface roughness, as shown in Figures 2-52 and 2-53, the free spaces to the gas flow become larger and in high number, resulting in shaft seal gas emissions. As the shaft seal represents the majority of the compressor emissions, see Table 2-7, the high emission rate of aged compressors results from the increase in the surface roughness.

The running mode leak test of compressors C1 and C2 showed the lower LFR values. These low gas emission values can be explained by the larger oil quantity trapped inside the surface asperities that facilitate the lubrication. The other factor affecting the shaft seal lubricant film is that PTFE material properties are time dependent and exposed to creep due to the permanent load and high temperature cycles. This material property reduces the interference load created during the seal installation resulting in the reduction of the PTFE lip load with time. A lower lip load helps the formation of thicker fluid films that enhance the seal lubrication.

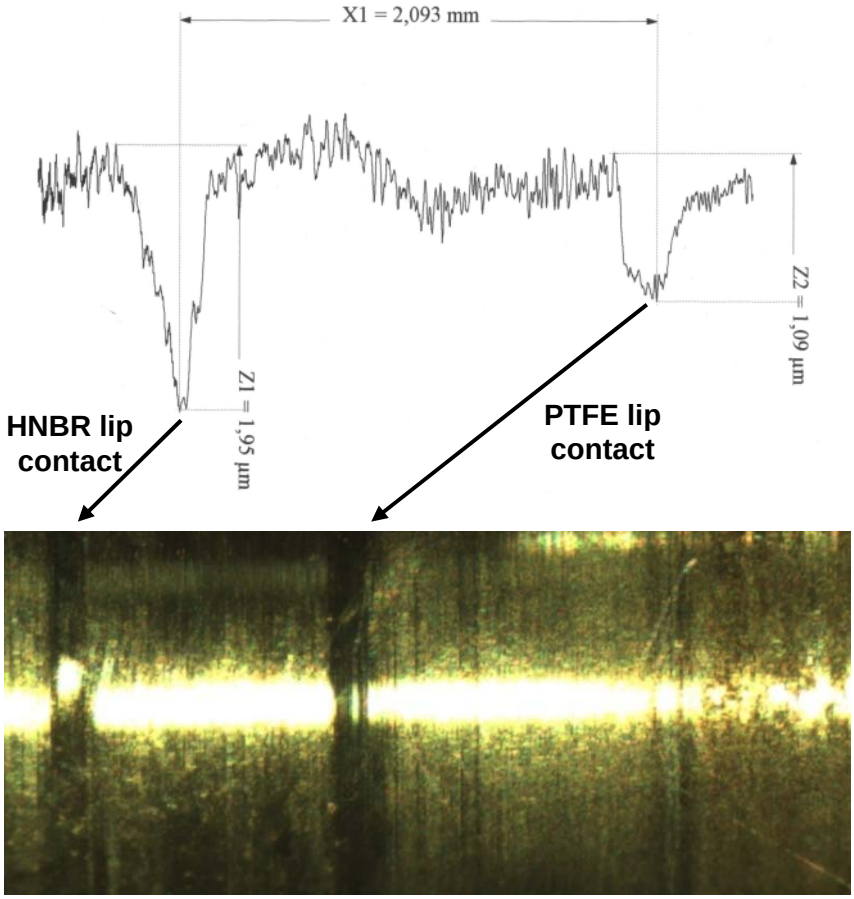

Figure 2-50 Profile of frictional tracks on the surface of a compressor shaft.

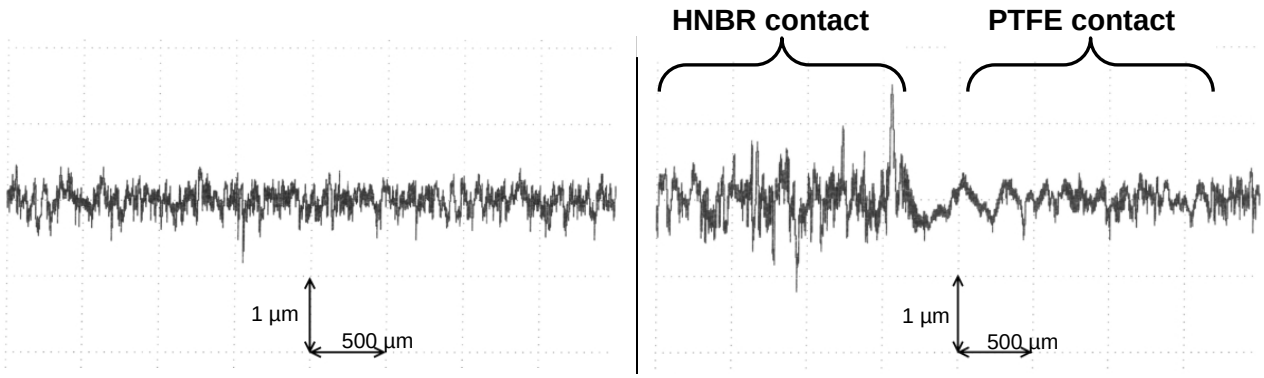

Figure 2-51 a) Roughness profile in the sealing zone of compressor shafts: a) Unused, b) B1.

2.12.4 Polymer transfer

The polymer transfer from the shaft seal lip rings to the shaft surface occurs during the shaft rotation. Figure 2-52 shows the rubber and PTFE transfer to the shaft surface. The transfer will impact the seal performance at different levels. First, it will generate polymer wear debris that will increase the wear rate of lips. Second, the polymer wear debris produced by the rubber lip will be mixed with the fluid, reach the PTFE lip contact, and also increase its wear rate. Finally, the polymer transfer can have a positive effect on gas emissions in standstill mode. By filling the free spaces among the shaft surface asperities, the polymer material deposit will work as a gas barrier by reducing the number and dimension of the gas leak paths.

The polymer deposit is not permanent since the fluid flow through the interface will expel some of the material stocked between the surface asperities, thus loosing the gas barrier effect.

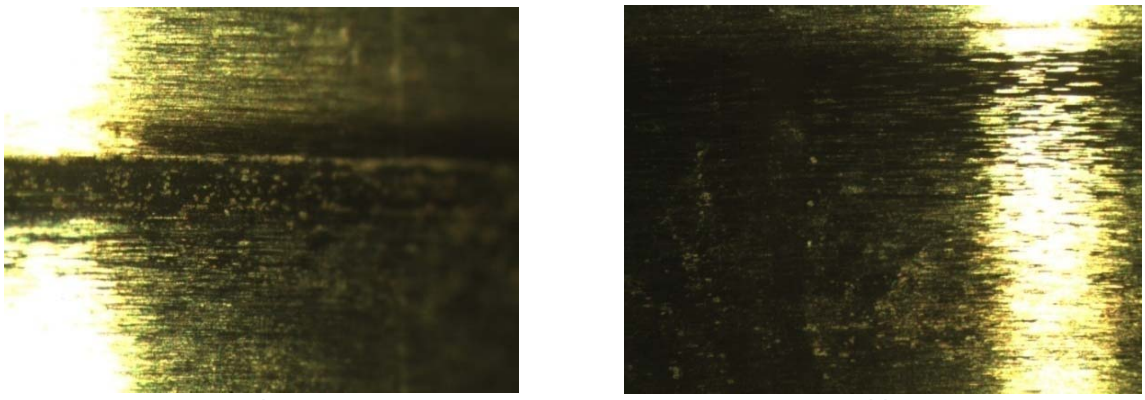

Figure 2-52 Polymer transfer to the shaft surface of compressor B1: a) HNBR; b) PTFE.

2.13. Shaft seal oil leakage

This chapter has shown that the lubricant oil in the shaft seal interface will be expelled by the gas flow when the shaft is stopped. Figure 2-53 shows the seal cases of the two compressors that have been aged, B1 and B2.

a) b)

Figure 2-53: a) Oil deposit near the B1 compressor shaft seal after endurance Step 10; b) Picture of the B2 compressor shaft seal after the endurance Step 7.

Compressor B1 experimented a shaft seal dry running after a long period at rest that proved that the seal contact was dry. During rotation, Compressor B1 presented relatively low LFR values showing that a lubricant film has been built in the shaft seal contact. Furthermore, emission increase of 800% was observed due to the shaft seal wear. The observation of the seal case shows an important oil leakage and proves that:

- Polymer wear debris are expelled by the oil flow,
- The seal contact dries because the oil is transported outside the seal,
- The oil flow ensures the seal correct lubrication thus reducing gas emissions in running mode.

Compressor B2 showed no dry running effect, a small oil effect on gas emissions at rest and high LFR values at rest and when running. The shaft seal degradation due to wear was also observed. The observation of the seal case shows no oil leakage, meaning that:

The oil remains effectively in contact on the shaft, thus maintaining a constant lubrication at rest,

The seal works with an extremely low lubricating film, which explains the high emission rate.

A picture of the compressor C1 seal case is presented in Figure 2-54. C1 is a 10-year old compressor with 300 000 km. The felt ring is oil saturated and the green color is due to the introduction of a fluorescent leak detector dye, miscible with the PAG oil.

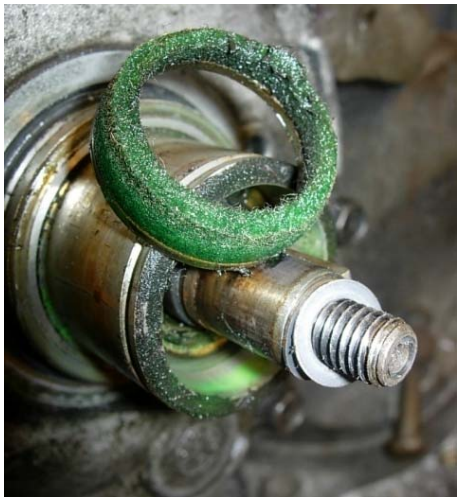

Figure 2-54 Felt ring of aged compressor C1 showing high oil leakage.

These observations show that a relation exists between the oil and the gas leakage. A shaft seal with high oil leakage performs better in running mode due to the formation of a thick fluid film. In standstill mode, gas emissions will be lower due to the gas barrier effect, but it is a temporary effect.

A shaft seal without oil leakage will not produce a thick lubricating film, thus allowing important gas emissions at rest and during rotation. Therefore, a solution must be found to produce a sufficient oil film to lubricate the seal contact during rotation and to work as a gas barrier in standstill mode.

2.14. Conclusions

In this chapter the compressor gas emissions of new and aged compressors have been studied. The compressor tightness has been investigated during the shaft rotation as well as when at rest. Leak sources have been identified:

- the sealing mechanism for the static seal
- The shaft seal for the dynamic sealing.

The new experimental setup has demonstrated that:

- Compressor emissions at rest are directly related to the square of the pressure difference between the compressor housing and the atmosphere,
- After a running period longer than 5 hours, the compressor emissions at rest can be divided by a factor 8 due to the lubricant oil in the shaft seal contact,
- At rest, oil is a barrier to the gas flow through the shaft seal, but it has only a temporary effect,
- After a stop period, the seal contact dries and when the compressor starts working, the shaft seal will run under dry conditions,
- In running mode, the gas LFR strongly depends on the lubricant film thickness in the shaft seal contact,
- LFR in running mode is directly related to the oil viscosity and increases when viscosity decreases,
- Shaft seal dry running is up to 9 times more emissive than under lubricated conditions,
- Shaft seal wear exponentially increases gas emissions,
- This aging process of the compressor leads to higher emissions at rest. It was observed an increase of 800% with compressor B1,
- A dry contact always results in higher emission rates compared to a lubricated one.

In the real life, compressor never runs under steady state oil lubricating regime since it can be achieved only after 15 hours running, thus increasing the shaft seal wear. Aged compressors C1 and C2 show that high emission rates result from the shaft seal wear. Although, the same wear improves the shaft seal lubricating performances, thus lowering emissions in running mode.

The shaft seal oil leakage can be related to the gas emissions. A shaft seal without oil leakage will not produce a thick lubricating film, thus allowing important gas emissions at rest and during rotation. Thick oil film lubrication reduces compressor gas emissions but increases the oil leakage. Therefore, a solution must be found to produce a sufficient oil film to lubricate the seal contact during rotation and to work as a gas barrier in standstill mode.

Next chapter will study the shaft seal in more detail. The shaft seal contribution to the compressor gas emissions in standstill mode will be presented.

2.15. Bibliography

[ACE07] European Automobile Manufacturers Association (ACEA), 2007. European automobile industry report 07/08.

[ASM85] American Society for Nondestructive Testing, American Society for Metals, 1982. Nondestructive Testing Handbook, second edition, volume 1. Robert C; McMaster, 816 P.

[CLO01] Clodic, D, Fayolle, F, 2001. Test-Bench for Measurement of Leak-Flow Rate of Mac Compressors. SAE technical paper 2001-01-0794.

[CLO05] Clodic, D, Palandre, D, 2005. Measurements of Leak Flow Rates of Mobile Air-Conditioning Systems. SAE technical paper 2005-01-1507.

[CLO07] Clodic, D, Yu, Y, 2007. Measurements of Leak Flow Rates of Mobile Air Conditioning (MAC) Components - How to Reach a Generic Approach. SAE technical paper 2007-01-1186.

[CLO96] Clodic, D., 1996. Zero leaks-Limiting emissions of refrigerants. Ashrae. 189 p.

[HAM04] Hamrock, B, Schmid, S, Jacobson, B, 2004. Fundamental of Fluid Film Lubrication. Marcel Dekker, 699p.

[HOR96] Horves, L.,1996 Shaft Seals for Dynamic Applications. Marcel Dekker, 485p.

[ISO93] Guide to the Expression of Uncertainty in Measurement. ISO, Geneva, Switzerland, 1993

[KIS99] Kishibuchi, A, Nosaka, M, Fukanuma, T, 1999. Development of a Continuous Running, Externally Controlled Variable Displacement Compressor. SAE technical paper 1999-01-0876.

[KLA86] Klaus, F, 1986. Friction and wear of polymer composites. Elsevier, 465p.

[MIL96] Miller, E, 1996. Introduction to Plastics and Composites. Marcel Dekker, 434p.

[MUL98] Müller, H, Nau, B, 1998. Fluid Sealing Technology. Marcel Dekker, 485p.

[PAR03] Park, Y, Kang, J, Yoo, J, Lee, J, 2003. Vapor Pressure of the 1,1,1,2-Tetrafluoroethane (R-134a) + Polyalkylene Glycol System. International Journal of Thermophysics, Vol. 25, No.6, November, p1849.

[SAR80] Sarkar, A, 1980. Friction and wear. Academic Press, 423p.

[SKI85] Skinner, T., Swadner, R., 1985. V-5 Automotive Variable Displacement Air Conditioning Compressor. SAE technical paper 850040.

[SOU07] Sousa, D, Clodic, D, 2007. Measurement of Mobile A/C Compressor Fugitive Emissions in Running Mode. 6th EDF-LMS Poitiers Workshop, September 27.

[STA05] Stachowiak, G, 2005. Wear – Materials, mechanics and practice. John Wiley & Sons, 458p.

[TOY07] Annual report, 2007. Toyota Industries Corporation

[YU08] Yu, Y, 2008. Generic Approach of Refrigerant HFC-134a Emission Modes from Mobile Air Conditioning. ENSMP, 179p.

[WAN98] Wandell, E., Dunn, W., Newell, T., 1998. Conditions that Limit Oil Circulation in a Mobile Air-Conditioning System. SAE technical paper 980286.

Chapter 3

SHAFT SEAL REFRIGERANT EMISSIONS

Introduction

In this third chapter, the shaft seal gas emissions in standstill mode are studied. The chapter starts with the description of the components that constitute the seal and their properties.

The study continues with the physical principles of the static sealing mechanism under dry and wet contact conditions. A brief design evolution of the shaft seal, from CFC to HFC compressors is performed.

Section 5 introduces the original experimental setup developed to study the seal gas emissions. Test results of different seal designs with different shaft surfaces under several test conditions are presented in Section 7.

This chapter closes with the seal contact visualization, which shows the deformation of seal components under different gas pressure levels.

3. Shaft seal refrigerant emissions

The shaft seal of current HFC-134a compressors has a unique design. It has been proved to be the most leak prone component of MAC systems (see Chapter 2). However, there are no publications reporting its refrigerant sealing mechanism and performance in order to quantify its contribution to the compressor gas emissions. The intent of this chapter is to determine experimentally the seal refrigerant gas emissions by developing an original test bench. Factors that contribute to the sealing performance will also be analyzed.

From now on, only refrigerant emissions in standstill mode will be studied (no shaft rotation), since they define the compressor gas emissions during its lifetime.

3.1. Shaft seal design

The shaft seal is composed of two sealing components in permanent contact with the shaft surface: the rubber lip and the plastic lip (see Figure 3-1). These two lip rings are bonded to a metallic structure composed of an inner and an outer cases. Peripheral rides or an o-ring are used as a sealing element between the seal metallic case and the housing, which also avoids the seal structure to move when the shaft rotates. To limit the deformation of the rubber lip with pressure, some seal designs incorporate a metallic support ring between the two lip rings.

The shaft seal is placed in the compressor front housing and the rubber lip ring faces the fluid pressure. The rubber lip has a sharp edge to maintain a contact line with the shaft surface. The plastic lip is typically 1-mm thick and contacts axially the surface over 0.5-1 mm.

The compressor is a permanently pressurized component. Therefore, the shaft seal is a static seal when there is no relative motion between the mating surfaces, and a dynamic seal when the shaft is rotating. The two working modes result in a complex sealing mechanism, whose performances vary along the time with the sealing surface wear (see Chapter 2).

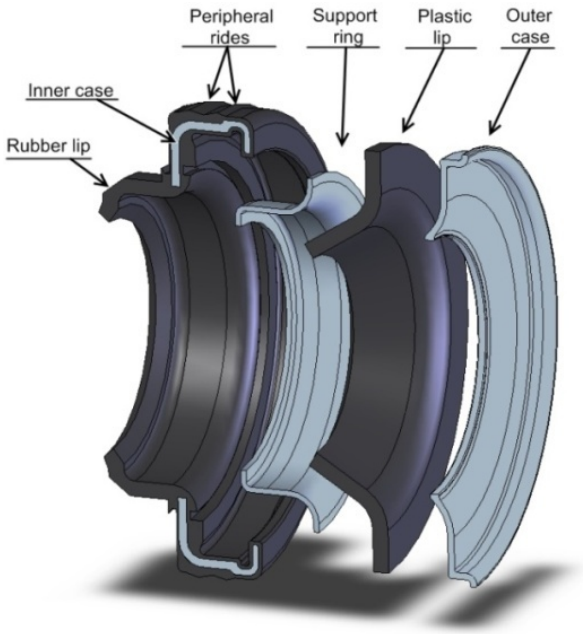

Figure 3-1 Exploded view of a usual shaft seal.

3.1.1 Closing forces

The sealing mechanism is based on the permanent contact between the sealing lips and the shaft during the seal life. The shaft seal lay-out and its sealing element deformation are presented in Figure 3-2. The sealing effect is achieved by the combination of two forces: the preload and the pressure load.

3.1.1.1 Preload

The inner diameters of lip rings, D_p *and* D_{sc}, are smaller than the shaft diameter D_{sh} (see Figure 3-2). On the contrary, the seal case outer diameter D_O is larger than the stationary housing bore D_h. The difference among the shaft seal dimensions, D_{sh} and D_h, is known as interference. When the seal is installed, the lip rings are stretched outward creating an initial contact stress between the lips and the shaft, σ_{r0} and σ_{p0}. At the same time, the peripheral rides are stretched inwardly to fit the housing bore, thus creating the initial contact stress σ_{pr}. If the interference is too small, then the lip contact stress will not be sufficient to leak tight the compressor when under pressure. During the shaft rotation, a small interference can avoid the lips to follow the shaft vibrations and the dynamic run-out. On the other hand, a high interference value will increase the contact stress of lip rings and will create a high under lip temperature, thus increasing the wear rate. The PTFE interference will be of primary importance since the lubricant film thickness varies inversely to the lip pressure load. Therefore, a shaft seal should always be used with the appropriate shaft diameter. A typical value of the shaft diameter tolerance is of ±0.08 mm.

The preload is necessary to ensure the sealing at the lip ring interface regardless of the fluid pressure. To maintain a constant preload around the lip ring mating surfaces and to avoid the angular misalignment with the shaft, the seal should be installed with care and using special tools. When the shaft seal is installed as presented in Figure 3-2, a snap ring is placed in the housing wall to limit the seal axial displacement with fluid pressure.

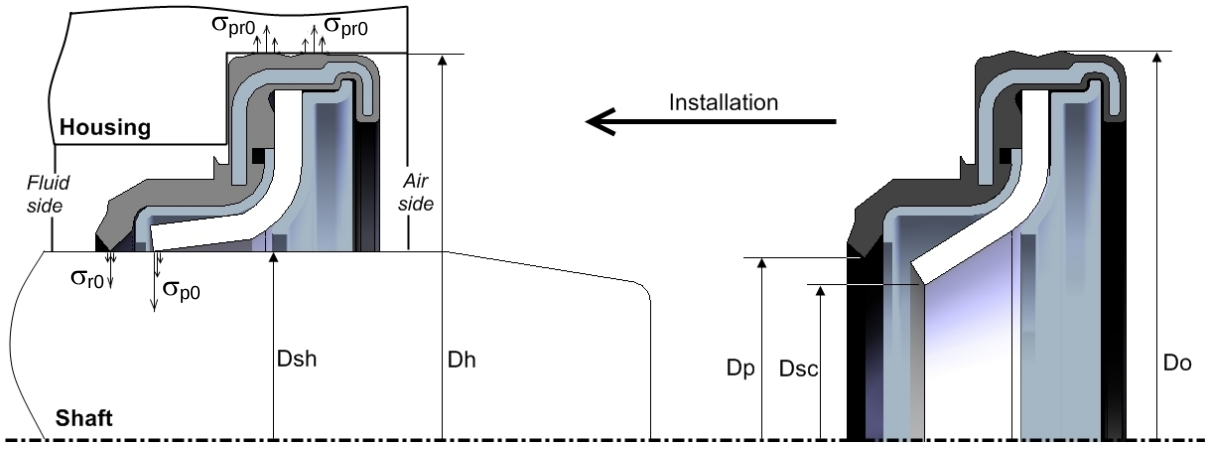

Figure 3-2 Shaft seal installation.

3.1.1.2 Pressure load

The compressor housing pressure acts on the seal. The resultant force will act on the rubber lip and the peripheral rides to complement the preload, thus maintaining a contact pressure higher than the fluid pressure to ensure a permanent contact. This static sealing effect can be easily maintained on the peripheral rides. However, an excessive contact pressure on the lip ring interface will reduce the sealing interface lubrication during the shaft rotation.

Therefore, the rubber lip ring is designed to limit the contact pressure and to facilitate the lubrication. The reduction of the lip load presents some advantages for the dynamic sealing performance (overheat reduction, low wear rate, and energy consumption), but it has a disadvantage for the static seal effect, since the higher the contact pressure, the better the sealing effect. So, a compromise must be found between improved performances at rest or in running mode.

3.1.2 Sealing modes

The shaft seal unique design is related to its ability to seal the fluid (gas + oil) when the compressor shaft is at rest, as well as when it is rotating.

When the shaft is not rotating, the fluid pressure acts on the rubber lip and a narrow contact is created in the sealing interface produced by the elastic deformation of the rubber lip. The resultant contact pressure is higher than the fluid pressure, thus preventing leakage.

When the shaft is rotating, the lubricant reaches the seal and is forced by the gas to enter the rubber lip contact, lubricating it. The oil will then reach the plastic lip to create a hydrodynamic fluid film that lubricates the contact. The fluid film has a double effect. First, it separates the mating faces reducing the surface wear. Secondly, it works as a barrier to the gas flow since it fills up the gap, or irregularities, of the mating surfaces.

In this chapter we will focus on new shaft sealing systems. The seal wear effect on gas emissions has been analyzed in the previous chapter.

3.1.3 Polymeric materials

The seal materials play a crucial role in fluid sealing. The compressor shaft is largely made of polymeric materials. Two different polymers are used in the compressor shaft seal: rubber and plastic. The material compound details are not revealed by the seal manufacturer. However, the name of the base polymer is normally referred to in the literature, but this clearly does not define the polymer material. The shaft seal base polymers are: Hydrogenated Nitrile Butadiene Rubber (HNBR) and PolyTetraFluoroEthylene (PTFE).

The elastic materials have a capacity to store mechanical energy with no dissipation of energy. They also offer a low adhesion, friction, and wear compared to metallic materials. Rubber is used in the shaft seal since it can produce large areas of contact, consequently, improving the gas sealing ability. However, for some elastic materials, the energy used for the deformation is not completely recovered when the load is removed. This is known as the visco-elastic effect, see Figure 3-3. The non elastic deformation of such materials is time-dependent and subjected to hysteresis losses created by the loading variation due to the compressor housing pressure variations. The polymer visco-elastic properties are highly dependent on the temperature and strain-rate evolution. Therefore, for the same contact conditions, the polymer deformation and, consequently, the contact stress will change along the time.

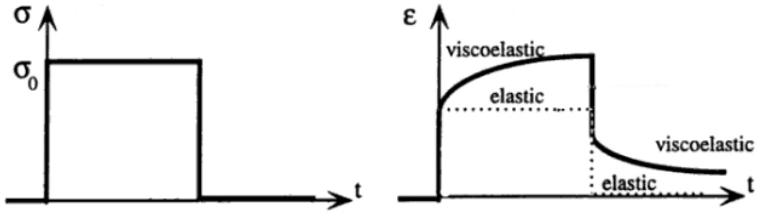

a) b)

Figure 3-3 Visco-elastic effect. a) applied stress and b) resultant strain.

The stress relaxation of polymers is an important aspect of seal tightness. When the seal is under a constant load, the initial contact stress decays along the time, thus the compressive stress drops increasing the seal leak flow rate (LFR).

The static seal effect is performed by the HNBR lip. This rubber material shares two important characteristics:

- Ability to withstand large deformation without rupture, and
- Ability to spontaneously recover their essential original dimensions upon release of load.

The properties of HNBR are mainly determined by the degree of hydrogenation and acrylonitrile (ACN) composition. The stress-strain properties of HNBR improve with the degree of hydrogenation, as shown in Figure 3-4. The glass transition temperature T_g of HNBR of different nitrile contents narrows between -15 and -40°C. T_g should be below the material use temperature.

For the majority of commercial applications, rubbers are used in complex formulations, also referred to as the rubbery system. This formulation includes the rubber (base polymer) with additives, fillers, reinforcing agents, among others, to meet the manufacturing process and the end-use application.

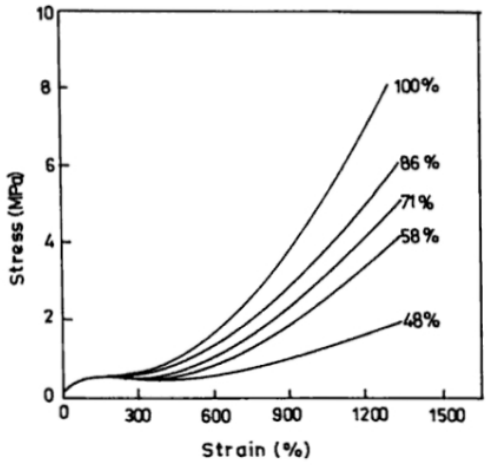

Figure 3-4 HNBR stress-strain curves with different degrees of hydrogenation, ACN = 40%. [CHE93]

3.1.4 Interface characteristics

The tribological contact of a shaft seal is composed of two different materials: polymer and metal. Surfaces of contact materials are described hereafter.

3.1.4.1 Polymer surfaces

Initially, polymer surfaces have a finish given by the manufacturing process. The PTFE surface is designed to improve the seal lubrication during the shaft rotation. One of the techniques to achieve such effect is to create a surface with micro pores that will stock oil improving the seal ability. A picture of a PTFE surface is shown in Figure 3-5a. The micro pores in the PTFE surface make it not adapted to the static sealing effect.

The static sealing effect is achieved by the narrow contact produced by the HNBR lip ring. The smooth surface of this rubber lip, associated with a lip edge high contact stress, produces the seal effect (see Figure 3-5b.

During operation, the profile of polymer surfaces changes due to several factors. The first one is related to the material wear that changes the lip geometry and produces a lip tip pattern with a multitude of micro-cavities. The second one is related to the material compatibility with the fluid to be sealed that can produce the chemical degradation of the base polymer. The heat generation in the seal interface accelerates the degradation processes described here. Therefore, the polymer surface texture changes with time, affecting the contact conditions at the sealing interface and leakage.

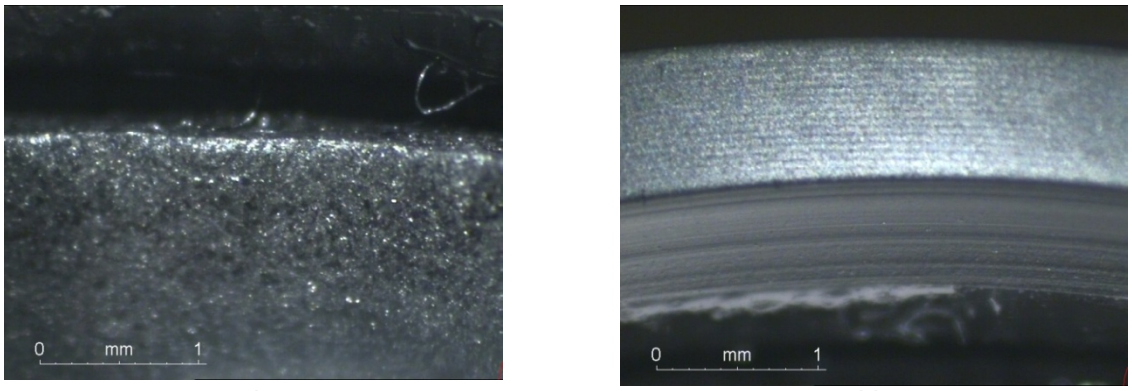

a) b)

Figure 3-5 Surface of lip seals in the contact zone; a) PTFE, b) HNBR.

3.1.4.2 Metallic surfaces

The shaft seal is in permanent contact with two metallic surfaces: housing and shaft. The metallic surface finish is critical to the proper functioning of the sealing system. During the metal cutting operation, a machined surface is created as the result of the tool edge movement relatively to the work piece. The surface condition of a machined part is affected by several cutting parameters such as tool nose radius, depth of cut, speed, feed and rate.

The surface profile or texture, of the machined surface represents the deviation from the nominal surface, the perfect flat surface, and includes roughness (nano and micro-roughness) and waviness (macro-roughness). Roughness is formed by fluctuations of the surface and characterized by hills or bumps, and valleys of short wavelengths. It is intrinsic to the production process. Waviness is the surface irregularity of longer wavelengths and may result from different production factors such as heat treatment, machine or work piece deflections or vibrations, chattering or warping strains.

The lay is also an important surface texture characteristic. It defines the principal direction of the predominant surface texture and is determined by the production method. Flaws are an additional deviation from the nominal shape and consist of unexpected and unwanted interruptions on the surface texture. Therefore, a machined surface texture is very different from the nominal surface. The metallic surface imperfections create channels to the gas flow: the higher the imperfection dimensions, the higher the gas leak rate.

The height parameter R_a, which is also known as center line arithmetic average, and the ten points height R_z are the most critical surface texture characteristics, although they are not sufficient to the complete characterization of a surface profile used in sealing technology. The R_a value is primary concerned with the vertical direction profile only; it omits the

information about waviness and the size of asperities. Additional surface roughness parameters should be recommended by seal manufacturers.

The shafts used in oil applications are generally made by plunge grinding since this manufacturing process produces a surface profile with low-lead generation, thus proving to be a reliable method for oil sealing applications. Hard turning has been acknowledged as an alternative to the plunge grinding manufacturing process. It presents the advantage of eliminating the hardening process, reducing the production costs [KUN05].

Imperfections and features of a real surface are crucial to the sealing performance, although the texture of the shaft surface is continuously changing. After the seal has run for a period of time, the shaft surface topography changes as shown in the previous chapter.

3.1.5 Permeation

Any polymeric material, when exposed to a pressure gradient, allows the transport of gas molecules through it as the result of intermolecular spaces or porosity. The movement of the gas molecules through the polymer, known as permeation, takes place in three stages: in the first stage, the gas dissolves into the polymer surface, then it will diffuse through the material due to the concentration gradient and, thirdly, it will evaporate at the low pressure polymer surface.

The diffusion process is described by the Fick law, Equation 2.4. The gas LFR, which is the ratio of the quantity of gas Q that goes through a membrane along the time t, is proportional to the permeability coefficient P_e, the membrane area exposed to the gas pressure and to the pressure difference through the membrane ΔP of thickness e.

3.2. Static interface sealing mechanism

When two surfaces are in contact, the surface roughness causes the contact in small areas distributed randomly (see Figure 3-6). Analytical studies and measurements show that areas of all contact spots and the real area of contact, are a small fraction of the nominal (apparent) area of contact W that would occur if surfaces were perfectly smooth [BHU99] [ILI80] [ZAM98]. The contact regions are recognized as being the small areas where asperities from one solid are squeezed against the asperities of the other solid. The free spaces among the contact surface asperities create tortuous paths to the fluid flow under a pressure gradient. The real contact area depends on the surface profile, properties of materials and interfacial loading conditions.

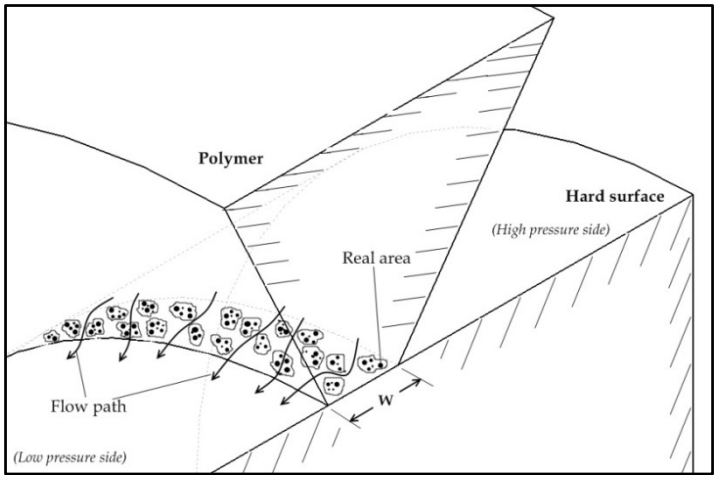

Figure 3-6 Leak paths in the contact between two round surfaces.

For elastic deformation at individual contacts, the contact area can be approximated by the Hertz analysis. If the contact asperity is modeled with two spheres, radius r_1 and r_2, in a solid contact with an applied normal load P_i, the resultant contact area is circular with a radius *a* and an elliptical contact pressure *p*. From the Hertz analysis, the contact radius is given by:

$$a = \frac{\pi pr}{2E_e} = \left(\frac{3P_i r}{4E_e}\right)^{1/3} \tag{3.1}$$

The corresponding area of contact is

$$A_i = \pi a^2 \tag{3.2}$$

The composite modulus is

$$E_e = \frac{1-\upsilon_1^2}{E_1} + \frac{1-\upsilon_2^2}{E_2} \tag{3.3}$$

The composite curvature

$$\frac{1}{r} = \frac{1}{r_1} + \frac{1}{r_2} \tag{3.4}$$

Parameters E and υ are the Young modulus of elasticity and the Poisson ratio, respectively. Subscripts 1 and 2 refer to the two spheres.

From Equations 3.1 and 3.2, it can be assumed that the area of contact increases with the applied normal load and decreases with the composite modulus. The rubber-like materials are characterized by a high Poisson ratio with a low elastic module resulting in a small composite modulus value when compared to a hard material. Therefore, the contact between a polymer material and a hard sphere will produce a higher contact area comparatively to the contact between two metallic spheres. Accordingly, the use of polymeric materials in a sealing system will reduce the difference between the real and the apparent contact areas, thus reducing the leak path dimensions and the leak flow rate.

There are two classes of properties to characterize the tribological contact: material deformation and surface topography. The time-dependent properties of polymers are not sufficient to set the real contact area equal to the nominal contact area. Therefore, the formation of leak paths is inevitable. Consequently, the shaft seal will always leak at a certain level, the issue being to limit the leak to the lower possible level.

The interfacial flow paths have very complex shapes. To make easier the gas flow study through the contact, the flow paths are assumed to be micro-channels with constant diameter ranging from 1 to 10 µm. The conditions encountered in a MAC compressor shaft seal interface result in a laminar viscous flow, which is defined by the Poiseuille law, see Section 2.3.

The Poiseuille law, Equation 2.3, establishes that the leak flow rate through a circular channel is directly proportional to the channel radius to the power of four and to the square of the pressure difference that causes the flow. The LFR is also inversely proportional to the leak tube length. Therefore, a tight static seal has to provide a wide contact surface with the shaft combined with a high load.

As mentioned before, the difficulty of the rubber lip design relies on the shaft seal double working mode, static and dynamic operations. The contact conditions that improve the static

seal effect will wear the seal tip prematurely. Accordingly, there must be an improved solution knowing that the shaft seal is 95 to 98% of its lifetime at rest and the fluid pressure during rotation is usually lower than at rest.

3.3. Wet contact

The shaft seal contact cannot be considered as permanently dry. The oil brought to the contact by the shaft rotation impacts the seal performance at rest. Experiments described in Chapter 2 have shown the oil effect on the seal static performances. The resultant reduction of gas emissions is explained by the spreading of the lubricant liquid flow throughout the interface.

When two surfaces are in contact and in the presence of a liquid film, the interface is not instantaneously in equilibrium. The liquid flow will spread over the surfaces during a certain time creating attractive forces with the surfaces until equilibrium is reached. The liquid spreading is driven by different mechanisms such as the surface tension gradients or the surface diffusion of liquid molecules. The liquid diffusion and attractive forces will reduce the refrigerant gas flow through the seal interface since the leak path number and dimensions are reduced.

3.3.1 Surface tension

If a liquid drop is placed on a solid surface, the liquid and the solid surfaces will come together at a characteristic angle called the contact angle or wetting angle θ (see Figure 3-7). For a liquid film on a solid surface, the wetting angle will also depend on other factors such as, the surface texture and the degree of oxidation.

Surface tension of liquids depends on the position of molecules in the interface liquid/solid. This surface tension is responsible for many remarkable properties of liquids, such as, the capillary action, the formation of spherical drops and bubbles, and the meniscus formation.

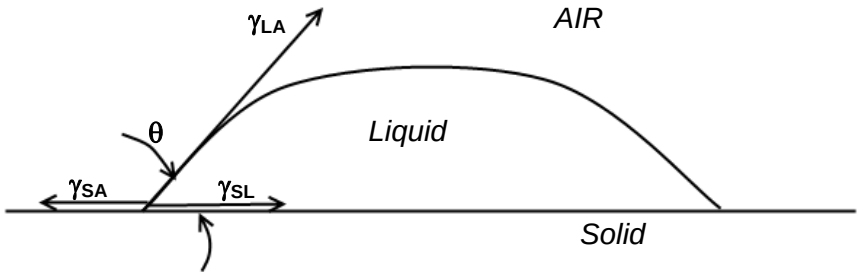

Figure 3-7 Liquid drop on a solid surface.

The surface tension for liquids γ, expressed in mJ/m^2, is the reversal work *W* required to create a unit area of surface A, at constant volume, temperature, and chemical potential, and is defined by:

$$\gamma = \frac{dW}{dA} \tag{3.5}$$

The surface tension is extremely important in adhesion since it defines the work of adhesion between the two surfaces. When a solid is in contact with a liquid, the molecular attraction across the interface can be expressed by the Dupré equation:

$$W_{SL} = \gamma_{SA} + \gamma_{LA} - \gamma_{SL} \tag{3.6}$$

W_{SL} is the work of adhesion per unit area between the two surfaces. γ_{SA} and γ_{SL} are the surface tensions of the solid against air and liquid, and γ_{LA} is the surface tension of the liquid against air. At the contact perimeter, the mathematical representation of the surface tensions can be expressed by Young equation:

$$\gamma_{SA} = \gamma_{SL} + \gamma_{LA} \cos\theta \tag{3.7}$$

This expression is applicable to $-1 \leq \cos\theta \leq 1$. By associating Young and Dupré equations, we obtain the expression of the work of adhesion, called the Young-Dupré equation:

$$W_{SL} = \gamma_{LA}(1 + \cos\theta) \tag{3.8}$$

The work of adhesion defines how a liquid spreads over a surface, known as wettability.

3.3.2 Wettability

Wettability is a term used to indicate how easily a lubricant will spread or flow over any surface and implies a contact angle θ between 0° and 90°. When θ is equal to 0°, the liquid will flow over the surface, thus improving lubrication. If θ is greater than 90°, then the liquid does not wet the surface, thus reducing the contact lubrication ability. Consequently, the liquid will spread when θ is equal to 0°: $W_{SL} = 2\gamma_{LA}$.

A liquid placed on a surface may be washed-out due to its small relative tangential displacement in a contacting area, called micro-slip. A high work of adhesion is achieved with a liquid of very low surface tension that increases the micro-slip. A lower value of W_{SL} is desirable for retarding spreading, thus reducing the oil transport through the seal contact in standstill mode.

3.3.3 Meniscus formation

When a liquid with a small contact angle is introduced between two contacting surfaces, it will go into surface cracks and pores and an oil meniscus may be formed around the asperities contact, see Figure 3-8. The meniscus can be assimilated to adhesive bridges formed by the proximity of two surfaces and the affinity of these surfaces to the liquid. The oil meniscus can be formed around an asperity contact, as well as around asperities that are in a closer contact. The meniscus formation can increase significantly the adhesion between surfaces. The adhesive force depends on:

- meniscus forces due to the surface tension, and
- viscous forces.

The small gaps and smoother surfaces increase the adhesive forces, thus reducing the oil transport through the seal interface in standstill mode.

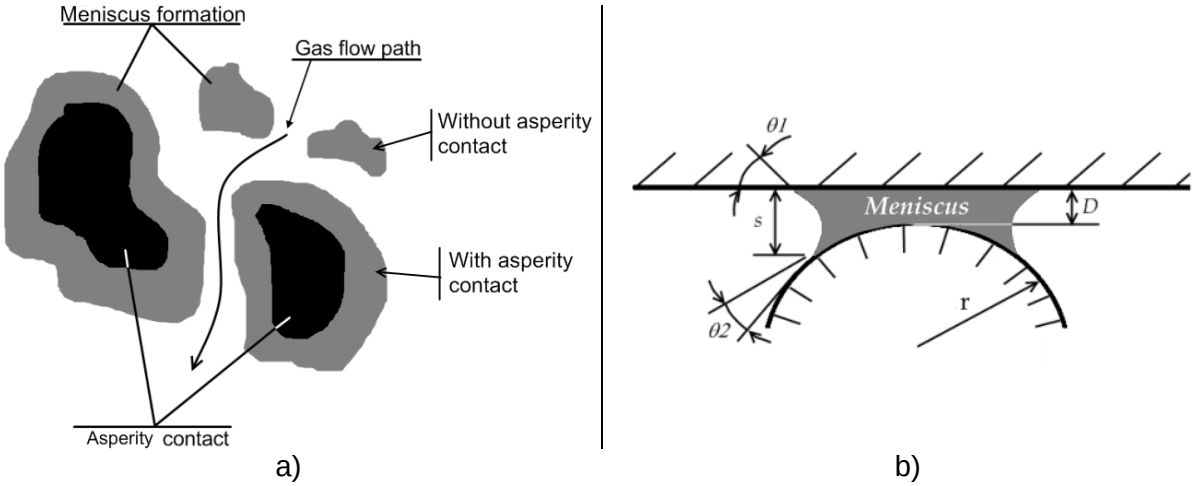

Figure 3-8 a) Meniscus formation around contact and non-contact asperities, b) meniscus attractive force parameters between a sphere and a plane surface.

The surface tension creates a pressure difference across the meniscus area, known as Laplace pressure. The resultant attractive force F_L depends on the geometries of asperities, the liquid surface tension, and the contact angle with the two surfaces. If we consider contact geometry between a sphere and a plane surface, as represented in Figure 3-8b, the meniscus attractive force is:

$$F_L = \frac{2\pi\, r\gamma_{LA}\,(\cos\theta_1+\cos\theta_2)}{1+{}^{D}/_{s}} \tag{3.9}$$

Where r is the sphere radius, γ_{LA} is the surface tension of the liquid, θ_1 and θ_2 are the contact angles between the liquid and the two surfaces, D is the surfaces separation, and s is the meniscus height. The maximum attraction force occurs when the asperities are in contact, D = 0 where the attraction force is independent of the liquid quantity. The higher the attractive force, the higher the duration of the shaft seal oil effect.

3.4. Design evolution

In the 80's, the shaft seal used in CFC-12 MAC compressors derived from other mechanical systems where rotating shafts required the leakage control of a pressurized fluid. Such operating conditions were usually found in process pumps, machine tools and gearboxes, among others. The shaft seal used in those machines was formed by the axial contact of two hard materials and is known as mechanical seal (see Figure 3-9).

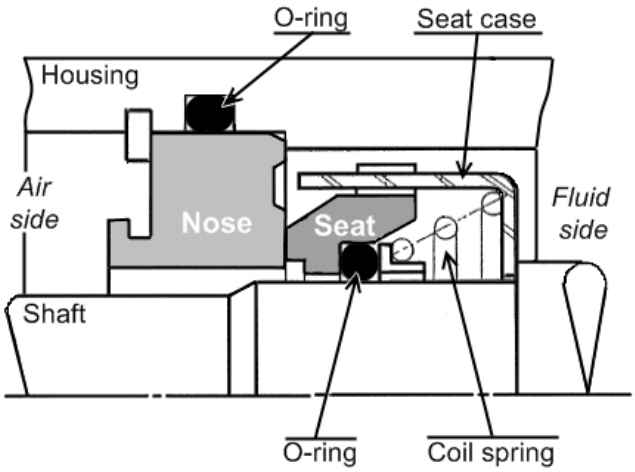

Figure 3-9 Mechanical seal used in MAC compressors.

The mechanical seal is an axial contact seal installed around the drive-shaft and is composed of a primary and a secondary seals. The primary one is a dynamic seal composed of two hard materials, the seat and the nose rings. The nose is a stationary fixed ring mounted on the compressor front housing. The seat ring is a floating ring that is mounted on the shaft and spring loaded to preload the rings. The seat ring is made of a harder material than the nose. The secondary seals are static seals, usually o-rings, installed between the primary seal and its support.

At rest, the nose and the seat rings are in mechanical contact, as well as the secondary seals, thus preventing the fluid leakage. However, when the seat rotates with the shaft, complex tribological interactions occur between the sealing faces and the fluid to be sealed.

During compressor rotation, the fluid, which is a mixture of oil and refrigerant gas, reaches the ring contact and penetrates the interface to establish a lubricant film. As the fluid flows through the interface, the fluid pressure drops progressively until reaching the atmospheric pressure at the air side. This hydrostatic pressure depends only on the pressure difference and the interface geometry. The seat ring rotation makes the fluid interact with the interface surfaces, creating a hydrodynamic pressure. The combination of the hydrostatic and the hydrodynamic effects produces a force component capable of splitting the mating surfaces creating a constant oil film typically of 1 μm. Accordingly, the seal will theoretically operate in a non-contacting condition that controls the fluid leakage, as well as the rings friction and wear.

The mechanical seal performance has been studied by different authors [LAB82] [SHI87] [SHI90] and was focused on the running mode scenario. The seal performance at rest has not been reported because the mechanical seals have been originally developed for applications where the fluid pressure difference only exists when the shaft rotates. The research activity was also more oriented to the oil leakage.

However, the fluid film formation in the seal interface is not always sufficient to avoid the metallic contact resulting on the surface wear and heat generation. The consequence is the modification of the mating surface textures as wear goes on. Formation of cracks and waves on the seal surfaces have been reported by different researchers [LAB82] [SHI87] and identified as the origin of important fluid leakage that can lead the compressor to break down due to the lack of refrigerant and lubricating oil.

In a mechanical seal, the primary sealing effect is achieved by the contact of two relatively hard surfaces. Considering the relatively low seat load, the resultant real contact area is

expected to be very low, thus producing numerous flow paths in the interface. Moreover, the flow path dimensions are expected to grow significantly with the wear of mating surfaces resulting in high refrigerant gas and oil leak flow rates, with a negative impact on greenhouse gas emissions and compressor performances.

The poor performance of mechanical seals led the seal manufacturers to develop a more reliable and tighter sealing system. In 1986, a new shaft seal concept has been presented by NOK Corporation Japan to reduce fluid emissions in running mode, as well as at rest. This new compact seal is represented in Figure 3-10 in its free position.

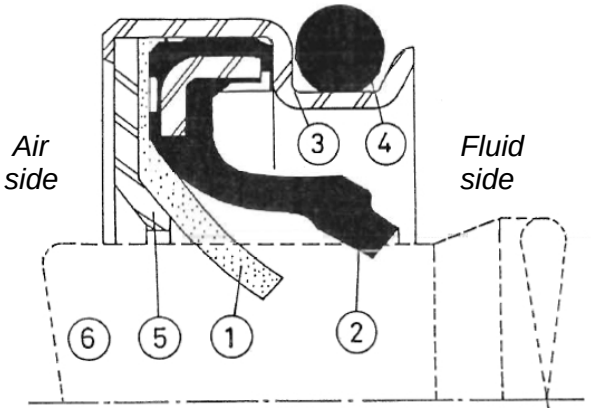

1 – PTFE lip ring
2 – Rubber lip ring
3 – Metallic case
4 – O-ring
5 – Holder case
6 – Shaft

Figure 3-10 MAC compressor lip-type seal initial concept [OHT86].

The lip-type seal was developed based on the PTFE seals used for oil applications. The PTFE lip *1* has been assembled with a rubber lip *2* in a rigid case *3*. The rubber lip has been used to help the PTFE lip to retain the fluid. A secondary seal is placed in the outer metallic case to seal the fluid between the compressor housing and the seal case. The major advantage of the lip-type seal compared to the mechanical seal was the reduction of gas leakage at rest [OHT86].

In 1989, the formation of cracks after a running period on the rubber lip edge has been reported [SHI89]. The destruction of the rubber lip contact was related to a large contact width with the shaft surface, which increases with fluid pressure and PTFE wear. This phenomenon was accelerated by the introduction of the variable displacement compressor, see Section 2.1, which increases the fluid pressure acting on the seal under certain operating conditions. The solution adopted by the seal manufacturer was to diminish the rubber lip contact width in order to reduce friction, thus decreasing the heat generation. Therefore, a support ring has been introduced between the two lips to control the rubber lip deformation (see Figure 3-1). Another positive effect of the support ring is the reduction of PTFE pressure load lowering the lip wear.

Since its introduction in 1986, the lip-type seal has proved to be the most appropriate shaft sealing technology for MAC compressors [CHI91]. Therefore, it has been adopted by the compressor manufacturers as the standard shaft seal for CFC-12, as well as for HFC-134a compressors.

After 1991, there is no published work concerning the oil and/or gas emissions from the compressor shaft seal. However, the design changes can be checked by looking at the seal patents. Almost all the shaft seal inventors had based their work on the seal design presented in Figure 3-10. Although, they work the shaft seal design and materials in order to improve the fluid emissions in running mode, the shaft seal emissions when the compressor is at rest are rarely mentioned.

To enhance the seal performance when the shaft rotates, some patents present a PTFE lip ring with spiral grooves that is believed to improve the seal performance by increasing the dynamic sealing mechanism [OBA99] [KAW00]. Helical grooves and irregularities were also introduced in the rubber lip contact surface to allow the oil leakage to the PTFE lip, thus improving the lubrication [YAM03a] [YAM03b] (see Figure 3-6a). The rubber lip lubrication is very important since it will affect the lip edge wear by reducing the friction coefficient.

The rubber lip design has been the main development issue. Different lip edges have been presented with the intent to reduce the contact pressure with the shaft to control its deterioration through use. Yamada [YAM03] has introduced grooves and undulations on the seal lip rings to improve oil lubrication during the shaft rotation (see Figure 3-11a). Kawagushi [KAW00] has increased the contact width of the rubber lip edge to a value higher than 0.6 mm to displace the maximum contact stress σ_{r0} to the low-pressure side and enhance the oil circulation to the PTFE lip. A different concept has been used by [HOS05] and [OSA05] to reduce the contact stress by the redesign of the rubber lip (see Figures 3-11 b and 3-11c). The first author introduced a concave element that will create a radial force opposite to the fluid pressure to reduce the contact pressure. The second author creates a hollow lip that will be elastically deformed by the refrigerant pressure, which results in a lip radial force reducing also the contact pressure. In 2006, Hosoi [HOS06] has coated the rubber surfaces that face the fluid with a soft material, such as tin. The rubber lip coating will reduce the material permeability to the refrigerant gas.

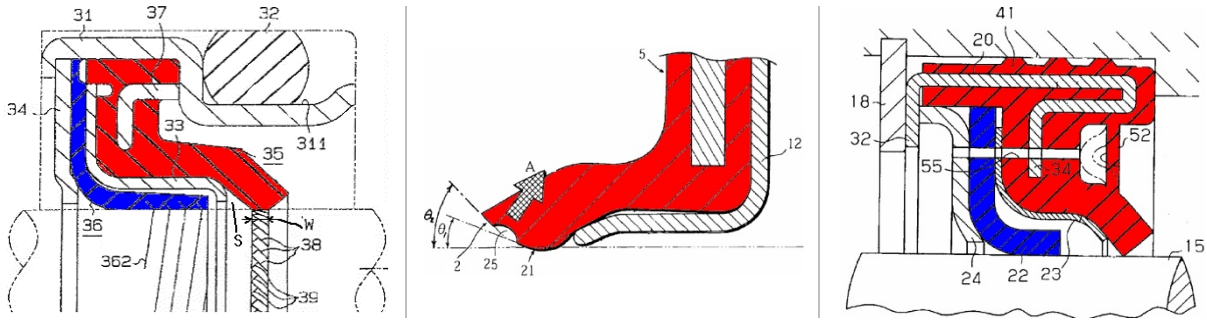

a) [YAM03] *b) [HOS05]* *c) [OSA05]*

Figure 3-11 Different lip-type seal concepts.

The development of carbon dioxide compressors is leading engineers to adapt the shaft sealing system to a high pressure gas. The new concept is based on the metal-to-metal contact, the mechanical seal [OTF03] [FRE05], used in the 80's with CFC-12 compressors and presented above. However, this sealing system presents high LFR values due to the combination of a low contact pressure with a high wear rate. Therefore, high CO_2 gas emissions are observed nowadays mainly during the compressor standstill mode. There is still a long development work to accomplish for CO_2 compressor shaft seals. This study deals only with the shaft seal designs used in HFC-134a compressors working under much lower pressure levels.

3.5. Shaft seal experimental setup

An original experimental setup has been developed in order to study the shaft seal gas emissions in standstill mode. This new apparatus has been developed to analyze different shaft seal designs, as well as shaft materials and roughness values in order to evaluate their impact on gas emissions. This experimental setup uses additionally a transparent shaft coupled with an image recording system to visualize the contact between the seal lip rings and the shaft surface.

3.5.1 Layout

The experimental setup (see Figure 3-12) is composed of two stainless steel chambers with rigid walls: at the right side the refrigerant chamber and, at the left side, the accumulation chamber. The shaft and the seal to be tested are installed between the two chambers. Therefore, the refrigerant gas that will flow through the seal will be recovered and accumulated in the right side chamber. The refrigerant gas concentration in the accumulation volume is measured by an infrared gas analyzer. The refrigerant properties are controlled by a heated refrigerant boiler and a heater placed in the high-pressure chamber to control the fluid pressure and the seal temperature independently.

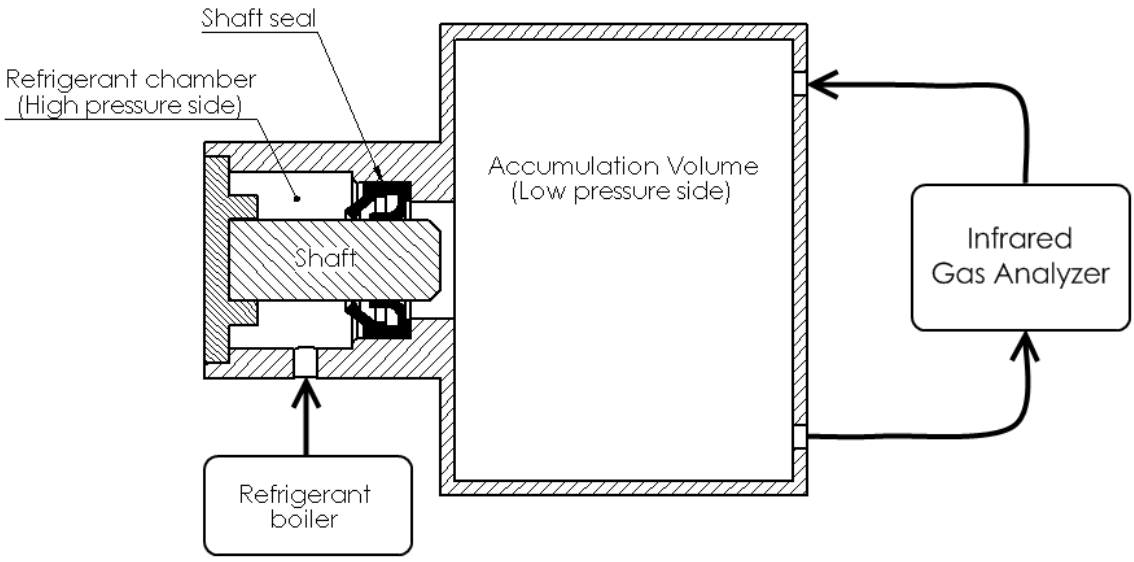

Figure 3-12 Experimental setup to study the shaft seal refrigerant emissions in standstill mode.

This experimental setup is designed to use not only the compressor original shaft, but also other manufactured shafts. A special shaft has been designed to allow the visualization of the shaft seal contact with the shaft surface. The shaft has been machined and polished to the same diameter as the application shaft. A chamfer is provided at the shaft end to protect the seal during the installation. The stainless steel shaft represented in Figure 3-12 has been replaced by a Poly-methyl methacrylate (PMMA) shaft, which is a transparent plastic acrylic material when polished that can be easily manufactured and used to replace the glass. The transparent shaft has a central hole to put in an endoscope to see the contact condition of the seal lip rings (see Figures 3-13a and 3-13b).

Accordingly, the experimental setup is composed of (see Figure 3-14):

- the refrigerant concentration measuring system where the seal to be studied is installed,
- the gas analyzer, and
- the visualization system.

The refrigerant concentration measuring system is composed of the refrigerant/seal chamber, at the front position, and the accumulation volume at the back position. The refrigerant chamber has an external heating system, comprising an axial fan and a heater, to control the gas refrigerant temperature, thus avoiding the refrigerant to condensate inside the seal chamber. A refrigerant boiler controls the refrigerant pressure and is installed under the experimental setup (not shown in Figure 3-14). The accumulation volume is a hermetical cylinder with an external mixing axial fan. Pressure and temperature sensors are used to monitor the tests. The refrigerant concentration measuring system includes a refrigerant

recovery unit and a vacuum pump to evacuate the seal chamber and the accumulation volume.

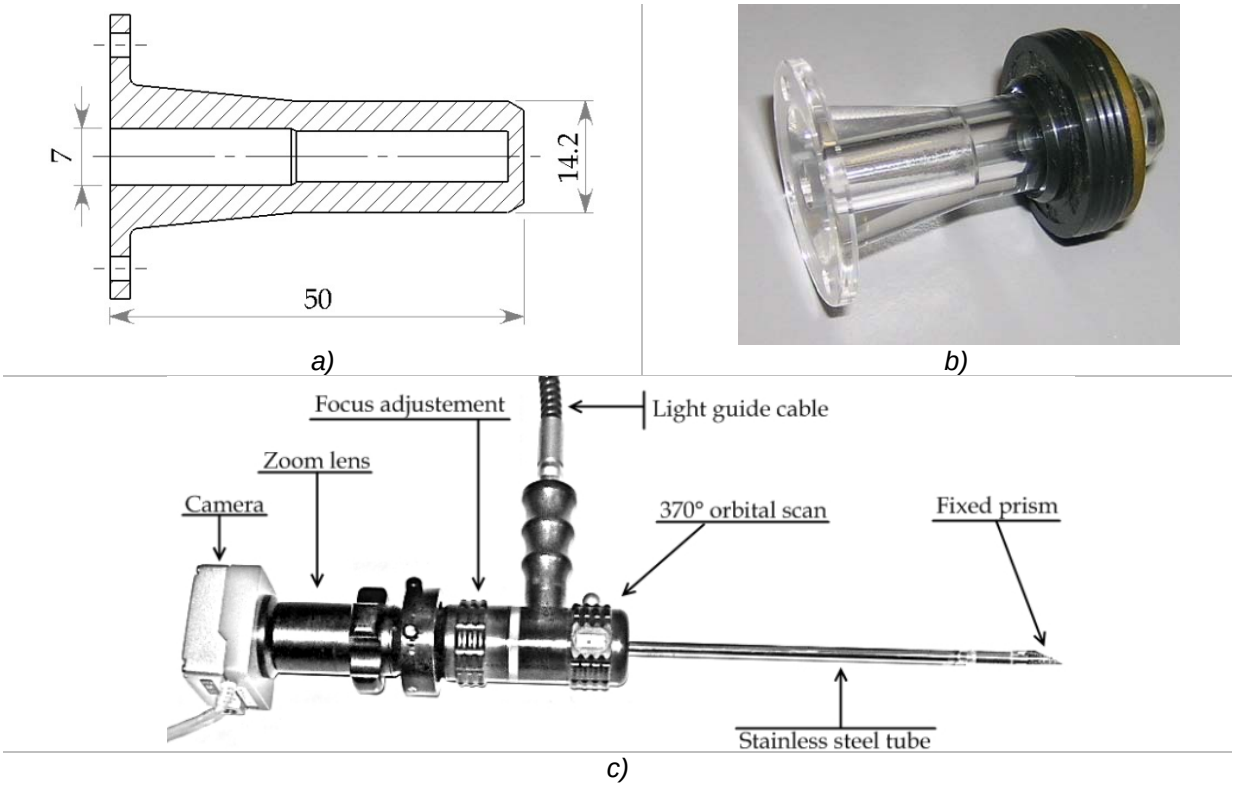

Figure 3-13 Shaft seal contact visualization system; a) sectional view and b)picture of the polished shaft; c) endoscope assemblage.

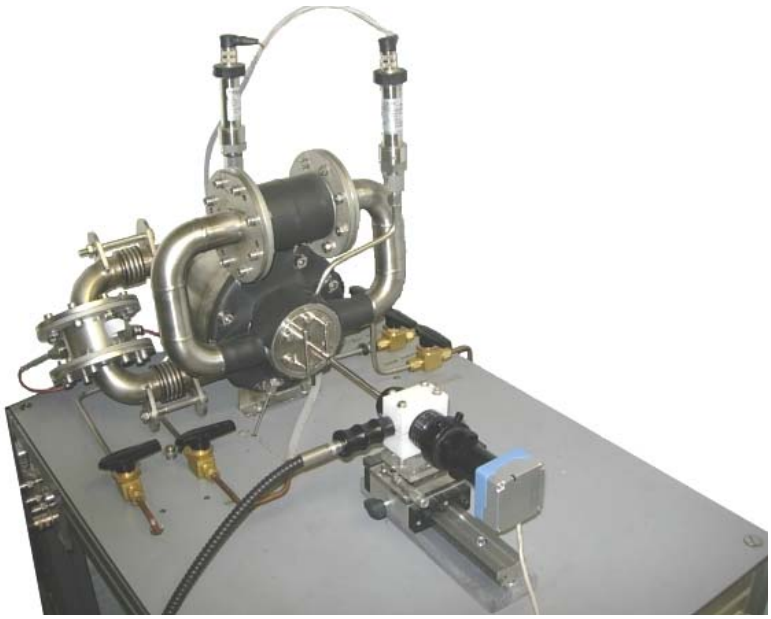

Figure 3-14 Experimental setup to study the shaft seal refrigerant emissions in standstill mode.

3.5.1 The visualization system

The visualization system is composed of a rigid endoscope, a light source, a zoom lens, and a video camera (see Figure 3-13c). The endoscope is a 6-mm diameter metal tube that incorporates a multiple-element relay lens to bring image and light, in separated channels, to the seal contact. The prism built in the steel tube sets the direction of view to 66° to an 80° overall viewing field. The view direction has been chosen to have the best image clarity. The prism can rotate 360° to inspect all around the seal lip contacts.

A video camera based on the Complementary Metal Oxide Semiconductor (CMOS) image sensor technology is used to capture images digitally with a resolution of 2.0 megapixels. The camera is connected to a zoom lens with adjustable focus coupled to the endoscope (see Figure 3-13c). This visualization system will be inserted in the transparent shaft central hole to record the seal lip rings deformation with pressure.

The visualization system is placed outside the experimental setup and in the seal chamber axis. A linear displacement system composed of a guide table sliding on an aluminum rail and a manual linear stage with a precision adjustment screw are used to place the endoscope viewpoint. The video camera is connected to a desktop PC to record the endoscope image.

3.5.3 The gas analyzer

The infrared spectrophotometer used in the compressor experimental setup presented in Chapter 2 and described in Section 2.4 is used to determine quantitatively the gas concentration inside the accumulation volume. The pressure and temperature sensors, as well as the refrigerant gas concentration, are connected to a programmable automation controller from National Instruments® and recorded by a LabWindows/CVI® program. The shaft seal leak flow rate is calculated using Equations 2.11 and 2.12.

3.5.4 Uncertainty analysis

The leak flow rate uncertainty value differs from the one of the compressor experimental setup, since the internal volume of the accumulation chamber is different. The volume is calculated by replacing the refrigerant chamber by a calibrated leak. The small accumulation volume will reduce the measuring time, thus increasing $u(^{\partial C}/_{\partial t})$. On the other hand, as the calibrated leak is placed outside the volume, the uncertainty due to the reservoir volume of the calibrated leak is not considered. Moreover, the seal to be tested is outside the accumulation volume, so there is no uncertainty due to the component volume. The volume is then calculated using a relatively low LFR, 6.7±0.3 g/yr at 20°C, to increase the measurement time. Therefore, by knowing the volume pressure and temperature, the reservoir leak flow rate and the gas concentration evolution with time, it is possible to calculate the accumulation chamber volume by using Equation 2.12. The volume combined standard uncertainty is:

$$\frac{u_{V_{ac}}}{V_{AC}} = \sqrt{\left(\frac{u(T_{amb})}{T_{amb}}\right)^2 + \left(\frac{u(P_{amb})}{P_{amb}}\right)^2 + \left(\frac{u(\dot{m})}{\dot{m}}\right)^2 + \left(\frac{u(^{\partial C}/_{\partial t})}{^{\partial C}/_{\partial t}}\right)^2} = 5.0\% \qquad (3.10)$$

The seal gas leak flow rate is calculated using Equation 2.14. Accordingly, the uncertainty of the seal leak flow rate is set to 5.2%. As explained in Section 2.5, the volume uncertainty defines the leak flow rate uncertainty.

3.5.5 Test procedure

The seal to be tested is inserted in the refrigerant chamber using a special installation tool to prevent the seal damage and the angular misalignment between the seal and the shaft. The refrigerant chamber and the accumulation volume are evacuated to 10 Pa abs. The accumulation volume is filled up with N_2 / O_2 (80 / 20%) and connected to the gas analyzer. The shaft seal is put under pressure by the external refrigerant boiler, which is heated to control the refrigerant pressure. The refrigerant chamber is heated just above the saturating temperature to avoid refrigerant condensation.

Before the gas concentration measurement, the seal is pre-conditioned during 72 hours at 55°C with a refrigerant pressure value set to 1320 kPa. The pre-conditioning process allows reaching steady state conditions of permeation through polymer materials.

Once the refrigerant chamber is at the temperature and pressure preset values, the gas analyzer will continuously measure the gas concentration in the accumulation volume. The continuous measurement allows identifying and quantifying any gas flow transitory phenomenon through the seal.

When a transparent shaft is used, the inspection system endoscope is inserted in the shaft and axially blocked. The video camera will record not only the lip ring contact surface, but also the rubber lip deformation with pressure.

3.6. Tested shaft seals

Different seal designs are available on the market. For this study, five different shaft seals from an original equipment manufacturer have been bought as spare parts and have been chosen considering the most recent designs for HFC-134a compressors. The selected shaft seals sectional view and the disassembled parts are presented in Figures 3-15 and 3-16 respectively.

3.6.1 Designs

Shaft seal samples A to E are made from the assembly of two lip rings and peripheral rides with a metallic structure. Main differences among these seals are: the rubber lip design and the use of a metallic part between the rings. Sample A is constituted of three parts only and has a very sharp rubber edge. Samples B and C incorporate a metallic washer between the rubber and PTFE lip rings. A separating part is used in samples D and E as well, but with a longer profile to support the rubber lip and to reduce its deformation with pressure. However, sample D has a longer rubber lip and its support ring covers only half of the lip compared to sample E, where the rubber lip is entirely sustained by its support (see Figure 3-1).

As explained in Section 3.1, the rubber lip edge is designed to generate a high contact stress on the shaft surface in order to leak tight the refrigerant gas. The contact stress value and distribution depend on the fluid pressure, the rubber lip position and the contact surface with the shaft surface. The two last factors will be defined by the lip deformation which, for the same fluid pressure, will be different for these five samples.

The shaft seal gas emissions are defined by the permeability of materials, as well as the contact conditions between the hard asperities and the rubber material. As previously described, the differences between these shaft seal designs are neither the materials nor the seal housing interface, but the contact interface of lip rings. Consequently, the differences of shaft seal leak flow rates result only from the contact conditions of lip rings with the shaft surface.

Figure 3-15 Sectional view of the shaft seals used in this study.

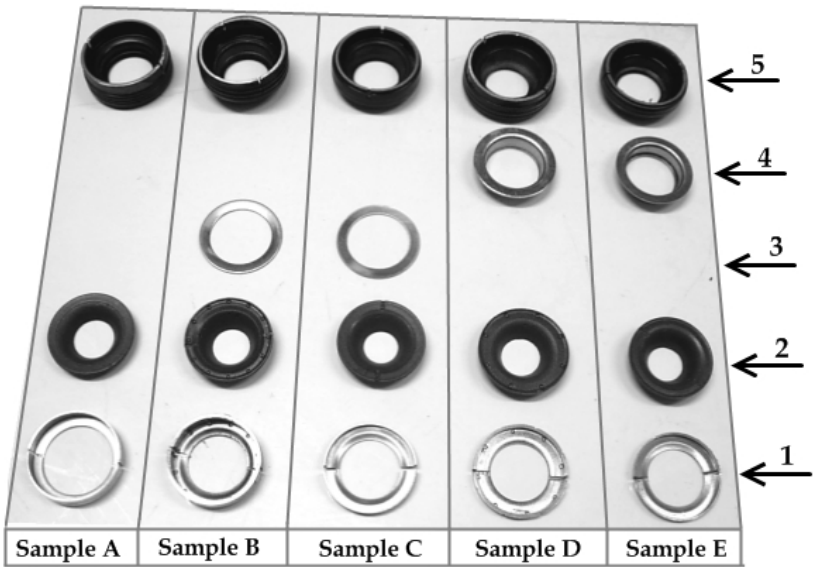

Figure 3-16 Shaft seals disassembled parts. *1*- Outer case; *2*- PTFE lip ring; *3*- Lip rings separating washer ; *4*- Rubber lip support ring; *5* – Metallic structure with the rubber lip and the peripheral rides.

3.6.2 Dimensions

The shaft seal dimensions in their free position are presented in Table 3.1. They have been obtained using a non-contact measuring device, a Light-Emitting Diode (LED) light micrometer. The object to be measured is placed between a light source and a receiver and its dimension is calculated using the shadow principle. The LED source produces a parallel light curtain that will reach the object to be measured. The high resolution Charge Coupled Device (CCD) camera will measure the contour formed by the object shadow and convert it into an electronic signal. The advantage of such a system is to measure accurately the shaft seal dimensions without deforming materials.

According to the manufacturer instructions, samples A, B, C, and E are installed on a shaft with a diameter of 14.2 mm and a housing diameter of 25.9 mm. Sample D is inserted on a 13.5 mm shaft diameter and a 27.0 mm housing. The PTFE lip ring high interference value results in a significant deformation during the shaft installation.

Table 3-1 Shaft seal dimensions before installation.

Sample	D_0 (mm)	D_{sc} (mm)	D_P (mm)
A	26.342	10.844	13.712
B	26.450	9.814	13.351
C	26.352	8.880	13.503
D	27.441	10.281	10.04
E	26.417	9.553	13.568

3.7. Shaft seal gas emissions

The seal samples A to E have been leak tested with original and new compressor shafts, thus ensuring a shaft without wearing tracks. Each seal has been tested at three different pressure levels with and without lubricant oil between the lip rings and the shaft (see Table 3-2). Test results are presented hereafter.

Table 3-2 Shaft seal temperature during the leak tests in standstill mode.

Pressure (kPa)	Seal temperature (°C)
770	35
1020	45
1320	55

3.7.1 Dry contact

The first test consisted of installing the shaft without addition of lubricant oil. The non-lubricated contact condition is achieved when the shaft has been stopped for some hours, depending on the fluid pressure and the mating surface roughness. The shaft seal samples A, B, C, and E have been tested using the compressor shaft no.4 with a diameter of 14.268 mm and the sample D with the shaft no.6 with a diameter of 13.489 mm. The shaft seal leak flow rates are presented in Figure 3-17. The used shafts were disassembled from two different compressor models.

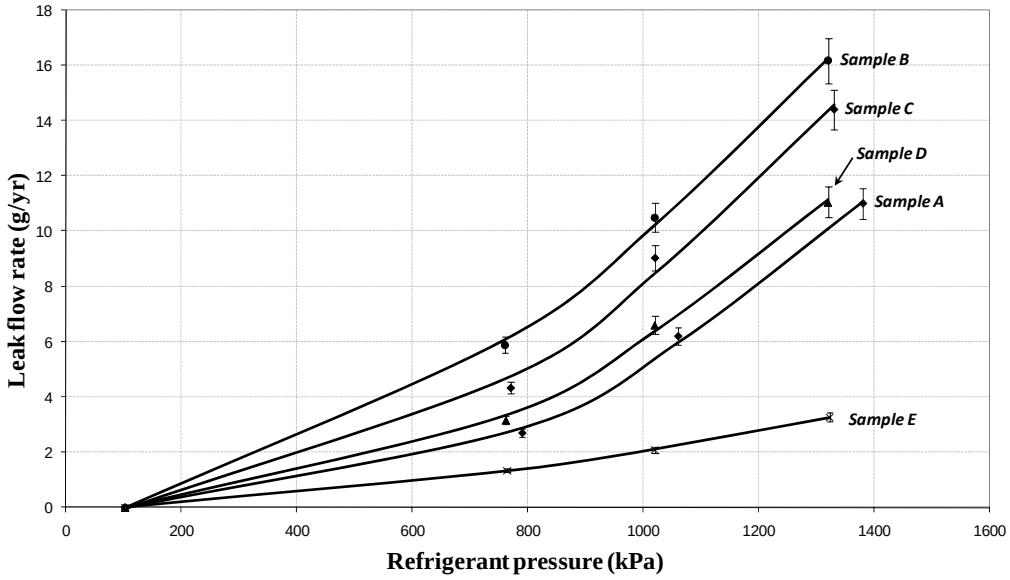

Figure 3-17 Refrigerant LFRs of five shaft seals with dry contact.

The graph presents the leak flow rate rise as a function of the refrigerant pressure. The emission results of each seal are fitted using the method of the least squares with a quadratic function. Emissions range from 1.3 g/yr at 764 kPa to 16.7 g/yr at 1320 kPa and confirm the shaft seal high emission rate. For the lowest pressure value, the leak flow rate difference among the five seals is very similar, about 1 g/yr. Although, this leak flow rate difference increases with the refrigerant pressure in particular for sample E, which is clearly the tightest shaft seal.

The shaft seal emissions in standstill mode increase exponentially with the gas pressure. The gas pressure rise impacts emissions at two levels:

1. increase in the driving force that causes the leak,
2. changing of the HNBR lip contact conditions.

At the first level, the fluid flow through the seal is described by the Poiseuille and Fick laws. In both cases, the increase in the gas pressure increases the LFR value. The second level deals with the definition of the leak path dimensions. As described by the Hertz theory, the real area of contact increases with load, thus reducing the leak path sectional dimensions, as well as the channel lengths. Accordingly, the higher the fluid pressure, the lower the LFR value. These test results show that the shaft seal gas emissions are driven mainly by the gas pressure.

Using these leak test results, it is possible to compare the shaft seal and the compressor gas emissions under the same pressure and temperature conditions. Considering the different shaft seal leak flow rates using the original shafts, an emission rate average value of 7 g/yr at 1020 kPa has been found. 24 new compressors have been leak tested at the laboratory according to the European regulation 706/2007. The resulting emission levels, without the Correlation Factor, range from 5 to 32 g/yr with an average value of 14 g/yr. Consequently, the shaft seal represents up to 50% of the gas emissions for new compressors in standstill mode.

According to these leak test results, it can be assumed that sample E seal design is the most suitable for static applications, especially for high fluid pressure levels. This performance is related to the combination of a rubber support ring with a short rubber lip that keeps a high contact stress with the shaft surface even with the fluid pressure increase. The rubber lip deformation for these samples will be measured using a transparent shaft, see Section 3.8, and simulated using a Finite Element Analysis, FEM, presented in next chapter.

3.7.2 Sample A

Sample A gas emissions behavior has been studied with different compressor shafts (see Figure 3-18). The shaft samples come from three different new compressor models.

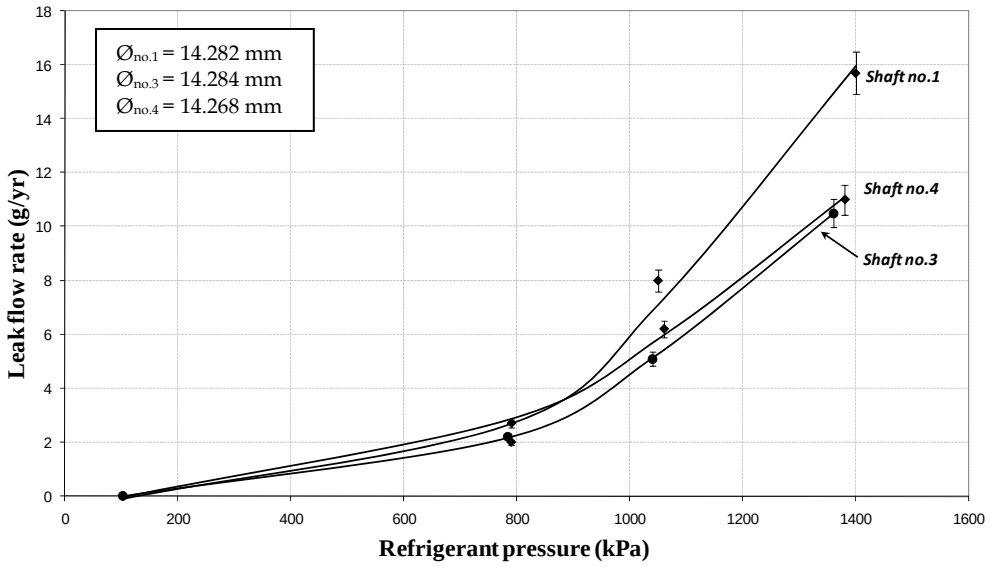

Figure 3-18 Sample A gas LFRs for different shafts with dry contact.

It was observed that gas emissions with shafts no.3 and no.4 are very similar. However, the leak flow rate with shaft no.1 is significantly higher at high pressure values. The gas emission behavior of these shafts is not related to their diameter. The higher diameter difference, 16 μm, is for shafts with equivalent emission levels. The most emissive shaft, shaft no.1, has the lowest diameter difference. Therefore, a shaft diameter difference of 16 μm does not change significantly the contact stress of seal lips with the shaft surface. The interpretation of these leak test results is directly related to the shaft surface roughness.

The surface roughness defines the leak path dimensions that can be assimilated to a circular channel of radius *r* and length *l*. In this case, the Poiseuille law, see Equation 2.4, defines the leak flow rate, which is proportional to the channel diameter, and so the higher the channel radius, the higher the leak flow rate. For low-pressure levels, the relatively low difference between roughness of shafts does not affect the gas viscous flow. As the gas pressure increases, the leak path dimensions become primordial for the LFR value especially for high LFR values.

3.7.3 Shaft surface with leads

A new shaft has been machined in a lathe to generate a surface with leads, shaft no.5. The shaft roughness profile is presented in Figure 3-19 and the roughness values are shown in Table 3-3. Shaft no.5 has a profile with valleys up to 4 μm depth and 0.5 mm large. The leak flow rate values for the seal sample C are presented in Figure 3-20 and compared to the original shafts 1 and 4. The shaft no.5 produces clearly the most emissive LFR with a value of 174 g/yr at 1380 kPa showing that the shaft surface roughness is of primary importance to define gas emissions in standstill mode. As for sample A (see Figure 3-18), shaft no.1 produces a higher LFR value compared to shaft no.4. Therefore, the shaft surface texture is a critical factor to the shaft seal gas emissions.

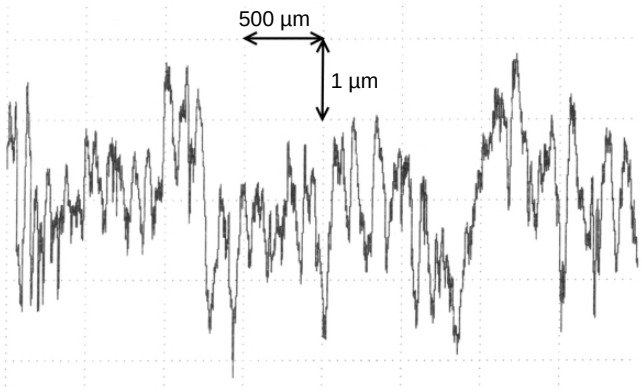

Figure 3-19 Roughness profile of shaft no.5.

Table 3-3 Surface roughness shaft no.5.

Diameter (mm)	Ra (μm)	Rz (μm)	R_{max} (μm)
14.212	0.58	3.27	3.92

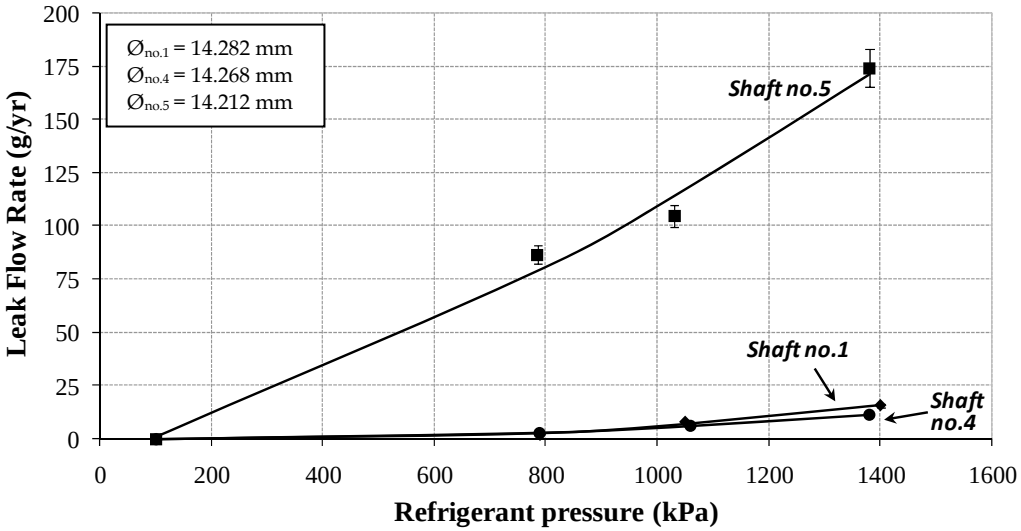

Figure 3-20 Sample C gas LFRs for different shafts with dry contact.

3.7.4 Wavy profile

The polished surface of a PMMA shaft has been slightly heated to create a surface texture with a wavy profile. The shaft was assembled with the seal sample A creating a dry contact and tested at three pressure levels, 1320 kPa, 1020 kPa, and 770 kPa. Figure 3-21 presents the refrigerant pressure and gas concentration evolution as function of time. The leak flow rate is calculated using the steady state regime and indicated on the graph by the dashed line.

It can be noticed that the shaft seal leak flow rate **increases** when the refrigerant pressure **decreases**: 0.7 g/yr at 1320 kPa, 1.0 g/yr at 1020 kPa, and 3.7 g/yr at 770 kPa. This behavior is opposite to what was observed until now, where the leak flow rate increases with pressure. This leak flow rate evolution is related to the combination of the elastic material properties with the wavy surface texture.

The contact between the wavy profile of the shaft surface and the rubber material is presented in Figure 3-22. The white spaces represent the free path for the gas flow. The PMMA surface “waves” can be assimilated to the asperities found on a metallic surface but with longer wavelengths. As the distance between the asperities is much longer in this wavy shaft, the elastic deformation of the rubber material will partially fill the valleys. A high gas pressure causes a high rubber elastic deformation, thus reducing the free spaces for the gas leakage. The fluid pressure decrease will reduce the rubber deformation, so reducing the contact area, increasing the leak path dimensions and, consequently, the gas LFR.

Therefore, the waviness surface parameter is very important to characterize the shaft surface texture.

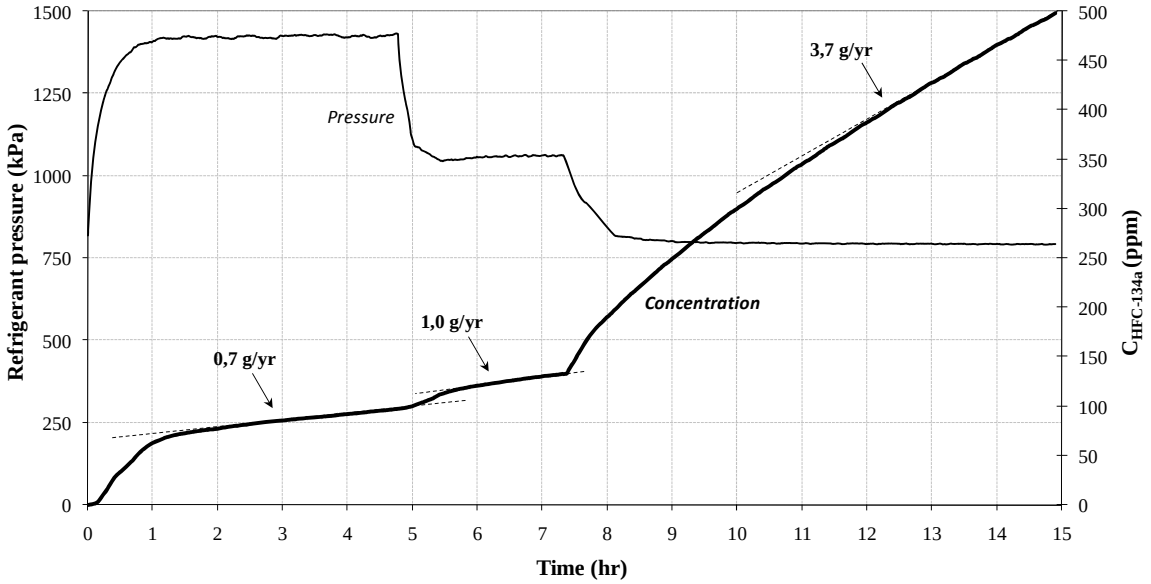

Figure 3-21 Sample A gas LFRs using a PMMA shaft with a waved surface.

a) High pressure *b) Medium pressure* *c) Low pressure*

Figure 3-22 Representation of the contact between the waved PMMA surface and the rubber lip.

3.7.5 Wet contact

The seal sample A has been leak tested using oil between the seal lip rings and the shaft. The shaft sample no.4 used for the previous tests has been coated with a thin layer of PAG-46 oil. The shaft is then inserted in the seal and the seal case is refrigerant charged. The evolution of the gas concentration in the accumulation volume for three different refrigerant pressures is plotted in a gas concentration vs. time curve (see Figure 3-23).

For each refrigerant pressure two different gas concentration slopes are observed. A slope is the gas concentration-time curve, which indicates a steady state gas flow through the seal. It has to be noted that the higher the slope, the higher the LFR. The existence of these two slope points indicates a transitory phenomenon that has not been observed with dry contact. Moreover there is a dramatic change of the seal LFR when comparing the initial and the final levels.

The first slope is obtained just after the test has been started and its duration depends on the fluid pressure. The shortest first slope duration corresponds to the highest fluid pressure. The second slope starts after a transition period and does not change with time. This is the same gas concentration evolution behavior found for MAC compressors when rotated by hand in an inclined position (see Section 2.8). This test result confirms the dominance of the shaft seal LFRs for the compressor.

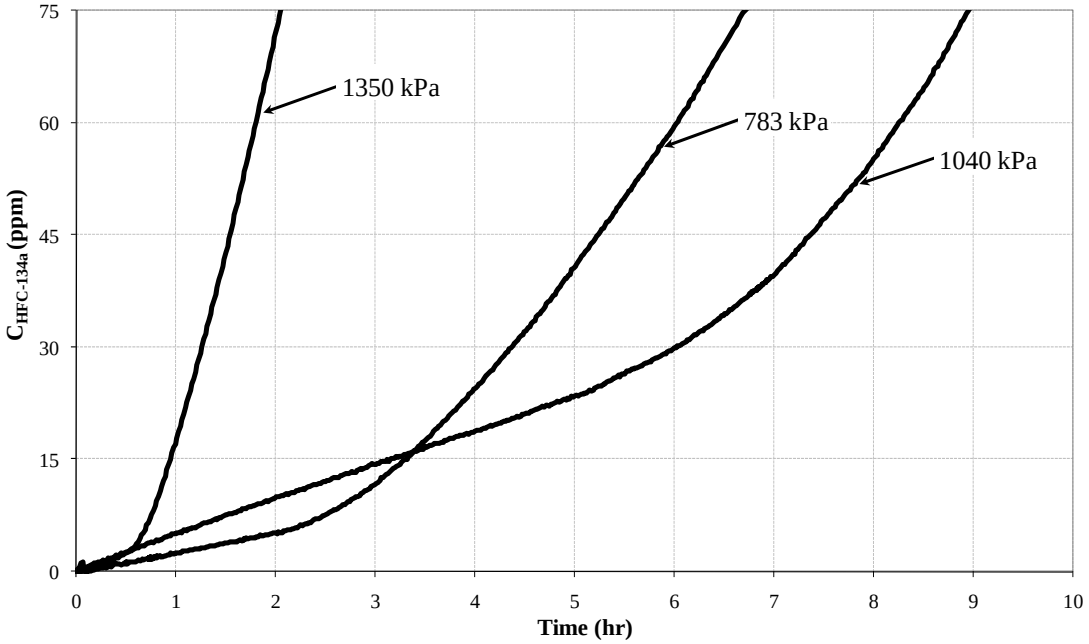

Figure 3-23 Refrigerant concentration evolution for shaft seal sample A with the original shaft and lubricated contact.

The leak flow rates corresponding to the first and the second slopes have been calculated and are presented in Figure 3-24. The LFRs for the first slope are relatively low and are not affected by the fluid pressure. On the contrary, the second slope LFRs are eight to eighteen times higher than those found for the first slope and are similar to the dry contact LFRs (see Figure 3-25). The transitory period increases with the decrease in the gas pressure. The first slope of the LFR value corresponds to the oil effect in the sealing interface. When the oil coated shaft is installed, there is still some oil on the lip rings trapped by the shaft surface imperfections. When the gas pressure starts acting in the seal interface, the oil is forced to leave the contact. The higher the gas pressure, the faster the oil leaves the contact, thus opening the leak channels to the gas flow. Therefore, as seen in Chapter 2, the lubricant oil in the seal contact has just a temporary effect.

In more detail, the oil effect consists in the oil meniscus formation around the asperities, thus filling, at least partially, the surface irregularities (see Section 3.3.3). This results in the decrease of the leak path dimensions and consequent reduction of the gas flow. The temporary effect of oil is related to the meniscus attractive force. The combination of the geometries of asperities with the oil surface tension generates an attractive force lower than the gas driving force. So, the meniscuses are continuously displaced along the seal contact to reach the air side. After a certain time, there is no more oil in the contact resulting in a LFR value which is the same as the one found for a dry contact. The lubricant oil that flows through the seal/shaft interface can be recovered at the seal low-pressure side, as shown in Figure 3-26.

As the pressure increases, a LFR difference is created to reach 2 g/yr at the highest pressure. This LFR difference is related to two different factors: the remaining oil in the contact that was not blown by the gas flow and the rubber lip position that varies with the coefficient of friction between the sliding surfaces, as it will be explained in Section 3.7.

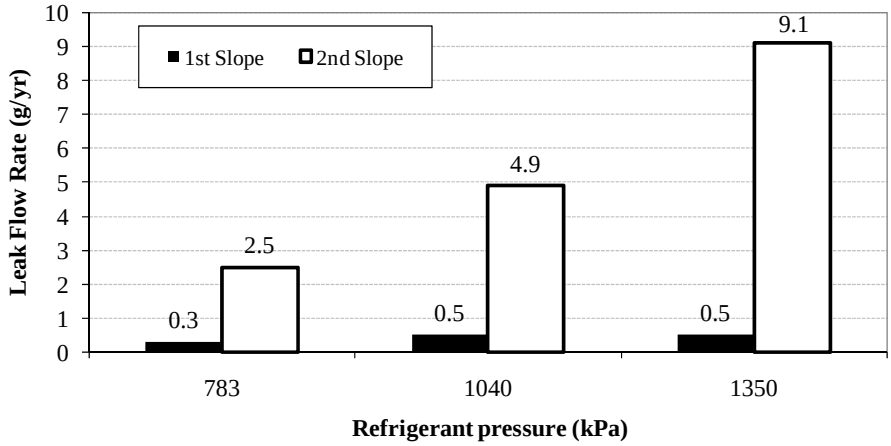

Figure 3-24 Refrigerant LFRs for shaft seal sample A with the original shaft and a lubricated contact.

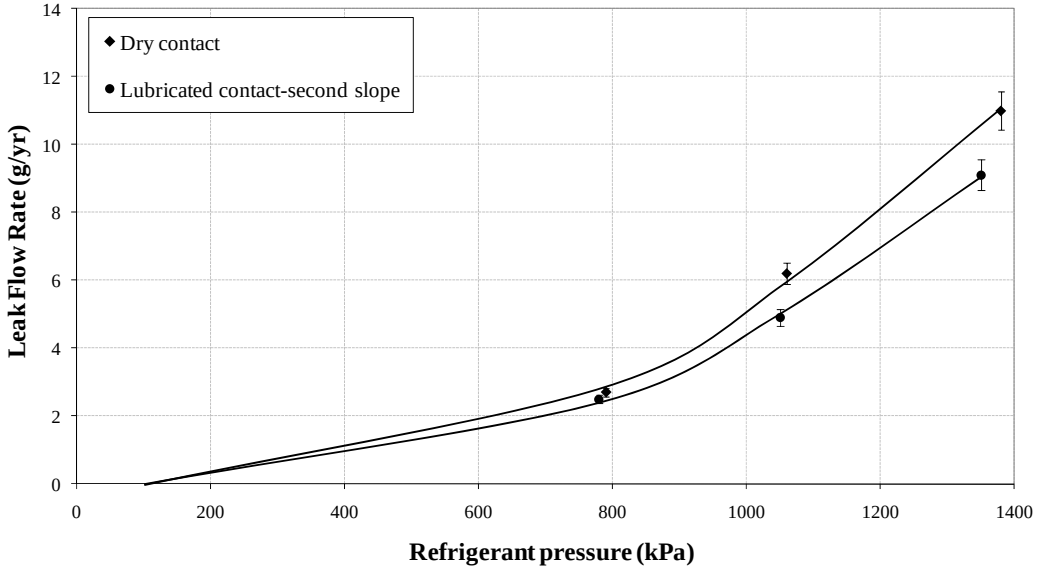

Figure 3-25 Refrigerant LFRs for shaft seal sample A with the original shaft.

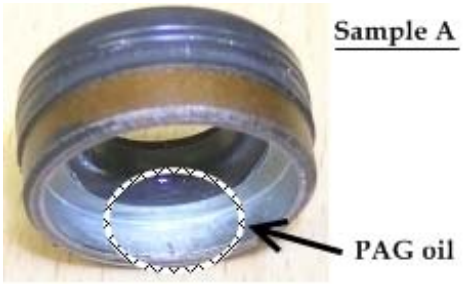

Figure 3-26 Lubricated oil at the seal low-pressure side resulting from its transportation through the seal contact.

As mentioned before, only the shaft surface has been coated with oil. The seal rubber lip that faces the fluid pressure, as well as the peripheral ride contacts, remain dry. Therefore, if we consider that the gas LFR of the first slope corresponds to the fluid flow through the dry leak paths, it becomes clear that it is very small comparing to the second LFR slope. Consequently, considering the shaft seal high gas emissions, the emissions resulting from the gas flow due to the permeation through the material, as well as the flow via the peripheral ride contacts, can be neglected.

3.7.6 Polished shaft

A polished PMMA shaft has been used to demonstrate the significance of the shaft surface roughness to the seal LFR. A picture of the PMMA shaft is shown in Figure 3-13b. The roughness profile and surface roughness values are presented in Figure 3-27 and Table 3-4, respectively. The PMMA shaft presents very low roughness values due to the polished operation. The shaft seal sample A has been leak tested with the polished shaft under dry and lubricated contact successively. Test results are presented in Figure 3-28.

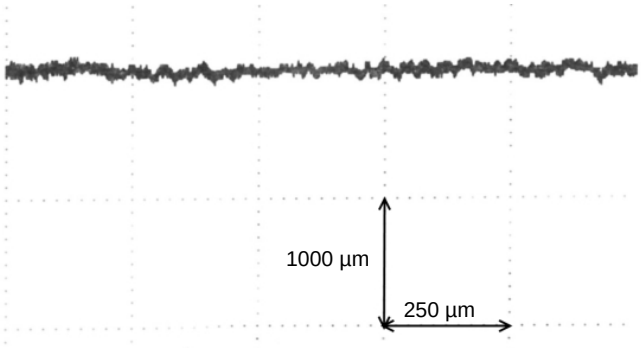

Figure 3-27 Roughness profile of the PMMA shaft.

Table 3-4 Surface roughness for the PMMA shaft.

Diameter (mm)	Ra (µm)	Rz (µm)	R_{max} (µm)
14.212	0.03	0.18	0.2

First, the polished shaft generates a LFR value up to 22 times lower than an original shaft. Therefore, it confirms the low contribution of permeation of materials and the peripheral ride contacts to the seal gas emissions and the importance of reducing the shaft surface roughness.

Second, the two different gas concentration slopes observed in Figure 3-23 for a lubricated contact do not exist. In other words, there is no oil effect with a polished shaft. The LFRs with a dry and a lubricated contact are identical. The oil effect does not take place since the real contact area has a value similar to the apparent contact area. In other words, there are an extremely high number of asperities in contact, which reduce the leak path dimensions and increase the oil meniscus attractive force to a value higher than the gas pressure. The result is a very low LFR.

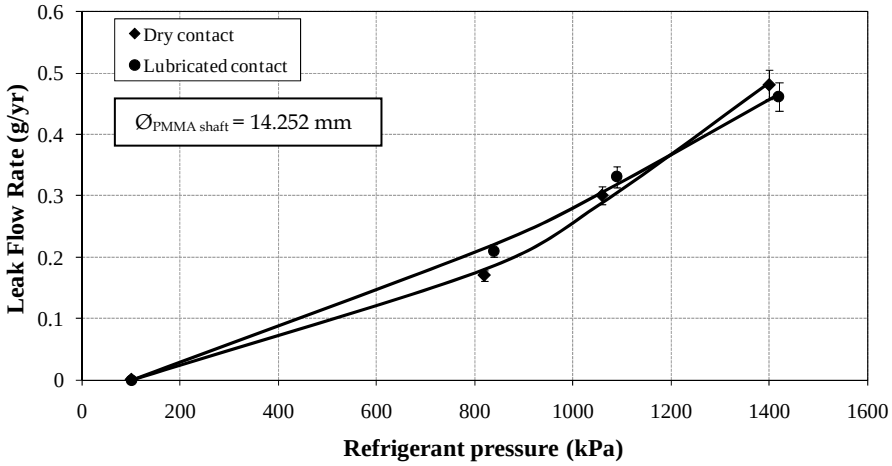

Figure 3-28 Refrigerant LFRs for the seal sample A with a PMMA shaft.

3.8. Seal contact visualization

The PMMA transparent shaft used for the leak tests presented above was also used to visualize the contact between the shaft surface and the lip rings. The visualization will give evidence of the lip deformation with pressure, as well as the lip contact surface evolution of some seal designs.

3.8.1 Deformation of lip rings

The captured image of sample A with its interpretation is shown in Figure 3-29. The image reveals the faces F1 and F2 of the rubber lip, the faces F3 and F4 of the PTFE lip, as well as the metallic support ring between the two lips, if installed.

The five shaft seal designs presented in Section 3.5 have been used to see the deformation of lip rings and the contact width deformation with pressure. The refrigerant chamber was filled up with N_2 / O_2 and the seal temperature set to 23°C. The contact images at four different pressures are presented in Figures 3-30 to 3-32.

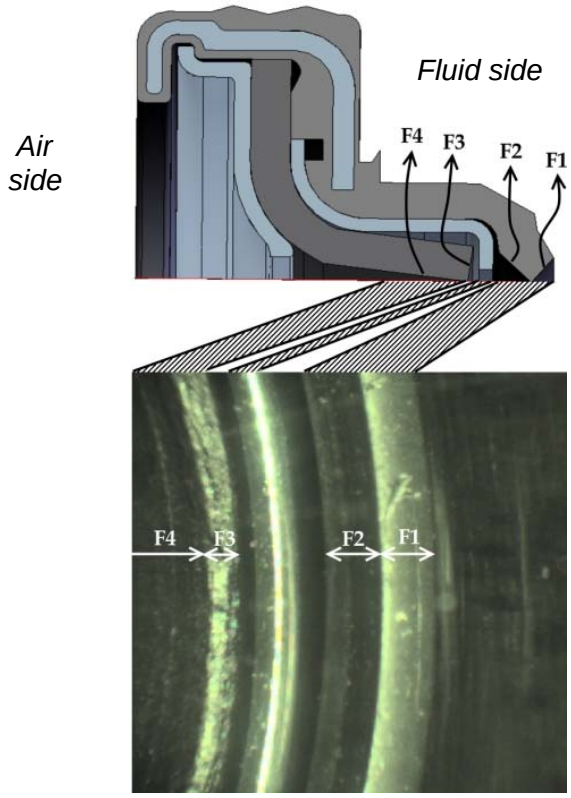

Figure 3-29 Interpretation of the captured image. *Up*- sectional view of a lip-type seal, *down*- endoscope image of seal sample E without fluid pressure (25x).

3.8.1.1 Samples A and B

Sample A rubber lip has a Contact Line, CL, with the shaft surface when exposed to the atmospheric pressure. The CL is the narrow circular interference between the rubber lip and the shaft surface. Face F2 is not in contact with the PTFE lip. The vertical dashed lines represent the axial displacement evolution of lips. When the gas pressure starts to increase under dry conditions, the rubber lip rotates around the CL, thus increasing the contact width *W* with the shaft surface (see Figure 3-30) and reducing the space between F2 and the

PTFE lip. The plastic lip is pulled down onto the shaft by the rubber lip deformation while F3 decreases. The gas pressure increment will make the rubber lip ring contact to grow and the plastic lip to move axially. At pressure level P_4, the plastic lip is squeezed by the rubber lip. When oil is added to the seal contact, the friction coefficient between the sliding surfaces is reduced. As the gas pressure starts to increase, the CL will move about 0.2 mm to fill the space between F2 and F3, thus creating a new contact stress. Accordingly, the leak flow rate of the second slope, see Section 3.6.2, will be different from the one obtained with a dry contact, since the contact conditions have changed.

When the shaft is not rotating, the fluid housing pressure will always generate a rubber lip contact higher than CL in sample A. Therefore, the rising of gas pressure increases the leak path length, which reduces the gas flow. When the shaft is rotating, the fluid pressure acting on the seal is about 300 kPa. At this pressure level, it is observed that the rubber lip contact of seal sample A is about 0.4 mm. Pictures also show the PTFE lip to be deformed by the action of the rubber lip ring. These two factors contribute to the increase in temperature and wear of lips. The rubber lip contact width is shown in Figure 3-31.

For sample B, the F2 rubber lip contacts the plastic lip at P1. When the gas pressure increases, there is no change on the rubber lip contact width under dry conditions. The only movement observed is the axial displacement of the lip rings with gas pressure increase: up to 0.1 mm. The presence of oil in the seal contact has generated no change on the deformation of lips.

The absence of movement from sample B rubber lip suggests that this one is supported by the PTFE lip. If we look carefully at the sectional view of seal sample B in Figure 3-15, we see that the movement of the PTFE lip during the shaft insertion will make the contact between the lip ends to be in the middle of F2 face. This position will work as a pivot to the rubber lip deformation. So, the increase in the rubber lip contact stress will be controlled by this rotation.

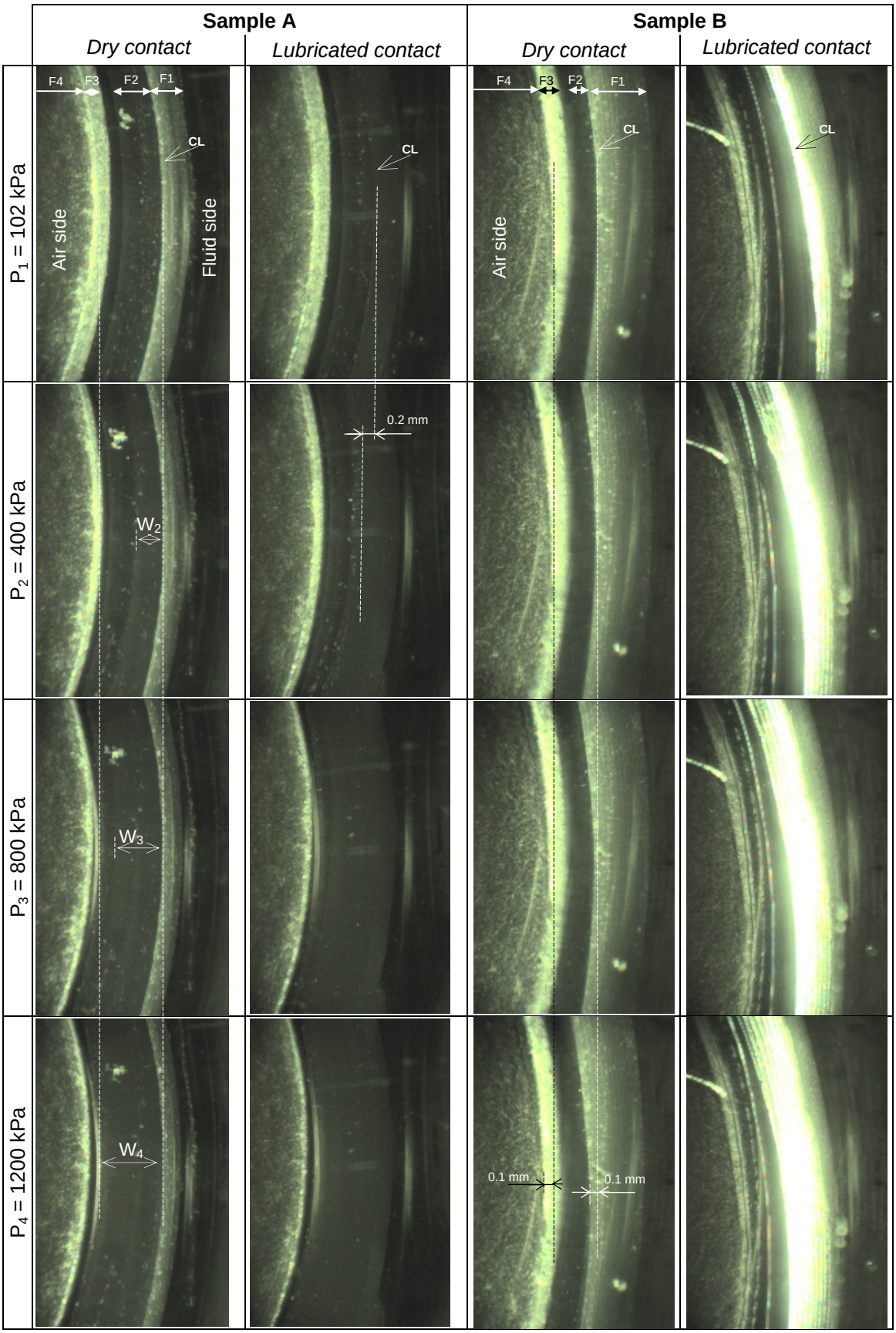

Figure 3-30 Samples A and B contact visualization.

3.8.1.2 Samples C and D

The rubber lip displacement of sample C is based on the lip rotation around the CL. A CL condition is maintained for low gas pressures. A low contact width is observed at P_4: 0.08 mm. The lubricated contact introduces a major change of the rubber lip deformation (see Figure 3-32). The rubber lip edge will be axially displaced with pressure, up to 0.6 mm, due to the low surface friction coefficient. This deformation will cause face F1 to contact the shaft surface, which is not supposed to happen. Therefore, the rubber lip load is entirely carried by F1 surface. F1 contact width evolution is shown in Figure 3-31.

The shaft seal sample D incorporates a metallic support ring that is recognizable in the seal contact picture on Figure 3-32. The rubber lip edge produces a CL with the shaft surface ,which remains unchanged with the gas pressure and lubrication. The rubber lip deformation is based on the rotation around the CL without increasing the contact width. The oil introduction in the seal contact does not change substantially the deformation of lips.

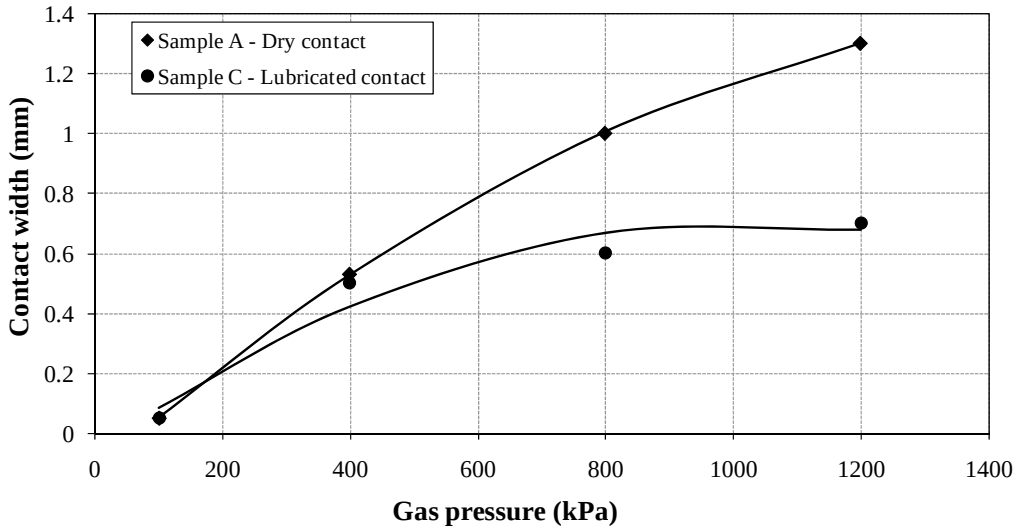

Figure 3-31 Rubber lip edge contact width evolution with the gas pressure.

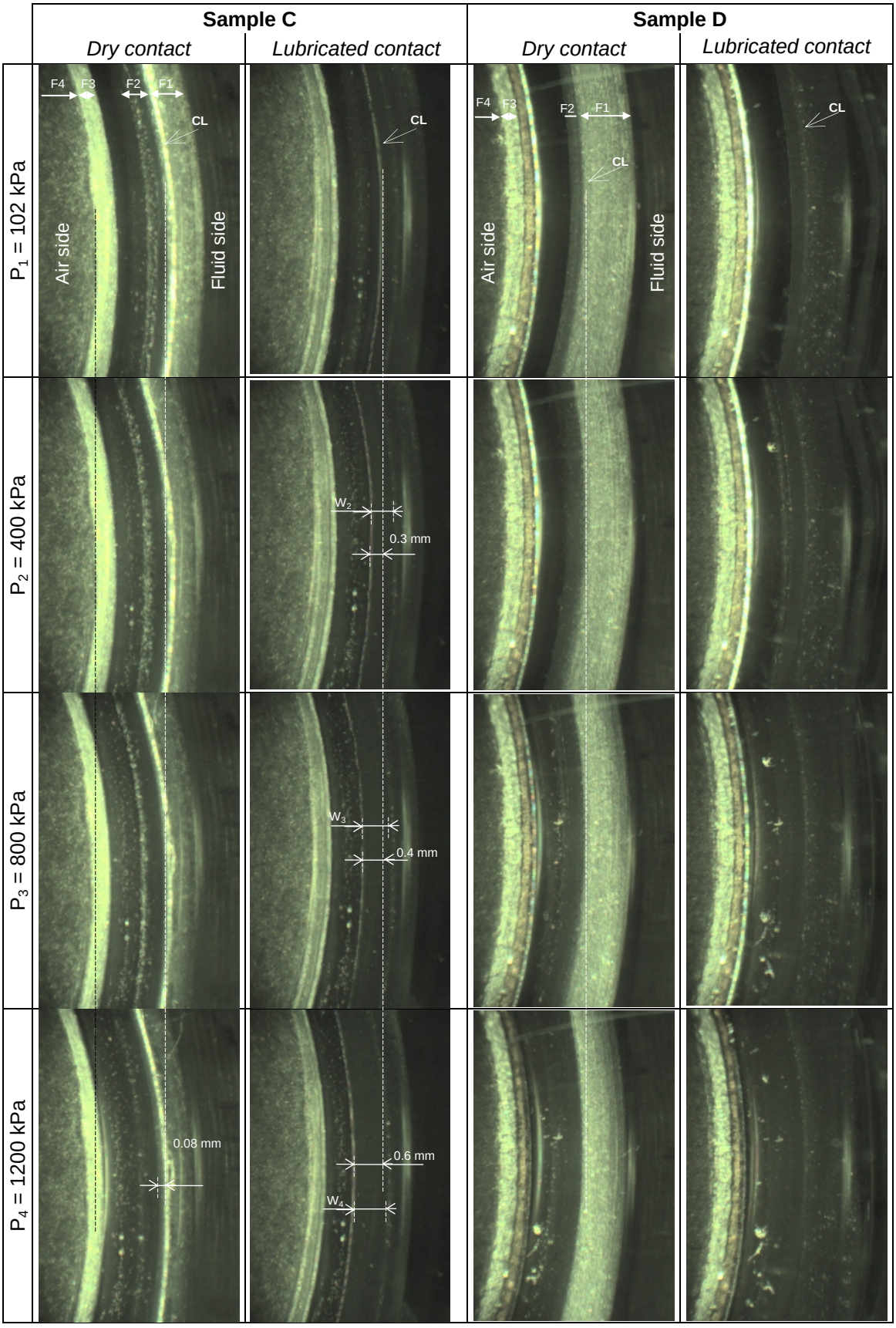

Figure 3-32 Samples C and D contact visualization.

3.8.1.3 Sample E

The contact visualization of seal sample E, the tightest seal in standstill mode, is presented on Figure 3-33). The visualization of the seal contact shows that the rubber lip contact width does not change with the gas pressure; the rubber lip simply rotates around CL. This scenario changes completely when the contact is lubricated. In this case, the gas pushes the rubber lip edge along the lubricated surface until it reaches the metallic support ring. The rubber lip edge displacement is higher than in sample C and has a value of 0.84 mm at 1200 kPa.

The high performance of sample E under dry contact at rest is not due to the increase in the leak path length. A finite element analysis should reveal the increase in the contact stress that justifies the seal performances, especially at high fluid pressure.

The five shaft seal samples generate different contact conditions with the shaft surfaces since they have a particular rubber lip design. After the installation, all rubber lip seal designs produce a CL with the shaft surface. Only sample A presents a significant contact width evolution under dry conditions. The shaft seal contact lubrication has proved to change the rubber lip deformation for three samples: A, B, and C. As the seal contact is lubricated during the shaft rotation and dries when stopped, the contact conditions of lip rings are always changing.

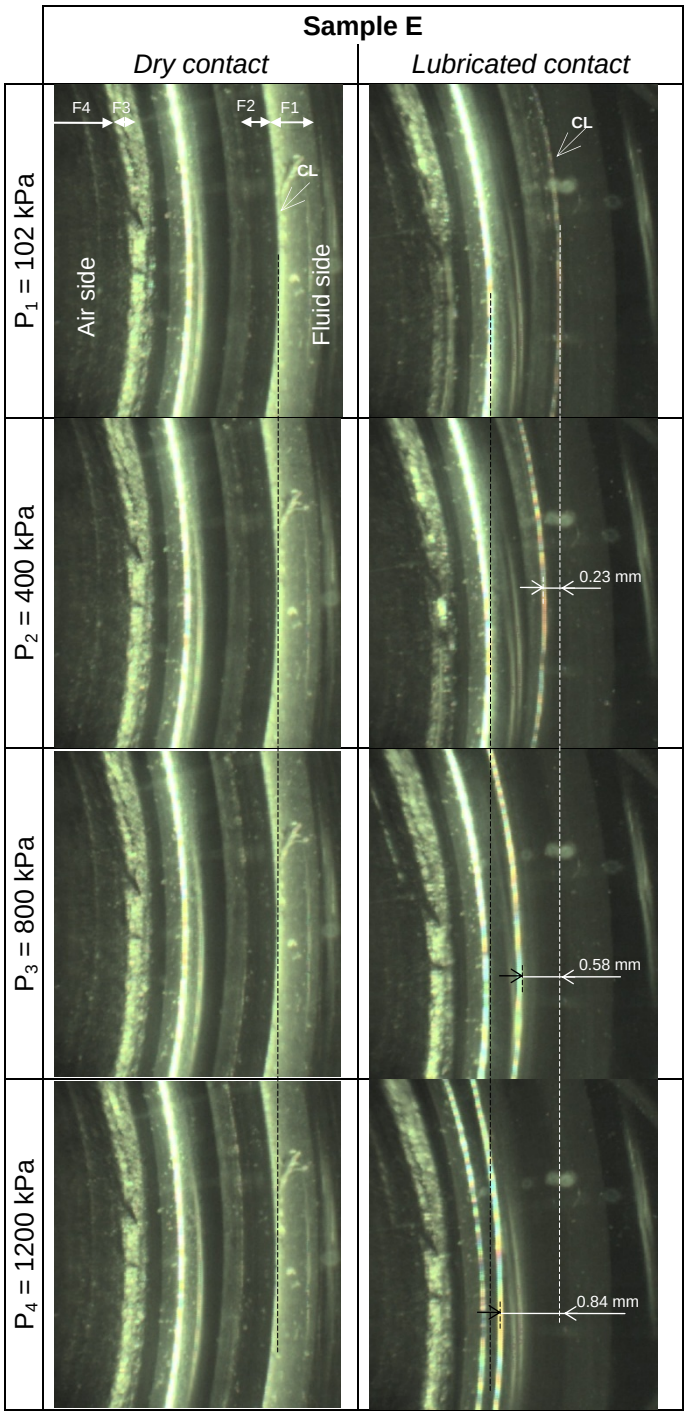

Figure 3-33 Sample E contact visualization.

3.8.2 Flow visualization

The refrigerant gas is a transparent media and its motion remains invisible to the human eye. However, the direct observation of a seal lubricated contact shows the formation of bubbles at the low-pressure side indicating the leak path exit (see Figure 3-34). In this continuous bubbling regime, gas bubbles are formed near the gas micro-channel exit at the seal interface, growing largely as they move on.

The refrigerant gas flows through the contact free spaces, the micro-channels, and transports the oil in the contact, thus creating gas bubbles when they reach the atmospheric side. Bubbles are visible in a lubricated contact since the oil surface tension provides the necessary wall tension to the formation of bubbles

Figure 3-34 shows the small formation of bubbles at the exit of the PTFE lip contact. The bubbles are not equally spread around the contact, showing the irregularity of the gas flow channels around the seal contact. This phenomenon is more pronounced in the PTFE lip contact since this plastic material has a rough surface when compared to the rubber producing higher gas leak flow rates.

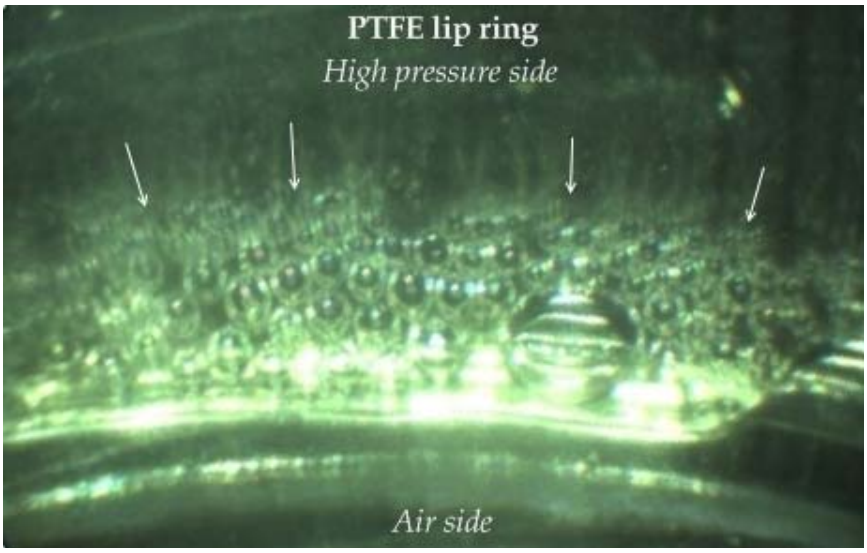

Figure 3-34 Formation of bubbles at the PTFE contact exit.

3.9. Conclusions

The gas emissions of several shaft seal designs used for HFC-134a compressors have been studied. The static sealing effect of such seals is based on the soft contact between rubber material, HNBR, and a metallic surface. As the metallic machined surfaces are characterized by a complex and irregular texture, the contact with the rubber material generates microscopic local contacts that are much smaller than the apparent contact area. The low real contact area allows the formation of micro-channels among the contact spots, which enable the gas flow and are the main cause of the shaft seal gas emissions.

The design evolution of the compressor shaft seal has been presented. It has been noticed the change from the leaky mechanical seals based on the metal-to-metal contact to the lip-type seal based on the soft contact that improves the seal performance.

An original experimental setup has been introduced and used to study the gas emissions of different shaft seal designs in standstill mode. The leak test results clearly show their high

LFR and set the shaft seal contribution to the compressor gas emissions up to 50%. The seal leak flow rate has proved to be very dependent on the shaft texture and the seal design. A factor of five has been found between the seal samples E and B for the same test conditions. By testing different shafts, it was possible to see that a higher surface roughness increases gas emissions.

The very low contribution of material permeability to the seal performance was also proved, as well as the oil barrier to the gas flow. The oil effect has shown a temporary effect since the gas pressure is responsible for the oil leakage, producing a dry contact.

The shaft seal contact visualization has shown the lip deformation and the contact width evolution with pressure under dry and lubricated contacts. After the installation, all seal designs present a contact line between the rubber lip and the shaft. As the pressure increases, the deformation depends on the seal design and the coefficient of friction between the mating surfaces. For two different seal designs, the presence of oil has considerably changed the rubber lip deformation, thus its contact stress. In dry conditions and for the majority of tested seals, the rubber lip movement is based on the lip rotation around its contact line. Only the rubber lip from sample A presented a significant contact width evolution, from 0.53 mm at 400 kPa to 1.3 at 1200 kPa. All the seal designs show the lip axial displacement up to 0.1 mm at high pressure. Therefore, the rubber deformation is very sensitive to the gas pressure variations, up to 0.8 mm for sample E with a lubricated contact.

The formation of bubbles on the seal contact exit was observed for a lubricated interface. It reveals the contact micro-channels location and the irregular distribution around the contact.

The last chapter deals with the finite element analysis of the seal deformation under pressure to determine the lips contact stress evolution of seal sample E.

3.10. References

[BHU99] Bhushan, B, 1999. Principles and Applications of Tribology. John Wiley & Sons. 1020 p.

[BRO99] Brown, R., 1999. Handbook of polymer testing. M. Dekker. pp. 751

[CHA91] Charrier, J, 1991. Polymeric materials and processing. Hanser publications. 663 p.

[CHI91] Chiba, K, Shimomura, T, Hirabayashi, H, 1991. Sealing Phenomena of a Lip-Type Seal for an Air Conditioning Compressor. SAE technical paper 910532.

[HOS05] Hosokawa, A., Nagaoka, H., Yamada, T, Keneshige, Y, 2005. Rotation Shaft Seal. US Patent No.:6,857,637.

[HOS06] Hosoi, H, Fukumuro, T, 2006. Sealing Member of a Compressor. US Patent 2006/0162546.

[ILI80] Iliuc, I, 1980. Tribology of Thin Layers. Elsevier Scientific Publishing Company. 225 p.

[KAW00] Kawagushi, M, Kubo, K, Yokono, T, Miura, S, Okuno, T, Tokunaga, E, Morishita, A, 2000. Sealing Structure for Compressors. US Patent No.: 6,123,514.

[KRA05] Kraus, R, 2005. Rotating Mechanical Seal. US Patent No.: 6,845,985.

[KUN05] Kunstfelt, T, Haas W, 2005. Shaft surface manufacturing methods for rotary shaft lip seals. Sealing technology, pp. 5.

[LAB82] Labus, T, 1982. A Comparative Evolution of Mechanical Seals for Automotive Air Conditioning Compressors. SAE technical paper 820076.

[MUL98] Müller, H, Nau, B, 1998. Fluid sealing technology. Marcel Deker. 485p.

[OBA99] Obata, H, Takeda, K, Hosokawa, A, 1999. Seal for Rotating Shaft. US Patent No.: 5,860,656.

[OHT86] Ohtaki, M, Yamamoto, Y, 1986. Development of New Lip Type Seals for an Automotive Air Conditioning Compressor. SAE technical paper 860493.

[OSA05] Osako, M., Yamada, T., Murase, M., 2005. Shaft Sealing Assembly. US Patent No.:6,886,834.

[OTF03] Otfried, S, 2003. A Mechanical Axial Seal for a Compressor. European Patent No.: EP1312841.

[PER05] Persson, B, Albohr, O, Tartaglino, U, Volokitin, A, Tosatto, E, 2005. On the nature of surface roughness with application to the contact mechanics, sealing, rubber friction and adhesion. Journal of Physics: Condensed Matter, Volume 17, Number 1, 12 January, pp. R1-R62.

[ROT94] Roth, A, 1994. Vacuum sealing techniques. American Institute of Physics. 845 p.

[SHI87] Shimomura, T, Yoshino, A, Matsumoto, S, Hirabayashi, H, 1987. Sealing Performance of End-Face Type Seals for an Automotive Air Conditioning Compressor. SAE technical paper 870513.

[SHI90] Shimomura, T, Nishihira, E, Chiba, K, Yoshino, A, Tanoue, H, Hirabayashi, H, 1990. A study of Cracking Phenomena on Carbon-Rings of Mechanical Seals for an Automotive Air Conditioning Compressor. SAE technical paper 900338.

[SOU08] Sousa, D, Clodic, D, 2008. Sealing Performance of a Mobile AC Compressor Shaft Seal. International Compressor Engineering Conference at Purdue, July 14-17.

[YAM03] Yamada, T, Imai, T, Yokomachi, N, 2003. Shaft Seal of a Lip Type With Fluid Guiding Components having the Same. US Patent No.: 6,592,337.

[CHE93] Cheremisinoff, N, 1993. Elastomer Technology Handbook. CRC Press, 1075p.

[YAM03b] Yamada, T, Imai, T, Ikeda, Y, 2003. Lip Seal. US Patent No.: 6;517,082.

[ZAM98] Zambelli, G, Vincent, L, 1998; Matériaux et Contacts. Presse polytechniques et universitaires romandes. 334 p.

Chapter 4

SHAFT SEAL STRESS ANALYSIS

Introduction

The last chapter presents the stress analysis of the shaft seal sample A. MARC software has been used to simulate all seal component deformations during installation of the shaft seal in its casing and around the shaft and pressurization by the refrigerant.

The stress analysis results are discussed in terms of contact stress evolution and deformation with the gas pressure. The oil effect in the rubber lip contact is also analyzed.

4. Shaft seal stress analysis

The Finite Element Method (FEM) is a computational technique that started in the 1950s as a tool for the stress analysis of complex geometries. The term stress analysis includes any kind of structural analysis. The stress analysis is an interdisciplinary subject since it brings together a detailed knowledge of the operating conditions of the system, the material(s) and the structural behavior, and the mechanics of the different materials. After 1980, the personal computer market increased in terms of quality, size, as well as computing speed, allowing the fast development of the finite element software, especially for the nonlinear analysis. Today, FEM analysis is a versatile and essential tool of the design engineering used worldwide in different areas of mechanical engineering: stress analysis, fluid flow, heat conduction and magnetic, among others.

In the last 20 years, the use of FEM has been expanded to investigate the behavior of polymers operating nonlinearly under large strains. From the use of nonlinear stress analysis in the shaft seal modeling, it is possible to demonstrate the behavior of the seal under different operating conditions in standstill mode. The purpose of the modeling is to calculate the predicted sealing stresses for a shaft seal rubber lip and peripheral rides.

The seal sample A has been chosen for this analysis due to its low gas emission levels when compared to the other seal designs (see Section 3.7). The shaft seal stress analysis has been performed considering all the seal structure components since they define the rubber lip position under load.

4.1. Materials properties

As presented in Chapter 3, the MAC compressor shaft seal is composed of two types of materials: metallic and polymeric. The metallic parts are used to rigidify the structure and the polymeric ones to perform the seal effect. However, these materials behave quite differently when loaded. Therefore, different approaches are needed to simulate their behaviors.

4.1.1 Metallic

The metallic parts of seal sample A are: inner case, support ring and outer case (see Figure 3-1). They are placed inside the polymeric materials, but they have radically different mechanical properties. The metallic parts are considered to have a linear stress strain relation. The metallic material properties are shown in Table 4-1.

Table 4-1 Metallic material properties.

Elastic Modulus (MPa)	1.93×10^5
Poisson ratio	0,27
Tensile strength (MPa)	5.8×10^2

4.1.2 Polymeric

The compressor shaft is mainly made of polymeric materials. Two different polymers are used in the compressor shaft seal: rubber and plastic.

Elastomers require a different approach from the metallic materials since they have the ability to withstand large deformations. The deformation of polymer materials due to loading and unloading is influenced by the value and duration of loading because of their visco-elastic properties. Visco-elasticity is a time dependent phenomenon that depends on the applied stress, loading rate, strain rate, and temperature.

Visco-elasticity is recognized by its two main aspects: creep and recovery (see Figure 3-3). Creep is the strain response to a stress that is constant with time and the recovery is the strain response to a stress that has been removed. Creep strain curves for rubbers often exhibit a highly non-linear dependence on stress.

Unfilled elastomers operating well away from their glass transition temperature can be considered as hyper-elastic (large strain elastic). There are many possible types of mathematical models for rubber materials (constitutive laws), such as the neo-Hookean law and the Mooney-Rivelin and Odgen series.

Hyper-elastic materials can be modeled by means of strain energy functions. For the stress analysis within elastomers, the Mooney-Rivlin constitutive law (material model) is known to be the most commonly used since it represents more accurately the stress strain behavior of rubber materials [LEE05] [KIM96] [SIL04]. For the Mooney-Rivelin law, the strain energy density involves powers of the first and second principal strain invariants, I_1 and I_2. The strain energy *w* for the Mooney-Rivlin model is defined by:

$$w = C_{10}(I_1 - 3) + C_{01}(I_2 - 3) \tag{4.1}$$

C_{10} and C_{01} are the material constants.

The rubber lip and the material of peripheral rides have been modeled as a hyper-elastic material with the following Mooney-Rivelin constants: C_{10} = 0.73 MPa and C_{01} = 0.38 MPa.

The plastic lip is made of a PTFE compound. This PTFE has a visco-plastic behavior radically different from that of the elastomeric material used for the rubber lip. This study will not treat the PTFE contact conditions. Therefore, to simplify the analysis, the plastic lip has been modeled as a linear elastic isotropic material.

4.2. Stress analysis software

In this study, the stress analysis is performed using MARC 2008r1 FEM software.

A FEM software is divided in three different parts:

- The pre-processor or solid modeling where the structure design is defined, as well as loads and materials properties,
- The solver constituting the heart of the FEM analysis. It uses the information created by the pre-processor to solve the problem and generates a “results” file, and
- The post-processor to help the user to interpret the results.

The objective of a FEM is the stress analysis. The calculation strategy is to calculate:

1st – the displacements {*u*},
2nd – strains {ε} from displacements, and
3rd – stresses {σ} from strains.

The problem domain is divided in a finite number of parts (elements), which can have a variety of shapes, such as triangles, rectangles, etc, known as discretization. The elements

are created to simulate the desired structural behavior. FEM allows each element to have its own shape, size, and material. Points defining and connecting elements are called nodes. Although elements are specified as joined at nodes, they are assumed to be continuous at boundaries.

4.2.1 Element stiffness

Interpolation functions are used to calculate the stiffness equations at an interior point of the element as a function of the nodal values. The element displacement is calculated using interpolation functions [*N]* as:

$$\{u\} = [N]\{u\} \tag{4.2}$$

The strain-displacement matrix [B] is given as:

$$\{\varepsilon\} = [B]\{u\} \tag{4.3}$$

Stress and strain can be related using the elastic matrix [D]:

$$\{\sigma\} = [D]\,\{\varepsilon\} \tag{4.4}$$

Nodal displacements are converted into stresses by combining [B] and [D] matrices:

$$\{\sigma\} = [B][D]\{u\} \tag{4.5}$$

The relationship among stiffness, applied forces, and nodal displacement is given by the global equation:

$$[K]\{u\} = \{f\} \tag{4.6}$$

Where [K] is the global stiffness, {u} the overall displacement vector, and {f} the overall vector of nodal forces.

4.2.2 Linear analysis

In a linear analysis, the material response is directly proportional to the load Hook's law. For the seal metallic parts, linearity is a good representation of the reality. It is assumed that rotations and displacements are small; the stress is directly proportional to strains and loads. The applied load maintains its original direction as the seal structure deforms. Equilibrium equations $[K]\{u\} = \{f\}$ are obtained for the elastic stress-strain relations. Displacements *u* are obtained in a single step of the equation solving.

Linear static analysis excludes large deflections that change how the loads are applied. Therefore, a non-linear analysis is needed to calculate the seal stresses.

4.2.3 Nonlinear analysis

The rubber material found in the shaft seal has a non-linear stress strain behavior. The rubber deformations due to the gas pressure are too high to consider that forces maintain the initial position, and the contact among the different parts is permanently changing. These are the main reasons to consider the shaft seal stress analysis as a non-linear problem.

Non-linearity complicates the stress analysis because equations describing the solution must incorporate conditions not fully known until the solution is determined. Therefore, the stress analysis solution cannot be obtained in one step as for the linear analysis. The solution is to perform several steps, update the tentative solution after each step, and repeat until a converge criteria is satisfied. Therefore, the non-linear problem is solved by taking a sequence of linear steps.

The FEM software allows the use of follower forces. This means that, as the rubber lip deforms, the pressure load follows the deformation to be permanently perpendicular to the surfaces exposed to the gas pressure.

4.3. Geometry definition and boundary conditions

The geometries necessary to the shaft seal stress analysis are created on the FEM software and are presented in Figure 4-1. The shaft seal sample E is represented in its free position according to the sectional view, see Figure 3-15. The rubber material is bonded on the metallic inner case and assembled with the other parts: support ring, PTFE lip, and outer case. The rubber edge radius is of 0.2 mm. The interference values are represented in Table 4-2.

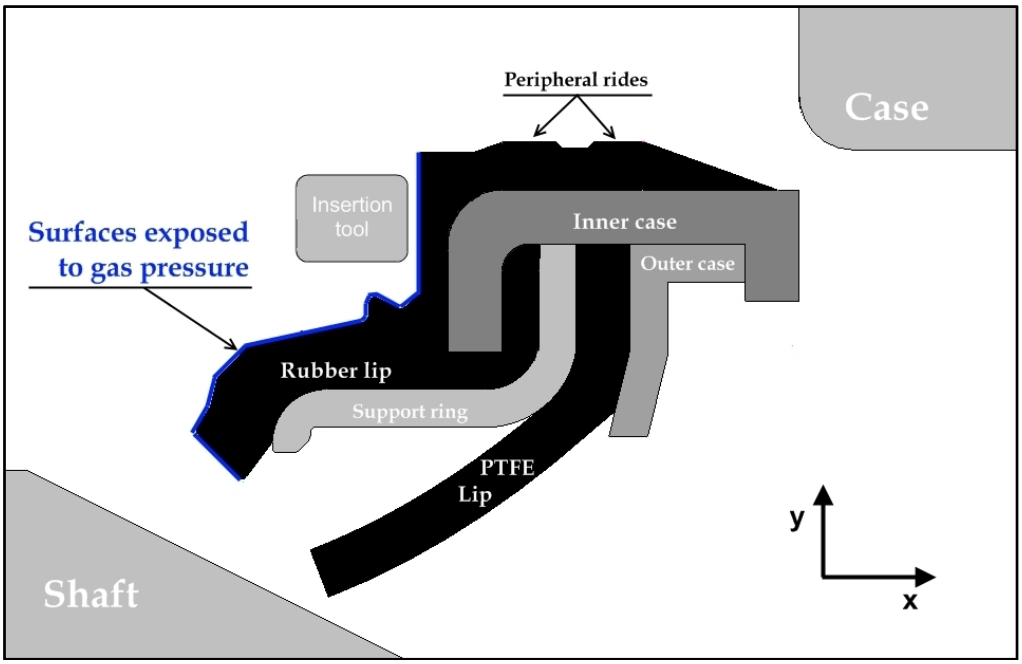

Figure 4-1 Shaft seal sample A geometry with installation components.

Table 4-2 Shaft seal interferences.

	Interference (mm)
Rubber lip/shaft	0.44
PTFE lip/shaft	4.7
Peripheral rides/case	0.32

The MAC compressor shaft seal can be considered as an axis symmetric problem. It has an axis of radial symmetry and all the surfaces are generated by revolving curves around the

axis of symmetry. As the shaft seal is loaded (fluid pressure) in a radially symmetric manner (axis symmetric), then the deflections, strains, and stresses are also axis symmetric and hence can be calculate along one dimension. Therefore, the seal stress analysis is transformed in a 2D axis symmetric problem. By using a plane stress formulation, it is possible to reduce the number of equations, thus the calculation time.

The seal stress analysis is divided in 3 steps:

1st – case insertion,
2nd – shaft insertion, and
3rd – gas pressure load.

First, the seal is inserted in the case by using a tool (movable rigid wall) corresponding to a displacement on the X direction. The peripheral rides are then deformed to fit the case bore and the seal remains fixed. The tool is then removed. In the second step, the shaft moves axially to deform the two lip rings: rubber and PTFE. Finally, the pressure acting on the rubber seal is activated.

The shaft seal FEM analysis requires the simulation of contacts among multiple surfaces. The presence of a contact can complicate the analysis since the changes in the contact area alter the boundary conditions and hence the material stiffness. The rubber material is considered bonded to the inner case and all other contacts are free to move along the mating surface. The friction coefficient can be independently controlled at each interface. It has been fixed to 0.3 at the interface of peripheral rides.

The shaft, the case, and the insertion tool have been modeled as rigid bodies, a reasonable assumption considering that they are made of steel. Rigid bodies are 1D elements and do not need to be meshed. The seal different parts have been meshed using incompressible axis symmetric elements. The mesh for all the seal components is represented in Figure 4-2.

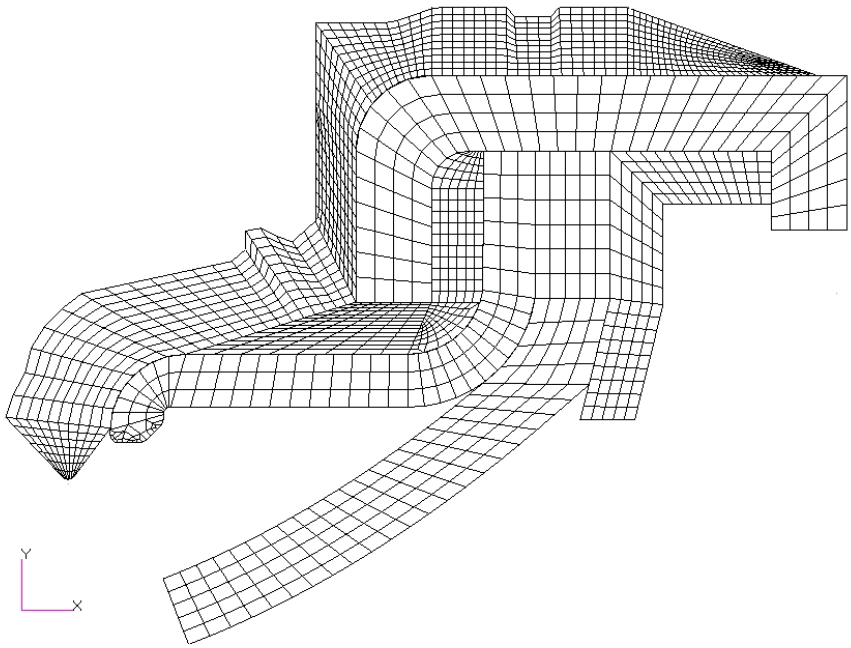

Figure 4-2 Shaft seal components mesh.

4.4. Sources of uncertainties

The stress analysis should be looked as a first intent to simulate the shaft seal behavior. The contacts between the shaft seal, the shaft, and the casing include a high number of variables difficult to fully determine. Therefore, there are some discrepancies between the finite element result and the seal actual behavior. Those uncertainties are related to:

- the model geometry,
- the Boundary conditions,
- the discretization, and
- the properties of the different materials.

When simulating materials with complex strain-stress relations, such as rubber, a special care should be taken when interpreting the results. Nevertheless, the stress strain analysis is a performing tool that can certainly help to the design of new shaft seals.

4.5. Results and discussions

As mentioned in Chapter 3, the gas leaks of the shaft seal are coming from:

- the interfaces between the shaft seal, the shaft, and the casing, and
- the permeation through elastomers.

Test results presented in the same chapter revealed a negligible effect of permeation and of the interface of peripheral rides. When performing the seal stress analysis, it is possible to find why the interface of peripheral rides has such a low contribution to the seal gas emissions.

Figure 4-3 presents the seal contact stress distribution on the rubber lip edge and the interface of peripheral rides. It can be seen that relatively to the rubber lip interface, the peripheral rides have higher:

1. contact stress values, and
2. contact area.

The Poiseuille law (see Equation 2.4) shows that the LFR through a circular channel is directly proportional to the channel diameter and inversely proportional to the channel length. The contact conditions encountered in the interface of peripheral rides produce a low channel diameter due to the high stress value and a long channel due to the important contact area. Therefore, the combination of these two factors leads to a low gas LFR. The rubber lip interface has a contact surface and stress lower than the peripheral rides, thus a higher LFR rate is related to the rubber lip.

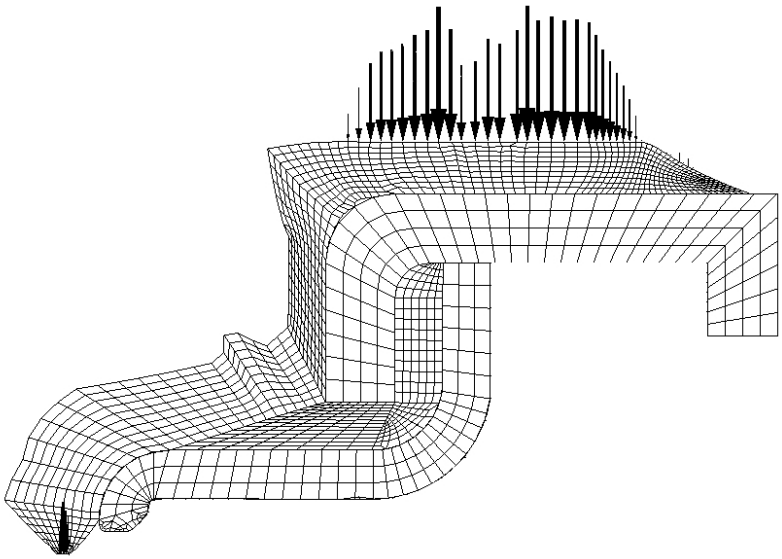

Figure 4-3 Sealing stress distribution on the shaft seal sample E after installation and pressurization.

The seal stress distribution along the peripheral rides is shown in Figure 4-4. The contact stress is distributed in a large area with a mean value of 3.15 MPa. The maximum contact stress is obtained in two different points with a value of 5.9 MPa. Therefore, the peripheral rides will produce a high sealing effect.

The stress values of peripheral rides are dependent on the interface with the case. The gas pressure variation will not change significantly the preload stress value.

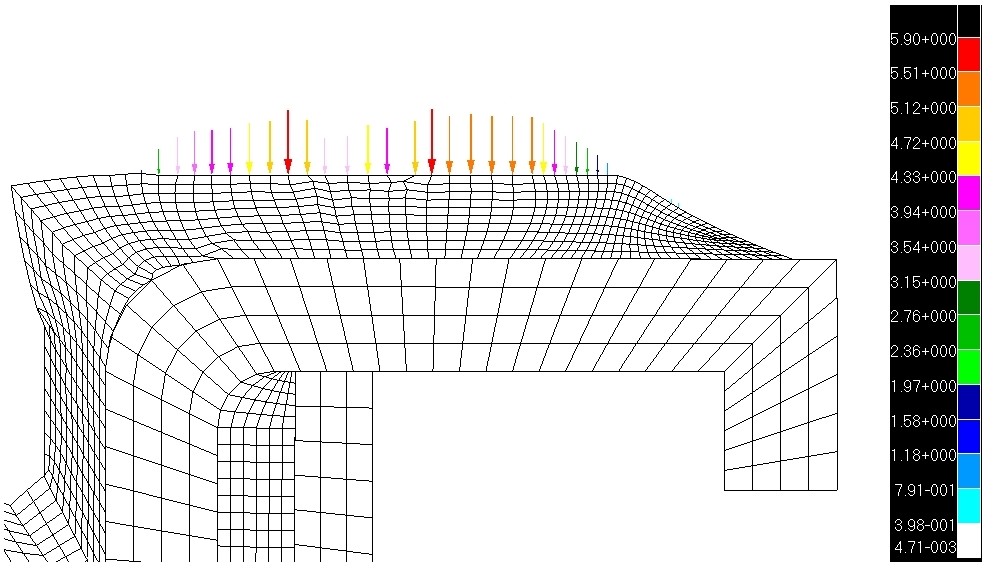

Figure 4-4 Peripheral rides deformation and contact stress distribution, P=0.3 MPa and μ=0.3.

The stress distribution in the rubber lip edge for two pressure levels is presented in Figure 4-5. The wireframe represents the edge initial position and the white color the positions and deformation after the analysis.

It is observed that the edge maximum contact stress is situated in the center of the contact and increases with the gas pressure as well as the material deformation. For the same gas pressure, the rubber maximum contact stress is nearly 3 times lower than the one obtained for the peripheral rides. However, the solution to improve the shaft seal gas emissions at

rest cannot be an increase in the rubber lip contact stress and contact surface, because it would also increase dramatically the wear rate during the shaft rotation.

It is observed that the support ring reduces the rubber lip deformation, thus avoiding the decrease in the contact stress with the gas pressure.

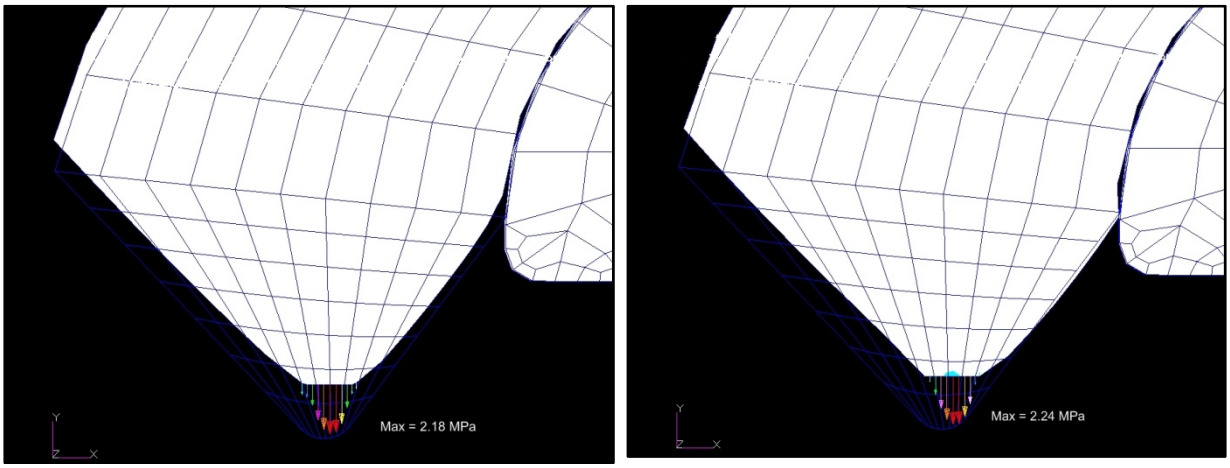

a) b)

Figure 4-5 Rubber lip edge contact stress with μ = 0.01, a) P = 0.3 MPa b) P = 0.5 MPa.

The shaft seal contact visualization presented in Section 3.8 shows different rubber lip deformations for dry and lubricated contacts. By reducing the rubber lip edge friction coefficient during the stress analysis, it has been possible to observe the same phenomena, (see Figure 4-6). So, it can be assumed that the stress analysis represents the rubber lip deformation in a very close way.

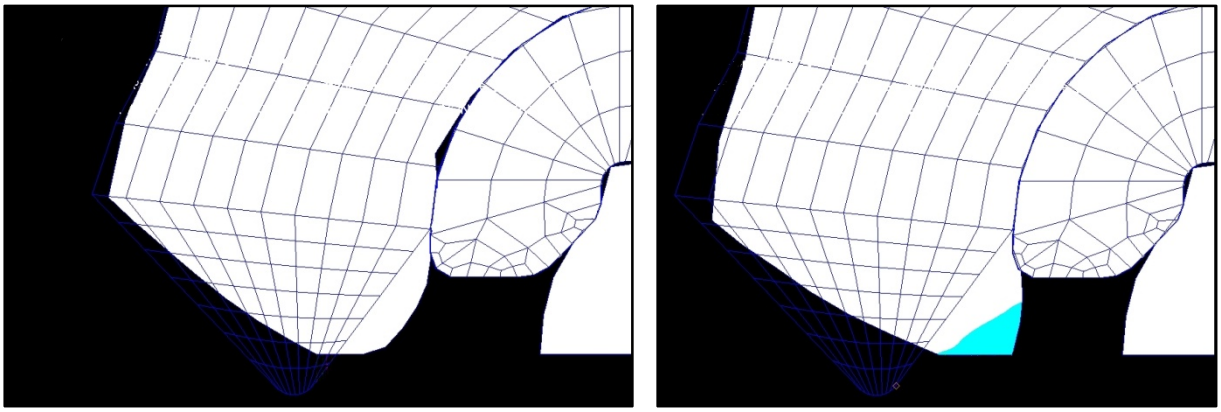

a) b)

Figure 4-6 Rubber lip deformation at P = 1.3 MPa; a) μ = 0.3, b) μ = 0.1.

The increase in the rubber lip deformation under low friction coefficients changes the contact conditions. Figure 4-7 shows the maximum contact stress evolution with the gas pressure for two different friction coefficients. For a low gas pressure, the friction coefficient does not change the maximum contact stress. As the gas pressure increases, the rubber lip maximum contact stress also rises, but the level for a lubricated contact is lower. Therefore, while the compressor is running at high compression ratio, the rubber lip position does not depend on the friction coefficient since the housing pressure is nearly 0.3 MPa.

The rubber lip static sealing effect is achieved by producing a contact stress higher than the gas pressure. It is observed that the rubber lip stress increases with the gas pressure and is 5 times higher than the gas pressure, thus ensuring the seal effect at rest.

By maintaining a high contact stress with the shaft surface, seal sample E performs better than other seal samples presented in Chapter 3, especially at high gas pressure levels, see Figure 3-17.

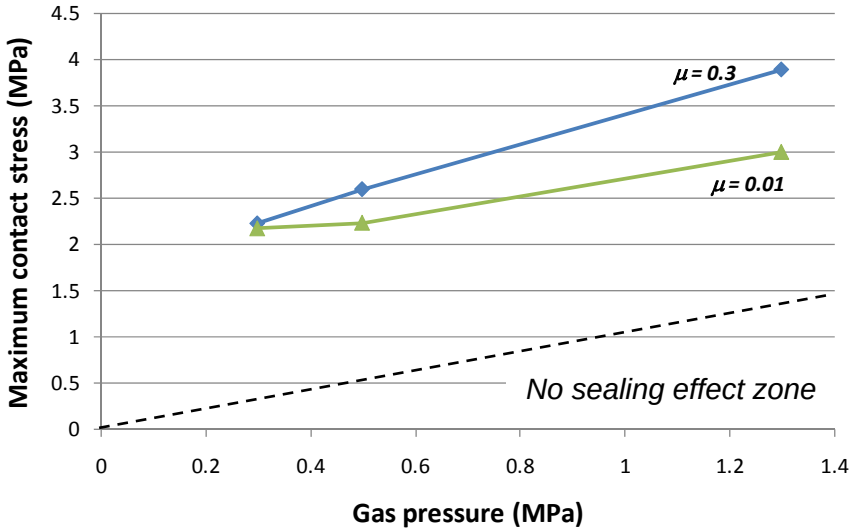

Figure 4-7 Rubber lip edge contact stress evolution with fluid pressure and friction coefficient.

4.6. Conclusions

In this chapter, the rubber lip and peripheral rides stress analysis of the shaft seal sample E has been performed. The seal installation was simulated before the seal pressurization to consider the interference contact stress.

The stress analysis results indicate a high deformation of peripheral rides and stress values relatively low for the rubber lip edge. These values are mainly defined during the seal installation. Those results explain the negligible impact of the peripheral rides on the seal gas emissions. The rubber lip position is maintained by the metallic support ring that ensures the increase in the contact stress with the gas pressure, thus improving the gas sealing ability. The control of the rubber lip edge deformation explains the sample E good sealing performances at high pressure levels when compared to other seal designs.

It has also been found that the contact stress value is also function of the rubber lip friction coefficient. The increase of the friction coefficient increases the rubber lip edge deformation and so reduces the contact stress.

The FEM has proven to simulate very closely the shaft seal contact stress and deformation behavior. It should be used in the future to develop new shaft seal designs in order to improve the gas leak tightness in standstill mode.

4.7. References

[BOA99] Boast, D, Coveney, V, 1999. Finite Element Analysis of Elastomers. Professional Engineering Publishing. 283p.

[KIM96] Kim, C, Shim W, 1996. Analysis of contact force and thermal behavior of lip seals. Tribology International Vol. 30, NO. 2. Pp. 113-119.

[KRI93] Krishnamachari, S, 1993. Applied stress analysis of plastics: A mechanical engineering approach. Van Nostrand Reihold, 593p.

[LEE05] Lee, C, Lin, C, Jian, R, Wen, C, 2005. Simulation and experimentation on the contact width and pressure distribution of lip seals. Tribology International, Elsevier.

[MSC04a] MSC.MARC User's guide, 2004. MSC. Software Corporation

[MSC05b] MSC.MARC Theory and User Information, 2004. MSC. Software Corporation

[SIL04] Silvestri, M, Prati, E, Tasora, A, 2004. Numerical analysis of sealing conditions in elastomeric rings. AIMETA International Tribology Conference, September 14-17, Italy.

[STE89] Steele, J, 1989. Applied finite element modeling. Marcel Dekker, 361p.

[ZIE05] Zienkiewicz, O, Taylor, R, Zhu, J., 2005. The Finite Elements Method: Its Basis & Fundamentals. Elsevier, 733p.

Conclusions

The MAC compressor is a permanently pressurized component whose sealing system continuously releases refrigerant to the atmosphere. Its dynamic seal, the shaft seal, is designed to contain the fluid when the compressor is running as well as when it is at rest. This two working modes result in a very complex seal design that should combine high contact stress and contact surface values at rest, and allow the contact lubrication when the shaft rotates. The shaft seal current design for HFC compressors combines two sealing materials: a rubber lip ring with a sharp edge for the static sealing and a plastic lip ring for the dynamic sealing.

The study of unused and aged compressor emissions has led the identification of the shaft seal sealing mechanism at rest, as well as in running mode. It has been demonstrated that the standstill mode defines the bulk of compressor emissions, which are directly related to the square of the pressure difference between the compressor housing and the atmosphere.

The running mode represents a small part of the compressor life. However, it is of major importance to the shaft seal performance. The leak test results showed that when the shaft starts rotating, there is a period of dry-running which is associated to high refrigerant emissions. This period can take about 15 hours. Once the shaft seal is lubricated, gas emissions are substantially reduced due to the formation of a lubricant oil film in the shaft seal interface. The shaft seal performance in running mode is mainly dependent on the fluid film formation at the seal interface. The increase in the lubricant film thickness creates the separation between the mating surfaces, thus reducing the leak flow path dimensions and so the LFR.

It has also been demonstrated that, when the compressor is at rest, the lubricant oil works as a gas barrier at the shaft seal interface. However, this is a temporary effect since the lubricant is transported through the seal contact, leading to dry contact and so increasing the LFR.

Along the compressor life, the shaft seal is continuously under dry and lubricated conditions. When the compressor works, the steady lubrication regime is scarcely achieved since the compressor usage lasts a short period of time. Even when the seal lubrication reaches a steady state regime, the oil film thickness is not sufficient to avoid the contact between the shaft surface and the seal polymeric materials. Therefore, the shaft and seal wear is inevitable and increases strongly gas emissions. An LFR increasing of 800% has been observed for the aged compressor B1. Compressors C1 and C2, two aged compressors recovered from old MAC systems showed emission levels at rest up to 1,780 g/yr. Accordingly, the wear of the shaft seal surfaces increases exponentially the MAC system emissions, which explains the high demand in refrigerant and the increase in the number of system recharges as the vehicle gets old. The leak detection tools used by the professional technicians are not adapted to leak check the shaft seal, which consequently result in a continuous release of refrigerant from aged vehicles.

The shaft seal contribution to the compressor emissions depends on the wear of sealing surfaces. For an unused compressor, the shaft seal represents up to 50% of emissions. For an aged compressor, the contribution value rises up to 93%. It has also been demonstrated that the shaft seal gas flow is mainly due to the leak paths between the seal and the shaft. The case interface flow and permeation contribution can be neglected.

The study of different shaft seal designs in standstill mode showed the importance of the rubber lip design to control the contact stress with the shaft surface. The higher the contact stress, the lower the leak path dimensions, thus the lower the gas flow rate. The shaft seal sample E is the tightest seal due to the deformation control of the rubber lip with pressure.

The stress analysis of seal sample E also indicates the increase in the rubber lip contact stress with the gas pressure showing one way to develop tighter shaft seals. It has also been noticed that the high contact stress values and contact surface of the seal peripheral rides explain their negligible contribution to the shaft seal emissions.

In summary, the MAC compressor is a leaky component mainly due to the shaft seal whose gas emissions increase exponentially with the wear of sealing surfaces. The wear effect is amplified by the start and stop of the compressor due to the dry-running effect.

Perspectives

The shaft seal development is directly related to the refrigerant used and policies to limit the MAC system emissions. The phasing out of HFC-134a from MAC systems is effective only in Europe. The choice of the next refrigerant will guide the shaft seal development, at least for the European market.

One of the possible candidates is carbon dioxide with a GWP of 1, which results in a compressor gas pressure 10 times higher than that of HFC-134a. The high pressure level represents a technological challenge to the shaft seal development. Until now, the development of CO_2 shaft seals is facing containment problems due to the gas pressure level and the wear of the seal metallic surfaces. The mechanical seal wear was the main reason to ban the mechanical seal from CFC-12 compressors. Another possible candidate is the new refrigerant R-1234yf with a GWP of 4, which presents a system pressure similar to HFC-134a, thus a similar design. However, this fluid is under development. This study was focused on the shaft seal design used for HFC-134a compressors that are still in use outside Europe.

The actual lip type seal design can be improved in two different areas:

- In running mode, and
- In standstill mode

In running mode, the dry-running time must be reduced by improving the oil circulation inside the compressor housing and the shaft seal lubrication, thus reducing the seal wear.

In standstill mode, the use of FEM analysis can improve the rubber lip design to obtain the highest possible contact stress value considering that the compressor housing pressure is higher in standstill mode.

A shaft seal will have low emission levels during its lifetime only if these two different areas are considered. Development work is necessary in those two areas in order to design new shaft seal with lower refrigerant emissions.

FRENCH SUMMARY

Introduction

Le système de climatisation est aujourd'hui un équipement incontournable des véhicules automobiles permettant d'améliorer le confort thermique ainsi que la sécurité des passagers. Ce système de climatisation utilise un fluide frigorigène halogéné, le HFC-134a, dont les émissions contribuent au réchauffement climatique. Le système de climatisation automobile présente des composants non-hermétiques qui sont susceptibles d'émettre du fluide frigorigène dans l'atmosphère. Parmi les différents composants du système, le compresseur a été identifié comme le composant le plus émissif et est responsable de 50 à 60 % des émissions globales du système. Au sein du compresseur, la contribution majeure aux émissions provient du joint tournant, comme cela est démontré dans ce travail.

Le mécanisme d'étanchéité du compresseur, et plus précisément du joint tournant, reste mal connu. La connaissance des paramètres d'étanchéité est nécessaire pour guider le développement dans le sens de la réduction des émissions de gaz.

Les objectifs recherchés sont l'étude des principes physiques et l'analyse des résultats expérimentaux en vue d'améliorer la compréhension des mécanismes fondamentaux et les paramètres qui contribuent aux émissions du joint tournant.

Une première partie fait référence aux impacts environnementaux liés à la climatisation automobile. Dans un deuxième temps, deux bancs d'essais innovants sont présentés et utilisés dans l'étude des émissions du joint tournant à l'arrêt ainsi qu'en fonctionnement. Les performances du joint tournant avec l'usure ont aussi été étudiées. La dernière partie introduit le calcul des contraintes d'un joint tournant qui sert de support à la compréhension des émissions à l'arrêt, ainsi qu'au développement de nouveaux designs.

Il s'agit ici de proposer une nouvelle approche dans l'étude du compresseur de climatisation automobile qui a permis d'identifier le mécanisme d'étanchéité du joint tournant en rotation ainsi qu'à l'arrêt. Les observations montrent la relation entre les émissions et le régime de lubrification, auquel s'ajoute l'effet transitoire de l'huile quand l'arbre est à l'arrêt. Cette étude montre aussi la dégradation importante de l'étanchéité du joint tournant avec l'usure, ce qui explique la forte demande de fluide frigorigène pour la maintenance et le nombre élevé de recharges effectuées sur les véhicules âgés. La méthode de calcul du débit de fuite par accumulation est au cœur de ce travail.

Tous ces résultats illustrent le débit de fuite élevé du joint tournant du compresseur, ainsi que la dégradation de l'étanchéité due au frottement. L'étude proposée n'a jamais été conduite jusqu'à présent et l'approche proposée est originale.

Chapitre 1

EMISSIONS DE FLUIDE FRIGORIGENE DES SYSTEMES DE CLIMATISATION AUTOMOBILE

Le HFC-134a est le fluide frigorigène unique des systèmes de climatisation automobile. Il s'est substitué au CFC-12 interdit par le Protocole de Montréal. Le système de climatisation automobile a été identifié comme le domaine le plus émissif avec 78 % des émissions mondiales de HFC, suivi par les systèmes de climatisation fixe avec 9 % (Figure 1). Cette proportion est aussi élevée car de nombreuses autres applications fixes fonctionnent encore avec des HCFC.

Les niveaux élevés d'émissions de fluides frigorigènes dus à la climatisation automobile sont directement liés à sa conception qui inclut un compresseur de type ouvert, des raccords et des flexibles en polymères utilisés pour connecter les différents composants. Ces composants n'existent pas dans le système de climatisation fixe et sont à l'origine des débits de fuite élevés de la climatisation automobile.

L'impact des émissions de fluides frigorigènes dans l'atmosphère peut être calculé en utilisant la notion de potentiel de réchauffement global (PRG *GWP*). Pour le HFC-134a, le GWP a une valeur de 1410, ce qui signifie que la perte d'un gramme de HFC-134a équivaut à l'émission de 1,' kg de dioxyde de carbone. D'où l'intérêt majeur de réduire les émissions des systèmes de climatisation automobile.

Ainsi, un véhicule dit « propre » doit absolument être équipé d'un système de climatisation avec de faibles taux d'émissions de fluides frigorigènes.

Par ailleurs, les émissions entraînent la perte de puissance frigorifique qui entrîne l'augmentation de la température de l'air soufflé dans l'habitacle. Par conséquent, dès que la température de soufflage atteint des valeurs proches de 18 °C, le conducteur va être amené à réparer le système de climatisation. L'intervalle de temps entre chaque réparation dépend du débit de fuite du système, ainsi que de la température d'entrée d'air dans l'évaporateur. Plus le débit de fuite et la température d'air extérieur sont élevés, plus le temps entre chaque réparation est réduit.

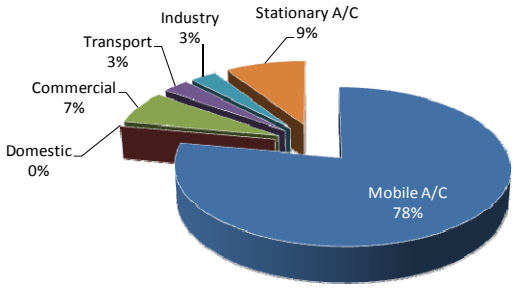

Figure 1 Emissions mondiales de HFC en 2003 reparties par domaine [CLO05]

Débit de fuite du système de climatisation

En 2006, le Centre Energétique et Procédés a réalisé, en collaboration avec l'Association des Constructeurs Européens d'Automobiles, une étude importante pour déterminer le débit de fuite des systèmes de climatisation installés dans les nouveaux véhicules. L'étude a analysé 10 types différents

de systèmes installés dans 39 véhicules et le résultat indique un débit de fuite moyen de 10 g/an. Les essais menés en laboratoire sur des systèmes et composants de climatisation neufs et à l'arrêt ont démontré que la somme du débit de fuite de chaque composant comprenant de(s) joint(s) d'étanchéité est égal au débit de fuite du système où les composants sont installés. Ce résultat est extrêmement important parce qu'il nous indique que l'étude de l'étanchéité des systèmes de climatisation automobile peut être réalisée composant par composant, connaissant ainsi l'impact que chaque amélioration aura dans les émissions globales du système.

Débit de fuite des composants

Grâce à cette étude, il a été possible de hiérarchiser le débit de fuite de chaque composant et de calculer sa contribution aux émissions du système de climatisation. Pour tous les systèmes, le compresseur est le contributeur majeur avec des valeurs entre 50 et 60 %. Les tubes en caoutchouc et polymères utilisés pour faciliter l'assemblage des composants et absorber les vibrations du moteur et du compresseur sont classés comme le deuxième contributeur. La plus faible contribution du compresseur (50 %) correspond à l'utilisation de tubes en caoutchouc avec un coefficient de perméabilité au HFC-134a élevé. La Figure 2 montre la contribution de chaque composant du système de climatisation.

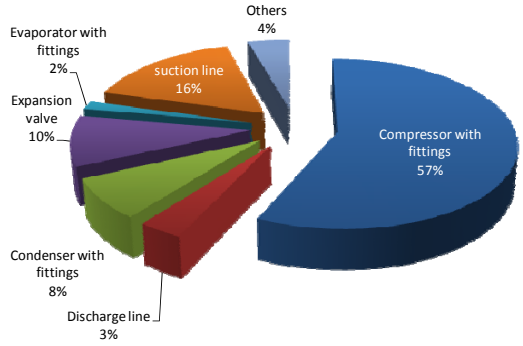

Figure 2 Contribution de chaque composant aux émissions du système de climatisation à l'arrêt et pour une pression de fluide frigorigène de 1020 kPa

Mode de fonctionnement

En Europe, le temps de fonctionnement annuel d'un véhicule est estimé entre 300 et 500 heures. De plus, le compresseur du système de climatisation n'est activé que 60 à 70 % du temps de fonctionnement, ce qui signifie que le compresseur de climatisation est à l'arrêt, de 95 à 98 % du temps, d'où l'intérêt de l'étude des émissions quand le système est à l'arrêt.

Types d'émissions

Les émissions liées au système de climatisation automobile sont divisées en deux groupes : les émissions directes qui résultent des défauts d'étanchéité du système et les émissions indirectes qui proviennent de la production d'énergie nécessaire pour le fonctionnement du système, notamment du compresseur. Dans cette étude, on ne discutera que des émissions directes.

Les émissions directes résultent de la différence de pression entre le fluide frigorigène et l'atmosphère. Elles existent pendant toute la durée de vie du système de climatisation, parce que le circuit est pressurisé non seulement en fonctionnement mais aussi à l'arrêt. En fonctionnement, deux niveaux de pression existent dans le système : condensation et évaporation. A l'arrêt, il n'y a qu'un niveau de pression qui correspond à la pression de saturation du point le plus froid du système, par exemple, 770 kPa à 30 °C.

Les émissions directes peuvent êtres divisées selon les trois phases de la vie d'un système de climatisation : la fabrication, l'usage et la fin de vie. Pendant la fabrication et la fin de vie, les émissions peuvent être contrôlées en établissant des procédures de remplissage et de récupération relativement simples. Le grand défi est dans le contrôle des émissions pendant l'usage du véhicule. Comment localiser les défauts d'étanchéité ? Quelle est la sensibilité des appareils de détection ? Quelle est la procédure pour la récupération et la recharge de fluide ? Est-elle respectée par tous les intervenants ? Combien de fois sont rechargés les systèmes de climatisation ? Les réponses à certaines questions seront données au cours de cette étude. Dans tous les cas, il faut sensibiliser tous les acteurs de la chaîne de la climatisation automobile, à commencer par les usagers.

Les émissions pendant l'usage du système de climatisation peuvent être régulières ou irrégulières. Dans le premier cas, on considère toutes les émissions correspondant à la perte progressive de fluide frigorigène. Elles sont liées à la conception du joint d'étanchéité ainsi qu'à la dégradation de ses performances avec le temps et la fréquence d'utilisation. Dans le deuxième cas, on considère toutes les situations où la dégradation de l'étanchéité est si importante qu'elle provoque la perte rapide et totale du fluide frigorigène contenu dans le système. C'est le cas des accidents de circulation, la rupture des joints d'étanchéité ou encore la perforation du condenseur due aux impacts de pierres provenant de la route. L'usure du joint tournant du compresseur peut aussi provoquer la perte rapide de fluide frigorigène, comme le montre l'analyse menée au cours de cette étude.

Les émissions régulières sont les plus importantes pendant l'usage du système de climatisation parce qu'elles existent dans tous les véhicules équipés d'un tel système, mais surtout parce que le débit de fuite du système de climatisation augmente très fortement avec l'usure du joint tournant du compresseur. Ce fait amène les usagers à réparer le système plusieurs fois dans la vie du véhicule, ce qui contribue aussi l'accroissement des émissions due aux manipulations de fluides frigorigènes.

Localisation des fuites

Les principaux outils utilisés pour la localisation des fuites dans un système de climatisation automobile pendant sa réparation sont : le détecteur portatif avec diode chauffée, les bulles de savon et le colorant traceur. Les points faibles de ces systèmes de détection sont la sensibilité et l'impossibilité de vérifier le joint tournant du compresseur, qui est le joint d'étanchéité le plus émissif du système de climatisation, comme cela est démontré aux chapitres 2 et 3.

En multipliant les émissions de fluide frigorigène par le GWP correspondant, on obtient l'équivalent en CO_2 qui permet d'estimer l'impact des émissions dans l'atmosphère. Ainsi, 115 et 47 millions de tonnes de CO_2 ont été rejetées respectivement par les Etats-Unis et l'EU25 (voir Figure 3). De ce fait, l'impact des émissions du système de climatisation automobile justifie bien l'étude et l'amélioration de son système d'étanchéité.

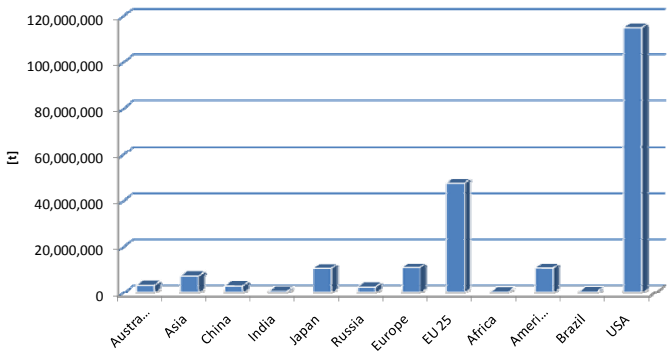

Figure 3 Emissions directes de la climatisation automobile en équivalent CO_2 en 2003.

Réglementation et marché de la climatisation automobile

La production mondiale de véhicules en 2006 était de 69,2 millions d'unités et continue à augmenter compte tenu de la forte demande notamment dans des pays comme l'Inde, la Chine et l'Ukraine. On sait aussi que 90 % des véhicules neufs sont équipés d'un système de climatisation, d'où l'impact important des émissions directes dans l'atmosphère. De plus, le marché de la climatisation automobile n'est pas exclusif des véhicules légers. Elle est aussi installée dans des véhicules commerciaux, cabines de camions, machines agricoles, bus et autocars.

L'Union Européenne a réglementé et rendu obligatoire la mesure du débit de fuite des systèmes de climatisation neufs utilisant un fluide frigorigène dont le GWP est supérieur à 150 et en imposant un niveau de débit de fuite maximal pour son homologation (Directive 40/2006). A partir de 2011, l'Union Européenne refusera toute homologation de véhicules équipés de systèmes de climatisation utilisant un fluide frigorigène avec un GWP supérieur à 150.

En Europe, le changement de fluide frigorigène est inévitable, ce qui contribue au développement de nouveaux fluides comme le R-1234yf dont le GWP est de 4, ainsi qu'au développement de systèmes de climatisation au CO_2. En dehors de l'Europe, il n'y a aucune restriction aux émissions des systèmes de climatisation automobile.

En résumé, le système de climatisation automobile est un équipement continûment sous pression, qui présente des taux d'émissions élevés dus en grande partie aux défauts d'étanchéité du compresseur. Le débit de fuite à l'arrêt définit les émissions du système de climatisation. L'amélioration de l'étanchéité du système de climatisation automobile est fondamentale pour réduire l'impact des émissions de HFC-134a dans l'atmosphère.

Chapitre 2

EMISSIONS DE FLUIDE FRIGORIGENE DU COMPRESSEUR DE CLIMATISATION

Au chapitre 1, le compresseur du système de climatisation a été identifié comme le composant le plus émissif. Dans ce chapitre, les différents types de joints d'étanchéité présents dans le compresseur sont décris ainsi que leur principe de fonctionnement.

Différents types d'étanchéité

Le compresseur est une structure en aluminium composée de l'assemblage de plusieurs pièces. De cet assemblage résulte l'introduction de joints d'étanchéité qui sont à l'origine de la perte continue de fluide frigorigène. Pour étudier les émissions du compresseur, on doit distinguer les deux types d'étanchéité : statique et dynamique.

L'étanchéité statique implique que la vitesse entre les deux surfaces à isoler est nulle. C'est le cas des joints du corps du compresseur comme les joints toriques et métalliques. Le joint placé entre l'arbre et la partie frontale du compresseur est nommé joint tournant et possède un mécanisme d'étanchéité plus complexe que les joints du corps. Le joint tournant est normalement vu comme un composant qui limite les pertes de fluide frigorigène et l'huile de lubrification uniquement quand l'arbre tourne. Dans ce cas, il est classé comme un joint dynamique. Cependant, dans un compresseur de climatisation, la pression du fluide est toujours supérieure à la pression atmosphérique, ce qui oblige le joint tournant à être aussi un joint statique quand l'arbre ne tourne pas. Alors, le joint tournant est à la fois un joint statique et dynamique. Ce double principe de fonctionnement résulte en un système d'étanchéité complexe qui sera analysé en détail dans ce travail.

L'introduction d'huile de lubrification dans le compresseur résulte de la nécessité de réduire le frottement entre les différentes parties en mouvement. Dans ce travail, on montrera que l'huile de lubrification a aussi un effet très important dans le mécanisme d'étanchéité statique ainsi que dynamique du joint tournant. De ce fait, la circulation d'huile dans le corps du compresseur devient aussi importante pour le système d'étanchéité. Dans un compresseur à pistons, l'huile circule avec le fluide frigorigène, ainsi que le mouvement des pistons et du plateau oscillant. Par conséquent, pour un compresseur à cylindrée variable, la circulation de l'huile dépend du taux de compression. Un autre facteur qui fait varier la distribution d'huile dans les joints d'étanchéité du compresseur est la circulation d'huile dans le circuit de climatisation. Comme l'huile est miscible avec le réfrigérant, il y a toujours une quantité qui circule dans le système, ce qui fait baisser le niveau d'huile du compresseur. Ce phénomène est plus intense lors du démarrage du compresseur où une grande quantité de lubrifiant est envoyée dans le système, réduisant significativement l'épaisseur du film d'huile entre les pièces en mouvement.

Etanchéité statique

Le mécanisme d'étanchéité d'un joint statique est basé sur la déformation élastique ou plastique d'un matériau plus mou que celui des surfaces à isoler. Ainsi, une fois le joint installé, il existe deux chemins de fuite possibles :

1. le contact entre le joint et les surfaces à isoler, et
2. la perméabilité à travers le matériau.

Dans le premier cas, le chemin de fuite résulte des irrégularités des surfaces en contact et le débit de fuite $\dot{m}$ peut être décrit par la loi de Poiseuille :

$$\dot{m} = \left(\frac{\pi r^4}{16 \mu_g l} \right) \Delta P^2$$

Le débit de fuite par le contact est ainsi proportionnel à la différence entre la pression atmosphérique et celle du fluide au carré ΔP^2 et au rayon du chemin de fuite r. Il est inversement proportionnel à la viscosité du fluide frigorigène μ_g et à la longueur du chemin de fuite l.

Dans le deuxième cas, le fluide frigorigène traverse la matière du joint et son débit peut être calculé par :

$$\dot{m} = P_e A \frac{\Delta P}{e}$$

Le débit de fuite par perméabilité dépend du coefficient de perméabilité du matériau P_e, de la surface en contact avec le gaz A ainsi que de la différence de pression entre les deux côtés du joint ΔP. Plus l'épaisseur de la matière e est importante, moins le débit de fuite sera élevé. Subséquemment, le débit de fuite d'un joint statique est l'addition du débit par contact et par perméabilité.

Etanchéité dynamique

Le mécanisme d'étanchéité du joint dynamique, le joint tournant, est basé sur la formation d'un film d'huile entre les surfaces en mouvement qui réduit non seulement la température de l'interface, mais aussi les dimensions du chemin de fuite, réduisant aussi le débit de gaz qui traverse le contact. L'épaisseur du film d'huile à l'interface dépend de la pression de contact, de la viscosité du fluide, du module d'élasticité et de la vitesse de rotation. Un régime de lubrification élastohydrodynamique est plus favorable aux émissions qu'un régime limite avec une moindre épaisseur de film.

La géométrie du joint tournant

Le joint tournant d'un compresseur est composé de deux lèvres pour l'étanchéité principale et d'ondulations pour l'étanchéité secondaire, voir figure 4. Quand le compresseur est à l'arrêt, l'étanchéité statique par contact est assurée par la lèvre en caoutchouc ainsi que par les ondulations. Quand l'arbre est en rotation, le film d'huile qui se forme dans l'interface avec la lèvre en PTFE assure l'étanchéité. Comme il n'y a pas de mouvement relatif entre le joint et sa fixation, les ondulations fonctionnent toujours en mode statique. La perméabilité est indépendante du mode de fonctionnement si on néglige l'effet de l'huile sur les surfaces des matériaux.

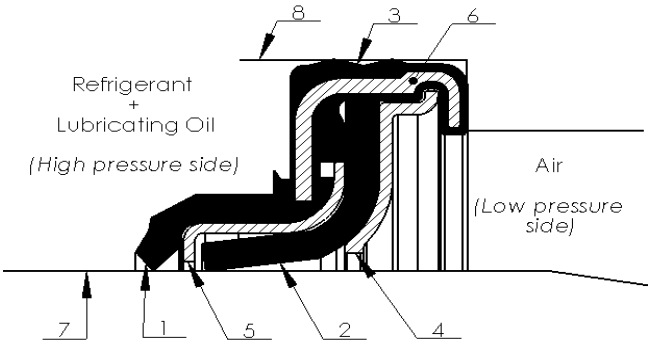

1) Lèvre en caoutchouc ; 2) Lèvre en PTFE ; 3) Ondulations ; 4) Support métallique ; 5) Support de la lèvre en caoutchouc ; 6) Structure métallique du joint ; 7) Surface de l'arbre ; 8) Surface de la fixation du joint

Figure 4 Vue en coup d'un joint tournant de compresseur

Banc d'essais du compresseur

Un banc d'essais innovant a été développé pour l'étude des émissions du fluide frigorigène du compresseur dans les deux modes de fonctionnement : à l'arrêt et en rotation. Le banc est composé d'une cellule hermétique où sont installés le compresseur et son moteur d'entraînement (voir figure 5). Les autres composants du circuit de climatisation sont installés à l'extérieur de la cellule. Ainsi, une fois le circuit sous pression, tout le gaz sortant du compresseur restera à l'intérieur de la cellule hermétique qui est à la pression atmosphérique. Un spectrophotomètre infrarouge est utilisé pour mesurer en continu la concentration de fluide frigorigène à l'intérieur du volume hermétique pour ensuite calculer le débit de fuite $\dot{m}$ en utilisant l'expression :

$$\dot{m}_{HFC-134a} = M_{HFC-134a} \frac{\partial n_{HFC-134a}}{\partial t}$$

Le débit de fuite du compresseur est le produit de la masse molaire du gaz *M* par la variation du nombre de moles de gaz *n* dans le temps à l'intérieur du volume hermétique. L'incertitude du débit de fuite est de 6 %.

La mesure de concentration en continu est un des points clés de cette étude puisqu'elle permet d'identifier tous les phénomènes transitoires importants pour les émissions de gaz.

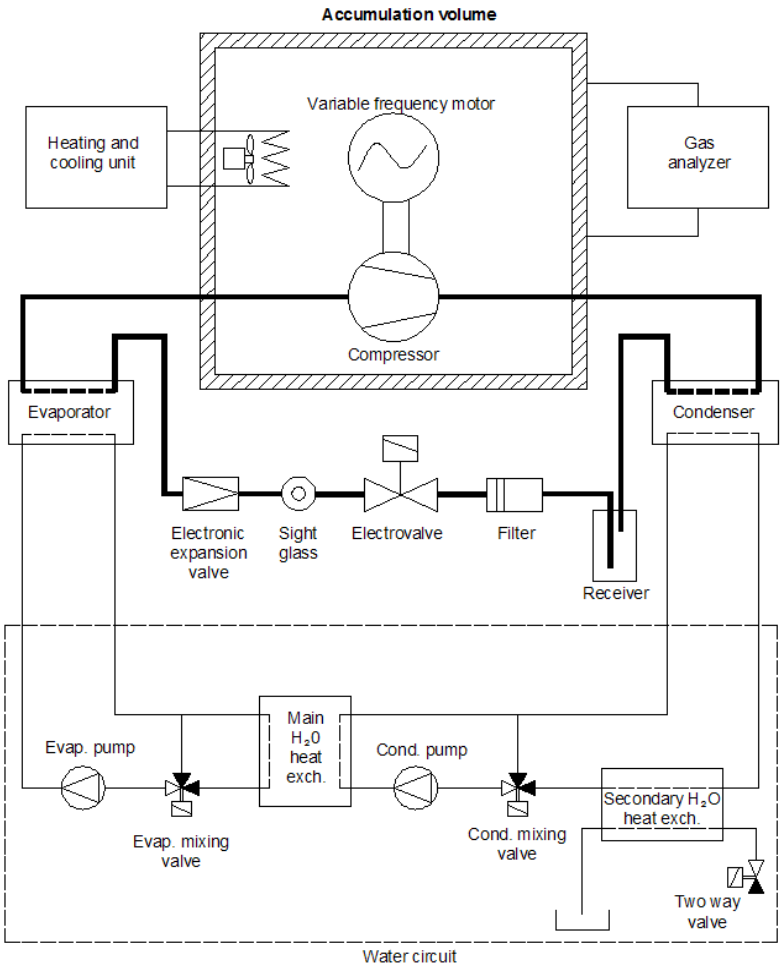

Figure 5 Banc d'essais pour l'étude de l'étanchéité du compresseur de climatisation à l'arrêt et en fonctionnement

Conditions de fonctionnement

L'étude considère les compresseurs à pistons à cylindrée variable parce qu'ils représentent plus de 80 % du marché de la climatisation automobile en Europe. Une étude préalable sur la pression et la température du fluide dans le carter du compresseur a été menée pour connaître les conditions de fonctionnement des joints statiques et du joint tournant afin de comparer ensuite les niveaux d'émissions. A l'arrêt, la pression du carter est égale à la pression du circuit et définie par la température du point le plus froid du circuit. La température du fluide résulte de l'équilibre avec la température du compartiment moteur. Quand le compresseur est en fonctionnement, la pression du fluide dans le carter est très proche de la pression d'évaporation. La température du fluide est directement liée aux pertes par frottement et augmente avec la vitesse de rotation, le taux de compression et la température du compartiment moteur.

L'augmentation du taux de compression produit des conditions à effets inverses pour les émissions de gaz. Premièrement, il a été vérifié que la pression du fluide dans le carter varie de manière inverse à celle du taux de compression, ce qui réduit la différence de pression responsable du débit de fuite. Deuxièmement, la température du fluide augmente avec le taux de compression, ce qui signifie une réduction de la viscosité du fluide qui affectera la formation du film de lubrification au joint tournant. Les émissions de gaz associées à ces conditions montrent que le débit de fuite du compresseur suit l'évolution de la température du fluide, ce qui prouve que le régime de lubrification du joint tournant est primordial pour établir le débit de fuite du compresseur en fonctionnement. A l'arrêt, c'est la pression du fluide qui définit le niveau d'émissions qui, comme le décrit la loi de Poiseuille, a une évolution quadratique avec la différence des pressions.

L'effet de l'huile de lubrification

L'effet barrière produit par l'huile dans le joint tournant a été mesuré. On constate une réduction du débit de fuite dans les premières heures d'essai qui peuvent atteindre 193 %. Cependant, l'effet barrière est temporaire. Il peut varier d'une heure jusqu'à quinze heures en fonction de la quantité d'huile présente dans le joint tournant. L'analyse détaillée de ce phénomène est présentée dans le chapitre 3.

L'usure du joint tournant

Deux approches différentes ont été réalisées pour déterminer l'impact de l'usure du joint tournant sur les émissions de gaz : mesure du débit de fuite de compresseurs usagés et vieillissement de compresseurs.

Deux compresseurs de climatisation ici nommés C1 et C2 ont été récupérés de véhicules ayant parcouru respectivement 300 000 et 85 000 km. Les essais menés à l'arrêt montrent des débits de fuite extrêmement élevés : 181 g/an pour le compresseur C1 et 1411 g/an pour le compresseur C2 pour une pression de fluide de 1030 kPa. Les mêmes compresseurs en fonctionnement présentent paradoxalement le débit de fuite le plus faible mesuré au cours de ce travail : 18 et 6 g/an à 4000 tr/min pour les compresseurs C1 et C2, respectivement. Ces résultats montrent plusieurs choses :

- les mécanismes d'étanchéité à l'arrêt et en rotation sont radicalement différents,
- l'usure du joint tournant a des effets catastrophiques sur les émissions à l'arrêt,
- la formation du film de lubrification au joint tournant est favorisée par l'usure, ce qui explique les performances en fonctionnement,
- les chemins de fuite situés dans le contact entre le joint tournant et l'arbre définissent le débit de fuite.

Les essais d'endurance ont été menés sur deux compresseurs neufs, nommés B1 et B2. Le premier essai consiste dans la mesure du débit de fuite à l'arrêt qui servira à évaluer la dégradation des performances selon le temps de fonctionnement. Le vieillissement consiste dans la répétition de cycles

NEDC, ainsi que des vitesses constantes intercalées de quelques essais à l'arrêt. L'évolution de la concentration a été enregistrée en continu.

Ces tests de vieillissement en laboratoire ne constituent qu'une première approche des conditions réelles de fonctionnement du compresseur. Il faut noter que le temps de fonctionnement en continu d'un compresseur est en moyenne de 2 à 3 heures si on considère un compresseur sans embrayage. Il sera encore plus réduit si on considère les compresseurs qui peuvent être arrêtés quand la demande de puissance frigorifique est nulle. Cette condition a un impact important sur l'usure du joint tournant parce qu'à chaque démarrage du compresseur, le niveau d'huile du compresseur baisse, ce qui augmente l'usure des composants en frottement. Les tests d'endurance présentent un nombre restreint d'arrêts pour limiter le temps de l'essai d'où un écart significatif par rapport à la vie réelle.

L'analyse en continu de la concentration du HFC-134a à l'intérieur du volume d'accumulation a permis d'identifier deux phénomènes :

1. l'effet temporaire de l'huile sur les émissions après une longue période d'arrêt,
2. le démarrage à sec du joint tournant.

Pour le compresseur B1, après une période d'arrêt qui varie entre 30 et 40 heures, le contact du joint tournant devient sec, ce qui entraîne une augmentation très importante du débit de fuite, comme indiqué dans la figure 6b. Le démarrage du compresseur sans huile au contact du joint tournant va entraîner des émissions de gaz extrêmement élevées pendant les cinq premières heures de fonctionnement, voir la figure 6a. Le film d'huile au contact du joint tournant sera complètement établi après plus de 17 heures de fonctionnement en continu, ce qui est identifiable par l'évolution linéaire de la concentration de gaz avec le temps. La fin de l'essai de l'étape 16 montre que l'élévation de la température du compresseur de 2 °C augmente le débit de fuite en 15 g/an en raison de la diminution de la viscosité de l'huile.

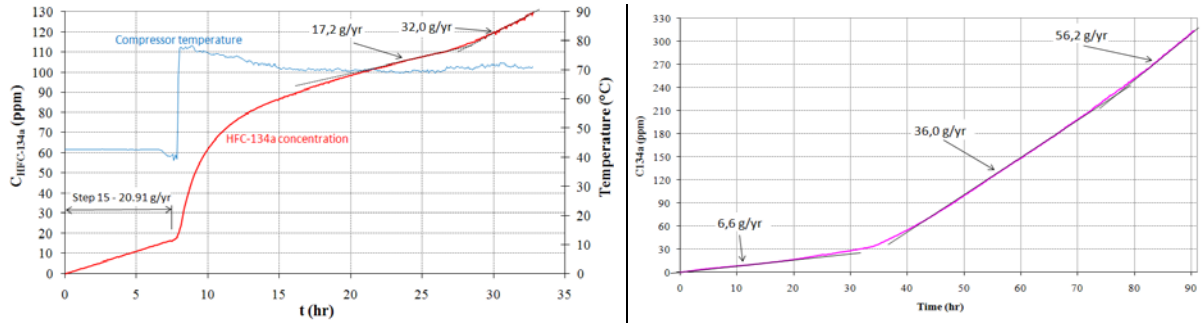

a) Step 16 *b) Step 17*

Figure 6 Evolution de la concentration du fluide frigorigène pour le compresseur B1 a) à 5 000 tr/min et b) à l'arrêt

Après un vieillissement de 872 heures, dont 584 en fonctionnement, le débit de fuite du compresseur B1 a évolué de 6,2 g/an à 56,2 g/an à l'arrêt pour une pression de fluide de 1020 kPa, ce qui résulte dans une augmentation de 800 % des émissions de gaz. A noter que la période de fonctionnement n'est jamais si longue pour un compresseur installé dans un véhicule. L'usure du joint tournant est accélérée par le démarrage à sec qui se répète des milliers de fois dans la vie d'un compresseur. La dégradation de l'étanchéité du joint tournant du compresseur B1 est encore plus importante dans la vraie vie du compresseur.

Le compresseur B2 ne possède pas d'embrayage, ce qui signifie qu'il fonctionne en continu avec le moteur du véhicule. Si le besoin de puissance frigorifique est nul, le taux de compression est ramené à zéro. Dans ce cas, la pression du circuit est définie par la température du point le plus froid du système mais elle est supérieure à la pression d'évaporation dès que la température extérieure est supérieure à 5 °C. Ce type de compresseur nécessite un système de distribution d'huile et de lubrification du joint tournant différent de celui du compresseur B1. Quand le taux de compression est nul, il y a très peu de

pièces en mouvement dans le carter et le fluide est à l'arrêt, ce qui rend difficile l'apport d'huile aux pièces en contact. De ce fait, le démarrage à sec, ainsi que l'effet de l'huile, sont beaucoup moins prononcés que dans le compresseur B1. Le joint tournant retient mieux l'huile, ce qui l'empêche de sécher complètement tout en réduisant l'effet de l'usure. Après 385 heures de fonctionnement et 272 heures à l'arrêt, le compresseur B2 présente une augmentation du débit de fuite de 40 % à l'arrêt pour une pression de 1020 kPa.

Le compresseur B2 présente une dégradation de l'étanchéité du joint tournant beaucoup moins importante que celle du compresseur B1, notamment à l'arrêt. Par contre, le débit de fuite en rotation est plus élevé pour le compresseur B2. Ceci montre que la présence quasi permanente d'huile dans le joint tournant réduit significativement l'usure. Pour un cycle NEDC, le débit de fuite du compresseur avec un taux de compression nul est supérieur au débit de fuite à l'arrêt. De plus, le temps de fonctionnement augmente l'usure du joint tournant. Ainsi, le compresseur B2 aurait un taux d'émissions annuel de gaz plus faible s'il était équipé d'un embrayage permettant de l'arrêter quand il n'y a pas de demande de froid.

L'effet de l'huile pendant les 30 à 40 premières heures d'arrêt du compresseur indique aussi qu'il y a un transport d'huile à travers le contact du joint tournant et qu'il serait plus important sur le compresseur B1. En démontant l'embrayage de ce compresseur, une quantité importante d'huile à été trouvée du côté extérieur du joint tournant, ce qui montre bien que le transport d'huile existe. Sur son chemin, l'huile transporte aussi des micro-débris résultants de l'usure des lèvres. Ce nettoyage du contact du joint tournant n'est pas complètement souhaitable puisque le dépôt de polymère remplit les irrégularités de la surface de l'arbre, c'est-à-dire, qu'il réduit la dimension des chemins de fuite, et par conséquence le débit de fuite à l'arrêt.

Débit de fuite du joint tournant

Un nouveau volume d'accumulation hermétique a été développé pour mesurer le débit de fuite du seul joint tournant. Il a été installé dans les compresseurs C1 et B1 et a permis le calcul du débit de fuite du joint tournant, ainsi que la contribution du joint tournant aux émissions du compresseur. Pour une pression de fluide de 1020 kPa, la contribution du seul joint tournant aux débits de fuite des compresseurs C1 et B1 est de 93 et 71 %, respectivement. Ce résultat montre clairement que le joint tournant est le joint d'étanchéité le plus émissif du compresseur et même de tout le système de climatisation.

Texture de l'arbre du compresseur

La dégradation de l'étanchéité du joint tournant a été étudiée par la mesure du profil de rugosité de l'arbre dans la région de contact avec les lèvres du joint. Ces mesures mettent en évidence la formation de pistes de frottement avec une profondeur maximale de 2 µm sur la surface de l'arbre. Ces pistes résultent de l'abrasion provoquée par les particules métalliques de taille micrométrique qui proviennent des pièces en mouvement du compresseur, notamment du roulement qui est placé juste à côté du joint tournant.

L'augmentation de la rugosité des surfaces en contact va influencer le débit de fuite à deux niveaux. A l'arrêt, elle se traduit par des chemins de fuite plus nombreux et de tailles plus importantes, ce qui augmente le débit de fuite. En fonctionnement, les défauts de surface fonctionnent comme des réservoirs d'huile, ce qui améliore la lubrification. Le comportement viscoplastique du PTFE joue aussi en faveur de la lubrification du joint tournant, puisque la réduction de la pression de contact avec le temps produit un film d'huile plus épais. La combinaison de ces deux effets est à l'origine de la meilleure étanchéité des compresseurs C1 et C2 en fonctionnement.

Chapitre 3

EMISSIONS DE FLUIDE FRIGORIGENE DU JOINT TOURNANT

Le chapitre 2 a montré la nécessité d'étudier le mécanisme d'étanchéité du joint tournant. Pour cela, les principes physiques pour un contact sec et en présence d'huile ont été étudiés dans le chapitre 3. Un nouveau banc d'essais a été développé pour étudier l'étanchéité du joint tournant à l'arrêt ainsi que pour visualiser le contact avec la surface de l'arbre.

Etanchéité statique

L'étanchéité statique du joint tournant est basée sur le contact permanent, d'une part, de la lèvre en caoutchouc et de la surface de l'arbre et, d'autre part, des ondulations avec la surface de fixation du joint (voir figure 3). La pression de contact nécessaire pour produire l'effet d'étanchéité est obtenue en combinant la pression de contact résultante de l'installation du joint avec la pression de contact provoquée par la pression du fluide.

La lèvre en caoutchouc a un profil aigu qui permet d'obtenir des pressions de contact élevées. Cependant, une surface parfaitement lisse n'existe pas. Toutes les surfaces ont des irrégularités qui résultent du processus de fabrication. De ce fait, quand deux surfaces sont en contact, on doit faire la distinction entre la surface de contact apparente *w* et la surface de contact réelle (voir figure 7). Cette dernière correspond aux quelques points des deux surfaces qui sont effectivement en contact. Les espaces qui sont autour de ces points de contact correspondent aux chemins empruntés par le gaz pour atteindre le côté à la pression la plus faible. L'amélioration de l'effet statique passe donc par la réduction du nombre et des dimensions des chemins de fuite, ce qui correspond à l'augmentation de la surface réelle de contact. Cette surface de contact effective peut s'agrandir par deux différentes approches : réduction de la rugosité des surfaces par modification de la méthode de fabrication et/ou, comme décrit par la théorie d'Hertz, en augmentant la pression de contact et en utilisant un matériau élastique. Une autre approche pour réduire le débit de fuite par contact passe par l'augmentation de la surface de contact apparente, ce qui augmente le nombre de points de contact et rend le chemin de fuite plus tortueux et long.

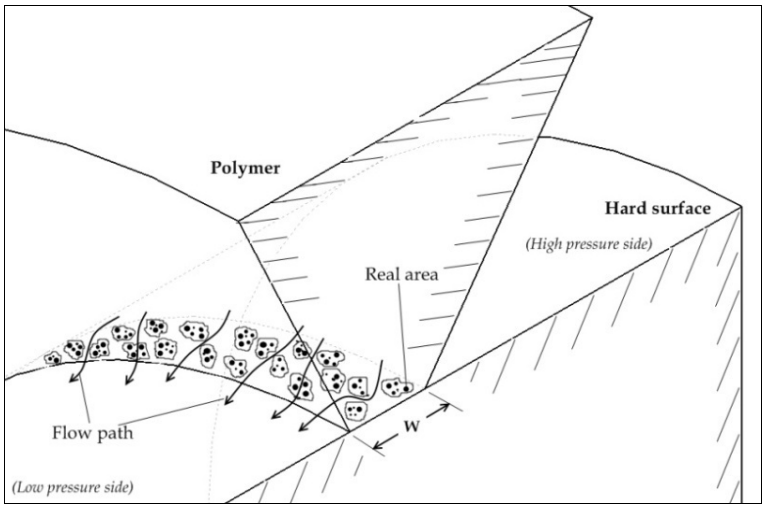

Figure 7 Chemins de fuite dans le contact entre la lèvre en caoutchouc et la surface de l'arbre

Cependant, la lèvre en caoutchouc est aussi soumise à la rotation de l'arbre du compresseur. Cela signifie que les conditions de contact doivent faciliter non seulement la formation d'un film d'huile pour réduire l'usure, mais aussi son transport à travers le contact pour permettre la lubrification de la lèvre en PTFE. Alors, l'effet statique est incompatible avec l'effet dynamique puisque les chemins de fuite empruntés par le gaz sont, dans une moindre mesure, empruntés par l'huile.

La perméabilité est une propriété intrinsèque du caoutchouc et définie par la loi de Fick. Le gaz en contact avec le caoutchouc commence à être absorbé dans la matière, ensuite, il va traverser la matière en raison de la différence de concentration, phénomène de diffusion, pour finalement s'évaporer du côté du caoutchouc à la plus faible pression. La perméabilité résulte du transport du gaz dans ces trois étapes.

Le débit par les contacts avec l'arbre et le support additionné au débit par perméabilité donne le débit de fuite total du joint tournant à l'arrêt.

L'effet de l'huile

La présence d'huile de lubrification dans un contact change le débit de fuite de celui-ci tout simplement parce que le nombre et les dimensions des chemins de fuite sont fortement réduits. Ce phénomène peut s'expliquer par la formation d'un ménisque d'huile non seulement autour d'un contact réel, mais aussi entre les aspérités qui sont proches du contact (voir figure 8a). Le ménisque va remplir et/ou réduire les dimensions des chemins de fuite, ce qui agit directement sur le débit de gaz qui traverse le contact.

Toutefois, la force exercée par le gaz peut vaincre la force d'attraction des ménisques. Dans ce cas, l'huile sera transportée à travers le contact. Cet effet est souhaitable quand l'arbre du compresseur est en rotation parce qu'il permet la lubrification du contact de la lèvre en caoutchouc et l'alimentation en huile pour la lèvre en PTFE. Mais à l'arrêt c'est tout le contraire. Il serait préférable de retenir l'huile dans le contact de la lèvre en caoutchouc pour éviter que le contact sèche. Il faut noter qu'à l'arrêt, le joint tournant n'est pas alimenté en huile, donc, une fois que la force d'attraction des ménisques n'est plus suffisante pour les fixer autour des aspérités, le contact devient progressivement sec.

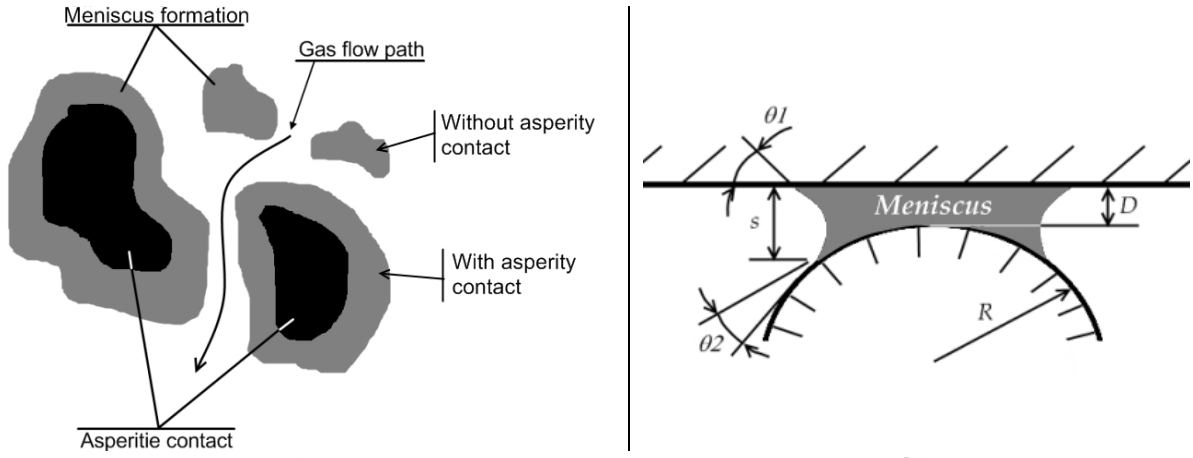

Figure 8 a) Formation d'un ménisque, b) Paramètres pour le calcul de la force d'attraction d'un ménisque entre une sphère et une surface plane

La force d'attraction d'un ménisque F_L peut être étudiée en considérant une géométrie de contact simple (voir figure 8b) :

$$F_L = \frac{2\pi r \gamma_{LA} (\cos\theta_1 + \cos\theta_2)}{1 + \frac{D}{f_S}}$$

La force d'attraction va donc dépendre de la géométrie des aspérités, de la tension de surface de l'huile γ_{LA}, de l'angle entre les deux surfaces, ainsi que de la distance entre les aspérités *D*. Plus la F_L est grande, plus l'effet d'huile perdure dans le temps.

Evolution de la conception du joint tournant

La conception du joint tournant du compresseur de climatisation automobile a beaucoup évolué depuis les années 80. A cette époque, la conception dérivait d'autres composants mécaniques où l'étanchéité de l'huile était importante. C'était le cas des pompes, des machines outils, des boîtes de vitesses, entre autres. L'étanchéité de ce joint tournant était basée sur le contact entre deux surfaces métalliques. Cependant, des débits de fuite très importants d'huile et de gaz, qui provoquaient même la panne du compresseur, ont été observés. Ces niveaux d'émissions étaient liés principalement à l'usure des surfaces métalliques.

En 1986, une nouvelle conception a été introduite sur le marché. Elle n'était plus basée sur un contact entre deux surfaces métalliques, mais plutôt entre deux lèvres en PTFE et HNBR avec la surface de l'arbre qui ont permis un gain très important en termes d'émissions. C'était une conception très proche de celle utilisée aujourd'hui. La littérature concernant ce type de joint tournant est presque inexistante et la seule façon d'accompagner l'évolution de la conception est par la lecture des brevets.

D'abord, on constate que le développement se fait presque uniquement à partir du mode fonctionnement. L'étanchéité du joint tournant à l'arrêt est très rarement mentionnée, or on sait qu'elle représente entre 95 à 98 % de son temps de vie et que l'effet du vieillissement fait augmenter très fortement le débit de fuite à l'arrêt. Au contraire de la lèvre en PTFE, la géométrie de la lèvre en caoutchouc présente plusieurs géométries qui visent surtout le contrôle de la pression de contact. On ne dispose d'aucune donnée pour évaluer la performance de tels designs.

Le récent développement des compresseurs au CO_2 pose de nouveaux défis pour la conception du joint tournant compte tenu de la pression élevée à l'intérieur du compresseur. La conception la plus répandue aujourd'hui pour les compresseurs à haute pression est le principe du joint mécanique utilisé dans les années 80 avec les compresseurs au CFC-12. Mais les performances n'ont pas changé puisque les compresseurs au CO_2 présentent encore des taux d'émissions très élevés. Dans cette étude, on étudie uniquement le joint tournant des compresseurs à basse pression.

Banc d'essais du joint tournant

Un nouveau banc d'essais a été développé pour étudier l'étanchéité du joint tournant du compresseur à l'arrêt. Ce nouveau banc est constitué de deux cellules hermétiques : fluide frigorigène et accumulation. Le joint tournant avec l'arbre sont placés entre les deux cellules. Ainsi, tout le fluide qui traversera le joint tournant sera mesuré dans la cellule d'accumulation (voir figure 9). La cellule d'accumulation est à la pression atmosphérique. Le principe de mesure est le même que celui présenté pour le banc d'essais du compresseur.

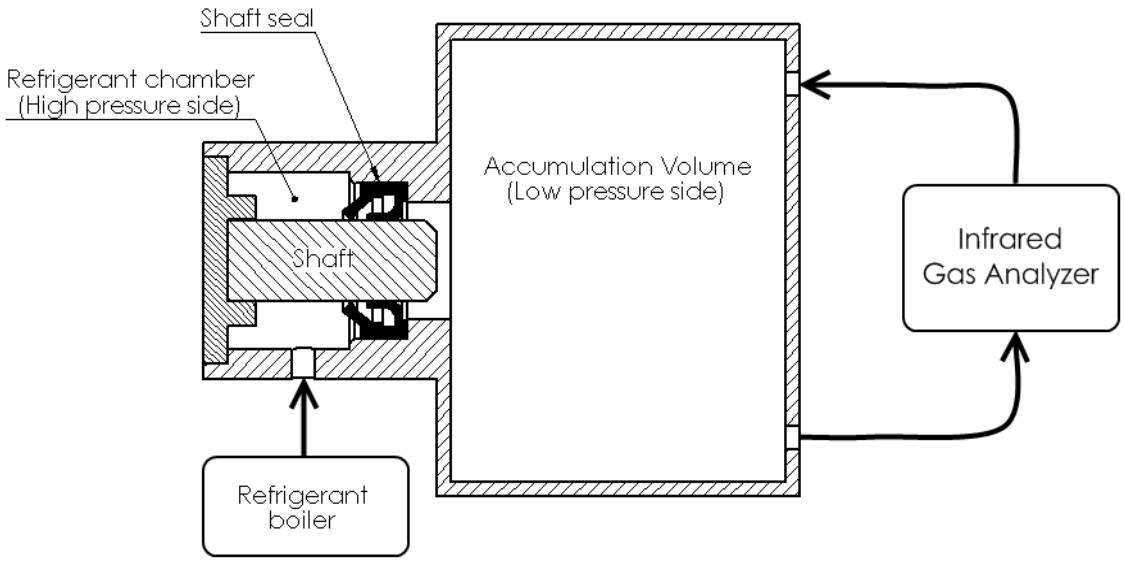

Figure 9 Principe du banc d'essais pour l'étude de l'étanchéité du joint tournant du compresseur

Ce banc permet l'étude de différents joints tournants, ainsi que d'arbres provenant de compresseurs ou de fabrication spéciale. Une autre particularité du banc réside dans la possibilité d'installer un arbre transparent à l'intérieur duquel on introduit un endoscope pour la visualisation du contact des lèvres. L'incertitude sur le calcul du débit de fuite est de 5,2 %.

Les différents joints tournants testés

L'étude des émissions et la visualisation du contact porte sur cinq types de joints tournants différents : A, B, C, D et E (voir figure 10). Leur grande différence est dans la géométrie de la lèvre en caoutchouc, ainsi que dans le contrôle de sa déformation avec la pression. Les joints tournants D et E présentent un support métallique entre les deux lèvres, ce qui permet de réduire la déformation de la lèvre en caoutchouc. Ces différences ont un impact direct sur les conditions de contact avec l'arbre, et par conséquent, sur le débit de fuite.

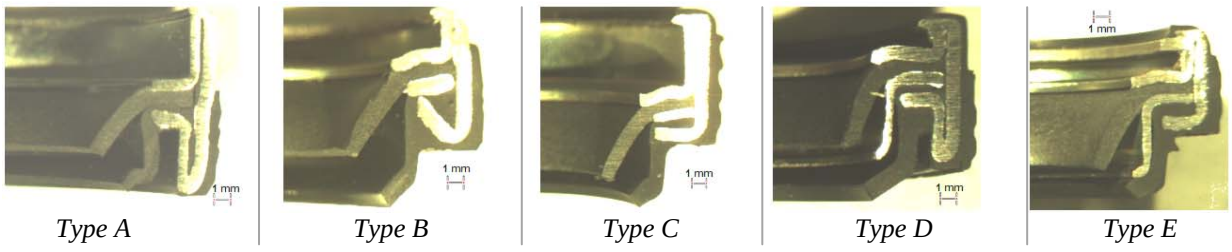

Figure 10 Vue en coupe des cinq joints tournants à étudier

Tous les joints tournants ont été testés avec des arbres de compresseurs neufs pour garantir l'homogénéité de la texture de la surface. Chaque type de joint tournant a été testé à trois niveaux de pression et température : 770, 1020 et 1320 kPa et 35, 45 et 55°C, respectivement.

Débit de fuite à sec

Les résultats des essais montrent que, comme pour le compresseur, la pression du fluide définit le niveau d'émissions du joint tournant (voir figure 11). L'évolution de la pression du fluide a deux conséquences :

1. augmentation de la différence de pression à l'origine du débit de fuite, et
2. déformation de la lèvre en caoutchouc, ce qui change les conditions de contact.

Dans le premier cas, le débit de fuite est décrit par les lois de Poisseuille et de Fick qui montrent que le débit de fuite augmente avec la différence de pressions. Le deuxième cas va définir le nombre et les dimensions des chemins de fuite. Cet essai montre que la déformation de la lèvre en caoutchouc du joint tournant E génère des conditions de contact plus favorables à la réduction des émissions. Effectivement, la lèvre en caoutchouc du joint tournant E est celle qui présente le moins de déformation avec la pression du fluide, ce qui permet d'augmenter la pression de contact avec la pression du fluide.

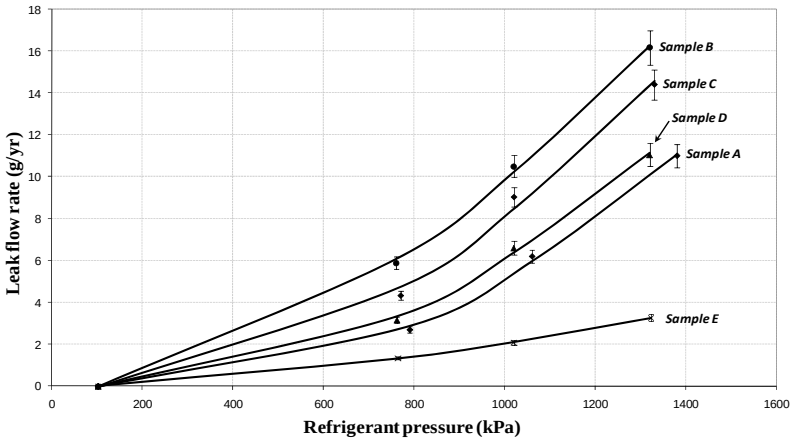

Figure 11 Débit de fuite de différents joints tournants à l'arrêt

Contribution des émissions du joint tournant

Avec les débits de fuite mesurés pour les cinq modèles, il est possible d'établir la contribution du joint tournant pour les émissions du compresseur. Si on compare ces résultats avec ceux obtenus pour 24 compresseurs neufs, on peut conclure que le joint tournant représente 50 % des émissions de gaz d'un compresseur neuf à l'arrêt.

Les paramètres d'étanchéité

Les essais menés avec différents arbres ont permis de conclure que :

- une variation de diamètre de 16 μm ne change pas le débit de fuite,
- la rugosité de la surface de l'arbre est primordiale pour établir le niveau d'émissions du joint tournant parce que la taille des chemins de fuite augmente avec la rugosité.

Un autre paramètre important pour la définition des chemins de fuite est l'ondulation. Un arbre transparent en PMMA a été chauffé pour provoquer un profil ondulé sur sa surface. Il a été observé qu'avec ce profil, le débit de fuite diminue avec l'augmentation de la pression : 0.7 g/an à 1320 kPa, 1.0 g/an à 1020 kPa et 3.7 g/an à 770 kPa. Cela semble contraire aux principes évoqués jusqu'à maintenant, mais en réalité ce n'est pas le cas. C'est une question de la définition du rayon du chemin de fuite décrit par Poisseuille. L'étanchéité statique du joint tournant du compresseur est assurée par la lèvre et les ondulations en caoutchouc, un matériau viscoélastique. La déformation de la lèvre dépend ainsi de la force appliquée.

A haute pression, la déformation significative du caoutchouc permet de bien remplir les espaces entre les piques des ondulations, ce qui réduit les dimensions des chemins de fuite, comme montré dans la figure 12a. A noter que la rugosité est extrêmement faible du fait du matériau. Quand la pression du fluide est plus faible, la force de déformation de la lèvre est aussi moindre. Par conséquent, les dimensions des chemins de fuite seront plus importantes, et donc le débit de fuite sera plus élevé (voir figures 12b et 12c).

Les valeurs et la variation des débits de fuites obtenus avec le profil ondulé indiquent aussi que le débit par perméabilité et par le contact des ondulations a un impact très faible sur les émissions du joint tournant. Ce sont alors les conditions de contact dans la lèvre en caoutchouc qui définissent le débit de fuite du joint tournant du compresseur à l'arrêt.

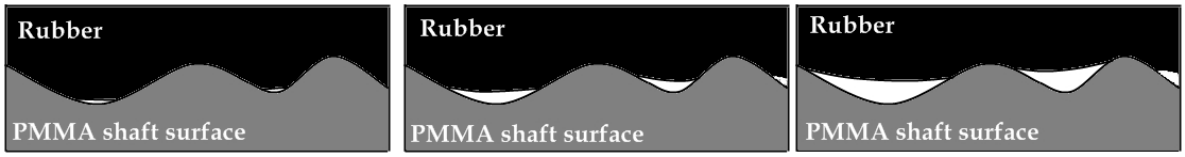

a) Haute pression *b) Pression moyenne* *c) Basse pression*

Figure 12 Représentation du contact entre la lèvre en caoutchouc et la surface ondulée de l'arbre transparent en PMMA

La présence d'huile dans le contact d'un joint d'étanchéité change le niveau d'émissions de gaz qui le traverse. Théoriquement, l'effet est expliqué par la formation d'un ménisque d'huile autour de chaque aspérité en contact ou proche du contact, ce qui réduit les dimensions des chemins de fuite.

La mesure du débit de fuite d'un joint tournant à l'arrêt en présence d'huile dans le contact de la lèvre en caoutchouc montre deux débits de fuite différents dans le temps. Dans un premier temps, le débit de fuite varie très peu avec la pression du fluide (voir figure 13). Cet intervalle de temps correspond à l'effet des ménisques d'huile. Mais comme la force d'attraction des ménisques est inférieure à la force exercée par le gaz, la formation des ménisques est rompue et l'huile est transportée par le gaz, ce qui rend le contact sec. A ce moment, on obtient le deuxième débit de fuite qui est approximativement égal à celui d'un contact complètement sec. La différence entre le deuxième débit de fuite d'un contact avec huile et celui d'un contact complètement sec est liée au changement de position de la lèvre en caoutchouc, comme cela a été déterminé pendant la visualisation du contact.

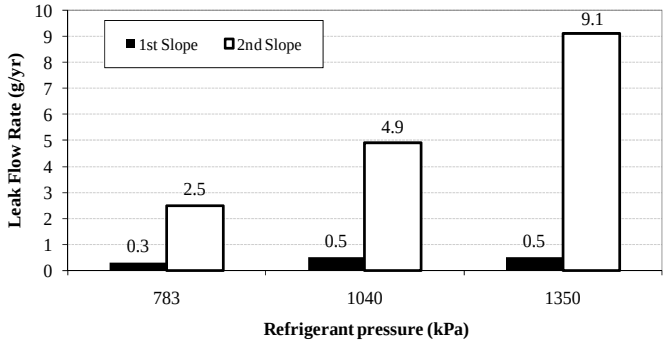

Figure 13 Débit de fuite du joint tournant A en présence d'huile dans le contact de la lèvre en caoutchouc et avec un arbre métallique

Le phénomène transitoire de l'effet d'huile implique le transport d'huile jusqu'au côté à pression atmosphérique. En outre, on démontre l'existence d'une fuite d'huile à l'arrêt. Ceci est facilement vérifiable par la visualisation directe du côté extérieur du joint tournant qui montre bien la présence d'huile et, donc, que la fuite d'huile à l'arrêt existe bien (voir figure 14).

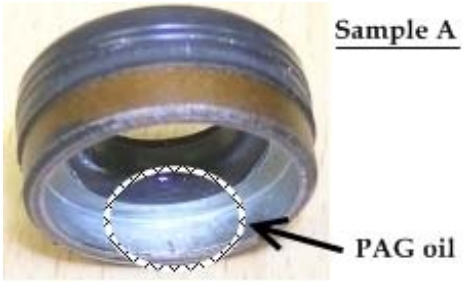

Figure 14 Présence d'huile du côté extérieur du joint tournant A qui montre la fuite d'huile à l'arrêt

Mais, quel est l'effet de l'huile quand la différence entre les surfaces réelle et apparente de contact est très faible ? La réponse est aucun effet, comme le montrent les résultats des essais présentés dans la figure 15. Quand la rugosité est très faible, comme sur la surface de l'arbre transparent, les chemins de fuite sont moins nombreux et de faible diamètre, donc, relativement à un arbre de compresseur:

- le débit de fuite est très faible, et
- l'huile n'a aucun effet sur les émissions de gaz.

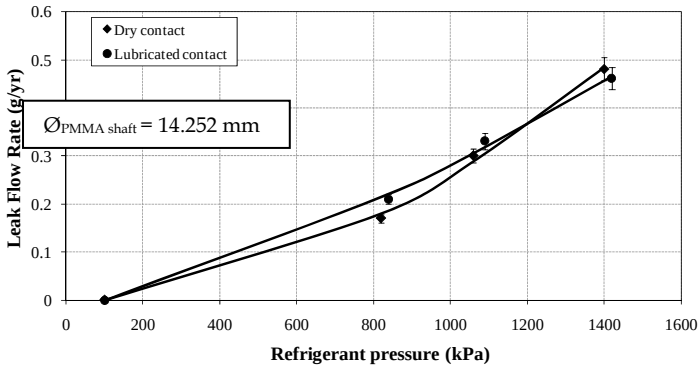

Figure 15 Débit de fuite avec un arbre transparent en PMMA, avec et sans huile

On peut donc conclure que, pour un joint tournant de compresseur à l'arrêt :

- le débit de fuite par le contact des ondulations et par perméabilité peut être négligeable,
- la rugosité de la surface de l'arbre détermine le débit de fuite du joint tournant.

Visualisation du contact

Un arbre transparent en PMMA a été utilisé pour visualiser le contact entre les lèvres du joint tournant et la surface de l'arbre. La visualisation a permis de déterminer l'évolution de la déformation et de la surface de contact avec la pression du fluide. Tous les joints tournants présentés précédemment seront testés. L'image du contact montre les deux lèvres ainsi que le support métallique de la lèvre en caoutchouc (voir figure 16).

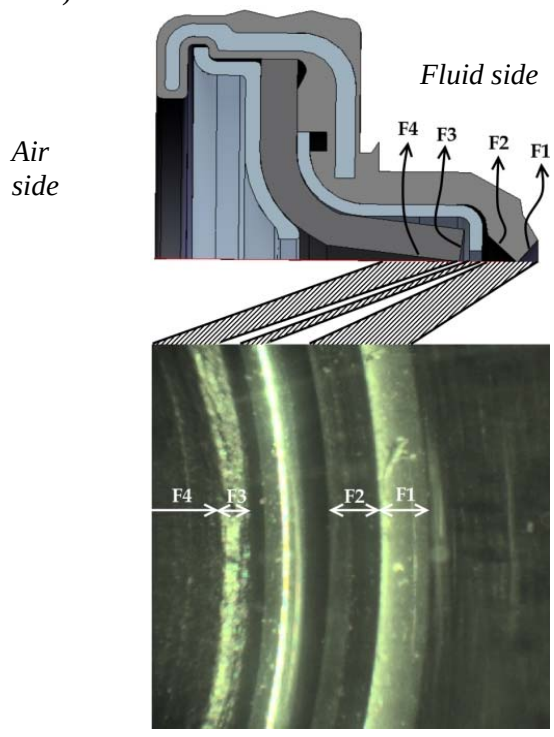

Figure 16 Visualisation du contact du joint tournant (25x)

Pour tous les modèles de joints tournants, le contact de la lèvre en caoutchouc se fait sur une ligne pour une différence de pressions nulle. Quand la différence de pression commence à augmenter, la déformation et la surface de contact varient avec la géométrie de la lèvre en caoutchouc, ainsi qu'avec le coefficient de frottement avec l'arbre.

Le joint tournant A présente l'évolution de la surface de contact la plus élevée. La largeur de contact de la lèvre en caoutchouc atteint 1,3 mm pour une pression de gaz de 1200 kPa (voir figure 16). Ce comportement change radicalement quand l'huile de lubrification est introduite dans le contact. La réduction du coefficient de frottement fait déplacer axialement la pointe de la lèvre en caoutchouc et change les conditions de contact. Ceci montre que la déformation de la lèvre en caoutchouc varie avec le coefficient de frottement, ce qui explique la différence entre les débits de fuite avec un contact sec et avec un contact lubrifié, dans le deuxième temps de l'essai. Les images montrent aussi la déformation de la lèvre en PTFE avec la force exercée par la lèvre en caoutchouc.

Le joint tournant B présente une très faible déformation avec et sans huile dans le contact. Les lèvres du joint tournant C montrent un déplacement axial de 0,08 mm à haute pression et pour un contact sec. Quand l'huile est introduite dans le contact, le déplacement axial et la largeur de contact augmentent dès 400 kPa. Le déplacement axial varie de 0,3 mm à 400 kPa à 0,6 mm à 1200 kPa. La variation de la largeur de contact avec la pression du gaz est montrée dans la figure 17.

Le joint tournant D possède un support métallique pour la lèvre en caoutchouc, ce qui fait qu'elle ne déforme pas la lèvre en PTFE. Le joint tournant E, le moins émissif des cinq testés, a aussi un support métallique pour la lèvre en caoutchouc. Quand le contact est sec, la lèvre en caoutchouc se déforme contre le support métallique sans changer la largeur de contact. En présence d'huile, le déplacement axial de la lèvre en caoutchouc devient très important. Dès que la pression du gaz augmente, la pointe de la lèvre s'approche du support métallique sans varier la largeur de contact. Pour 1200 kPa, le déplacement axial est stoppé par le support métallique et a une valeur de 0,84 mm.

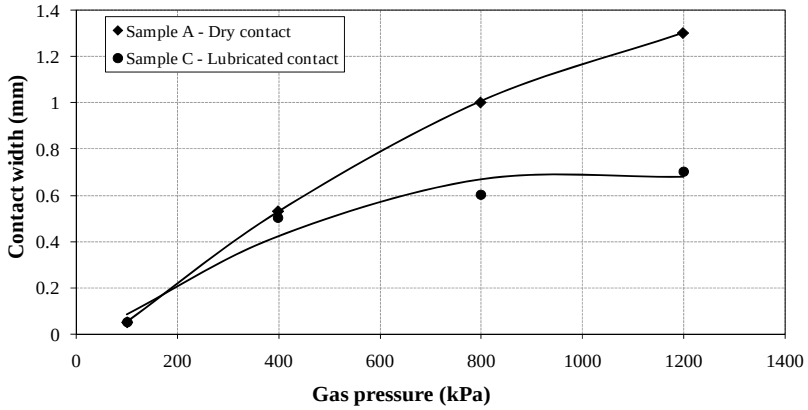

Figure 17 Evolution de la largeur de contact de la lèvre en caoutchouc

La visualisation du contact des lèvres du joint tournant a permis aussi d'apercevoir l'écoulement de gaz à travers le contact. La tension superficielle de l'huile provoque la formation de bulles de gaz à la sortie des chemins de fuite. Ceci permet de localiser les chemins de fuite et de conclure qu'ils sont distribués d'une façon hétérogène autour du contact.

Chapitre 4

CALCUL DES CONTRAINTES DU JOINT TOURNANT

Le dernier chapitre présente le calcul des contraintes d'un joint tournant de compresseur de climatisation automobile. Le joint tournant à analyser est le modèle E qui présente le plus faible taux d'émission de gaz relativement aux quatre autres modèles qui ont été testés.

Les matériaux

Le joint tournant est composé de matériaux ayant différentes propriétés mécaniques. La lèvre en caoutchouc, celle qui définit l'étanchéité à l'arrêt, présente un comportement viscoélastique, donc, non-linéaire. La lèvre en PTFE présente elle un comportement viscoplastique, donc, non-linéaire aussi. La structure métallique peut être modelée selon la loi d'Hooke. Les différentes lois de comportement des matériaux rendent le calcul complexe.

Le calcul a été réalisé avec le logiciel de calcul d'éléments finis MARC 2008r1. Le modèle considère tous les composants du joint tournant ainsi que les étapes de fixation et d'insertion de l'arbre (voir figure 18). Pour simplifier l'analyse, la lèvre en PTFE est modelisée comme un matériau élastique. La lèvre en caoutchouc est modelisée selon la loi de Mooney-Rivelin avec C_{10} = 0,73 MPa et C_{01} = 0,38 MPa.

La géométrie

La géométrie du joint tournant est présentée figure 18 dans sa position initiale. Le caoutchouc est considéré attaché à la structure métallique et en contact avec le support. Compte tenu de sa géométrie et de la nature du chargement, le calcul des contraintes du joint tournant est considéré comme un problème axisymétrique.

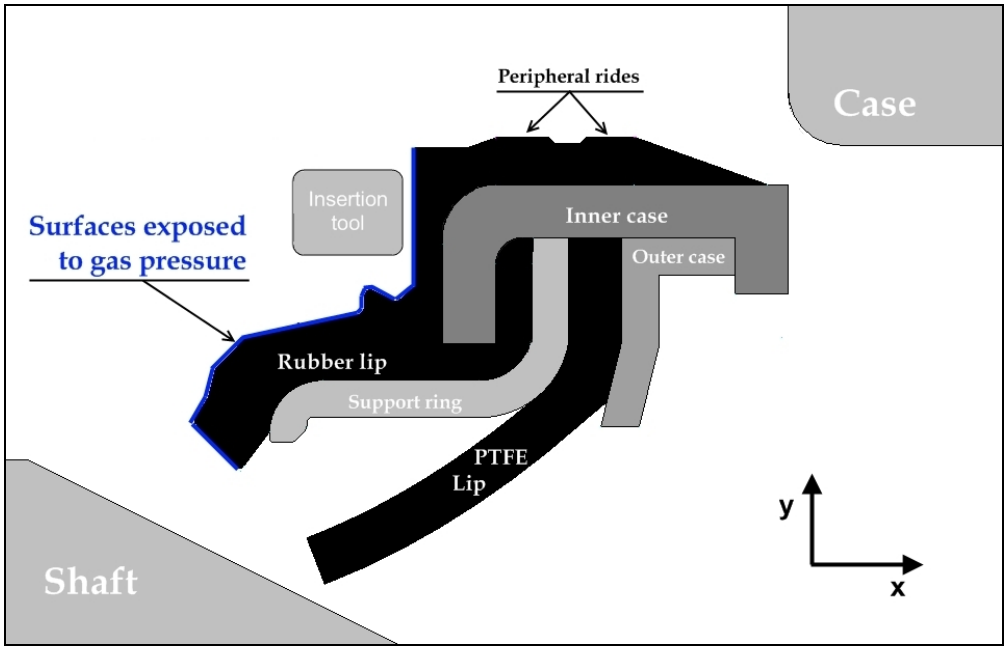

Figure 18 Géométrie du joint tournant E avec les composants nécessaires à son installation

Séquence du calcul

L'analyse se déroule en trois temps. D'abord, l'outil insère le joint tournant dans sa fixation et, ensuite, est enlevé. Avec le joint en position, l'arbre avance pour déformer les lèvres. Finalement, la pression est appliquée sur la lèvre en caoutchouc.

Résultats des calculs

L'analyse de la tension et de la surface de contact dans les ondulations et dans la lèvre en caoutchouc montre pourquoi le débit de fuite par le contact des ondulations peut être négligé relativement à celui de la lèvre (voir figure 19). D'une part, la tension de contact dans les ondulations est deux fois supérieure à celle de la lèvre, ce qui permet de réduire le rayon des chemins de fuite et, par conséquent, le débit de gaz. D'autre part, la surface de contact des ondulations est beaucoup plus grande, ce qui crée des chemins de fuite plus longs et ainsi réduire le débit de gaz. La combinaison d'une tension élevée et d'une grande surface de contact rend le débit de fuite par les ondulations beaucoup plus faible que celui de la lèvre.

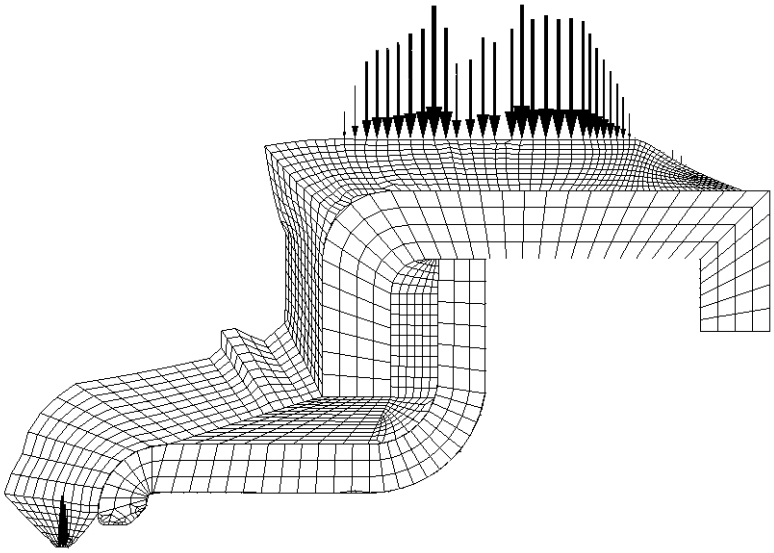

Figure 19 Distribution de la pression de contact et déformation du joint tournant E après installation et application de la pression de gaz

La réduction du coefficient de frottement entre la lèvre en caoutchouc et la surface de l'arbre a permis de voir les différentes déformations de la pointe de la lèvre. Le même comportement avait été trouvé pendant la visualisation du contact.

La pression de contact de la lèvre en caoutchouc dépend à la fois de la pression du gaz et de la surface de contact. En faisant varier le coefficient de frottement, la déformation de la lèvre va aussi changer et, par conséquent, la surface de contact. L'effet du coefficient de frottement sur la tension de contact est montré figure 20 pour trois pressions de gaz différentes et deux coefficients de frottement.

Une pression de gaz faible cause aussi une faible déformation de la lèvre avec un contact sec ou lubrifié, ce qui fait que la pression de contact est approximativement la même. Quand la pression du gaz augmente, la déformation de la lèvre augmente aussi, particulièrement pour de faibles coefficients de frottement. Cette différence dans la déformation va créer une surface de contact plus importante pour un coefficient de frottement plus petit qui résulte en une pression de contact plus faible. L'effet du coefficient de frottement est plus prononcé dans les plus grandes déformations.

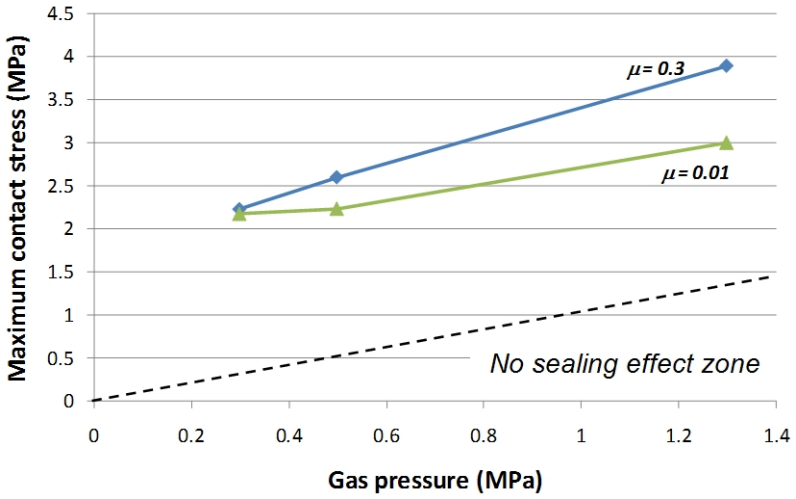

Figure 20 Evolution de la pression de contact avec la pression du gaz et le coefficient de frottement

Ces résultats montrent que le coefficient de frottement a aussi un effet sur le débit de fuite du joint tournant du compresseur. Lors de la comparaison du débit de fuite entre un contact sec et un contact lubrifié, on a noté qu'il y avait une différence significative. Cette différence s'explique précisément par la différence entre les pressions de contact obtenues dans les deux cas.

La méthode des éléments finis a permis une bonne simulation des déformations du joint tournant du compresseur. La définition de ce modèle peut être améliorée pour la conception de joints tournants plus étanches.

Conclusions

Le compresseur de climatisation automobile est pressurisé non seulement en fonctionnement mais aussi à l'arrêt. Il s'agit d'un compresseur non-hermétique qui utilise un fluide frigorigène halogéné dont les émissions contribuent au réchauffement climatique. Le joint tournant présente un double système d'étanchéité qui lui permet de retenir le fluide aussi bien compresseur en fonctionnement qu'à l'arrêt. Ce double principe de fonctionnement résulte en un système d'étanchéité complexe qui doit combiner une pression élevée sur le joint et une grande surface de contact à l'arrêt et permettre la lubrification en fonctionnement.

L'étude des émissions de compresseurs neufs et usagés a permis d'identifier les mécanismes de fuite à l'arrêt ainsi qu'en fonctionnement. Il a été démontré que le mode arrêt est l'élément dominant des émissions du compresseur, qui sont directement liées au carré de la différence des pressions.

Le mode fonctionnement représente une petite partie de la vie du compresseur. Cependant, il a une importance capitale dans l'évolution du débit de fuite du compresseur dans le temps. Les essais en fonctionnement montrent des problèmes de lubrification du joint tournant pendant le démarrage qui accélèrent l'usure. Le niveau d'émissions du compresseur en fonctionnement est directement lié à la lubrification du joint tournant. La présence d'huile dans le joint tournant, quand le compresseur est à l'arrêt, est aussi très bénéfique pour réduire les émissions de gaz. Néanmoins, il s'agit d'un effet temporaire car l'huile migre, ce qui rend le contact sec.

L'effet de l'usure du joint tournant a été évalué à deux niveaux : l'étude des émissions des compresseurs usagés et le vieillissement sur banc d'essais. Dans ces deux cas, l'usure du joint tournant a augmenté très significativement les émissions à l'arrêt, 800 % pour le compresseur B1. Pourtant, les compresseurs plus émissifs à l'arrêt sont les plus performants en fonctionnement, compte tenu de la meilleure lubrification du joint tournant rendue possible par le changement de la texture des surfaces en contact dans le joint tournant.

La contribution du joint tournant aux émissions du compresseur dépend de l'usure du joint. Si le compresseur est neuf, la contribution est de 50 %, sinon, elle peut atteindre 93 %. Il a été prouvé que le débit de fuite du joint tournant du compresseur provient quasi exclusivement du contact entre la lèvre en caoutchouc et l'arbre. Le débit de fuite correspondant au contact avec la fixation et par perméabilité peut être négligé.

L'étude de différentes conceptions de joints tournants a montré l'importance de limiter la déformation de la lèvre en caoutchouc pour obtenir des pressions de contact élevées. Le calcul des contraintes d'un joint tournant a mis en évidence la différence entre la pression de contact maximale et la surface de contact entre l'arbre et la fixation du joint qui justifient le débit négligeable de ce dernier. Le coefficient de frottement affecte aussi la pression de contact de la lèvre en caoutchouc, ce qui fait de lui un contributeur aux émissions du joint tournant.

Le compresseur de climatisation automobile est un composant très émissif en raison du mécanisme d'étanchéité complexe de son joint tournant. L'usure de celui-ci est le facteur déterminant pour la dégradation de l'étanchéité, ce qui explique la forte demande de fluide frigorigène pour la maintenance et le nombre élevé de recharges effectuées sur les véhicules âgés.

Perspectives

Le développement du joint tournant est directement lié au fluide frigorigène utilisé et à la politique de limite des émissions de gaz des systèmes de climatisation automobile. Dans tous les cas, le développement d'un joint tournant doit se faire dans deux domaines différents :

- en rotation (étanchéité dynamique), et
- à l'arrêt (étanchéité statique).

En fonctionnement, le démarrage à sec du joint tournant doit être supprimé en améliorant la lubrification des lèvres ainsi que la circulation d'huile à l'intérieur du compresseur.

A l'arrêt, le calcul par éléments finis amènera au changement de la géométrie de la lèvre en caoutchouc pour obtenir la pression et la surface de contact qui réduiront les chemins de fuite sans pour autant mettre en cause la lubrification du joint une fois en fonctionnement.

La priorité de développement est indiscutablement la réduction de la dégradation du joint tournant avec l'usure. Toutefois, il se fera uniquement si les deux modes de fonctionnement sont pris en compte.